Barts and The London
School of Medicine and Dentistry

Development of a Novel In-vivo Setting Bone Graft Substitute From Bioactive Glass

Thesis submitted in fulfilment of the requirements for the degree of Doctor of Philosophy in the Faculty of Dentistry, University of London

Niall William Kent

May 2014

Centre for Oral Growth and Development
Institute of Dentistry
Bart's and the London School of Medicine and Dentistry
University of London

Abstract

Calcium phosphate cements are in-vivo setting, injectable calcium phosphate based biomaterials. They are made of calcium phosphate salts which when mixed with water react to form apatite, the mineral phase of bones and teeth. This study investigates a novel way of forming calcium phosphate cements using bioactive glasses. The aim of the work was to discover a novel route of synthesis using a silicate bioactive glass.

Fifteen glass compositions were produced designed to investigate P_2O_5 content, CaF_2 content and calcium to sodium ratio within the glass. Glasses were produced via a melt-quench route before being milled and sieved to below 38 μm. The bioactive glass and $Ca(H_2PO_4)_2$ powders were mixed in an overall calcium to phosphate ratio of 1.67. The cement powder was then reacted with a 2.5 % solution of Na_2HPO_4. The paste was then mixed and then placed into cylindrical moulds. Eight samples were immersed into Tris buffer solution for 1 hour, 1 day, 7 days or 28 days. The compressive strength was measured for each specimen as well as SEM performed and the setting times for each composition was studied using the Gilmore needle test. The cement phase was analysed using ^{31}P & ^{19}F MAS-NMR, FTIR and XRD.

The results showed that both compressive strength and setting time was dependent upon glass composition. As sodium content was increased both the initial and final setting times decreased. Increased fluoride addition caused a decrease in the setting time. In the fluoride free compositions octacalcium phosphate was identified in all compositions. The cement setting

reaction for these compositions followed a similar reaction of first forming dicalcium phosphate dihydrate which transformed to octacalcium phosphate then eventually hydrolysing to hydroxyapatite. When fluoride was incorporated into the cement the phases formed were fluoridated-apatite and DCPD. In conclusion a novel method of producing calcium phosphate cements was discovered using a bioactive glass as a reactive precursor. It was shown that the cement phase, setting time and compressive strength could all be altered by changing the glass composition.

Foreword

This thesis contains the discovery of and subsequent in-vitro characterisation of a novel calcium phosphate cement formed through the reaction where at least one of the reactive precursors is a bioactive glass. Each glass composition was used to produce a cement which was then characterised for compressive strength and cement phase after immersion for various time points in Tris buffer solution. The effect of glass composition on the cement properties and cement phase is then discussed. This novel method was patented, a copy of which is included in the appendix. A six and twelve week in-vivo ovine animal study was subsequently performed on this material a report of which is also included in the appendix of this thesis.

Table of Contents

List of Figures

List of Tables

Appendices

Appendix A: Required statement of originality for inclusion in research degree theses.

Appendix B: Patent filed as a result of this work.

Appendix C: Results of an animal study conducted on the cements developed in this project in collaboration with University College London.

Appendix D: Journal article published ‘Effects of Fluoride on in vitro Enamel Demineralization Analyzed by ^{19}F MAS-NMR’

List of Abbreviations

HAP - Hydroxyapatite

AP - Apatite

OCP – Octacalcium Phosphate

DCPD – Dicalcium Phosphate Dihydrate

DCPA - Dicalcium Phosphate Anhydrous

FAP - Fluorapatite

TTCP – Tetracalcium Phosphate

XRD – X-ray Diffraction

FTIR – Fourier Transform Infrared

MAS-NMR – Magic Angle Spinning Nuclear Magnetic Resonance

SEM – Scanning Electron Microscopy

DSC – Differential Scanning Calorimetry

Acknowledgements

My utmost and most sincere gratitude is for my supervisors Dr Natalia Karpukhina and Professor Robert Hill. Who have guided and pushed me throughout the completion of my PhD.

Mother and Father I thank for raising and supporting me. For my brothers Frank and Luke who taught me the force of will and the strength of personality, without which I would not have finished.

To all of my fellow PhD students in the dental physical sciences department who made my time funny, easy and enjoyable. In particular I would like to thank Samera, Nasrine and Navina.

I would also like to thank both Professor Ishikawa and Professor Matsuya at Kyushu University for welcoming me to Japan and allowing me to work in their institution.

For the various funding I have received during my PhD I would like to thank:

The Medical Research Council and Bart's and The London Dental School for jointly providing the funding for my PhD.

The Japan Society for the Promotion of Science for funding my three month research fellowship at Kyushu University in Japan.

Queen Mary innovation for providing funding for the undertaking of an in-vivo animal study of the bioactive glass cement developed during this project.

Chapter 1: Introduction

The aim of this project is to develop novel calcium phosphate cements (CPCs) setting *in vivo* which are produced through reaction where at least one of the precursors is a bioactive glass.

CPCs are calcium phosphate based synthetic bone graft materials which form conventionally as a result of the reactions between calcium phosphate salts. On mixing with water the salts react to form apatite, the mineral phase of bones and teeth. CPCs have uses in both orthopaedics and dentistry where they are used as bone substitute materials to replace missing or diseased bone. They are advantageous because of their injectability which allows the surgeon to inject the setting cement paste into the implantation site minimally invasively. These materials are also *in vivo* setting which allows them to mould to the shape of the implantation site once implanted which ensures complete void filling. Unlike CPCs, pre-set bone substitutes do not have this advantage and cannot set *in vivo*.

The disadvantages of currently used CPCs are that firstly the calcium phosphate salts used lack sufficient solubility which leads to poorly controllable setting times. Salts are also fixed in their stoichiometry meaning they are restrictive when alteration of composition is desired to improve the properties of these materials. CPCs also suffer from low early water stability caused by their poor setting characteristics. On incomplete setting the cement mixed with body fluid can be dislodged from the implantation site.

This has the potential for large surgical complications and even mortality for the patient if untreated.

Bioactive glass has also been used as bone-substitute materials. They are amorphous materials and are produced from SiO_2-P_2O_5-CaO-Na_2O where the SiO_2 is the glass network forming oxide. They are defined a class A bioactive materials as they are osteoinductive (Hench, 2006). The initial commercial examples were based on the glass composition 45S5 (46.1 mol% SiO_2, 26.9 mol% CaO 24.4 mol% Na_2O and 2.5 mol% P_2O_5) developed by Hench et al. in the late 1960's. Later examples has been developed notably StronBone®, a strontium containing bioactive glass indicated for bone substitution (O'Donnell et al., 2010). The material is implanted as granules where the granular mixture is mixed with the patients' blood and then impacted into the implantation site.

The advantages of bioactive glasses are that they show good biocompatibility, forming a strong interfacial bond with host bone. This intimate bone is caused by apatite formation on the surface of the glass and in-growth of host bone in the material (Hench et al., 1971). By definition glass allows significant variation in compositions which enables alteration of the properties in order to optimise notably solubility and biocompatibility. The disadvantages of bioactive glass as a bone-substitute materials are that they are non-injectable. Bioactive glasses are implanted during the surgery which is considerably more invasive method than injection of CPCs. Bioactive glasses also have no inherent strength once implanted. Whilst neither CPCs nor bioactive glasses can be used for load-bearing application, CPCs do set

during their implantation forming a uniform material which is resistant to forces applied to it preventing material migration from the implantation site. Bioactive glasses however remain particulate until either material induced apatite formation or host bone formation which can take at least a few weeks. Meaning the glass granules are susceptible to deformation or migration from the implantation site which is undesirable.

The intention of this project is to combine the advantages of both a bioactive glass and calcium phosphate cements and produce a novel biomaterial which is superior in its properties to both CPCs and bioactive glasses. This will widen both the applications and effectiveness of current bone grafting materials available to surgeons. The advantages of using this approach are outlined below.

Glasses exist in a higher energy state than their crystalline counterparts. As a result of this the glasses are more soluble than the equivalent crystal structure. The solubility of a glass can also be manipulated at will through alterations in the design of the composition. This gives a wider control of setting times through changes in glass composition when glasses are used to produce *in vivo* setting synthetic bone graft. Thus the setting times of these materials can be more readily controlled through glass composition and particle size distribution rather than just particle size as with CPCs.

Glass compositions can also accommodate substantial incorporation of therapeutically useful ions. It is desirable in certain applications to produce substituted apatites (fluoride & strontium) during the setting reaction of CPCs. This has been attempted by introducing additional salts that contain

the desirable ion to the salt powders. However, this has been shown to have deleterious effect on the setting reaction of CPCs (Bohner et al., 2005). It is hypothesised that introducing these ions from the glass structure would avoid these complications enabling the beneficial effect of the ions without affecting the cement properties.

Using bioactive glass also introduces the silicate phase which is a potential site for heterogeneous nucleation and has been proposed as such by Hench et al (Hench, 2006) in the bioactivity mechanism of bioactive glasses. In conventional CPCs (without hydroxyapatite seed crystals added to the formulation) the nucleation is likely to occur via homogenous nucleation. Heterogeneous nucleation has a lower energy barrier than homogeneous nucleation meaning it occurs more commonly in a system. This means that potentially cement developed using glasses would nucleate more rapidly and thus set more rapidly than conventional CPCs.

Another advantage of using the glass is that it has been identified that the release of silicon and calcium ions into the site of implantation improves the biocompatibility of the material. 17 – 20 ppm soluble Si species and 88 – 100 ppm soluble Ca ions release from bioactive glasses increases the rate of osteoblast proliferation and differentiation (Sun et al., 2009) (Xynos et al., 2000, Xynos et al., 2001, Hench et al., 2002). Bioactive glasses are examples of class A bioactive materials, only class A bioactive materials induce rapid new bone formation *in vivo* (osteoproduction). Comparing Class A bioactive materials with Class B, like dense HA substrates, or inert materials shows that class A materials are the only examples capable of

forming new mineralised bone. This will result in a new glass-based *in vivo* setting bone graft substitute being more biocompatible and osteoinductive compared to a conventional CPC.

Therefore the resulting material will be an *in vivo* setting bone-substitute with a range of potential advantages over both bioactive glasses and CPCs. The new CPCs made from bioactive glasses will have improved setting time and be injectable which makes them considerably easier and less invasive than all non-injectable bone substitutes like bioactive glasses, porous bone scaffolds, or HA granules. In conclusion these novel materials will be far superior to current orthopaedic materials available to surgeons.

Chapter 2: Literature Review

2.1 Calcium Phosphates

2.1.1 Hydroxyapatite

Hydroxyapatite is a common mineral which is the major inorganic phase of bone and teeth. It is a type of calcium phosphate with the chemical formula $Ca_{10}(PO_4)_6(OH)_2$. It has extensive use in biomaterials, especially for bone substitution, given its affinity with bone.

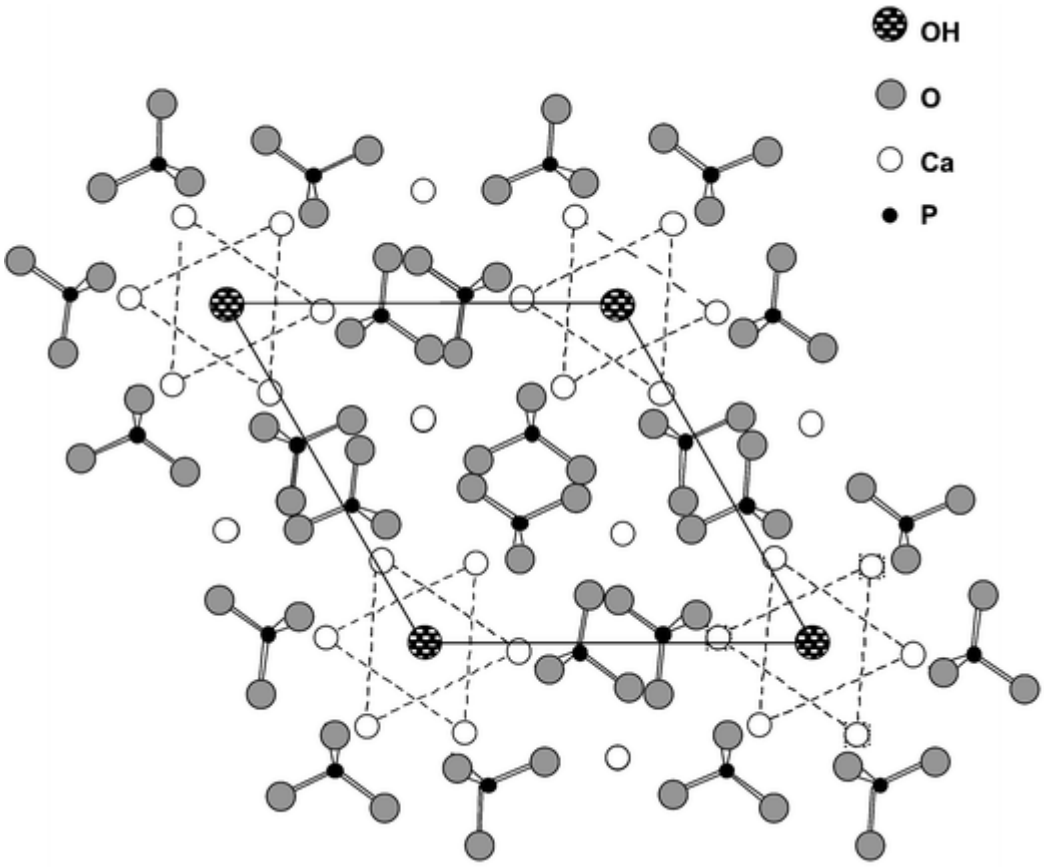

Figure 1 Crystal structure of monoclinic hydroxyapatite (Cazalbou et al., 2004)

2.1.1.1 Structure

Pure hydroxyapatite (s-HAP) is monoclinic with space group $P2_1/b$ and lattice parameters a = 9.4214(8), b = 2a, c = 6.8814(7) Å, $\gamma \neq 120°$ (White and Dong, 2003) (See Figure 1). Ns-HAP (non-stoichiometric) has a slightly

different crystal structure to s-HAP (stoichiometric), it is in an hexagonal form with space group P63/m *a* = 9.4240, *b* = 9.4240, *c* = 6.8790 Å (Kay et al., 1964). Hydroxyapatite has a similar structure to octacalcium phosphate (OCP) ($Ca_8(HPO_4)_2(PO_4)_4$) and there is a strong relationship between these two compounds. Hydroxyapatite has an OH^- column running vertically down its structure (White et al., 2005). This column is easily substituted and common substitutions for the hydroxyl groups include F^-, Cl^- and CO_3^{2-}. These hydroxyl ions are aligned in one orientation along the column OH-OH-OH-OH this induces hydrogen bonding down the structure and provides stability. Slight impurities of fluoride ions can cause 'flipping' of the alignment of the hydroxyl ions OH-OH-F-HO-HO (Elliott, 1994).

2.1.1.2 Nucleation and Crystal Growth

The nucleation of hydroxyapatite is a complicated process and depends upon reaction conditions. In highly supersaturated solutions at neutral or alkali pH conditions it was shown that amorphous calcium phosphate first forms which then transforms to OCP which then hydrolyses to hydroxyapatite (Elliott, 1994). Studies where seeded crystals were added to calcium phosphate solutions with altering conditions showed that the rate of crystal growth is largely determined by the degree of the supersaturation of the surrounding solution (Moreno et al., 1977, Moreno and Varughese, 1981). Kinetic analysis showed that linear growth rate was dependant on the square of the degree of supersaturation of the solution (Moreno and Varughese, 1981, Moreno et al., 1977).

2.1.1.3 Substitution in Hydroxyapatite

Substitution in apatites is very common and indeed it is actually incredibly difficult to synthesise pure stoichiometric, monoclinic, s-hydroxyapatite. Virtually all naturally occurring apatites have some degree of substitution within their structure. Substitution for the hydroxyl ions in apatite is common and it is known that F^-, Cl^-, CO_3^{2-}, O_2^{2-}, and SO_4^{2-} can all substitute at this site in various degrees. The structure of apatites is not generally known and it should be noted that sizes of different anions should be taken into account as this can distort the apatite crystal structure. Another factor with this type of substitution is that it can alter the substitution in other sites of the apatite structure, particularly at the Ca sites (Elliott, 1994). As substitution of OH^- ions for larger or smaller ions will alter the sizes of ions that can substitutes for Ca^{2+} or PO_4^{3-} ions. The most common substitution for OH^- is F^-, and fluorapatite is more stable than hydroxyapatite (Elliott, 1994). There are two routes by which this substitution can occur. The first is through ion exchange where already formed apatite crystals undergo ion exchange where OH^- ions are replaced without dissolution of the apatite crystal. It should be noted that the degree of substitution will depend on the concentration of the ion to be substituted also this method will not give 100% substitution (Braun et al., 1995). The second route is incorporation of these ions during formation through precipitation from solution where fluoride ions or chloride ions are added to the reaction solution and they enter the apatite structure during apatite formation. Addition of fluoride ions to the apatite formation reaction will cause the substituted apatite to form directly without going via an OCP

intermediate (Muragalelli et al., 1992, Shiwaku et al., 2010a, Shiwaku et al., 2010b).

There is much substitution in apatites at the calcium sites which are numerous and complex. Two calcium sites exist within the apatite structure Ca(I) and Ca(II), the distribution of substitution is often different between the two sites. There are four Calcium occupying site I and six Calcium occupying site II within one hydroxyapatite unit cell (LeGeros, 1991). The distribution between the two sites will be affected by charge as if the charge of the ion substituting the calcium ion is different from 2+ (as in calcium ions) then the charge compensation mechanism will affect distribution and the size of the substituting cation in relation to the two sites. Other factors affecting distribution include polarisability, ability to form partial covalent bonds, extent of substitution, temperature, thermal treatment and method of preparation (Elliott, 1994). The coordination number of the Ca(I) site is nine, whereas for Ca(II), it is seven. Based on this it has been suggested that the Ca(I) site should be preferentially occupied by larger cations than the Ca(II) site. The most common and most relevant substitution occurring at the calcium sites are Sr^{2+} and Na^{+}, a full list of possible substitutions can be found in the literature (Elliott, 1994).

2.1.1.4 Carbonated Apatite

Understanding the structure and chemistry of carbonated-apatite is important, as it is the main form of apatite found in bones and teeth and it is also a very common substitution in apatites. There are two distinct types of carbonate substitution, type A and type B. Type A substitution occurs when

the CO_3^{2-} ion is substituted at the position of the hydroxyl groups to give a formula of $Ca_{10}(PO_4)_6CO_3$. Type B substitution is for a PO_4^{3-} ion in the apatite lattice, this further induces substitution of a Ca^{2+} ion for a Na^{+} ion to provide charge balance in the resulting structure, $Ca_9Na(PO_4)_5CO_3(OH)_2$. Type A substituted carbonated-hydroxyapatite is produced through solid-state reactions at 1000°C, only a small fraction of biological apatite is believed to be type A. Whilst the solubility effects of type A substitution have not been measured, it is hypothesized that this substitution will cause higher solubility of the apatite due to weaker bonds introduced by the carbonate substitution (LeGeros, 1991).

Type B substituted carbonated-hydroxyapatite can be prepared through direct precipitation or hydrolysis of OCP or dicalcium phosphate dihydrate (DCPD). The degree of substitution is dependent upon the amount of CO_3^{2-} in solution. A maximum substitution level of 22 wt% exists as carbonate can only replace a maximum of three PO_4^{3-} ions in the apatite lattice. Type B substitution has a number of effects on the apatite these being (I) decrease in *a*-axis and an increase in *c*-axis dimensions compared to carbonate-free apatites; (II) decrease in crystal size; (III) increase in crystal strain; (IV) change in crystal morphology; (V) increase in solubility. The increase in solubility is caused by the decrease in crystal size that increases the total surface area. Additionally, the Ca-CO_3 bond is weaker than the Ca-PO_4 bond, making the apatite more susceptible to acid dissolution (LeGeros, 1991).

FTIR is a good method of both identifying carbonate substitution and confirming which type is present. Bands present give bands at 1474 and 1406 cm^{-1} for type B, 1541 and 1449 cm^{-1}, for type A 1563, 1506, 1541 and 1453 cm^{-1} (Fleet and Liu, 2004).

It is also possible to obtain apatites with mixed type A and B incorporated into the apatite structure (Gibson and Bonfield, 2002). Samples have been synthesised in-vitro using $Ca(OH)_2$ and H_3PO_4 with CO_2 gas bubbled through the reaction solution, the powder was then synthesised calcined at temperatures between 500° and 1100°C for 2 h, with a heating rate of 2.5°/min. (Gibson and Bonfield, 2002). FTIR was used to identify incorporation of carbonate into the apatite structure. Bands at 1570, 1545, 1504, 1498, 1466, 1455, 1410 (all CO_3 v_3), 880, 873 (CO_3 v_2) and 755 cm^{-1} (CO_3 v_4) all show carbonate substitution.

2.1.1.5 Identification
Infrared and Raman Spectroscopy

Table 1 IR and Raman Peak Positions of Hydroxyapatite (Elliott, 1994)

IR[a]	Raman[a]		Assignment
3572	3572 m		OH stretch
1087	1075 s	1046 s	ν_3 PO_4
~1072 sh[a]	1061 w,sh	1039 m	
1046	1053 sh	1028 s	
~1032 sh			
	962 vs		
962		948 m	ν_1 PO_4
	641 vw		
630		630 vw	OH libration
	615 m		
601	608 s	593 s	ν_4 PO_4
571		580 s	
	447 s		
474		432 s	ν_2 PO_4
~462 sh			
	376 w		lattice mode
	333 w[b]		
~355 sh			Ca_3-(OH) "ν_3 stretch"
343			
	306 w[b]		
	289 w[b]	175 w	
	267 w[b]	157 w	
	237 w	153 w	
~290	222 w	140 w	Ca-PO_4 lattice modes
~275	206 w	132 w	
~228	196 w	114 w[c]	

vs, very sharp; vw, very weak; w, weak; m, medium; s, strong; vs, very strong; sh, shoulder (Elliott, 1994).

IR performed on apatite and calcium phosphates in general can be a useful and fast technique used for their identification. Additional bands to those listed above have been used as methods of determining common substitutions in apatite structures, peaks of note include, 3545 & 3572 cm^{-1} which are assigned to fluorohydroxyapatite; 3498 & 3570 cm^{-1} which are assigned to chlorohydroxyapatite; and 872, 879, 1410, 1450, and 1541 cm^{-1} indicating presence of carbonate (CO_3^{2-}) substitution in the apatite structure

NMR spectroscopy

In ^{1}H MAS-NMR of hydroxyapatite at 500.13 MHz and a spinning speed of 7.3 kHz a sharp resonance was present at 0.2 ppm relative to trimethyl silane which was attributed to the proton in the OH^- group, a second resonance at 5.6 ppm as identified which was attributed to surface adsorbed water (Yesinowski and Eckert, 1987). Additionally ^{43}Ca MAS-NMR has been performed on hydroxyapatite) samples attempting to distinguish between the two calcium sites present in the crystal structure (53.784 MHz, spinning speed 4 kHz). The authors were able to distinguish between the two sites with the Ca(I) site being located at -1.8±0.8 ppm and the Ca(II) site at 11.2±0.8 ppm (Laurencin et al., 2008). ^{31}P MAS-NMR studies performed on hydroxyapatite (68.42 MHz, spinning speed 2.5 kHz) gave a resonance at 2.8 ppm relative to 85% H_3PO_4. The authors also produced a number of calcium-deficient apatites with Ca/P = 1.46 & 1.58 these also gave resonances at 2.8 ppm indicating no difference in peak position with changing stoichiometry (Rothwell et al., 1980).

X-ray Diffraction

The XRD pattern below is of hydroxyapatite. A characteristic diffraction line to look for is a triplet of peaks around 32 degrees 2 theta (31.7 (211), 32.1 (112) and 32.8 (300) degrees 2 theta). There is also a characteristic diffraction line at 25.8 (002) degrees 2theta. These characteristic diffraction lines are especially useful when identifying small apatite crystals.

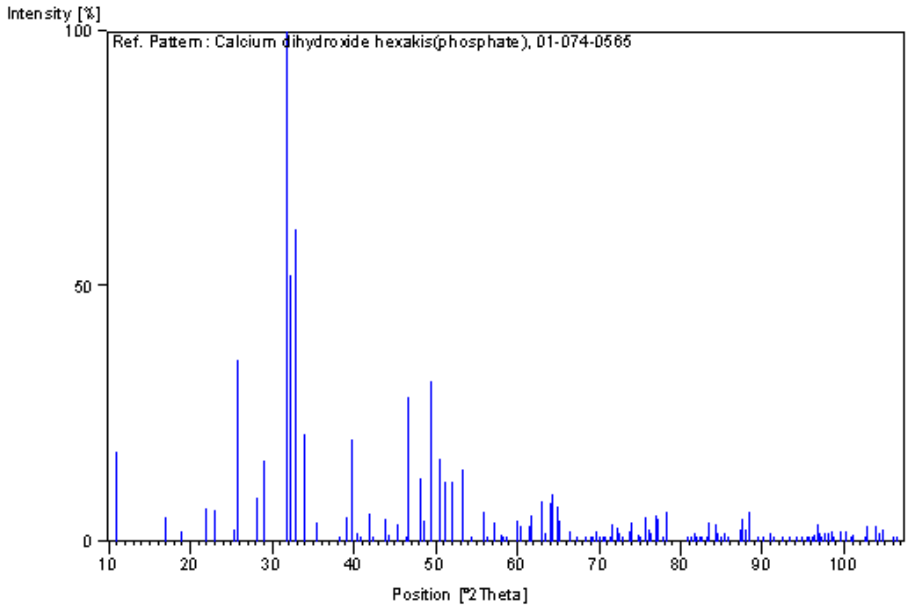

Figure 2 X-ray Diffraction Pattern and relative intensities of Hydroxyapatite ICSD reference code 01-074-0565 from (Sudarsan.K and Young, 1969).

2.1.2 Fluorapatite

Due to Fluorapatite (FAP) being the least soluble of the apatite mineral series it is found in nature, a notable example is in marine organisms (Puura and Nemliher, 2001). Fluorapatite has been found in many types of marine invertebrates, notable examples are in brachiopods, crustacean exoskeletons, coral, and sharks teeth (MacFadden et al., 2004). Sharks teeth are examples of placoid scales and are made of apatite. Apatite in shark teeth resembles FAP with OH^- ions hydrogen bonded to nearby F^- ions in a linear fashion along the c-axis (Ogaard et al., 1991).

2.1.2.1 Structure

FAP is hexagonal with space group P63/m and lattice parameters, a = b = 9.36 Å, c= 6.88 A. The fluoride ions occupy the centre of calcium (II) ‘triangles’ found at z= 1⁄4 and z= 3⁄4. Fluoride ions (1.36 Å) are smaller in

comparison to hydroxyl ions (1.40 A) fitting into the calcium ‘triangles’ (Elliott, 1994). The substitution of F^- for OH^- ions causes a reduction in the volume unit cell, which causes the lattice to become denser. This increase in density causes enhanced stability because of electrostatic bonds formed between F^- and adjacent ions.

2.1.2.2 Effect of Fluoride Substitution

The incorporation of fluoride ions into the apatite structure to form either fluorohydroxyapatite ($Ca_{10}(PO_4)_6(OH)_{2-x}F_x$) or pure fluorapatite ($Ca_{10}(PO_4)_6F_2$) has a number of effects upon the properties of the apatite which includes (I) an increase in structural stability due to a better fit of fluoride in the Ca ‘triangles’; (II) contraction of the *a*-axis but no change in the *c*-axis dimensions; (III) increase in crystallinity which induces increased crystallite size and a decrease in crystal strain; (IV) a stoichiometry of apatite closer to that of pure apatite (Ca/P = 1.67); (V) decrease in solubility (LeGeros, 1991).

2.1.2.3 Identification

By far the best way of identifying the presence of pure fluorapatite is by ^{19}F Magic Angle Spinning Nuclear Magnetic Resonance (MAS-NMR) a technique that can be run on solid samples and will show the individual presence of any fluoride environments within a specimen. On an ^{19}F MAS-NMR spectra FAP will appear at -101 ppm (relative to $CFCl_3$) (Brauer et al., 2010c) or 64 ppm (relative to C_6F_6) (Braun et al., 1995). Mixed substituted-fluorapatite with either OH- or Cl- groups will be distinguished from pure stoichiometric FAP, as will possible fluoride containing impurities (for instance CaF_2). Unpublished work has been completed where ^{19}F MAS-NMR

has been used to confirm sharks teeth are made of fluorapatite and that fluoride containing bioactive glasses form fluorapatite on immersion (Brauer et al., 2010a).

FTIR has been used to identify the formation of FAP by the absence of a band at 3572 cm^{-1} which is the OH peak in hydroxyapatite, the logic being that if it is absent then pure FAP must be present. This is however a flawed method, a paper which used a solution route to synthesize various degrees of substituted fluorohydroxyapatite shows that this peak is not present after $Ca_5(PO_4)_3OH_{0.8}F_{0.2}$ degree of substitution meaning it cannot be used as a reliable method to assess the formation of pure FAP (Wei et al., 2011).

X-ray Diffraction has been used to identify the formation of apatite in circumstances where fluorapatite or mixed fluorohydroxyapatites have been synthesized (Azami et al., 2011). XRD will tell the investigator if the reaction has reached completion to confirm that apatite has been produced without impurities and starting materials are no longer present. XRD cannot however distinguish easily between hydroxyapatite and fluorapatite and thus cannot be used on its own to show FAP formation. The reason for this is that while there are some slight differences between degrees 2 theta positions these differences are minor and cannot be, with confidence, used to confirm the presence of fluorapatite. In addition to this if substitution is not 100% fluoride for hydroxide ions then this difference between lines decreases further.

A number of studies have used F-electrode analysis to show the presence of fluoride in an apatite sample (Takagi et al., 2010, Azami et al., 2011). The suspected FAP should first be dissolved in an acidic solution, perchloric acid

($HClO_4$) has been used for this purpose. Then an F-electrode can be used to assess concentration of fluoride present in the sample. This can then be compared against Ca and P concentrations to assess whether the sample has the correct Ca/F ratio (0.200) for stoichiometric fluorapatite. SEM-EDX has also been used to measure fluoride concentration in synthesized FAP samples (Azami et al., 2011), however this is an inaccurate method due to fluoride being a relatively light element. Both of these two methods are inaccurate methods for measuring fluoride concentrations and while they will indicate the presence of FAP when used in conjunction with XRD analysis it will not be possible for the investigator to confirm with complete certainty as to whether a sample is pure FAP.

2.1.3 Octacalcium Phosphate

Octacalcium phosphate (OCP) has the chemical formula $Ca_8(HPO_4)_2(PO_4)_4.5H_2O$, the composition of OCP was first described by Berzelium in 1836. OCP is an important calcium phosphate phase as it is regarded as a transient intermediate in the formation of the thermodynamically more stable hydroxyapatite (Elliott, 1994). Its ability to act as an intermediate to hydroxyapatite formation is due to the fact that it nucleates and grows more readily than hydroxyapatite. This intermediary however is thought to be pH dependent. At reaction conditions with a pH between 5.0-9.0 OCP will be an intermediate phase before hydroxyapatite formation whereas if reaction conditions are above pH 9.0 then hydroxyapatite will precipitate directly (Chow, 2000). This is most likely due to the relative lack and abundance of OH^- or H^+ ions at the different pHs. As hydroxyapatite synthesis requires the presence of sufficient OH^- ions

whereas OCP incorporates two acidic protonated phosphates (HPO_4^{2-}) in its structure.

Understanding the formation and hydrolysis of OCP is then important in the mineralization of bones and teeth, remineralisation of carious lesion, and formation of hydroxyapatite-based biomaterials. OCP has been found as a component of dental calculus and other calcifications (Kakei and Yoshikawa, 2003). It is also thought that OCP is an intermediate mineral phase in bone formation with X-ray diffraction studies showing the presence of OCP in bone of metaphysis of a two day old rabbit (Elliott, 1994).

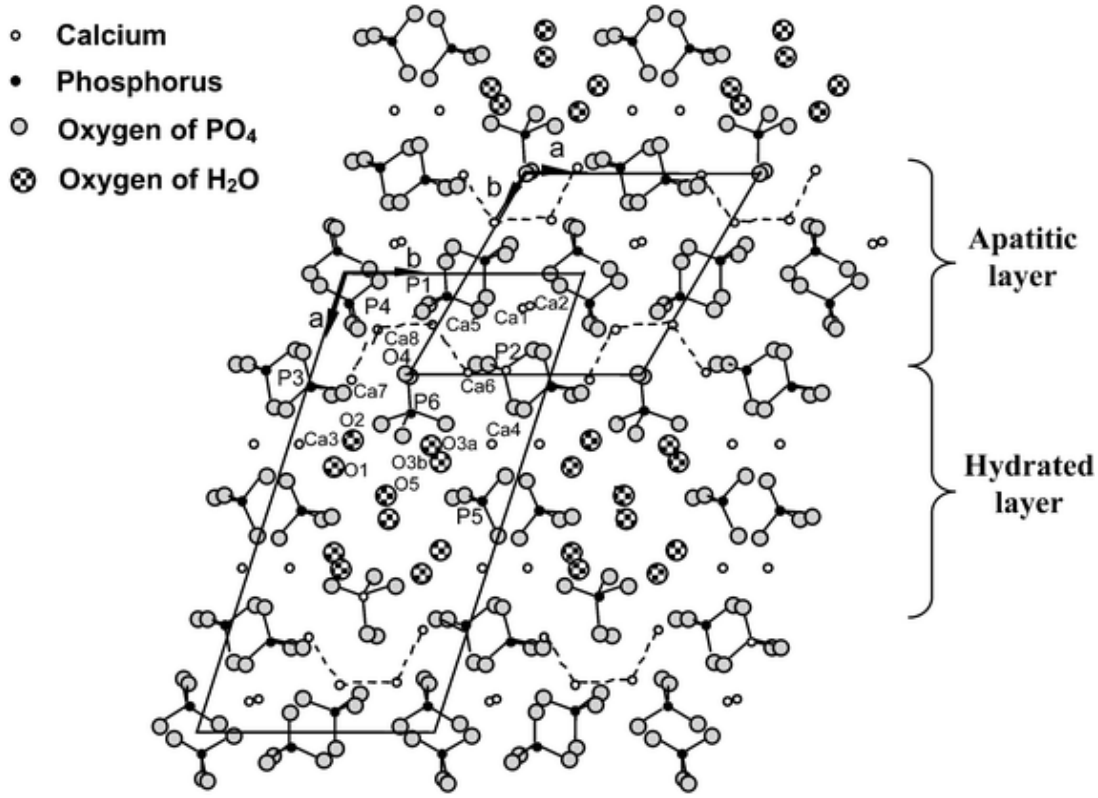

Figure 3 Crystal structure of octacalcium phosphate (Cazalbou et al., 2004)

2.1.3.1 Structure

OCP has a triclinic lattice, space group *P*1 and unit cell *a* = 19.692(4), *b* = 9.523(2), *c* = 6.835(2) Å and α = 90.15(2), β = 92.54(2) and γ = 108.25(1)°

(Mathew et al., 1988). The asymmetric unit (the largest structural unit in where none of the atoms are related through symmetry) is $Ca_8H_2(PO_4)_6.5H_2O$, there are two asymmetric units per unit cell. The OCP structure consists of two 'layers' being the '*apatite'* layer and '*water'* layer. The 'apatite' layer is approximately 1.1 nm thick and is alternating with the 'water' layers (sometimes referred to as 'hydrated' layer) which are approximately 0.8 nm thick parallel to (100) and are a clear feature of the OCP structure (Elliott, 1994).

The 'apatite' like layer provides an explanation for the similarities seen in the lattice parameters of OCP and hydroxyapatite (*a* = 9.4176, and *c* = 6.8814 Å). This 'apatite' layer is made of alternating sheets of phosphate ions with Ca^{2+} ions. The water layer consists of phosphate ions more widely spaced than the apatite layer and Ca^{2+} ions with a slightly variable amount of water molecules between them. The constituent ions in the OCP structure are distributed between these two layers differently. Six Ca^{2+} ions and two of the six phosphates are located in the apatite layer. The 'water' layer is made of two Ca^{2+} ions and a single phosphate ion. This leaves three phosphate ions which are located in the junction between the apatite' and water layers. Two of the phosphate ions are protonated, the phosphate ion in the water layer and one of the phosphate ions located at the inter layer junction (Elliott, 1994).

2.1.3.2 Hydrolysis and Role in Calcium Phosphate Chemistry

There are two reactions that contribute to the hydrolysis transformation of OCP to hydroxyapatite:

$$Ca_8(HPO_4)_2(PO_4)_4.5H_2O + 2Ca^{2+} \Rightarrow Ca_{10}(PO_4)_6(OH)_2 + 3H_2O + 4H^+$$

$$1.25Ca_8(HPO_4)_2(PO_4)_4.5H_2O \Rightarrow Ca_{10}(PO_4)_6(OH)_2 + 1.5H_3PO_4 + 4.25H_2O$$

The reaction of hydroxyapatite formation from OCP has been studied using a number of techniques. Single crystal X-ray diffraction and polarized light microscopy showed that during the phase transformation of OCP to hydroxyapatite, pseudomorphs of OCP were produced (Elliott, 1994). The pseudomorphs properties approached those of hydroxyapatite as the reaction progressed. It is believed that the reaction from OCP to hydroxyapatite occurs through crystal transition rather than dissolution and reprecipitation. This idea is supported by a number of studies showing intercrystalline mixtures of OCP and hydroxyapatite. A crystal of partly hydrolysed OCP when studied on XRD gave the pattern of OCP and hydroxyapatite with the *b*- and *c*- axis collinear (Elliott, 1994). This suggests an intercrystalline mixture of the two crystals given the similarity in their crystal structure. High-resolution electron microscopy studies were performed on partially and fully hydrolysed OCP crystals (Nelson and Mclean, 1984). Partially hydrolysed OCP crystals showed periodic contrast variations that had a periodicity of 16.5 Å. This was interpreted as regions of OCP that had lost water causing a 2.4 Å contraction of the *a*-axis parameter. The fully hydrolysed OCP crystals contained similar contrast variations surrounded by apatite. This evidence supports the idea the calcium-deficient hydroxyapatite is a mixture of OCP and hydroxyapatite, rather than a separate crystal phase itself. This is again supported by ^1H MAS-NMR performed on a calcium-deficient hydroxyapatite with a Ca/P = 1.50 which showed equal amounts of HPO_4^{2-} and OH^- present the sample (Elliott, 1994).

Orientation growth of OCP on an ion selective membrane was performed. The system used consisted of three chambers, the central chamber was formed by a cation and anion selective membrane 2 mm apart. The central chamber was kept at a constant by pH-stat controlled addition of acid or base. Various concentrations of calcium and phosphate solutions were pumped through the outer chambers. When the pH of the central chamber was 7.4 and calcium and phosphate concentrations of 12 and 7.2 mmol l^{-1} respectively were used then well crystalline ribbons of OCP grew. These ribbons grew along their *c*-axis and were perpendicular to the membrane inner surface. Identification was performed using XRD and SEM. It was shown that addition of Ca^{2+} ions caused these ribbons to transform over 7 days to well-orientated hydroxyapatite (Moriwaki Y, 1983). This supports the idea that OCP is the intermediate in biological apatite formation as it shows that OCP formed in an ordered structure would remain in this orientation during transformation to apatite. This fits with the strong and defined orientation seen in biological apatite making up bones and teeth.

The effect of other ions on the hydrolysis of OCP to hydroxyapatite has been studied also. Carbonate ions have been shown to decrease the rate of transformation, these are also retained into the final apatite structure giving a carbonated apatite. The amount of carbonate incorporated has been shown to depend upon which alkali carbonate is used to donate the carbonate to the reaction (Elliott, 1994). Another study measuring the transformation of OCP using SEM and IR spectroscopy showed that Mg^{2+}, citrate and pyrophosphate ions inhibit the transition (Sharma et al., 1992). The same

study also showed that F^-, CO_3^{2-}, HPO_4^{2-}, and Ca^{2+} ions facilitated OCP to apatite transformation. Other factors shown to influence this reaction are solution pH, ionic concentrations and OCP crystal size (Elliott, 1994).

The effect of fluoride is believed to be due to the fluoride inducing the formation of fluorapatite which has greater stability than hydroxyapatite which creates a larger driving force for the formation of fluorapatite over hydroxyapatite and at a faster rate (Elliott, 1994). Heat and fluoride ions were shown to accelerate the transformation of OCP to hydroxyapatite at 40°C and 0.01% NaF respectively, these conditions increased the rate considerably (Elliott, 1994). Very interestingly addition of fluoride to reaction conditions which have been shown to form OCP showed formation of fluorapatite directly (Shiwaku et al., 2010a, Shiwaku et al., 2010b, Muragalelli et al., 1992).

2.1.3.3 Identification

Infrared and Raman Spectroscopy

A study synthesized OCP using a method originally produced by LeGeros et al (Legeros, 1985), with modification to the method by Tomazic et al (Tomazic et al., 1989). The authors produced two forms of OCP which they refer to as polymorphs. Form A is the directly synthesized OCP whereas form B is a version of form A that has been exposed to water. This is probably not two polymorphs of OCP and is perhaps rather a calcium-deficient apatite consisting of intercrystalline mixtures of OCP and hydroxyapatite. As is shown above OCP is easily hydrolysed to

hydroxyapatite in the presence of water and the difference in the specimen could be explained by this (Fowler et al., 1993).

Table 2 IR and Raman Peak Positions of Octacalcium Phosphate. [a] Infrared band positions for A form and B form OCP at 48 °C and wavenumber differences between forms (A-B). [b] Raman band positions for excitation with 488.0-nm radiation a t low (L), medium (M), and high (H) power levels (L = 50-85 mW; M = 175-200 mW, H = 350-400 mW) and wavenumber differences between excitation at high and low powers (H - L) where discernible. The spectrum has a broad unresolved water band that extends from about 3700 to about 2000 cm^{-1}. [d] Very broad weak band. [e] Center of 1048 and 1052cm^{-1} doublet. [f] From average of 360 and 345 cm^{-1} bands. NM = not measured, w = weak, mw = medium to weak, m = medium, s = strong, v = very, sh = shoulder, b = broad. (Fowler et al., 1993)

infrared[a]			Raman[b]				
A form	B form	Δ cm^{-1} (A – B)	H	L	M	Δ cm^{-1} (H – L)	assignment
	~3600 vvw, sh						ν_3, ν_1 stretch of H-bonded H_2O, HPO_4 (OH stretch)
~3555 m, b	3525 m						
	~3300 m, b		NM[c]	NM[c]	NM[c]		
~2950 m, b	~3090 m, b						
~2400 vw, b	~2440 vw, b						HPO_4(6) (OH stretch)
1629 w	1642 w	−13	NM[d]	NM[d]	~1630 vw, b		ν_2 H_2O bend
~1298 vw	1295 w	+3					HPO_4(6) (OH in-plane bend)
1207 w	1193 w	+14					HPO_4(5) (OH in-plane bend)
1138 vw, sh	~1137 vvw, sh	+1					ν_3 HPO_4 stretch
1118 s	1121 s	−3					ν_3 HPO_4(6) stretch
1109 s	1103 s	+6	~1105 vw	~1112 w	~1109 vw	−7	ν_3 HPO_4(5) stretch
1093 s							
1086 s	1077 s	+9	1084 vw	1079 vw	1079 vw	+5	ν_3 HPO_4, ν_3 PO_4 stretch
				~1052 w	~1052 vw		
						1050[e] w	
1056 s	1055 s	+1					
			~1048 w	1048 w			ν_3 PO_4 stretch
1038 s	1037 s	+1	1036 w	~1036 vw	1036 vw		
1023 s	1023 s	0	~1025 vw	~1027 vw	~1025 vw		
	~1000 vvw, sh		1008 m	1011 m	1010 m	−3	ν_1 HPO_4 stretch
				~1005 w, sh	~1005 w, sh		
967 w			967 vs	966 s	966 s	+1	ν_1 PO_4 stretch
963 w	962 w	+1	956 vs	959 vs	957 vs	−3	
913 w	917 w	−4	913 w	916 w	916 w	−3	HPO_4(6) [P–(OH)] stretch
873 w	861 w	+12	884 w	874 w	879 w	+10	HPO_4(5) [P–(OH)] stretch
~650 vw, b			~630 vw	~631 vw	~630 vw		H_2O libration
627 vw	627 vw	0					H_2O(4) libration
608 vvw, sh			617 vw, sh	619 vw, sh	618 vw, sh	−2	ν_4 PO_4 bend
599 m	601 m	−2	606 mw	609 mw	609 mw	−3	
578 w	575 w	+3	588 m	591 m	591 m	−3	ν_4 PO_4, ν_4 HPO_4 bend
			578 m	577 m	578 m	+1	
561 m	560 m	+1					ν_4 PO_4 bend
			~556 vw, b		~556 vw, b		
529 w	524 w	+5	533 w, b	523 w, b	527 w, b	+10	ν_4 HPO_4 bend
465 vw	466 vw	−1	449 m	451 m	450 m	−2	ν_2 PO_4 bend
			426 m	427 m	426 m	−1	
445 vw	449 vw	−4					H_2O libration
			~413 m, sh	409 m	413 m, sh	+4	ν_2 HPO_4 bend
			371 w	353 w	356 w	+18	ν_2 HPO_4(5) bend
	360 w						
337 m	~345 w	~−15[f]					Ca–H_2O translation

In infrared experiments on the OCP there are a number of bands that allow the differentiation of OCP from apatite. The peaks that refer to HPO_4 groups can be used to distinguish between OCP and apatite. The bands at 3300, 2950, 1298, 1207, 1138, 1207, 1138, 1118, 1109, 1086, 913, and 873 cm^{-1} can be used to identify OCP in IR measurements. For Raman spectroscopy bands at 1112, 1079, 1052, 1011, 1005, 916, and 874 cm^{-1} can be used.

NMR spectroscopy

^{1}H MAS-NMR performed at 500 MHz and a spinning speed of 7.8 kHz showed the presence of a chemical shift at 13 ppm referenced to trimethyl silane and this was assigned to an acidic proton of a HPO_4^{2-} ion located in the junction between the apatite and 'water' layers. The other HPO_4^{2-} located in the water layer was not found, the failure to find a clearly resolved resonance was attributed to positional disorder of this ion and overlap with resonances with the structural water found in OCP. Chemical shift at 1.1 and 1.5 ppm were detected and were assigned to protons on an isolated water molecule found in the OCP water layer. At 5.5 ppm there was an intense spinning sideband pattern that was assigned to relatively immobile structural water groups. The intensity of this resonance was attributed to a more mobile water species either in the OCP water layer or on the OCP surface. ^{1}H MAS-NMR studies performed on thermally dehydrated OCP (a process known to induce OCP to hydroxyapatite transformation) gave a resonance at 0.2 ppm which was attribute to the OH^- found in hydroxyapatite. This was attributed to as evidence of the theory that the structural water in OCP can relocated themselves to a nearby PO_4^{3-} ion to form HPO_4^{2-} and OH^- in a dehydration reaction of OCP to form hydroxyapatite (Elliott, 1994).

A ^{31}P MAS-NMR study performed on OCP (121.5 MHz, spinning speed 6 kHz) prepared through a reaction of sodium phosphate monobasic dihydrate ($H_2NaPO_4.2H_2O$) and calcium nitrate tetrahydrate $Ca(NO_3)_2.4H_2O$. The OCP sample gave four resonances relative to 85% H_3PO_4 at -0.2, 2.0, 3.3 and 3.7 ppm with an approximate intensity ratio of 3:1:1:1 respectively. The authors were able to distinguish where the different phosphate groups appeared on

the MAS-NMR spectra. The resonance at -0.2 ppm was assigned to P5 and P6; the resonance at 2.0 ppm was P3; 3.3 ppm was P2 and P4; lastly 3.7 ppm was attributed to P1. Phosphates labelled P1-4 are the PO_4^{3-} ions in the OCP structure and P5 & P6 are the HPO_4^{2-} ions (Tsai et al., 2010, Tseng et al., 2004, Davies et al., 2012).

X-ray Diffraction

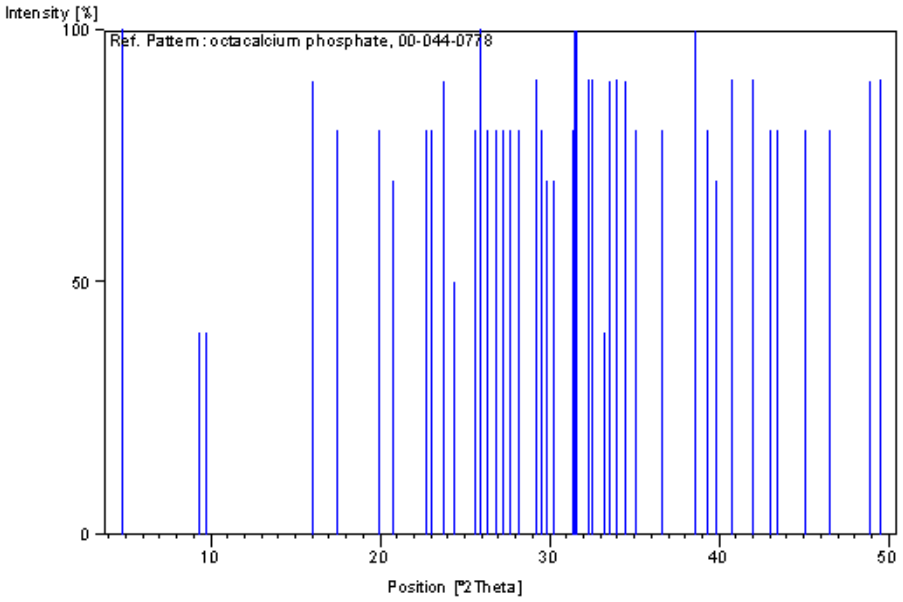

Figure 4 XRD Reference Pattern and Relative Intensities of Octacalcium Phosphate ICSD reference code 00-044-0778

The above figure 2 shows the reference XRD pattern of OCP. Given the similarities between the pattern for OCP and apatite the only diffraction line where OCP can be distinguished from apatite is the diffraction line at 4.7˚ 2θ, which in highly crystalline OCP will give an intense diffraction line.

2.1.4 Brushite

Brushite or dicalcium phosphate dihydrate (DCPD) has a formula of $CaHPO_4.2H_2O$. Brushite was discovered in 1865 in phosphatic guano in the Caribbean. Brushite typically occurs in rock formations and encrusted on

ancient bones, dental calculus and pathological calcifications (Walther et al., 1996). It is proposed that Brushite is an intermediate for apatite formation indeed if Brushite is placed into a pH solution outside of its solubility range then apatite will form (Elliott, 1994).

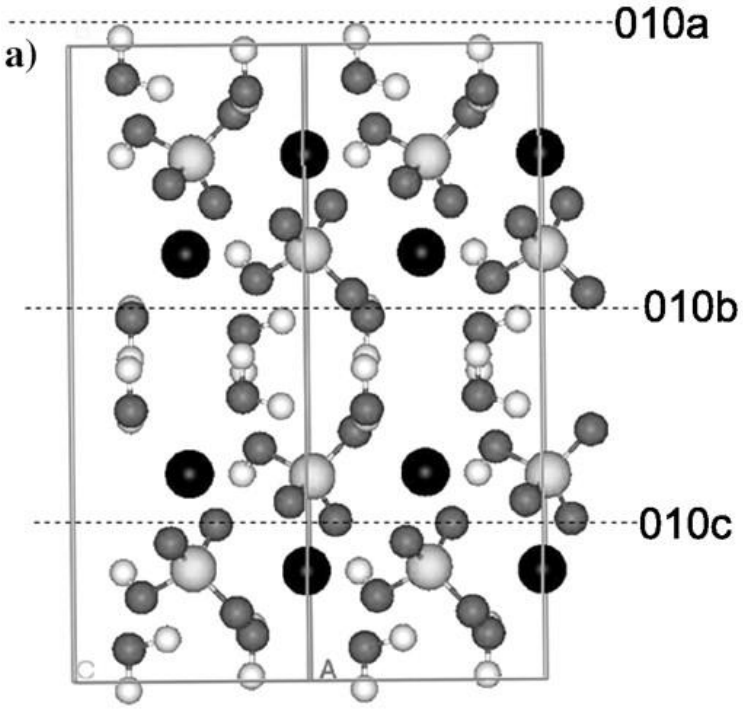

Figure 5 Crystal structure of DCPD; Black sphere = calcium, light grey sphere = phosphorus, dark grey sphere = oxygen, white sphere = hydrogen (Sainz-Diaz et al., 2004)

2.1.4.1 Structure

DCPD is monoclinic, space group *Ia* with lattice parameters *a* = 5.812±0.002, *b* = 15.180±0.003, *c* = 6.239±0.002 Å and β = 116° 25±2'. Four formula units are present per unit cell with an asymmetric unit $CaHPO_4.2H_2O$, none of the 5 hydrogen atoms are related by symmetry (Curry and Jones, 1971). The structure of DCPD consists of columns that are parallel to the short diagonal of the (010) face of the unit cell, of alternating Ca^{2+} and PO_4^{3-} ions. The columns are joined together to form corrugated sheets, a conspicuous

feature of the structure. The sheets have the composition of $CaHPO_4$ and are linked together by water molecules (Gashti et al., 2013). Similarly structured sheets are also notably found in the structure of $Ca(H_2PO_4)_2.H_2O$ (Elliott, 1994).

2.1.4.2 Hydrolysis and Role in Calcium Phosphate Chemistry

Hydrolysis of DCPD will ultimately lead to formation of hydroxyapatite, however, unlike the structural relationship between OCP and hydroxyapatite, DCPD is not a pseudomorph of apatite (Elliott, 1994). Where the transformation from OCP to hydroxyapatite goes via a phase transition the single crystal unit is altered chemically to give the formula of hydroxyapatite. In DCPD to apatite transformation the route of formation is through dissolution of DCPD then precipitation of hydroxyapatite which can go via OCP as an intermediate depending upon reaction conditions.

DCPD will transform to OCP if in a solution with a pH range 6.2 – 7.4 and at a temperature within 25 – 37 °C (Tung et al., 1985). If reaction conditions have a higher pH or temperature than this then it is believed the apatite will precipitate directly. The reason for this is that the precipitation and growth rate of hydroxyapatite is slow if the pH or temperature is not high; this is in contrast to OCP which has a lower solubility than DCPD and will form readily in mild conditions. The formation of apatite from DCPD has been shown to be inhibited by addition of Mg^{2+} and pyrophosphate ion (Rowles, 1968). Addition of F^- ions during hydrolysis will cause the direct precipitation of either pure fluorapatite or fluorohydroxyapatite even at conditions where

without fluoride OCP would form as an intermediary for hydroxyapatite formation (Tung et al., 1985, Chow and Brown, 1973) (White et al., 1988).

2.1.4.3 Identification

IR and Raman

Below are the IR and Raman frequencies for DCPD. DCPD can be distinguished from its bands at 875 cm^{-1} (IR) and 880 cm^{-1} (Raman), which are P-O(H) stretching.

Table 3 IR and Raman Peak Positions of DCPD (Elliott, 1994). a vw, very weak; w, weak; m, medium; s, strong; vs, very strong; br, broad; sh, shoulder

IR	Raman	Assignments
3547 s		
3492 s		O–H Stretching of water
3295 s		
3171 s		
2964 sh		O–H Stretching
2386 w		$2 \times 1218 = 2436$
2270 vw		$1218 + 1066 = 2284$
2128 vw		$2 \times 1066 = 2132$
1720 sh		$2 \times 875 = 1750$
1651 s		H_2O Bending
1218 s		O–H In-plane bending
1141 s	1119 w	
	1083 m	
1066 s	1060 m	PO Stretching
1006 sh		
998 s	998 vs	
875 s	880 m	P–O(H) Stretching
795 s	784 w, br	H_2O Libration
665 m		
578 s	588 m	
530 s	525 m	PO Bending
	414 m	
	383 m	H_2O Translation
	323 w	PO Bending
	280 w	
	209 m	
	179 w	Lattice vibration
	144 m	
	112 w	

NMR spectroscopy

^{31}P MAS-NMR (2 kHz, spinning speed) ^{1}H decoupled at 68 MHz studies performed on DCPD samples have shown a resonance at 1.7 ppm relative to 85% H_3PO_4. ^{1}H MAS-NMR studies have shown resonances at 6.4 and 10.4 ppm referenced to trimethyl silane which were attributed to structural water and acidic protons respectively. This was performed at both 200 and 500 MHz with a spinning speed up to 8 kHz (Miquel et al., 1990).

X-ray Diffraction

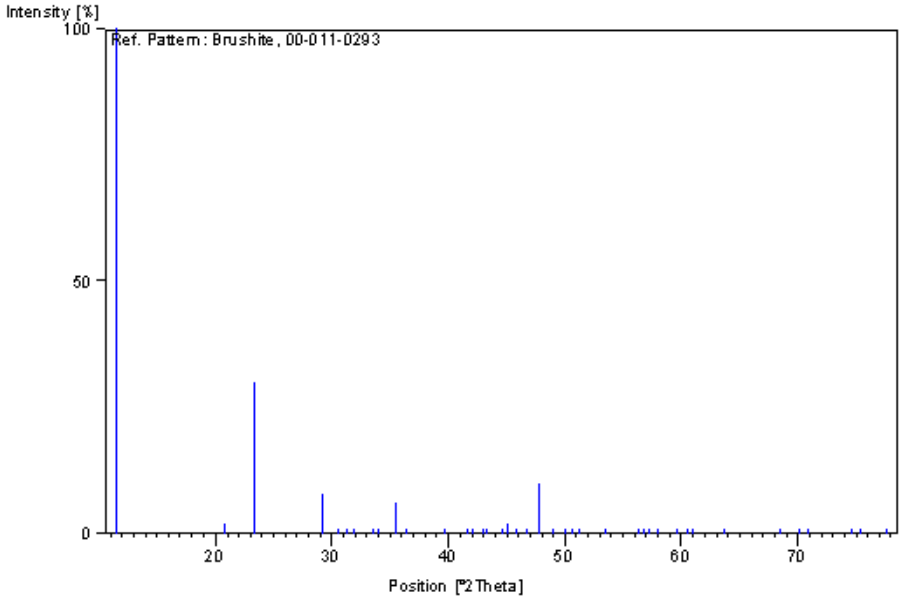

Figure 6 XRD pattern and Relative Intensities of DCPD

In order to distinguish DCPD from apatite and OCP the peak at 11.607˚ 2θ can be used to distinguish, as apatite does not possess a diffraction line at this angle.

2.2 Nucleation Theory

Nucleation is the localized formation of a thermodynamic system. In this project nucleation theory is specifically applied to the nucleation of crystalline

phases. There exist two mechanisms of nucleation, homogeneous and heterogeneous nucleation. This is an important process involved in the setting of calcium phosphate cements. Traditionally calcium phosphate cements form their cement phases (apatite or DCPD) via homogeneous nucleation. However examples exist where cement systems have been seeded with hydroxyapatite crystals in order to facilitate heterogeneous nucleation and shorten setting times.

Nucleation theory has also been applied to explaining fracture mechanics of ceramic systems. Griffith suggested that the thermodynamics associated with nucleation could also be applied in the formation of cracks from defects in ceramics (Griffith, 1921). The formation of the crack (or surface) requires energy to form the new surface (interfacial energy). Another application of nucleation theory is in formation of glass-ceramics where crystalline phases can form within an amorphous glass phases. Understanding nucleation theory is essentially important in understanding the reaction mechanism for many cement systems as it can play a large role in understanding the reaction mechanism. It can also aid in the tailoring of setting times and compressive strengths, important factors when developing a cement for commercial use.

2.2.1 Homogeneous Nucleation

Homogeneous nucleation is the spontaneous formation of a new thermodynamic system within the interior of a uniform system. This nucleation is then the formation of an interface at the boundaries of a new phase. Supersaturation is the driving force for nucleation (Abraham, 1968).

Supersaturation occurs when the pressure in the newly formed solid is less than the liquid pressure, and brings about a change in free energy per unit volume, G_V , between the liquid and newly created solid phase. The change in free energy is balanced by the energy released through the creation of the new phase (volume free energy), and the energy required to form a new interface (interfacial energy). If the overall change in free energy, ΔG, is negative, nucleation is favoured.

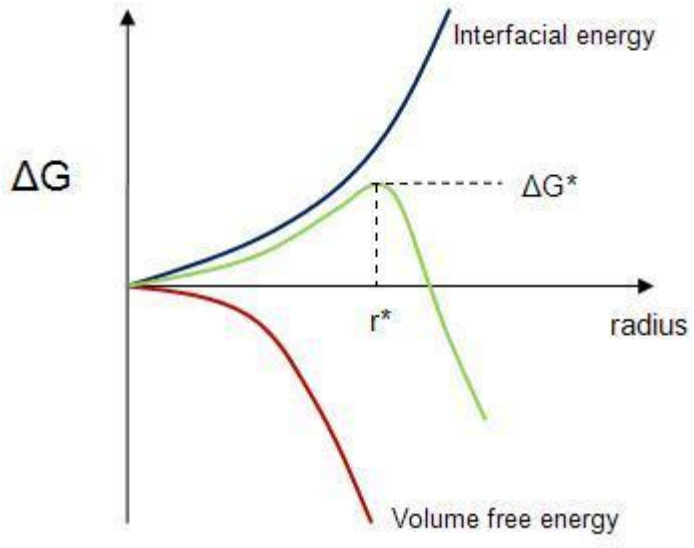

Figure 7 the change in free energy resulting from the formation of a spherical nuclei of solid in a liquid. (Hacker)

Energy is consumed to form an interface; the exact energy required depends upon the surface energy of each phase. Nuclei are measured in terms of their radius. It is only when nuclei are larger than the critical radius (r^*) that they are stable and nucleation and potential growth proceed. If hypothetical nuclei form that are smaller than the critical radius then the energy released by forming its volume is less than the energy required to form its surface. If this occurs then nucleation will not proceed. If the radius of the nuclei is

larger than the r^* then nucleation proceeds because the net ΔG is negative meaning the nucleation is thermodynamically favoured (Oxtoby, 1998).

If a spherical nuclei of particles is forming then $-G_v$ Joules cm^{-3} of energy is liberated during formation, energy is required to form the surface interface, which is G_s Joules cm^{-2}. The energy to form a spherical cluster of a new phase of a specific radius r is equal to:

(1) $$\Delta G = -\frac{4}{3}\pi r^3 G_v + 4\pi r^2 G_s$$

Where

G_v = Energy of formation

G_s = Interfacial energy

ΔG = Net free energy

If the radius of the nuclei is $<r^*$ then the overall ΔG increases when adding molecules or atoms to the nuclei until the r* is reached at which point the $\Delta G<\Delta G^*$. The addition of further atoms or molecules to the nuclei gives an overall release of energy, favouring the growth of the nuclei.

(2) $$r^* = -\frac{2G_s}{G_v}$$

To equate the maximum free energy change for the formation of a nuclei at the critical radius (ΔG_r^*), the expression below defines the relationship of the interfacial energy and free energy per unit volume.

(3) $$\Delta G_r^* = \frac{16\pi(\Delta G_s)^3}{3(\Delta G_v)^2}$$

The formation of nuclei involves the addition of atoms or molecules and if this process involves energy then the likelihood of this occurring is low. Considering the entropy of the solid-liquid interface, the following expression can be formed on the basis of the rate of nuclei formed by recognizing this event as an activated process:

(4) $$n_{r^*} = n \exp\left(\frac{-\Delta G_r^*}{kT}\right)$$

Where:

n_r^* = number of nuclei per unit volume

n = number of atoms or molecules per unit cell

k = Boltzmann's constant

T = Absolute temperature

When the nuclei radius is $\geq r^*$ then addition of further molecules or atoms to the nuclei means energy available for work (ΔG) is released, rather than is used. At this point the rate of growth is not limited by nucleation but instead limited by diffusion of particles to the nuclei. An additional element to nucleation is then the rate at which atoms are attached to the nucleus. An atom or molecule at the liquid-solution interface must acquire an activation energy (ΔG_a) in order to join the nuclei. The probability of this occurring is defined by the expression:

(5) $$P = v_o \exp\left(\frac{-\Delta G_a}{kT}\right)$$

Where:

P = Probability

V_o = Vibrational frequency of an atom attempting to cross nuclei-liquid boundary

Combining the previous two equations the rate of homogeneous nucleation is expressed as:

(6) $$I = nv_o \exp\left[-\left(\frac{N\Delta G_r^* + \Delta G_a}{RT}\right)\right]$$

Where:

N = Avogadro's number

R = Universal gas constant

The equation presented above calculates the rate of nucleation at differing temperatures. The nucleation rate describes a nucleus being formed (ΔG_r^*) and its rate of growth determined by the rate of atom attachment (ΔG_a) at the nuclei-liquid interface (Abraham, 1968).

2.2.2 Heterogeneous Nucleation

Heterogeneous nucleation is nucleation that occurs at phase boundaries or on impurities with the system. It requires less energy to occur than homogeneous nucleation due to the ΔG_a being lower because the surface energy barrier is lower. Heterogeneous nucleation may be either intrinsic (occurring within the liquid, for instance on nucleating agent) or extrinsic (liquid surface). Heterogeneous nucleation has a lower free energy barrier than homogeneous nucleation; this then makes it more likely to occur. A heterogeneous nucleus is a spherical cap which has a lower free energy barrier to formation than a nucleus formed through homogeneous nucleation with equivalent volume (Gao, 2004).

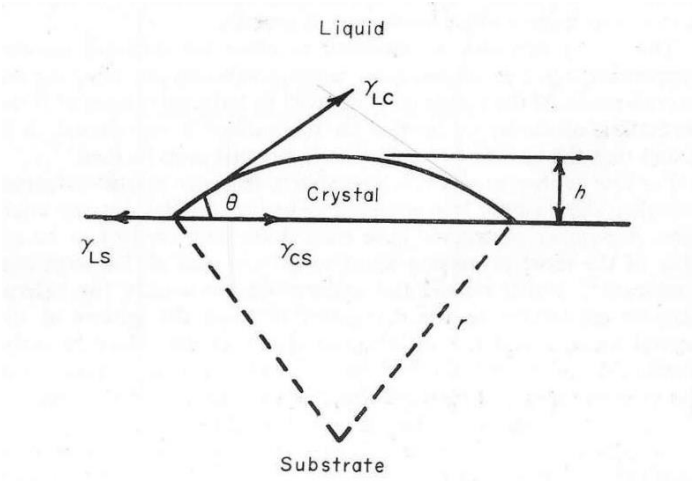

Figure 8 Wetting angle determination of nuclei on a substrate facilitating heterogeneous nucleation. (Chung et al., 2010)

A nuclei forming on a substrate generates two interfacial surface energies. These being substrate-nuclei interfacial energy (ΔG_s^b) and liquid-nuclei interfacial energy (ΔG_s^c). The total surface energy is then expressed as:

(7) $$\Delta G_s = \Delta G_s^b Cos\theta + \Delta G_s^c$$

Where:

θ = Contact angle

ΔG_s = Total interfacial energy

As the contact angle decreases towards zero, the surface energy also decreases. Consequently the barrier to nucleation is reduced (ΔG_r^* decreases). For a contact angle greater than zero, the free energy barrier for nucleation is expressed as:

(8) $$\Delta G^*_{r\,heterogeneous} = \Delta G^*_{r\,homogeneous} f(\theta)$$

Heterogeneous nucleation will only be favourable if $\Delta G_r^*{}_{heterogeneous} < \Delta G_r^*{}_{homogeneous}$. $f(\theta)$ Is a term which represents the strength

of the inter-atomic attraction between the nucleus and the substrate and is measured from the contact angle,θ.

(9) $$f(\theta) = \frac{(2+\cos\theta)(1-\cos\theta)}{4}$$

The total free energy for the formation of a nucleus with the critical radius in a heterogeneous nucleated system is expressed as:

(10) $$\Delta G_r^* = \frac{16\pi(\Delta G_s)^3}{3(\Delta G_v)^2} f(\theta)$$

Regarding the contact angle, (θ), there are four incidences which determine how the substrate-nuclei interaction will determine how the nucleation occurs.

If θ ≥180°, then no wetting of the substrate will occur. In this instance only homogeneous will occur as the spherical cap is now a sphere and not associated with the substrate.

If θ ≥90° to <180°, the contact angle approaches 180° and approaches the Cosθ approaches -1. A reduction in the wetting of the substrate by the nucleus will result in an increase likelihood of homogeneous nucleation.

If θ = 0° to <90, the contact angle approaches 90° then Cosθ approaches 0.the energy barrier of heterogeneous nucleation can be reduced to half that of homogeneous nucleation.

If $\theta = 0°$, then $\cos\theta = 1$. This means the substrate is completely wetted by the nuclei. There is no barrier to nucleation ($\Delta G_r^* = 0$).

2.3 Solubility of Calcium Phosphates in Calcium Phosphate Cements

Phase transition based on dissolution-precipitation reactions are well documented for the setting and hardening of calcium phosphate cements. A requirement for this process to occur is moderate instability i.e. the precursor for the reaction to proceed should be more soluble than the product phase. The monophasic system of the production of calcium deficient hydroxyapatite (CDHA) from α-tricalcium phosphate (α-TCP) is an example of this.

$$3\alpha\text{-}Ca_3(PO_4)_2 \Leftrightarrow 9Ca^{2+} + 6PO_4^{3-}$$

$$Ca_9(HPO_4)(PO_4)_5(OH) \Leftrightarrow 9Ca^{2+} + 6PO_4^{3-} + H_2O$$

$$3\alpha\text{-}Ca_3(PO_4)_2 \Rightarrow Ca_9(HPO_4)(PO_4)_5(OH)$$

Since at physiological pH CDHA is the less soluble than α-TCP (Ishikawa, 2010), CDHA is the more thermodynamically stable phase and thus its formation is favoured. When α-TCP is placed into solution it will partly dissolve in order to reach equilibrium. Ca^{2+} and PO_4^{3-} will be released into solution from dissolution of α-TCP. These ions will precipitate to CDHA as it is the most thermodynamically stable phase. This then encourages continual dissolution of the α-TCP and precipitation of CDHA. The dissolution-precipitation then continues until the α-TCP has completely dissolved and the CDHA has formed completely. The crystals are interlocked forming a hard, set cement.

Figure 6 (below) shows solubility of a range of calcium phosphates at a range of pH's at ambient temperature. The diagram indicates that hydroxyapatite is the least soluble phase in the wide pH range so generally its formation is favoured thermodynamically. The diagram indicates the role the pH plays in determining which phases form. Other factors will also play a role in determining the phases that form namely stoichiometry and temperature of formation.

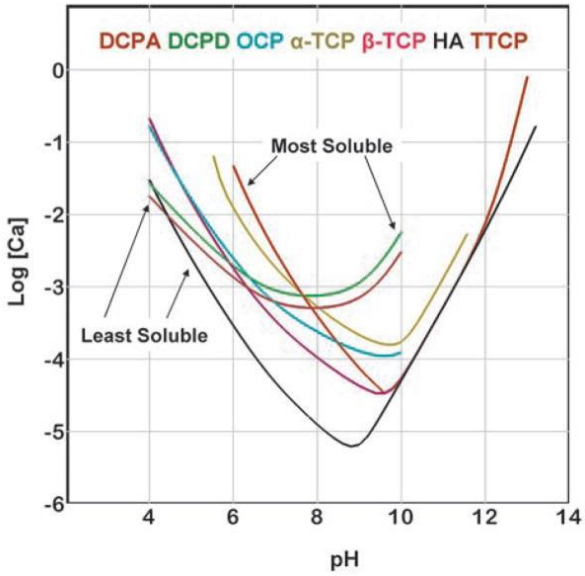

Figure 9 Solubility phase diagram of various calcium phosphate phases at pH range 2-14. (Chow, 2009)

Table 4 Calcium phosphate salts with formulas, calcium to phosphate ratio (Ca/P), and respective abbreviations listed. Ksp = Solubility constant (Chow, 2009)

Compound	Abbreviation	Formula	Ca/P Ratio	Ksp.
Monocalcium Phosphate Monohydrate	MCPM	$Ca(H_2PO_4)_2.H_2O$	0.50	Highly soluble
Monocalcium Phosphate Anhydrous	MCPA	$Ca(H_2PO_4)_2$	0.50	Highly soluble
Dicalcium Phosphate Dihydrate / DCPD	DCPD	$CaHPO_4.2H_2O$	1.0	$10^{-6.59}$
Dicalcium Phosphate Anhydrous / Monetite	DCPA	$CaHPO_4$	1.0	$10^{-6.90}$

α-Tricalcium Phosphate	α-TCP	α-$Ca_3(PO4)_2$	1.50	$10^{-25.5}$
β-Tricalcium Phosphate	β-TCP	β -$Ca_3(PO_4)_2$	1.50	$10^{-28.9}$
Amorphous Calcium Phosphate	ACP	$Ca_xH_y(PO_4)_z$.nH2O	1.20-2.20	$10^{-25.2}$ – $10^{-24.8}$
Tetracalcium Phosphate	TTCP	$Ca_4(PO_4)_2O$	2.00	10^{-38}
Hydroxyapatite	HAP	$Ca_{10}(PO_4)_6(OH)_2$	1.67	$10^{-116.8}$
Octacalcium Phosphate	OCP	$Ca_8(HPO_4)_2(PO_4)_4$	1.33	$10^{-96.6}$

2.4 Calcium Phosphate Cements

2.4.1 Calcium Phosphate Cements: History

The first published data on calcium phosphate biomaterials was in 1920 by (Albee, 1920), who first developed the concept of using these materials for medicinal applications and provided the basis for what has been developed since. The research conducted used what the authors describe as “triple calcium phosphate”, using this to promote bone growth at a fracture site comparing their results to a control. The authors injected triple calcium phosphate into the gap formed in the occurrence of a bone fracturing in canine cranial defects. The results showed that addition of triple calcium phosphate showed a faster bone growth and union compared to a control where no triple calcium phosphate was used. Query remains as to what specifically was used in this study as the solution injected was described as “5 % triple calcium phosphate suspension in distilled water”. (Chow, 2009) points out that it is unclear whether the calcium phosphate used was “precipitated or ceramic material and whether it was powder or granular form”. Regardless of this criticism of the lack of specificity on the authors’ behalf, in its very fundamentals this paper demonstrated that a material containing calcium and phosphate will promote and improve the healing of

fractures and so must take premier position in the origins of calcium phosphate biomaterials in orthopaedic medicine.

It was not until 1951 when the next noticeable step in this field occurred; Ray and Ward (Ray and Ward, 1951) investigated granular synthetic hydroxyapatite and its effectiveness at repairing defects in the long bones of dogs and the crania of cats. The authors created defects surgically in the bones then inserted the granular synthetic hydroxyapatite and compared the results to those obtained from autogenous bone grafts. The results from this study showed that while the granular synthetic hydroxyapatite was replaced by bone it was slower at doing so than autogenous bone grafts.

Koester et al (1976) produced 7 calcium phosphate ceramic formulations and tested their bioresorbability in the fibula of dogs. After 6 months they showed that their formulations had been replaced by bone tissue, thus demonstrating the ability of these materials to be implanted, integrate and eventually be replaced by bone. They also noted that for biocompatibility a Ca/P ratio in the material had to be between 2:1 and 4:1, and that the optimum was 3:1.

The idea for the first calcium phosphate cement was proposed by LeGeros in 1982. In the first patent on calcium phosphate cements tetracalcium phosphate (TTCP) and dicalcium phosphate anhydrous (DCPA) (or dicalcium phosphate di-hydrous (DCPD) were used as initial reagents. The authors discovered that leaving these mixtures in test tubes led to a ‘hard’ deposit after a few hours. These compounds are more soluble at neutral pH than hydroxyapatite (Hwang et al., 1986) and when mixed with water produce HA. As a consequence of this discovery various animal studies were

conducted (Costantino et al., 1992, Friedman et al., 1991, Costantino et al., 1991) which demonstrated precipitation of nano-crystalline HAP in these compositions. On implantation highly biocompatible HA was readily replaced by new bone. This cement composition using TTCP and DCPA (or DCPD) was approved by the FDA in 1996 and became the first commercial calcium phosphate cement.

2.4.2 Applications and Formulations

2.4.2.1 Orthopaedic Applications

These cements have varied medicinal applications and are specifically useful in orthopaedic medicine due to the compositional similarity to bone. They are implanted into bone in many procedures, they are used in skeletal fractures, hip replacements, vertebroplasty, kyphoplasty and in other corrective and restorative orthopaedic procedures.

Vertebroplasty and kyphoplasty were introduced in 1987 and are minimally invasive surgical procedures designed to reduced pain of those afflicted which is conducted on the vertebrae in the treatment of osteoporosis-induced vertebral compression fractures (McGirt et al., 2009). The two procedures differ slightly in their methodology, Vertebroplasty involves injecting the cement into the compressed vertebrae to stabilise the site and prevent further damage and hopefully decrease the pain to the patient. Kyphoplasty involves inserting a balloon, inflating this balloon then filling the cavity produced with the cement, this is a corrective surgery designed to repair the site of vertebral collapse (Lewis, 2006).

There is also an application of calcium phosphate cements in treating common fractures. While it may not be worthwhile in small fractures because of the risks/benefits associated with the surgery, due to their properties these cements would be very useful when the fracture site is large or if metallic implants are used as the use of cements has been shown to speed up the healing process by increasing the rate at which new bone is formed (Aberg et al., 2012). This would be hugely popular with patients as it could potentially speed up the recovery time from these fractures meaning that the patient could be mobile more quickly allowing a faster return to regular physical condition.

2.4.2.2 Dental Applications

Alveolar ridge preservation is a surgical procedure in which a bone graft material is placed in the alveolar socket of tooth at the time of extraction to preserve the alveolar ridge from its physiologic resorption. Among the numerous available filling materials used to prevent alveolar ridge resorption, allografts and xenografts are limited because of problems of supply and risks of cross contamination. To overcome these limits, many synthetic bone substitutes have been proposed foremost amongst these are calcium phosphate materials.

Calcium phosphate materials offer great potential for bone regeneration since they have a chemical composition close to the biological apatite of bone tissue. They are biocompatible and the ability to act as a substrate for bone growth makes them a favourable material for use in dentistry. The rationale behind their use in socket filling procedures is that they will prevent

the physiological resorption of the alveolar crest after tooth extraction. Because of its osteoconductive properties, a calcium phosphate based biomaterial will enhance the growth of blood vessels and proliferation of bone cells within the material, thereby promoting biomaterial resorption and subsequent replacement by new bone. Their efficiency as bone substitute materials has already been proven in different human applications including the alveolar ridge preservation and the bone regeneration around defects in dental implants usually in combination with barrier membranes (Guided Bone Regeneration).

Guided bone regeneration (GBR) has been combined with dental implants to encourage bone regeneration and enhance osseointegration. It is based on the concept that by using barrier membranes it is possible to separate the bone from the soft tissues and at the same time create the space into which new bone can grow. The use of an osteoconductive graft material, such as calcium phosphate based material, when combined with GBR at the time of implant placement may enhance the potential for complete bone regeneration and osseointegration. At present, guided bone regeneration is basically applied in the oral cavity to support new bone tissue growth on alveolar ridge to allow stable placement of dental implants.

Currently one option available when filling the alveolar socket or undertaking guided bone regeneration for fixation of an implant is granular calcium phosphate ceramic materials. These materials are typically hydroxyapatite ($Ca_{10}(PO_4)(OH)_2$) or tricalcium phosphate ($Ca_3(PO_4)_2$) or biphasic mixtures of both. These materials have been used successfully offering an

osteoconductive and somewhat resorbable bone substitute material. Their disadvantages however are:

1. Deformation of Implantation Site – Granules by their nature have no inherent bulk strength until they have been fully osseointegrated, which can take weeks to occur. Until this point they can easily be deformed by the application of pressure and force upon them. This could cause the formation of voids in the material and a modification in shape where the new bone forms.

2. Migration from Implantation Site – Similarly to the potential for deformation of the implant site there is also, for the same reason, potential for migration of the granules from the implantation site. During healing, displacement of graft material can lead to incorrect or incomplete guided bone regeneration.

3. Difficult Preparation – Granular bone substitutes are typically mixed with patients' blood or saline solution prior to implantation. The surgical time is lengthened by the need to extract or collect the patients' blood and this method does not give replicable results.

4. Low Resorption Rate – In some clinical situations it is desirable that after use of a bone substitute material rapid resorption and replacement with host bone occur. This facilitates a return to normal bone structure and typical load distribution ensuring healthy bone quality and appearance. As hydroxyapatite is a stable crystalline phase resorption is strictly cell mediated

which can take many years to complete, or in some instances may never occur.

All of these problems lead to unnecessary discomfort for the patient, difficulty for the clinician, lengthening of surgical time and compromised in-vivo performance. There is a clear need for a novel material to address these problems.

2.4.2.3 Typical Formulations

The field of calcium phosphate cements (CPC) appears a comprehensively studied field with most or all combinations of calcium and phosphate containing salt having been prepared and tested, leading to a recent review on these materials stating "…every possible combination of the cement formulation has already been tested…". As example of this the interested reader is referred to a paper published (Driessens et al., 1993) where the authors produced 108 different combinations of numerous calcium phosphate salts in order to measure their setting times.

In the almost three decades since the first calcium phosphate cement was developed numerous research groups have produced many different types of CaP cement which form a wide range of cement phases. There are two classes of CPC's which exist, Apatite and DCPD cements.

Table 5 Commercial compositions of calcium phosphate cements (Bohner et al., 2005)

Company	Cement /name	Components	End Product
ETEX	a-BSM	Powder: ACP (50%), DCPD (50%); Solution: H_2O (unbuffered saline solution)	Apatite
	Embarc		
	Biobon		
Stryker-Leibinger Corp	BoneSource	Powder: TetCP (73%), DCPD (27%); Solution H_2O, Na_2HPO_4, NaH_2PO_4	Apatite
	HydroSet		

Teknimed	Cementek	Powder: a-TCP, TetCP, Na Glycerophosphate; Solution: H_2O, $Ca(OH)_2$, H_3PO_4	Apatite
	Cementek LV	Powder: a-TCP, TetCP, Na Glycerophosphate, dimethylsiloxane; Solution: H_2O, $Ca(OH)_2$, H_3PO_4	
Biomet	Calcibon	Powder: a-TCP (61%), DCP (26%), CaCO3 (10%), HAP (3%); Solution: H_2O, Na_2HPO_4	Apatite
	Mimix	Powder: TetCP, a-TCP, $C_6H_5O_7Na.2H_2O$	
Mitsubishi materials	Biopex	Powder: a-TCP, TetCP, DCPD, HAP, $Mg_3(PO_4)_2$, $NaHSO_3$; Solution: H_2O, sodium succinate, sodium chondroitin sulphate	Apatite
	Biopex-R	Powder: a-TCP (75%), TetCP (18%), DCPD (5%), HA (2%); Solution: H_2O, sodium succinate, sodium chondroitin sulphate	
Kyphon	KyphOs	Powder: a-TCP (77%), $Mg_3(PO_4)_2$ (14%), $MgHPO_4$ (4.8%), $SrCO_3$ (3.6%); Solution: H_2O $(NH_4)_2HPO_4$	Apatite
Shanghai Rebone Biomaterials Co, Ltd	Rebone	Powder: TetCP, DCPD; Solution: H2O	Apatite
Synthes-Norian	Norian SRS	Powder: a-TCP (85%), $CaCO_3$ (12%), MCPM (3%); Solution: H_2O, Na_2HPO4	Apatite
	Norian CRS		
Kasios	Eurobone	Powder: b-TCP (98%), $Na_4P_2O_7$ (2%); Solution: H_2O, H_3PO_4, H_2SO_4	DCPD
Synthes	ChronOs inject	Powder: b-TCP, MCPM, $MgHPO_4.3H_2O$, $Na_2H_2P_2O_7$; Solution: NaH_2PO_4, H_2O, sodium hyaluronate	DCPD

DCPD and apatite cements both have excellent biocompatibility (Elliott, 1994) and have excellent potential for their common applications. DCPD cements have a higher rate of resorbability, which is believed to be due to DCPD being more soluble than CDHA and HA (Dorozhkin, 2008) and in fact DCPD cements have been shown to resorb faster than apatite cements (Klein et al., 1985, Liu et al., 1999, Apelt et al., 2004), as a consequence of this DCPD cements suffer from a rapid decrease in strength, though overall strength of implanted bone increases due to bone ingrowth (Nishimura et al., 1991).

Apatite cements do have better ‘material’ properties than DCPD cements, for instance DCPD cements have considerably short setting times (~30 s) (Mirtchi et al., 1991, Mirtchi et al., 1989) compared to apatite cements (10 min). The extremely short setting times is a considerable disadvantage as in order for these materials to be used clinically then the surgeon must be allowed sufficient time for the paste to be loaded into the implantation device

and implanted before the material sets. Various attempts have be used to lengthen the setting times of DCPD cements firstly via using less soluble reactants, addition of pyrophosphates which have been shown to inhibit setting. An attempt has been tried to where the cement is frozen during storage and delivery (Grover et al., 2008).

Another potential disadvantage of DCPD cements is that inflammation has been seen in certain conditions (Tamimi et al., 2012). In some instances DCPD cements have been shown to convert to apatite *in vivo (Dorozhkin, 2008).* While on the face of it this does not seem a large problem given the biocompatibility of apatite, the crystal growth associated with this reaction has been shown to cause tissue damage and inflammation, to address this issue magnesium is added to some formulations which acts as an inhibitor to apatite formation. Another cause of tissue inflammation associated with DCPD cements is potentially when too much DCPD is present in the cement mixture (Apelt et al., 2004, Grover et al., 2003, Flautre et al., 1999) causing inflammation for the initial implantation period, due to the acidity associated with DCPD.

It cannot be ignored that apatite cements have wider clinical use than DCPD cements. Currently there are 18 different formulations (Bohner et al., 2005) of apatite cements available compared to 3 DCPD cements formulations (Tamimi et al., 2012). Given the similar biological properties these cements share why are there so many more apatite cements than DCPD cements? Especially given the considerable advantage DCPD cements have in being resorbed faster than apatite cements. In his review (Dorozhkin, 2008)

suggests that ultimately the reason for this imbalance was due to simply that apatite cements were developed before DCPD cements. While there perhaps is some truth in this it is possibly a little simplistic. This is due to a number of reasons including the number of additives required to simply match the properties of apatite cements, the poor strength of DCPD cements, and the greater amount of research which has gone into apatite cement development along with the fact that apatite cements were developed first.

2.4.3 Chemistry of Setting in Calcium Phosphate Cements

2.4.3.1 Hydroxyapatite Cement

Hydroxyapatite cements represent the most common and widely used commercially group of CPC's. There are a number of different types within this one group but all have their formula based on that of apatite $Ca_{10}(PO_4)_6(OH)_2$.

Introduction: HAP cements were the first composition developed by Brown and Chow in 1986 and the setting reaction is listed below.

Setting reaction*:* The very basic setting reaction for the formation of HAP cement is listed below:

$$10Ca^{2+} + 6PO_4^{3-} + 2OH^- \rightarrow Ca_{10}(PO_4)_6(OH)_2$$

This is a very simplified reaction, but it highlights which ions are required for HAP formation. Obviously there must be a source of Ca^{2+} and PO_4^{3-} ions which are traditionally delivered in the form of various calcium phosphate salts. This reaction also highlights the requirement for OH^- ions which

suggests the importance of a high pH (at least above pH 7) to provide a source of hydroxyl ions during the setting reaction.

$$CaHPO_4 + Ca_4(PO_4)_2O \rightarrow Ca_5(PO_4)_3OH$$ (Fukase et al., 1990)

The above reaction is a reaction between tetracalcium phosphate (TTCP, $Ca_4(PO_4)_2O$) and dicalcium phosphate anhydrous (DCPA, $CaHPO_4$). The authors confirmed using XRD that the reaction is 100% complete (i.e. 100% apatite formation) after 4 hours. The compressive strength also reached a maximum (36 ±0.3 MPa) at 4 hours, demonstrating compressive strength is proportionally related to the completion of the reaction. Though the formation of poorly crystalline HAP was shown, further studies revealed that this setting reaction eventually goes to calcium deficient hydroxyapatite ($Ca_{10-x}(HPO_4)_x(PO_4)_{6-x}(OH)_{2-x}.nH_2O$,CDHA) (Ishikawa et al., 1999) initially formed HAP acts as a nucleus for CDHA. A further study suggests that the HAP formed in the initial setting reaction reacts with excess DCPA to form CDHA (TenHuisen and Brown, 1994). Because of this it may be the case that in actual fact no cement systems exist which actually form stoichiometrically pure Hydroxyapatite free from substitutions at all, it appears after conducting a literature review no hydroxyapatite forming cements have been found.

2.4.3.2 Calcium-deficient Hydroxyapatite Cement

CDHA cements are perhaps the most common form of apatite cements. It is believed the CDHA is formed via the intermediate phase of OCP meaning OCP forms first and then rapidly transforms to CDHA. Bones and teeth mostly consist of CDHA which is what contributes to the excellent osteo- and bio- compatibility.

Given the vast amount of publications where the cement phase is CDHA there is an equally large range of reactions where it is formed.

$3Ca_3(PO_4)_2 + H_2O \rightarrow Ca_9(HPO_4)(PO_4)_5OH$ (Monma and Kanazawa, 2000, Fernandez et al., 1996, Gbureck et al., 2004b, Bohner et al., 2006, Brunner et al., 2007, Alves et al., 2008, Jack et al., 2008, Gbureck et al., 2004a, Gbureck et al., 2003)

$Ca_xH_y(PO_4)_z.nH_2O + H_2O \rightarrow Ca_{10-x}(HPO_4)_x(PO_4)_{6-}x(OH)_{2-x} + nH_2O$ (Knaack et al., 1998, Tofighi et al., 2000)

$3Ca_4(PO_4)_2O + 3H_2O \rightarrow Ca_9(HPO_4)(PO_4)_5OH$ (TenHuisen and Brown, 1998)

The reactions stated above also require a phosphate solution to react or to speed up their reaction; because of this many formulations require either NaH_2PO_4, Na_2HPO_4 or H_3PO_4 as part of the liquid phase used to initiate the setting reaction. Most reactions have been shown to happen in one step (see reactions listed above) though it should also be mentioned that CDHA has been found to form via an intermediary phase of DCPD in the cement system involving a reaction between MCPM and CaO.

$$CaO + Ca(H_2PO_4)_2{\cdot}H_2O \rightarrow 2CaHPO_4.2H_2O$$

$$6CaHPO_4.2H_2O + 3CaO \rightarrow Ca_9(HPO_4)(PO_4)_5OH + 2H_2O$$

The first step involves rapid precipitation of DCPD following by further reaction of CaO with the DCPD to form the CDHA.

2.4.3.3 Carbonated Apatite Cements

Carbonatapatite ($Ca_{8.8}(HPO_4)_{0.7}(PO_4)_{4.5}(CO_3)_{0.7}(OH)_{1.3}$) is a form of apatite which is substituted by carbonate groups.

Setting reaction:

$$5.2CaHPO_4.2H_2O + 3.6CaCO_3 \rightarrow Ca_{8.8}(HPO_4)_{0.7}(PO_4)_{4.5}(CO_3)_{0.7}(OH)_{1.3}$$

Two commercial cement samples are examples of these types of cements Biocement D® and Norian SRS® (Fernandez et al., 1999b, Constantz et al., 1995) (see table 5) it has been shown that these two commercial samples are formed via a two-step process. The first step involves precipitation of DCPD which then further reacts to form carbonated apatite (Boudeville et al., 1999).

$$\alpha\text{-}Ca_3(PO_4)_2 + Ca(H_2PO_4)_2.H_2O + 7H_2O \rightarrow 4CaHPO_4.2H_2O$$

$$5.2CaHPO_4.2H_2O + 3.6CaCO_3 \rightarrow Ca_{8.8}(HPO_4)_{0.7}(PO_4)_{4.5}(CO_3)_{0.7}(OH)_{1.3} + 2.9CO_2 + 12H_2O$$

In the first reaction DCPD forms rapidly. Subsequent the pH drop increases the $CaCO_3$ dissolution which then initiates the second reaction to form the carbonated apatite. The second reaction is slower than the first.

2.4.3.4 Brushite (DCPD) Cements

DCPD cements were discovered and developed after the discovery of apatite cements in 1987 by two independent research groups Mirtchi and Lemaitre (Mirtchi et al., 1990) and also Bajpai et al. (1991). The first DCPD cements were prepared by mixing together MCPM and β-TCP, then adding water. The resulting paste was shown to set in an exothermic reaction over time to give a hard cement material consisting of DCPD, known as the mineral Brushite.

Setting reaction*:* There are a number of different reactions to form DCPD cements, listed below is a selection of these.

$$Ca_4(PO_4)_2O + 2H_3PO_4 + 7H_2O \rightarrow 4\ CaHPO_4.2H_2O$$

$$\beta\text{-}Ca_3(PO_4)_2 + H_3PO_4 + 6H_2O \rightarrow 3\ CaHPO_4.2H_2O$$

$$\beta\text{-}Ca_3(PO_4)_2 + Ca(H_2PO_4)_2 \rightarrow 4CaHPO_4.2H_2O$$

$$\beta\text{-}Ca_3(PO_4)_2 + Ca(H_2PO_4)_2.H_2O \rightarrow 4CaHPO_4.2H_2O$$

The setting mechanism for DCPD cements involves 4 steps: (1) the constituents of the cement starting material powder dissolve in water; (2) the dissolved ions form a super-saturated gel; (3) nucleation of DCPD crystals occurs within the gel phase; (4) crystal growth from the nucleated small crystals, these crystals interlock giving a hard set cement (Tamimi et al., 2012). DCPD can only precipitate at a pH <6 due to its solubility at higher pH. DCPD cement pastes must be acidic during setting therefore an acidic component must be incorporated into the starting materials for DCPD cements. The DCPD cement system using the reactants β-TCP and MCPM has had the pH studied over the course of setting, initially the MCPM starts to dissolve which causes a rapid decrease in pH to 2.5 (Bohner and Gbureck, 2008, Bohner et al., 1997) and then pH increases during the setting reaction to pH 5. The pH in the cement system can be altered (pH 2.5-6) by using different ratios of each of the starting materials; if more MCPM is used the pH will remain low even after setting has completed whereas if excessive β-TCP is used the pH can be almost neutral at pH 6 (Bohner et al., 1997).

In another DCPD cement reaction MPCM was replaced with orthophosphoric acid. The advantages of this system over the β-TCP/MCPM system are (1) good control over reactivity and composition; (2) Faster preparation; (3) longer setting times and higher tensile strengths; it should be pointed out however that because orthophosphoric acid is more acidic than the MCPM it replaces, the pH of the cement drops dramatically to 2.5 and stays at this level even after setting and therefore there are concerns that the lower pH

may give problems relating to the biocompatibility (i.e. inflammation) (Bohner et al., 1997).

Thermochemical studies have been performed on the setting reaction of DCPD cements. In the MCPM cement system, after mixing with water the MCPM hydrolysis is an endothermic reaction (ΔH= 23.0 kJ mol^{-1}) to form phosphate and calcium ions (Bohner and Gbureck, 2008).

$$Ca(H_2PO_4)_2.H_2O \rightarrow Ca^{2+} + 2H_2PO_4^- + H_2O$$

At the same time as the previous reaction is taking place the β-TCP dissolves after exposure to protons in an exothermic reaction (ΔH= -66.0 kJ mol^{-1}) to also produce form dihydrogen phosphate and calcium ions (Bohner and Gbureck, 2008).

$$\beta\text{-}Ca_3(PO_4)_2 + 4H^+ \rightarrow 3Ca^{2+} + 2H_2PO_4^-$$

The exothermic (ΔH= -10.0 kJ mol-1) precipitation of DCPD then occurs which causes a jump in pH (Bohner and Gbureck, 2008, Nurit et al., 2002).

$$Ca^{2+} + 2H_2PO_4^- + 2H_2O \rightarrow CaHPO_4.H_2O + H^+$$

The overall reaction is thus exothermic (ΔH= -83kJ mol^{-1}) which is why these cements warm up when setting.

$$\beta\text{-}Ca_3(PO_4)_2 + Ca(H_2PO_4)_2.H_2O + 3H_2O \rightarrow 4CaHPO_4.H_2O$$

DCPD or Brushite has been found to transform into CDHA (Xie et al., 2001), about which it has been hypothesised that this can cause tissue inflammation potentially caused by either crystal growth or orthophosphoric acid release caused by the transformation reaction. The reaction is caused by dissolution of the DCPD which the precipitates to CDHA (Xie et al., 2001).

$$(10\text{-}x)CaHPO_4.2H_2O \rightarrow Ca_{10-x}(HPO_4)_x(PO_4)_{6-x}(OH)_{2-x} + (4\text{-}x)H_3PO_4 + (18\text{-}x)H_2O$$

To avoid the aforementioned side effects two available solutions were suggested. (1) To introduce excess β-$Ca_3(PO_4)_2$ which could react with the orthophosphoric acid released thus limiting damage to tissue (Grover et al., 2003); and (2) to add magnesium ions to the formulation which have been shown to inhibit apatite precipitation (Bohner, 2000, Bohner, 2001).

At of the time of writing there are currently 3 different commercial DCPD cements which are listed in table 5. From looking at the commercial examples of DCPD cements it can be seen that all three have an acidic phase (PA or MCPM) and all use β-TCP in their preparation. The addition of the acidic phase is explained by the need for an acidic environment for DCPD to precipitate. The addition of these acidic starting materials provides the acidic setting medium which causes DCPD to be the most favourable product to precipitate. The use of β-TCP in all three commercial samples appears less clear as it has be shown that β-TCP is not essential for the formation of DCPD and there are many examples of DCPD cement reactions which do not involve β-TCP, so why is β-TCP used in all the preparations? The explanation of this is simply the production of β-TCP is the cheapest out of all the possible alternatives (TTCP, ACP and α-TCP) to manufacture, TTCP has a highly energy demanding route of synthesis (Moseke and Gbureck, 2010) and α-TCP can be produced in a similar method to β-TCP the only difference being α-TCP requires a higher temperature for synthesis (Cicek et al., 2011).

2.4.4 Effects of particle size upon calcium phosphate cement setting

Monophasic systems are relatively simple systems to document and study. Apatite cements involving the reactions of two or more calcium phosphate salts in the setting reaction is a more complicated system. The relative solubility's of the different salts used as well as their respective particle sizes will affect both the dissolution and precipitation of the cement phase. The first calcium phosphate cement was prepared via a reaction between Monetite ($CaHPO_4$, DCPA) and tetracalcium phosphate ($Ca_4(PO_4)_2O$, TTCP). In essence the dissolution-precipitation method for cement formation is the same as with the setting reaction of α-TCP. The TTCP and DCPA both dissolve releasing Ca^{2+} and PO_4^{3-} ions, which then precipitate to CDHA, the most thermodynamically favourable phase in this system at physiological pH. For optimal cement properties (compressive strength and setting times) the particle sizes of the two salts in this instance must be carefully considered. TTCP is more soluble than DCPA and thus will release its ions in their respective ratios in a different rate than DCPA. The results of alterations in particle size are listed in table 6. For optimal results the TTCP must have a larger particle size than the DCPD, then complete dissolution of both precursors will take place and the CDHA will precipitate.

Table 6 Effects of particle size upon compressive strength of calcium phosphate cement formed through the reaction of tetracalcium phosphate and dicalcium phosphate anhydrous (Ishikawa, 2008)

Average particle diameter (μm)		**Ratio of the average particle diameter of TTCP/DCP**	**Compressive Strength (MPa)**
TTCP	**DCPA**		
1.6	11.9	0.13	0 (no setting)

12.4	11.9	1.04	7.1 ± 1.0
1.6	0.9	1.78	21.8 ± 4.4
12.4	0.9	13.78	51.0 ± 4.5

Table 6 above demonstrates the importance of particle size in biphasic system. TTCP is a more soluble salt at physiological pH than DCPA, therefore when the particles are small for TTCP and large for DCPA no setting was achieved because of an imbalance of the dissolution of the two phases. Optimal compressive strength was observed when the particle size of the TTCP was large and DCPA was small. In this case the two phases dissolved at similar rates allowing similar dissolution profiles for both salts meaning they dissolved and apatite precipitated at a constant rate.

2.4.5 Substitution in Calcium Phosphate Cements

2.4.5.1 Fluoride

Fluoride-substituted apatite cements form fluorapatite, which has novel advantages and applications. Hydroxyapatite cements resorb gradually under cell-mediated acidic conditions and are replaced by host bone. This ability has been seen as a key attribute contributing to their use as bone filling materials. However, there are applications where materials which are biocompatible and osteoconductive but not bioresorbable would be advantageous. This could potentially be accomplished by producing apatite cements with a range of resorption rates. Apatite cements which are more stable under acidic conditions would be capable of achieving this given the mechanism of cement resorption. It should be noted DCPD cements are more stable than apatite cements under acid pH but they are converted to

apatite under physiological conditions *in situ.* Therefore, CPC's which have little or no solubility under acidic conditions would be ideal. Partially or fully fluoride substituted apatites have been demonstrated to have considerably lower solubility in acids than hydroxyapatite (Takagi et al., 1998). So fluorapatite forming cements would be anticipated to show decreased resorption rates compared to apatite (HA, CDHA) cements.

As of the time of writing two fluorapatite cements systems have been described in the literature (Wei et al., 2011, Takagi et al., 2010), The first system was a reaction between TTCP and DCPA with a solution of 2 M H_3PO_4 also containing 3 concentrations of HF as a source of fluoride with a L/P = 0.5 (ml/g). The cement mixtures with the three fluoride concentrations 0.2%, 2.0% and 4% were prepared. A control with no fluoride was also produced. The method used to identify fluorapatite was by dissolving prepared samples in $HClO_4$ and then analysing for fluoride ions using a fluoride-ion selective electrode. The study confirmed fluoride was present and the amounts were proportional to the percentage substitutions (0.2, 2 and 4%). This study also performed *in vivo* rat studies using these cements, the results were very encouraging. The control cement was found to have 'significantly resorbed'; the 0.2% sample was shown to have considerably less resorption than the control; the 2% cement only showed 'slight resorption'; and the 4% cement showed 'no resorption'. This study then demonstrated the hypothesis of decreased resorption of FAP cement to be correct.

A second study on fluorapatite cement involved a reaction between TTCP and NaF powders with a liquid phase of 17% (v/v) H_3PO_4.

$$5Ca_5(PO_4)_2O + 2H_3PO_4 + 4NaF \rightarrow 2Ca_{10}(PO_4)_6F_2$$

The authors (Takagi et al., 2010, Wei et al., 2011) used the cement to fill carious cavities. The method the authors used to determine that they had formed fluorapatite was by performing FTIR and looking for an absence of OH bands at 3571cm^{-1} and 632cm^{-1} (OH Stretch). The authors performed cytotoxicity studies on the produced cements and found no significant difference between the FAP cement and the non-fluoride containing control on the cell density which allowed them to conclude that these cements are not cytotoxic.

A big criticism of these studies is in the methods they use to identify the formation of fluorapatite, it is very difficult to confirm the presence of fluorapatite as XRD and FTIR which are the most common techniques used to identify phases in CPC's will not differentiate between HAP and FAP. The method of identification used in the second study mentioned give extremely uncertain results, the OH band in the apatite that appear on the FTIR spectra is not a sharp band and so using this data to conclude that FAP had formed is not done with a high degree of confidence. A considerably better way of showing fluorapatite formation would be using ^{19}F MAS-NMR, which would indicate the various fluoride containing phases within the cement sample and is perhaps the only method FAP can be identified with a high degree of confidence.

2.4.5.2 Strontium

Addition of strontium can be very beneficial for calcium phosphate cements and could potentially allow CPC's to be used to treat osteoporosis. Osteoporosis is a metabolic disease which causes decreased bone mass resulting in decreased bone strength and increased risk of fracture (Mallette et al., 1989, Sandhu and Hampson, 2011). The consequences of this for an individual suffering from osteoporosis is an increase in disability and mortality and generally causes a difficulty in performing normal daily duties. Current treatments for osteoporosis included selective oestrogen receptor modulators and strontium ranelate (Burlet and Reginster, 2006). Strontium ions have been shown to stimulate the cell replication of preosteoblasts which ultimately increase the rate of new bone formation, it has also been shown to decrease bone resorption by inhibiting osteoclast differentiation and activity (Marie et al., 2001, Grynpas et al., 1996, Canalis et al., 1996).

Strontium has also been shown to be radio-opaque, a study conducted in 2010 (Romieu et al., 2010) attempted to establish whether strontium-substituted cement would produce radio-opaque cements. The authors produced a strontium-substituted cement from 6DCPD + 2.5CaO + 1.5$SrCO_3$, the resulting cement was then assessed for radiopacity and it was concluded that strontium addition improved the visibility of the cement in X-rays. This would be highly beneficial as currently CPC's are difficult to see in X-rays. Cements which are more radiopaque would be more easily tracked for their resorption and replacement by bone.

To date a number of attempts at strontium substitution have been done. Addition of strontium has been achieved via three routes (i) addition of soluble strontium salts to the liquid phase used to begin the cement reaction; (ii) producing strontium substituted salts as the powder starting materials; (iii) strontium is added as a separate powder phase (e.g. $SrCO_3$ or $SrHPO_4$).

Two routes used where strontium salts were introduced into the powder mixtures used strontium hydrogen phosphate (Guo et al., 2008, Guo et al., 2005) and strontium carbonate (Boudeville et al., 2010). Both systems were designed to produce strontium-substituted apatite (Sr-HA). The study using strontium carbonate found addition of strontium caused a decrease in the reaction rate, as without strontium X-ray diffraction showed the starting materials (DCPD + CaO) disappeared after 2 hours whereas with the introduction of strontium carbonate the $SrCO_3$ was still present after 4 weeks and not found after 3 months. The authors did however conclude that the developed cement does have potential for clinical use as they produced a cement with an optimal setting time of 15 min, a compressive strength of ~20 MPa after 1 day, and confirmed that the strontium did become part of the apatite structure. When $SrHPO_4$ was used as the powder phase the authors used DCPA and TTCP with 0.5M PA (phosphoric acid) as the liquid phase and then added various amounts of $SrHPO_4$ to give 0%, 5%, and 10% substitution. The authors found strontium can actually increase the compressive strength at an optimum degree of substitution. 5% Sr substitution consistently gave higher compressive strengths, at 5 days the 0% Substitution had a compressive strength ~50 MPa whereas the 5% had

an compressive strength of ~63 MPa. It should also be noted that 10% substitution had a negative effect on compressive strengths when compared with the 0% substitution. The production of a Strontium-substituted DCPD cement was attempted (Alkhraisat et al., 2008) where strontium chloride was added in different amounts to a cement system consisting of β-TCP and DCPD. The authors found using XRD that strontium ions did substitute into the DCPD crystal lattice which caused the lattice to expand. The effect of the strontium on the final setting time is interesting, the authors found that 10% Sr substitution increased the setting time to 8.3 min from 1.3 min in 5% substitution (the authors did not determine setting time of 0%). In apatite cements increased setting time is usually detrimental to the clinical applications of these cements. In DCPD cements a major criticism of them is their very short setting times (30 s). Strontium addition could actually be beneficial in DCPD cements not only for their biological effect of strontium but also for the use in being able to extend the setting times.

In two studies (Yu et al., 2009, Pina et al., 2010) the authors synthesised Strontium-substituted α-TCP, which was used to produce CPC's, interestingly one study produced a DCPD cement and the other an apatite cement. The DCPD cement was formed with the Sr-α-TCP and solutions containing 10 wt.% PEG (poly(ethylene glycol) and 20% wt.% citric acid sol or 0.5 wt.% HMPC (hydroxyl propyl methylcellulose), 10 wt.% PEG and 20 wt.% citric acid. The results showed the mixtures formed DCPD after the initial set which after immersion in SBF for 15 and 30 days formed an apatite phase, addition of strontium increased the setting time from 3 ±0.5 min with

no substitution to 7 ±0.5 min with strontium substitution. Finally the authors also showed that the strontium substitution of 11.74% increased the compressive strength compared to the non-substituted samples. The authors attribute this to a lower content of DCPD phase present in the Sr containing samples, however, this is perhaps inaccurate and an alternative theory is presented below.

A recent study (Boanini et al., 2010) assessed the effect of strontium ions of the hydrolysis of α-TCP, by immersing α-TCP powder in solution and then introducing strontium via the solution phase by dissolving $SrCl_2$ into the solution at various substitutions (0, 5, 10 and 20%), the authors found that in the 0% substitution CDHA was detected after 2 days (at 30 °C) and the sample was completely CDHA after 3 days, with 5% substitution CDHA was only found after 10 days and in the higher substitutions CDHA was not found after the longest time point the authors attempted (14 days).

2.4.6 Criticisms of the Literature on Calcium Phosphate Cements

2.4.6.1 Immersion media

In the literature there are considerable differences in protocols when producing and analysing calcium phosphate cements. Particularly many different solutions have been used to immerse these cements into including, physiological-like solution (PLS), simulated body fluid (SBF), Tris buffer, and deionised water. The problem with using different solutions is they will have different effects upon the immersed cements. PLS contains phosphate and calcium ions which if compared to a solution without these ions may give different reaction rates for instance addition of these ions may cause the

reaction to reach 100% completion before the same cement in a solution devoid of these ions. SBF has problems which have been outlined a particular problem is presence of Mg^{2+} and Cl^- ions, Mg^{2+} has been shown to inhibit apatite formation (Giocondi et al., 2010). Using deionised water is a problem as immersing the cement may alter the pH of the solution which may affect the rate of reaction completion and this does not adequately match what the cement faces when implanted during use. Ideally a pH ~7.2 buffered solution without other ions present should be used, which is why Tris buffer has been used to immerse the cement in these experiments.

2.4.6.2 Compressive Strength

Compressive strength is a particularly poor technique to analyse these materials, especially for applying the results gained to their application. Firstly the compressive strength is not a particularly useful technique as the flexural strength is a much more useful technique in imitating the forces these materials are under when implanted. Secondly often when making the cement cylinders for testing their compressive strengths the cylinders are manipulated to give artificially higher compressive strengths. This is achieved by loading the cement paste under pressure into the moulds when the cylinders are produced. This produces much denser specimens which as a result have higher compressive strengths compared to samples which are simply pressed into the cylinder by hand. This is not applicable for when they are used clinically because when the surgeon implants the material it is injected into the site without excessive force. Flexural strength matches the real stresses these materials face when they are implanted, though these are rarely published due to poor strengths being achieved (Moreau et al., 2009).

2.4.6.3 Categorisation

There is a strong tendency to categorise these cements into the products they form during their setting reaction (i.e. apatite, DCPD etc.) a tradition that has been carried on in the previous section out of a desire not to stray from convention. The problem with this categorisation is that these materials are strongly related and will each form into each other depending upon reaction conditions. For instance an 'OCP cement' may form OCP initially but will convert to apatite over time in a basic of neural pH. Is the OCP merely a transition stage to apatite formation and it should be called an apatite cement. A 'DCPD cement' placed into neutral or basic pH will convert to apatite and does so in the body causing negative effects. If $Ca_2(H_2PO_4)_2$ is placed into solution it initially dissolves then reprecipitates into $CaHPO_4.2H_2O$ which if with another source of calcium is present will form OCP. Should this be called a DCPD cement due to presence of $CaHPO_4.2H_2O$ in its very early setting reaction.

2.4.6.4 Characterisation

Analysing the phases present in calcium phosphate cements has been typically poorly conducted and inconsistently studied. Typical methods of characterisation of calcium phosphate cements have been done using X-ray diffraction and FTIR. A few studies have used ^{31}P MAS-NMR to characterise cement phase but these are dramatically in the minority (Legrand et al., 2009). The problem with relying predominantly of X-ray diffraction as the primary method of characterising cement phase is that whilst it is a very useful technique it also has several disadvantages. Typically investigators perform XRD measurements with a scanning range beginning above 10 °2θ

because of this octacalcium phosphate, due to its similar XRD pattern to hydroxyapatite is rarely found as a cement phase. In addition to this XRD gives very little information regarding substitutions in apatite meaning it cannot be used on its own to confirm carbonate of fluoride substitutions for instance.

2.5 Bioactive Glass

Bioactive glasses are silicate-based glasses that in contact with physiological fluids form apatite on their surface. The original compositions of bioactive glasses included SiO_2, P_2O_5, CaO, and Na_2O although many other species have been incorporated since including K_2O, SrO, CoO, CaF_2, NaF, ZnO, and MgO amongst others. The glasses have a number of medical uses as they are biocompatible, resorbable and osteoinductive. The advantages of bioactive glasses is their ability to react on their surface rapidly. This enables fast bonding to bone and other body tissues making them an excellent bone-substitute material. The main disadvantages of bioactive glass when used as bone-substitute materials is their poor mechanical properties. This means they are unable to be used for load bearing applications as the tensile bending strength of most compositions range between 40-50 MPa (Hench, 2006). Also the granular nature means implantation can be very invasive compared with an injectable bone substitute. Lastly dissolution of the glass *in vivo* can cause a high pH rise above body pH that causes problems during osseointegration and can lead to voids in the centre of the implant site.

2.5.1 Introduction to Glasses

The first definition of a glass was by Tammann who defined a glass as a vitreous state and regarded it to be an extremely undercooled liquid. Later X-

ray studies allowed the structure of glasses to be determined (Vogel, 1985). Glasses have a random arrangement of atoms lacking in long-range order unlike crystalline materials which have a structure consisting of regular repeating units. Glasses are amorphous (non-crystalline) materials.

The conventional method of producing a glass involves rapidly cooling a liquid at a rate which prevents crystallization of the material. As the fluid material rapidly decreases in temperature the material begins to rapidly increase in viscosity this prevents the glass constituents arranging themselves into a crystalline arrangement. This continues until solidification of the material occurs. Glasses are thermodynamically unstable but are kinetically stable due to a high E_a required for molecular rearrangement (Kohne et al., 2011).

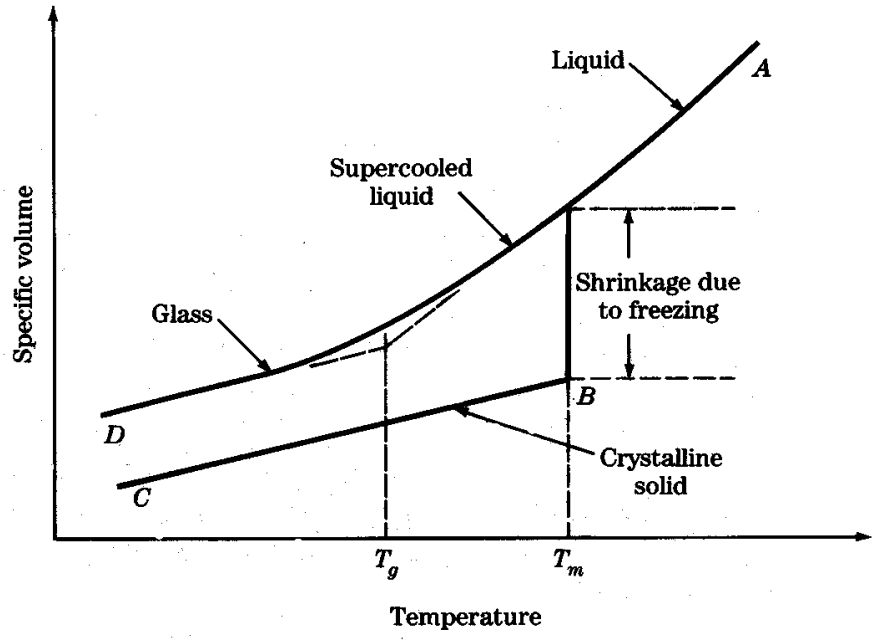

Figure 10 Specific Volume-Temperature graph of glass formation. (Best, 1990)

Figure 7 above shows changes of specific volume (volume/unit mass) that occurs if a molten liquid is cooled from its liquid state to form either a crystalline material or a glass material. In the first instance if the molten liquid is cooled at a low rate then when the material reaches its melting point (point B) it crystallizes. At the melting point there is an abrupt decrease in the specific volume caused by the formation of the crystalline phase.

If that same molten liquid is now instead cooled at a rapid rate below its T_m then there is no abrupt change in the specific volume at any temperature. The change in specific volume instead occurs continuously (point A to D) over a large temperature range and the result of this is that a glass is formed. At the lower temperatures (below T_m) the rate of the change in specific volume is similar in both the formation of either crystalline or glass phases. Although as is visible the magnitude of the difference in specific volume between crystalline and glass is large due to the large decrease in the formation of the crystalline form.

The glass transition temperature (T_g) in silicate glasses is related to the energy required to break and re-form covalent bonds in an amorphous (or random network) lattice of covalent bonds. The T_g is not fixed for all silicate glasses and depends largely upon the composition. A more disrupted glass network causes a decrease in T_g due to fewer covalent bonds in the structure. Addition of network modifiers will cause a more disrupted structure. The charge and size of the network modifying agent will cause different effects on the T_g. Rapid cooling a molten glass mixture below its T_g is essential in glass formation (Holloway, 1973).

2.5.2 Zacharaisen's Random Network Theory

Zachariasen proposed a theory of the network structure of glass in the early 1930's (Zachariasen, 1932, Vogel, 1985). The model proposes the relationship between the structure of the glass and the glass properties. Supported by X-ray diffraction studies this theory provides the basis of understanding glass structure (Zarzycki, 1991). In this model, the internal energy of the amorphous and crystalline phases of the same stoichiometry/composition are assumed to be similar and that the inter-atomic interactions within the amorphous and crystalline are also similar (Ray, 1978).

The polyhedral structure is found in both crystalline and amorphous states of the same material. The random network in the glass is facilitated by the change in both bond length and dihedral angles in the polyhedral (Zarzycki, 1991). This then led Zachariasen to suggest that the structure of a glass is composed of a three dimensional network made of an irregular arrangement. This irregular structure is what differentiates between glass and crystalline materials (Holloway, 1973). The two-dimensional structural differences in amorphous and crystalline SiO_2 based structures are represented below.

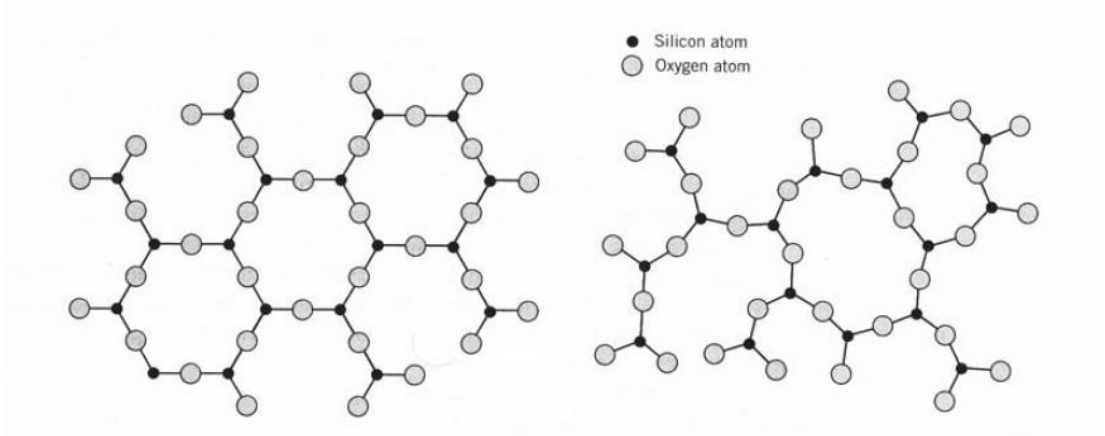

Figure 11 Structural differences of pure SiO_2 in its crystalline (left) and amorphous configuration (right). (Anac, 1992)

In this model it is proposed that the ideal condition for glass formation is when it is formed of structural components which are capable of forming an extended three-dimensional network that does not possess long range order. Zachariasen then proposed four basic rules required for glass formation (Zachariasen, 1932, Vogel, 1985).

- The constituent polyhedra should link together to form a three-dimensional network.
- A network forming cation must have a low-coordination number otherwise there is an increase likelihood of crystallization.
- An oxygen atom may be bonded to no more than two cations.
- The oxygen polyhedra share corners and not faces or edges.

Further to these rules, additional rules were proposed which relate to the formation of low-order three-dimensional networks. Typically those glasses formed of compounds such as SiO_2, P_2O_5, GeO_2 and B_2O_3 (Vogel, 1985).

- A compound tends to form a glass if it has the ability to easily form polyhedral groups of small building units.
- No more than one corner of the constituent polyhedra should be shared.
- Anions in the glass such as O^{2-} should not bind to more than two central atoms of a polyhedron. Therefore, in simple glass anions will form bridges between polyhedra. For example in silicate glasses Si-O-Si bonds will form between SiO_4 tetrahedron.

- The number of corners of the polyhedra making up the structure should be optimally 4 or less and should not exceed 6.
- Three of the corners of each polyhedra must be connected to neighbouring polyhedra.

Addition of oxides such as Na_2O or CaO will cause bridging oxygen atoms between tetrahedra to break to form negatively charge non-bridging oxygen atoms. The oxygen associated with the added oxides will become bound to one of the tetrahedra lacking an oxygen induced by the severing of the Si-O-Si bond between the tetrahedra. The cation will then be bound ionically to the non-bridging oxygen atom. The cation will sit in the cavity formed by the severing of the tetrahedral bond (Vogel, 1985). This is represented in figure 9 below.

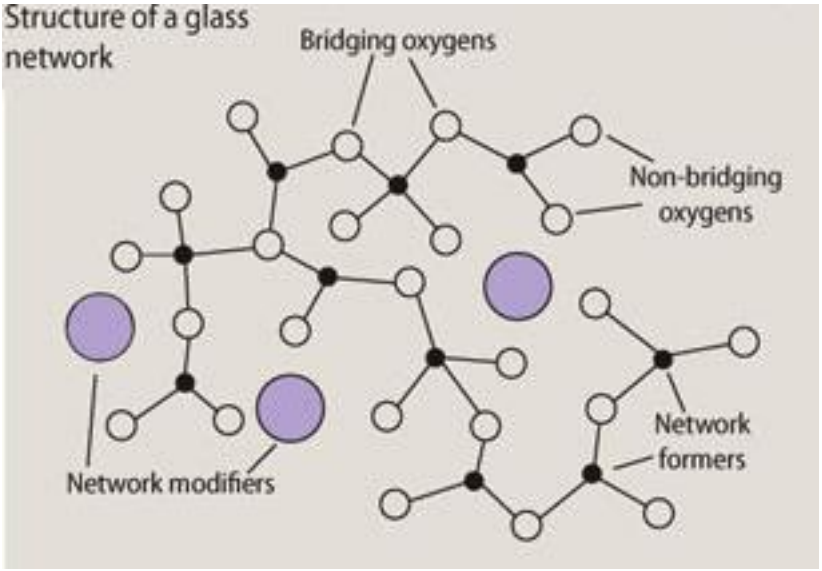

Figure 12 illustration of effect on glass structure of addition of network modifying agents. (Coleman, 2013)

Cations have been classified by the manner in which they affect glass formation and the structure of the glass. These have been classified into

three types network formers, network modifiers and intermediates (Vogel, 1985).

Network Formers, are the backbone of all oxide glasses and are the units which build the three-dimensional networks. For instance, in a pure SiO_2 glass the basic unit is a tetrahedron of a silicon atom surrounded by four bridging oxygen atoms. Network formers typically have a coordination number of 3 or 4, other than Si typical network formers are P, B and Ge. Silicate glasses are three-dimensional structures of tetrahedrons consisting of silicon and oxygen atoms. In a glass consisting of only silica, this is built of SiO_4 tetrahedra, in this structure each silicon atom is covalently bonded to four oxygen atoms which are each bonded to two silicon atoms.

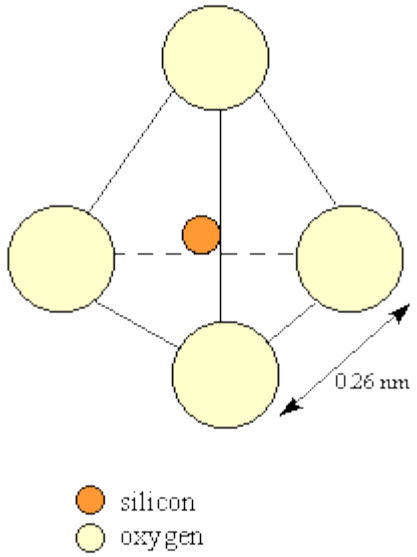

Figure 13 SiO_4 Silica tetrahedron unit. (Grundwald, Publication year not stated)

Network modifying oxides, do not form a glass network on their own and are incapable of doing so. These cations act to disrupt the glass structure by creating non-bridging oxygen atoms. The creation of non-bridging oxygen atoms causes a weakening of the glass structure as for each network

modifying oxide added one bridging oxide is broken to form two non-bridging oxygen atoms. Increasing the amount of network modifying oxides causes a gradual breakdown of the silica network. This is not necessarily a detrimental effect as this has been harnessed to produce disrupted and soluble bioactive glasses which are extremely useful. Common network forming oxides include CaO, Na_2O, K_2O, SrO and BaO.

Intermediates are oxides which alone are not capable of forming glass networks. However, they can reinforce the network or disrupt it. They can either bond to network forming tetrahedrons via bridging oxygen atoms forming a more cross-linked network. Alternatively, they can act to form more non-bridging oxygen atoms leading to a more disrupted glass network. Examples of intermediates include Ti, Zn, Pb, and Al.

2.5.3 History of Bioactive Glass

The concept of bioactive glasses began in 1967 as a result of research to find a material that would not be rejected by the body and was bioinert. It was discovered by Hench (1972) that certain glass compositions can bond to bone in so produced the world's first bioactive glasses. Orthopaedic materials used before had previously been metallic or plastic in nature and tended to form scar tissue in the interfacial layer between the material and host tissue. What was required was an implant material that would form a bond between material and tissue.

Research began in 1969 and was based on a simple hypothesis that if a material formed hydroxyapatite on its surface then it would give an increase in bioactivity compared to other metallic or plastic materials used at the time.

A hydroxyapatite-forming material was desired because hydroxyapatite is the main mineral phase of both bones and teeth (Hench, 2006).

Initial work done by Hench et al. (1972) discovered that certain composition ranges produced glass that would bond to bone. These were termed bioactive glasses and were made of SiO_2, Na_2O, CaO and P_2O_5. Hench investigated changes in these four component systems. The P_2O_5 content was maintained at 6 wt % whilst the amounts of the other three components was altered to see the respective bioactivity of the alteration in compositions (Hench, 2006). The compositional effects on the bone-bonding ability when the composition is shown in figure 14.

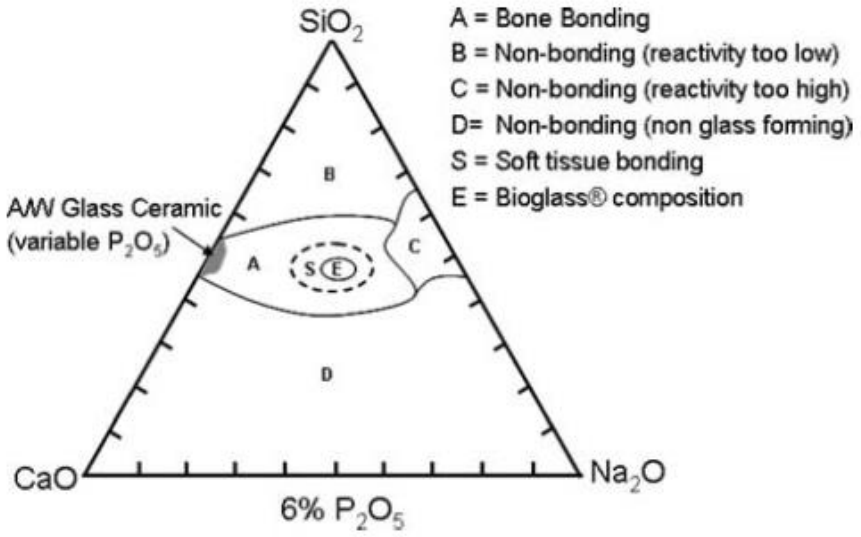

Figure 14 Ternary phase diagram of bioactive glass compositions relating to bioactivity. (Hench, 2006)

Areas labelled B and D showed no bone bonding this is caused by problems within the glass network. Compositions in section D did not form glasses, they likely crystallized during quenching. The cause of this is mostly likely because the amount of network modifier was too high and produced a very disrupted network which did form glass but converted to a partially crystalline

solid which is more thermodynamically stable and less reactive than glass. Area B, whilst it did produce a glass, the glass produced was most likely ‘too stable’ due to a high amount of bridging oxygen atoms. This prevents opening of the structure to release the requisite ions for apatite formation and thus increased bioactivity. Section A was an optimal region for bone-bonding of the glass compositions, then inside this region glass with a composition inside the S section were able to bond to soft tissue. The optimal composition was section E and led to the glass 45S5 used for bond-substitution the composition was 45% SiO_2, 24.5 Na_2O, 24.5% CaO and 6 % P_2O_5 (these are all weight percent).

A criticism of this initial work done by Hench et al was their choice to design compositions using weight percent of components. This effectively ignores Zachariasen random network theory and suggests the researchers were simply concerned with discovering an optimal composition by doing an exhaustive search, rather than understanding the science of the glass structure which would have enabled them to design the glasses based on their structure which may have led them to discover more bioactive glasses than 45S5. It is also somewhat puzzling that the P_2O_5 content was not altered to investigate its effect on bioactivity. Given that the authors themselves state that their aim was to produce apatite, a high phosphate containing mineral. It seems logical that increasing the amount of phosphorus in the glass would increase bioactivity and this has been since shown (O'Donnell et al., 2008b).

2.5.4 Structure of Bioactive Glass

Bioactive glasses consist of two major types of component, network formers and network modifiers. 45S5 is perhaps the most widely known bioactive glass composition 46.1 mol% SiO_2, 26.9 mol% CaO 24.4 mol% Na_2O and 2.6 mol% P_2O_5. The SiO_2 and P_2O_5 components act as network formers and CaO and Na_2O components acting as network modifiers. It was initially believed that in '45S5 bioactive glass' the SiO_2 and P_2O_5 network forming components were bonded together with Si-O-P bonds existing within the glass structure. This idea was based upon molecular dynamic (MD) computer simulations (Tilocca et al., 2007, Tilocca and Cormack, 2007). However, Pedone et al has shown Si-O-P bonds do not exist within the glass structure (Pedone et al., 2010). This is consistent with ^{31}P MAS-NMR data gained which has shown that the P_2O_5 exists as orthophosphate $(PO_4)^{3-}$ (Q^0_p) within the glass network (O'Donnell et al., 2008a, Brauer et al., 2009). This promotes the idea that the glass is a split network with the phosphate component existing within the silica network (Eden, 2011).

2.5.5 Q Structure and Network Connectivity

Glass Q structure refers to the structure and quaternary/tetrahedral coordination of the network forming units which the glass consists of.

Q^1 has 1 bridging oxygen and 3 non-bridging oxygen's meaning the network former in the glass is structured so the individual units are dimers.

Q^2 structure has 2 bridging oxygen's and two non-bridging oxygen's meaning the network former forms long chains or possibly rings.

Q^3 structure has 3 bridging oxygen's and 1 non-bridging oxygen meaning it has a 3D structure, similar to the Q^4 structure which has 4 bridging oxygen's.

The Q structure has a great deal of influence on the properties of the final glass. A trend tends to exist that the lower the Q structure the higher the solubility of the resulting glass. Although there is obviously a limit on how low a NC (network connectivity) can be as glasses with a NC below 2 tend to become hard to produce because they have a high chance of crystallising during the quenching process.

Hill presented a calculation to determine the theoretical network connectivity. Network connectivity (NC) is the average number of bridging oxygen atoms per network forming unit. The calculation published was (Brauer, 2011):

(11) $$NC = 2 + \frac{[(2 \times SiO_2) + (2 \times P_2O_5)] - [2(M_2^IO + M^{II}O)]}{SiO_2 + (2 \times P_2O_5)}$$

In this equation M^I refers to the molar concentration monovalent cations and M^{II} refers to divalent cations. This equation has it flaws as it assumes that phosphate exists as part of the glass network and can, depending upon composition exist with a range of Q^n structures. However, as explained previously phosphate in bioactive glass exclusively exists as orthophosphate regardless of composition. Therefore this equation has been updated to account for the role of phosphate in the glass.

(12) $$NC = 2 + \frac{[(2 \times SiO_2) - [2(M_2^IO + M^{II}O) + (6 \times P_2O_5)]}{SiO_2}$$

This equation gives a strong tool for predicting the average Q structure of a bioactive glass. This is excellent when designing novel bioactive glass compositions as it allows you to tailor the bioactivity of designed glasses. Whilst the network connectivity model has it benefits it should be noted that there are drawbacks in following this model exclusively. The NC model does not take into account the nature of the modifying cations or the charge to size ratio and the influence they have on the glass network. Another caution should be noted is that the NC model aims to produce the most soluble glasses and whilst the bioactivity of a bioactive glass is directly related to its ability to form apatite, its ability to form apatite is not directly related to its solubility.

The Q^n structure of the silicate phase depends somewhat on the ratios of the network forming and network modifying components. It has been shown that replacing the SiO_2 for P_2O_5 will cause an increase in Q^3 and a decrease in Q^2 in the glass network of the silicate phase (O'Donnell et al., 2008a).

The structure of a bioactive glass directly influences the physical properties of the resulting glass including mechanical properties and solubility. The structure of the glass can be predicted using its molar composition. Zachariasen's random network model states that bridging oxygens (BO) are distributed randomly throughout the glass (Zachariasen, 1932). The number of bridging oxygens per network former determines the Q^n structure of the glass, using Zachariasen's model means that the Q^n is dependent upon the relative concentrations of network former and modifier. Phillips and Thorpe have proposed the percolation theory which predicts that the glass network

will become rigid if the average number of bridging oxygens is greater than 2.4 (Phillips and Thorpe, 1985). This theory is supported up by experimental work reviewed by Brauer and Hill where the ability to form apatite was minimal when the average BO was 2.4 (Brauer, 2011).

When designing a bioactive glass the general consensus in the literature suggests a NC between 2.0 and 2.4 is optimal for apatite formation. Hill recommends a network connectivity close to 2.0, this is supported by experimental data with 45S5 Bioactive glass having a of NC = 2.11 (Hench, 2009) and various experimental work showing increasing the NC from 2.0 shows a decline in apatite formation in simulated body fluid (SBF). Edén suggests a broader range between 2.0 and 2.6, it is also predicted that a NC <1.8 and NC >2.7 would be unfavourable for apatite formation (Eden et al., 2011, Eden, 2011). Experimentally it is difficult to produce glasses with a NC <2.0 due to their tendency to crystallize during quenching.

2.5.6 Effect of Phosphate Content on Glass Structure

Increasing phosphate content in bioactive glasses was investigated by O'Donnell et al (O'Donnell et al., 2008a). The authors increased the phosphate content in a series of bioactive glasses. Two series of glasses were produced, Series 1 replaced silicon with increasing amounts of phosphate whilst keeping the ratios of calcium and sodium constant. Series 2 increased the phosphate content but kept the theoretical network connectivity constant by charge balancing the orthophosphate phase with calcium and sodium. The rationale behind the work was to establish how

phosphate existed in the glass structure. The compositions of the produced glasses are listed below.

Table 7 Glass Composition Produced to Investigate Phosphate Content in Two Series of Glasses by O'Donnell et al.

Name	Mol %					
	SiO_2	Na_2O	CaO	P_2O_5	NC	NC'
Series 1						
ICIE1	49.46	26.38	23.08	1.07	2.04	2.13
ICSW2	47.84	26.67	23.33	2.16	2.00	2.18
ICSW3	44.47	27.26	23.85	4.42	1.92	2.30
ICSW4	37.28	28.52	24.95	9.25	1.75	2.62
ICSW5	40.96	27.87	24.39	6.78	1.83	2.44
Series 2						
ICSW1	51.06	26.10	22.84	0.00	2.08	2.08
ICSW6	48.98	26.67	23.33	1.02	2.00	2.08
ICSW7	47.07	27.19	23.78	1.95	1.92	2.08
ICSW8	43.66	28.12	24.60	3.62	1.79	2.08
ICSW10	40.71	28.91	25.31	5.07	1.67	2.08
ICSW9	38.14	29.62	25.91	6.33	1.56	2.08

Na/Ca = 0.87. NC assuming phosphate enters glass structure. NC' assuming two phase system.

The glass structure was investigated using ^{29}Si and ^{31}P MAS-NMR. The ^{29}Si MAS-NMR performed on series 1 show an increase in peak asymmetry with increasing phosphate content. This fits with the hypothesis that phosphate exists as orthophosphate as when the phosphate content increases then more Na and Ca ions are required to charge balance the orthophosphate PO_4^{3-} which increases the polymerisation in the silicate network causing more Q^3 distribution agreeing with the results seen by ^{29}Si MAS-NMR. ^{31}P MAS-NMR drew the same conclusions, in series 1 the phosphate existed as an orthophosphate species. This peak shifted as NC' increased for series 1 but, the peak position in series 2 did not change. The results here show that the P_2O_5 introduced into the glass exists as a separate orthophosphate

phase within the final glass composition. The results here also show that when designing a glass which incorporates P_2O_5 this should be assumed to exist as orthophosphate and therefore should be charge-balanced. If the phosphate is not charge-balanced then this will cause the silicate phase to be more cross-linked which will have a highly negative impact on the glass bioactivity.

The same authors also investigated the physical properties of the glasses produced (O'Donnell et al., 2008b). This included measuring the density, glass transition temperature (T_g), crystallisation temperature (T_c), and thermal expansion coefficients.

Table 8 Glass Transition Temperature, Glass Crystallization Temperature, Thermal Expansion Coefficient and Densities of two Series Investigating Phosphate Content by O'Donnell et al.

Name	T_g/°C	$T_{p1,c}$/°C	$T_{p2,c}$/°C	α/x10-6/°C^{-1}	ρ/g cm^{-3}
Series 1					
ICIE1	513	629	676	-	2.715
ICSW2	511	636	679	15.70	2.719
ICSW3	491	655	674	16.18	2.719
ICSW5	485	605	625	-	2.696
ICSW4	482	543	617	18.88	2.788
Series 2					
ICSW1	519	614	642	-	-
ICSW6	515	620	653	-	2.721
ICSW7	513	642	692	-	-
ICSW8	509	652	669	16.37	2.727
ICSW10	496	619	-	16.54	2.748
ICSW9	491	580	613	-	2.787

The theoretical density of the glasses was calculated using the Doweidar model and these were compared with the experimental values, a modified Doweidar model (Doweidar, 2009) was also used to compensate for the existence of the orthophosphate phase. A decrease in density was seen in series 1 with increasing phosphate content. The experimental values showed

a much better fit to the theoretical density values which used the modified Doweidar model which took into account the orthophosphate phase. An anomalous result was seen with glass ICSW4, which showed an out of sequence dramatic decrease in density. This was attributed to crystallisation in the glass during quenching which was detected using XRD.

T_g and T_c was measured using differential thermal analysis, the working range was also calculated which is the temperature range between T_g and T_c (Working Range = T_c - T_g). For T_g in both the series the T_g decreased with increasing phosphate content, this is somewhat unexpected in both cases. For series 1 it may be expected that the T_g would increase because of the results shown by NMR which demonstrated a more cross-linked silicate network formed as the phosphate content increased. In series 2 it would be assumed that the T_g would be kept constant regardless of the phosphate content because the phosphate was charged balanced meaning no effect was seen on the cross-linking in the silicate phase. The explanation for the decrease in the T_g was attributed to increase in the orthophosphate phase as the P_2O_5 content increased. This meant the glass had more pockets of orthophosphate droplets leading to a more open and more disrupted glass network. The T_c seems independent of phosphate content, though inclusion of phosphate does allow crystallisation at lower temperatures.

The thermal expansion coefficients of the glasses were measured by comparing theoretical values calculated form the Appen model with experimental values from dilatometry experiments. For both series of glasses the thermal expansion coefficient increased with increasing phosphate

content, with the experimental values fitting well with the experimental values. This was explained by the increasing orthophosphate phase interdispersed through the silicate phase causing a higher glass expansion as the phosphate content increases. The thermal expansion coefficient is important for bioactive glass compositions which are used as implant coating materials.

XRD studies on the glass series showed all except glass ISCW4 were amorphous. This glass had the highest P_2O_5 content of all glasses at 9.24 mol %. This suggests that there is a maximum P_2O_5 content that can be incorporated without the glass crystallising. The nearest P_2O_5 content was 6.78 mol % indicating the maximum P_2O_5 content lies in between 6.78 and 9.24 mol %.

Recently another publication has focussed on the relationship between phosphate content and bioactivity (Mathew et al., 2014). The authors produced a number of glass compositions altering the network connectivity (2.11, 2.15, 2.50, 2.74 and 2.93) and producing two series at different network connectivity's (2.50 and 2.93) with increasing phosphate content from 0 – 6 mol%, the sodium to calcium ratio was maintained at 1.54. The aim of the study was to study P and Si Q speciation's in bioactive glasses and how these relate to bioactivity by performing NMR and molecular dynamic (MD) simulations of a range of glass compositions. From ^{31}P MAS-NMR measurements and subsequent deconvolution the authors discovered the presence of phosphate species within the glass structure of both Q_P^0 and Q_P^1, with the being Q_P^0 the vast majority in all compositions. The authors did

discover a trend of increasing Q_P^1 relative speciation as the network connectivity was increased from 4.1% (NC = 2.1) to 20.5% (NC = 2.9). When P_2O_5 content was increased in the glass composition the authors did not measure a difference between Q_P^0 and Q_P^1 ratios. With relation to phosphate content in the glass the authors concluded that bioactivity is maximised by altering two factors (1) lowering the silicate network connectivity to between 2.0 and 2.6[1], preferably lower as this reduces the potential fraction Q_P^1 species which does not precipitate to apatite. (2) Increasing P_2O_5 content in the glass, preferably above 6.0 mol%. One should be careful though as other work has concluded that P_2O_5 contents above 8 mol% induce crystallization in the glass during quenching (O'Donnell et al., 2008b).

2.5.7 Effect of Fluoride on Glass Structure

The structural role of fluoride was investigated by Brauer et al (Brauer et al., 2010c). The authors produced a series of bioactive glasses with fluorine incorporated. The series of glasses produced had increasing amounts of CaF_2 incorporated. The ratio of network formers and network modifiers was kept constant this maintained the NC of the glasses so any changes seen in the glass were due to fluoride inclusion rather than changes in glass Q^n structure. Table 9 below shows the glass compositions that were produced.

Table 9 Glass Compositions Produced by Brauer et al. to Investigate Fluoride Effect on Glass Structure. Amounts mol%.

Glass	SiO_2	P_2O_5	CaO	Na_2O	CaF_2	NC	NC'
A	49.47	1.07	23.08	26.38	-	2.13	2.13
B	47.12	1.02	21.98	25.13	4.75	2.13	1.82
C	44.88	0.87	20.94	23.93	9.28	2.13	1.49

[1] A result partially confirmed by the conclusions of previous work conducted by a different author.

D	42.73	0.92	19.94	22.79	13.62	2.13	1.15
E	40.68	0.88	19.98	21.69	17.76	2.13	0.78
F	36.83	0.80	17.18	19.64	25.54	2.13	-0.01
G	33.29	0.72	15.53	17.75	32.71	2.13	-0.9
H	44.88	0.97	44.87	-	9.28	2.13	1.49

The design of the glass was based on the hypothesis that in the glass structure the fluorine exists as a fluorine-calcium complex rather than fluorine forming non-bridging fluorine attached to the Silicon in the glass. How the fluorine exists would have a direct influence on the structure of the glass. The calculated network connectivity is listed as NC and assumes the fluorine is in a complex with calcium. The hypothetical network connectivity (NC') is also listed if the glass formed non-bridging fluorine in the glass structure.

The glasses produced were characterized using differential scanning calorimetry that measured glass transition (T_g) and crystallization temperatures (T_c). XRD was performed to conform that the glasses were amorphous after quenching. ^{19}F, ^{31}P and ^{29}Si MAS-NMR was also performed on the glass samples to determine the various fluorine, silicon and phosphorus environments within the glass.

No Si-F bonds were detected using ^{29}Si MAS-NMR, a large peak at -80 ppm corresponded to Q^2 in the glass structure, a relatively small shoulder was detected at -92 ppm which shows the presence of Q^3_{Si}. The presence of a majority of Q^2_{Si} with a lesser amount of Q^3_{Si} and absence of Si-F bonds agrees with the hypothesis that the fluorine exists bound to the calcium, most likely as CaF^+. This then also agrees with the hypothesis used to design the glasses so the actual NC is likely to be close to the intended NC of 2.13. This

result concurs with the findings of Lusvardi et al. who performed MD simulations of fluorine containing bioactive glasses and also did not find the presence of any Si-F bonds.

The ^{19}F MAS-NMR performed on this glass series found that the fluoride is present as complexes with either sodium, calcium or mixtures of both (Brauer et al., 2010b). The sodium-free glass in the series showed the formation of a F-Ca(n) species with a peak at -89 ppm. Hexa-coordinated species of F-Na(6) were found at -220 ppm and peaks at -115 and -165 ppm indicated the presence if mixed calcium-sodium fluoride species. As well as the ^{29}Si MAS-NMR data the ^{19}F MAS-NMR agrees with the idea that Si-F bonds do not form in the glass structure and rather forms calcium and/or sodium fluoride complexes. Brauer explains the result seen by suggesting that due to silicon having a higher affinity for oxygen than fluorine and the fact that in these glass non-bridging oxygens are abundant then the formation of Si-F bonds is unfavourable.

The T_g of the series produced by Brauer et al. showed a decrease in Tg with increasing CaF_2 content. Furthermore the onset of crystallization (measured using DSC) decreased with increasing fluoride content. This was explained due to the formation of the calcium-fluoride complexes (CaF^+) which reduce the charge from Ca^{2+} in a glass without fluoride to CaF^+ with fluoride. This reduction from a 2+ to 1+ charge in calcium reduces the potential for calcium ions cross-linking silicate chains leading to a more disrupted structure.

In summary, fluoride is readily incorporated into a bioactive glass structure. When incorporated it has been conclusively proven that the fluoride forms

complexes with sodium and calcium ions and does not form Si-F bonds. Incorporation of fluoride in the glass leads to a more disrupted glass structure indicated by a decreasing T_g with increasing amounts of fluoride in the glass composition. Given that Si-F bonds do not form in the glass network when designing bioactive glass with fluoride the fluorine should be added but the ratios of all other components (network former and modifiers) should be kept constant. This will mean the NC is not affected by fluorine addition.

Lusvardi et al. (Lusvardi et al., 2008) performed MD simulations of fluorine containing bioactive glasses and did not find the presence of Si-F bonds. The authors introduced CaF_2 into the glass by replacing network modifiers, this caused an increase in the NC' of the final glass caused by the reduction in network modifier content. When introducing fluoride into the glass composition then the ratios of the other components must be adjusted to account for the addition so that the glass NC is not adjusted. As this means that any changes in structure or bioactivity may be due to changes in glass network rather than the addition of fluoride.

A recent paper has also studied the incorporation of fluorine in bioactive glasses (Pedone et al., 2012). The authors compared ^{23}Na, ^{31}P and ^{19}F NMR results and MD simulations of a bioactive glass composition containing fluoride from (Christie et al., 2011). The authors looked at the local environments of the fluoride ions and confirmed that the F ions were associated with the Ca^{2+} and Na^{+} ions within the glass structure and did not form Si-F bonds.

2.5.8 Mechanism of Bioactivity

The dissolution of bioactive glasses is important to understand their bioactivity. The bioactivity of these glasses is defined as their time to form apatite in solution. The bond-bonding ability of bioactive glass implants depends on the surface reactions taking place on the bioactive glass. It is generally presumed that for a composition to be bioactive a layer of hydroxycabonated apatite must precipitate on the implant surface before it bonds to tissues. The ability of the glass to release ions for forming apatite will determine their bioactivity.

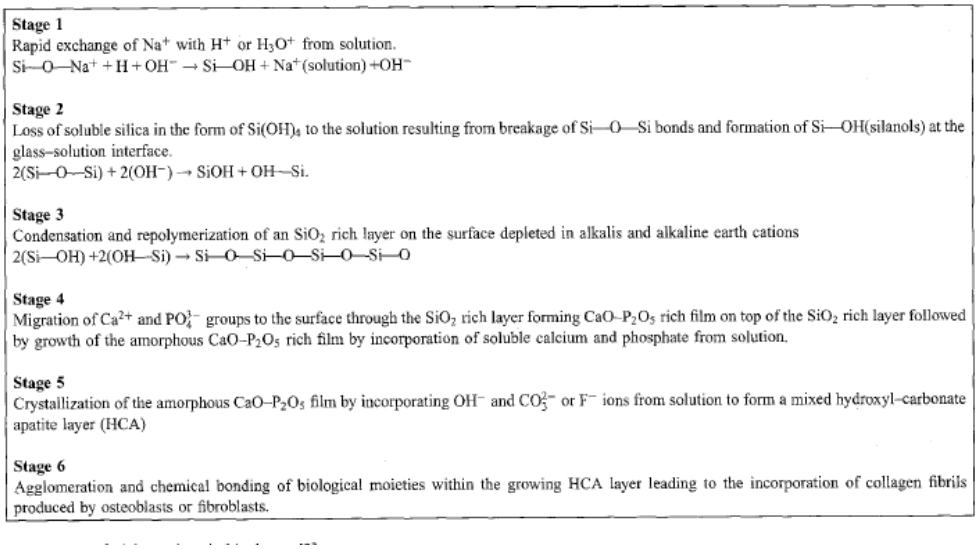

Figure 15 Mechanism of bioactivity of bioactive glass proposed by Hench et al.

Figure 15 shows the widely accepted mechanism proposed by Hench (Hench, 2006) to explain the bioactivity of bioactive glasses. The first step is the ion exchange of Na^+ ions from the glass for protons in the form of H^+ or H_3O^+ in the surrounding solution. This then induces an increase in the local pH due to the build-up of OH^- hydroxyl ions. This causes the breakage of the Si-O-Si bonds in the glass network by the hydroxyl ion, forming SiOH silanol groups at the interface between glass and surrounding solution. Breakage of

the silicate network opens the glass network which allows Ca^{2+} and PO_4^{3-} ions to migrate to the surface of the glass. An amorphous $CaO\text{-}P_2O_5$ film forms at the surface of the glass. This film then grows drawing Ca^{2+} and PO_4^{3-} ions from the surrounding solution. The layer then crystallizes and incorporates ions from the surrounding solution, namely OH^- and CO_3^{2-} ions. A mixed hydroxy-carbonated apatite layer then forms which allows the incorporation of collagen fibres and ultimate formation of new bone.

This mechanism gives no indication on how glass composition influences apatite formation. Numerous studies show that there is a large difference in the rates of apatite formation when the composition is altered. Hill suggests (Hill, 2012) that for apatite formation the surrounding solution must become super-saturated with PO_4^{3-} and Ca^{2+} ions, therefore altering the glass composition to maximize this (increasing CaO relative to Na_2O and increasing P_2O_5 content) would give a more rapid formation of apatite. Previous published work where the authors produced series of glasses with these modifications have increased the apatite forming ability of bioactive glasses (O'Donnell et al., 2008b). The Hench mechanism indirectly suggests that increasing the solubility of the glass would increase the rate of formation. From this mechanism, it would be expected that glasses with little or no sodium would not be bioactive or would exhibit limited bioactivity. It has been recently discovered that new sodium-free or low sodium-containing silicate glasses are exceedingly bioactive and form apatite in less than 4 hours.

Since Hench proposed his mechanism of bioactivity of bioactive glasses the split network model has been proposed. The orthophosphate existing in the

glass structure as droplets affects this mechanism. It is known the Ca and Na are distributed evenly between the silicate and phosphate phases within the glass network. A $CaNaPO_4$ in its amorphous form would be very soluble; therefore it is possible that the actual dissolution mechanism could be slightly different from what Hench suggests. It may be the case that when the glass particles enter solution the orthophosphate phase is released rapidly from the glass network this would also release the associated calcium and sodium ions. Insufficient calcium ion concentration would then limit apatite formation meaning the rate limiting step for apatite formation and thus bioactivity is release of calcium ions from the silicate network. Explaining why glasses with high Ca/Na ratios have seen rapid apatite formation.

Chapter 3: Techniques

3.1 X-ray Diffraction

The process of X-ray diffraction involves shooting a beam of X-rays at a sample and when these X-rays interact with the sample secondary diffracted beams of X-rays are created which are related to interplanar spacing in the crystalline powder, which can then be interpreted to produce a pattern identifying the crystalline components of the sample. It is based on constructive interference of monochromatic X-rays and a crystalline sample (Zolotoyabko, 2014). These X-rays are generated by a cathode ray tube, filtered to produce monochromatic radiation and focussed toward the sample. The interaction of the incident rays with the sample produces constructive interference (and a diffracted ray) when conditions satisfy Bragg's Law:

(13) $$n\lambda = 2d \sin \theta$$

Bragg's Law relates the wavelength of electromagnetic radiation to the diffraction angle and the lattice spacing in a crystalline sample. These X-rays once diffracted, are then detected, processed and counted (Zolotoyabko, 2014). By scanning the sample through a range of 2θangles, all possible diffraction directions of the lattice should be attained due to the random orientation of the powdered material. Conversion of the diffraction peaks to d-spacing's allows identification of the mineral because each mineral has a set of unique d-spacing's. With the aid of reference patterns, X-ray diffraction will be used to identify which crystalline products have formed in the cement reactions; and also used to ensure that the glasses are amorphous as when X-ray diffraction is performed on amorphous materials no sharp lines are present on the pattern, only broad amorphous halos are present.

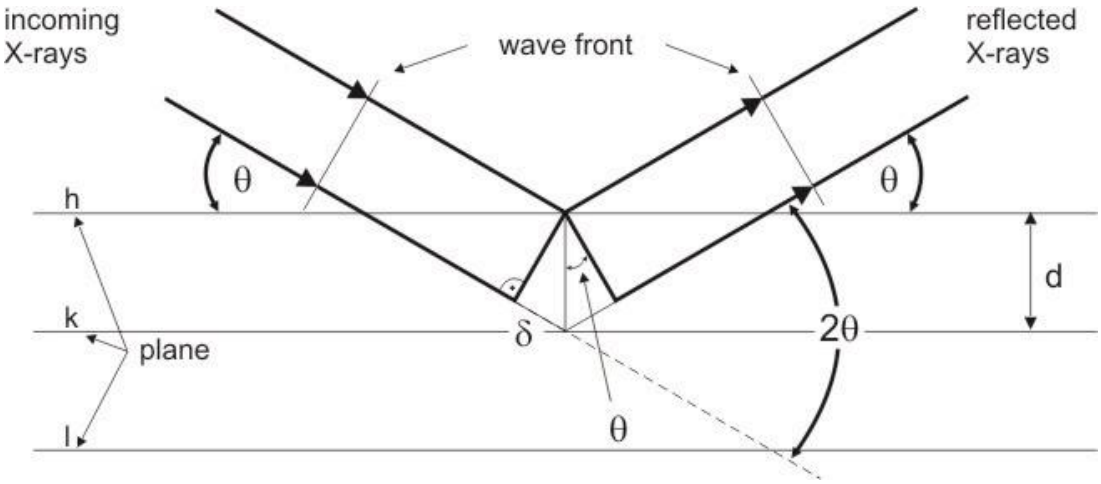

Figure 16 Representation of diffraction of X-rays from a crystal in X-ray diffraction analysis.

Applications and Use

In this project X-ray diffraction will be used to analyse both the cements and glasses produced. It will be used to determine the phases formed in the cement setting reaction, X-ray diffraction will be able to distinguish between the various potential phases formed in the setting reaction. X-ray diffraction patterns provide peaks which define the phases formed in the sample; each different phase present has its own specific finger print allowing its identification. Glasses are defined by their amorphous nature which when analysed using X-ray diffraction does not give diffraction lines. Ensuring the glasses are amorphous is important. Firstly if a glass-ceramic forms then it may be less reactive than its amorphous counterpart. Secondly small amounts of crystalline phases in glasses are hard to reproduce between different batch productions, therefore two batches of the same glass composition may give very different types and amounts of crystallisation which would not give reproducible glass properties.

A particular advantage X-ray diffraction gives for this project is its ability to distinguish between octacalcium phosphate and hydroxyapatite. Octacalcium phosphate has an almost identical X-ray diffraction pattern to hydroxyapatite except octacalcium phosphate has a prominent peak at 4.7 degrees 2 theta which is absent in hydroxyapatite patterns. A disadvantage in relation to this project is its inability to distinguish between fluorapatite and hydroxyapatite. On X-ray diffraction pattern both hydroxyapatite and fluorapatite share identical peaks, this is a particular disadvantage for this project that aims in part in to produce both hydroxyapatite and fluorapatite forming cements.

3.2 Magic Angle Spinning Nuclear Magnetic Resonance

Nuclear magnetic resonance relies on the phenomenon that nuclei in a magnetic field absorb and then re-emit electromagnetic radiation. Atomic isotopes with a magnetic moment can be studied for NMR spectroscopy. When placed into a magnetic field these isotopes exist in two spin states which either align with or against the magnetic field. If the nuclei are then irradiated with energy corresponding to the exact spin state of the specific nuclei causes those aligned against the magnetic field to 'flip' to align with the magnetic field. The energy difference (ΔE) between the two states is the energy released during this 'flipping' and is detected within the NMR probe. For ½ spin nuclei the energy difference between the two spin states at a given magnetic field strength is proportional to their magnetic moment (Keeler, 2010). However the individual environments of each isotope affect this energy difference slightly, causing chemical shifts. These chemical shifts can be used to identify nuclei within a specific molecule and also nuclei within different environments in the same compound (Keeler, 2010).

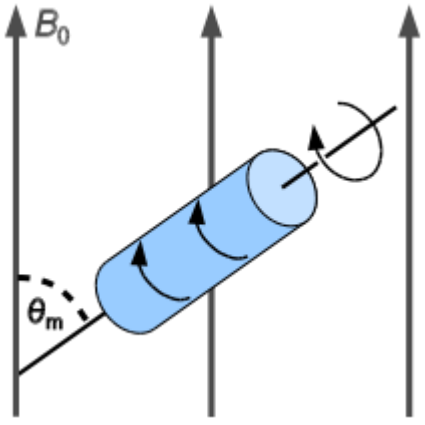

Figure 17 Representation of MAS-NMR rotor at magic angle (θ_m)

Magic-angle spinning (MAS) is a technique used in nuclear magnetic resonance to perform experiments in solid-state NMR spectroscopy. In a condensed phase there are main three interactions (dipolar, chemical shift anisotropy, quadrupolar) which often lead to very broad lines. Spinning the sample at the magic angle (ca. 54.74°, where $\cos 2\theta_m = 1/3$) with respect to the direction of the magnetic field, causes these broad lines to narrow, increasing the resolution allowing identification and analysis of the spectrum produced from the sample. In liquids (for instance compounds in solution) the interactions outlined above are averaged out due to the fast, time-averaged motion of the molecules in solution, on the contrary in solids this does not occur. This magic angle spinning of a solid mimics the orientation averaging in solution. Magic angle spinning causes the signal to become much narrower, giving rise to the isotropic value and spinning sidebands which occur at multiples of the spinning speed. At the magic angle the nuclear dipole-dipole interaction, between magnetic moments of nuclei averages to zero. The chemical shift anisotropy is a nuclear-electron interaction and averages to a non-zero value during magic angle spinning. The quadrupolar interaction is only partially averaged by spinning at the magic angle leaving a residual secondary quadrupolar interaction (Keeler, 2010).

Applications and Use

In this project MAS-NMR will be used to characterize the products of the cements developed, it will also be used to assess the setting mechanism of the cements developed in this study with the potential to work with other (conventional) CaP cements in order to assess them using NMR.

Identification of the formation of apatite in the cements will be important as this is the desirable product of the cement formation, to identify apatite ^{31}P MAS-NMR will be used, apatite appears on the spectra at 2.8 ppm (Kaflak-Hachulska et al., 2003) and should produce a narrow peak which is indicative of a crystalline product. ^{19}F NMR will be useful to firstly to ensure that glasses produced which include fluoride in their composition actually have it once they have be produced, also ^{19}F NMR is one of the only techniques which allow the confirmation of the formation of fluorapatite as the production of fluorapatite in a cement composition will not only be novel but will also increase the applications of current calcium phosphate cements.

Advantages and Disadvantages

Advantages of MAS-NMR are that it can detect very sensitive and depending upon abundance of the nuclei and number of scans it can be used for analysis of small amounts of sample, so if a sample is multi component and a probed species is present is very small quantities then NMR is likely to detect it where other techniques may not show it presence. Also NMR can be used to quantitatively analyse a sample and with deconvolution can be used to determine relative of fractions of components in a sample. Disadvantages of NMR are firstly that it can be hard to interpret the spectra and successful interpretation requires references from literature sources and analysis using other techniques. Secondly detection depends upon an atom having a detectable isotope that is in detectable amounts. For instance, ^{19}F is a spin ½ nucleus and at 100% natural abundance, all F atoms in a sample can be detected with no difficulty even at very low levels (White et al., 1988).

Table 10 Range of calcium phosphate compounds with their formulas and ^{31}P MAS-NMR chemical shifts relative to 85% H_3PO_4.

Compound	Abbreviation	Formula	^{31}P Chemical Shift	Ref
Fluorapatite	FAP	$Ca_{10}(PO_4)_6F_2$	2.8 (±0.2)	(Rothwell et al., 1980)
Hydroxyapatite	HAP	$Ca_{10}(PO_4)_6(OH)_2$	2.8 (±0.2)	
Octacalcium Phosphate	OCP	$Ca_8(HPO_4)_2(PO_4)_4.5H_2O$	-0.2, 2.0, 3.3, 3.7	(Tseng et al., 2004)
Na_2HPO_4	-	Na_2HPO_4	6.6	
Dicalcium phosphate dihydrate/Brushite	DCPD	$CaHPO_4.2H_2O$	1.7 (±0.3)	(Rothwell et al., 1980)
Dicalcium phosphate anhydrous/Monetite	DCPA	$CaHPO_4$	-1.5 (±0.4) 0.0 (±0.4)	(Rothwell et al., 1980)
Monocalcium phosphate anhydrous	MCPA	$Ca(H_2PO_4)_2$	-0.1 (±0.3) -4.6 (±0.3)	(Rothwell et al., 1980)
Monocalcium phosphate monohydrate	MCPM	$Ca(H_2PO_4)_2.H_2O$	0.5 (±0.4) -0.5 (±0.4)	(Rothwell et al., 1980)

3.3 Fourier Transform Infrared Spectroscopy

Infrared spectroscopy is an important technique in chemistry. It is an easy way to identify the presence of certain functional groups in a molecule. Also, it can use the unique collection of absorption bands to confirm the identity of a pure compound or to detect the presence of specific impurities. It is a technique which is used to obtain an infrared spectrum of absorption and emission scattering of a solid, liquid or gas.

An FTIR spectrometer scans a sample, rapidly, at all infrared frequencies done using an interferometer. The interferometer produces a unique type of signal which has all of the infrared frequencies “encoded” into it. Most interferometers employ a beamsplitter which takes the incoming infrared beam and divides it into two optical beams. One beam reflects off of a flat mirror which is fixed in place. The other beam reflects off of a flat mirror which is on a mechanism which allows this mirror to move a very short distance from the beamsplitter. The two beams reflect off of their respective

mirrors and are recombined when they meet back at the beamsplitter. Because the path that one beam travels is a fixed length and the other is constantly changing as its mirror moves, the signal which exits the interferometer is the result of these two beams “interfering” with each other. The resulting signal is called an interferogram which has the unique property that every data point which makes up the signal has information about every infrared frequency which comes from the source. Once detected the interferogram must be converted into a frequency spectrum which is done using Fourier mathematics which allows interpretation of the bands present within a sample.

FTIR works by the bonds in a molecule absorbing infrared light at a certain wavelength which is specific for that chemical bond. The electrons within a chemical bond absorb the light at a specific frequency (its resonant frequency) and are elevated into an excited state, which causes the bond to vibrate. A bond can vibrate in many different ways; typically these are symmetrical stretching, antisymmetrical stretching, scissoring, rocking, wagging and twisting. Infrared light which is absorbed by the molecule is not detected by the detector and compared with the reference beam the sample is lacking energy at certain wavelengths. The bonds in a molecule that are IR active all contribute to make a specific ‘fingerprint’ spectrum for each specific molecule, allowing for its identification.

Applications

In this project FTIR will be used for cement characterisation. FTIR is advantageous because it rapidly allows the analysis of samples, with typical

spectrum taking less than 2 minutes to obtain. FTIR allows the characterisation of the phosphate groups within the apatite structure (Elliott, 1994) as well as the water molecules and OH groups in apatite, octacalcium phosphate and DCPD (Elliott, 1994). It will be especially useful in this project for looking for any carbonate substitution within the apatite and is the only technique used in this project that can accomplish this (Kolmas et al., 2011).

Chapter 4: Aims and Objectives

4.1 Aims

The aim of the project is to develop a novel method of forming calcium phosphate cements using bioactive glasses as a reactive precursor. It is also an aim to develop glasses that can be used as ion delivery vehicles for the formation of novel cements. Fluoride and strontium will be added to glass compositions with the aim of producing both fluorapatite and strontium-substituted calcium phosphate cements. ^{31}P and ^{19}F MAS-NMR as well as X-ray diffraction will be used primarily to assess the viability of the glasses for forming calcium phosphate cement phases. Production of fluorapatite will be assessed by ^{19}F and ^{31}P MAS-NMR and XRD.

4.2 Objectives

Produce novel calcium phosphate cements where at least one major component of the setting reaction is a bioactive glass.

Confirm that the bioactive glass is providing Ca^{2+} and PO_4^{3-} for the cement phase to form and that the presence of the bioactive glass is essential for formation of the cement phase. This then confirms that the glass is taking part in the reaction rather than acting as a filler in the cement phase. This can be achieved using ^{31}P MAS-NMR to confirm dissolution of the orthophosphate phase with in the glass.

Establish optimal glass compositions for producing novel calcium phosphate cements. Optimal properties are defined as compressive strength (4-15

MPa), setting times (Gilmore needle test) (between 5 and 30 minutes), rheology (injectable through a needle) and porosity (high interconnectivity of pores). Glasses that vary calcium to sodium ratio and P_2O_5 content will be produced to measure effect on cement properties.

Introduce fluoride in the form of CaF_2 into the glass composition with the aim of producing a calcium phosphate cement which the main cement phase[2] is fluorapatite. A series of glasses will be produced to establish optimal fluoride contents for maximum fluorapatite formation in the cement phase.

Compare setting times, compressive strengths and phases formed against those of the commercially available calcium phosphate cement, HydroSet.

[2] Main cement phase is defined as the major phase present in the resulting cement after reaction. It is also the phase that primarily contributes to the compressive strength and setting times of the resulting cement. In this project the main cement phases may be octacalcium phosphate ($Ca_8(HPO_4)_2(PO_4)_4.5H_2O$), hydroxyapatite ($Ca_{10}(PO_4)_6(OH)_2$, carbonated-hydroxyapatite (type A or B), Brushite ($CaHPO_4.2H_2O$), Monetite ($CaHPO_4$), fluorapatite ($Ca_{10}(PO_4)_6F_2$), or a biphasic system consisting of a mixture of any of the above.

Chapter 5: Materials and Methods

5.1 Cement Starting Material Production

5.1.1 Glass Compositions

The following glass compositions were designed to assess the influence of P_2O_5 content, CaF_2 content and calcium to sodium ratio on cement formation and properties. The network connectivity of the glasses was maintained constant for all series of cement compositions in order to not change the degree of connectivity within the silicate glass phase.

Series 1 (QMNWKPaG01-05), investigating P_2O_5 content, increased P_2O_5 content in 2.00 mol% increments from 0.00-8.00. As a major component of hydroxyapatite, the effect of phosphorus content within the glass was studied to observe what effects it would have upon cement properties and chemistry. These amounts were selected because they range from zero phosphorus oxide to 8.00 mol% which is probably near the limit of incorporating ions into a glass according to previous work (O'Donnell et al., 2009).

Series 2 (QMNWKPaG06-11) investigated fluoride content from 2.00-4.50 mol% in 0.50 increments. It was unknown how fluoride content in the glass would affect cement properties and the ability to form fluorapatite. These amounts were chosen because they would give a range of potential fluoride substitutions in any apatite they may potentially form.

Series 3 altered the calcium to sodium ratio within the glass. It was believed that additional sodium may increase the rate of glass dissolution (based on the Hench glass dissolution mechanism (Hench, 2006)) which would then, in

turn, decrease setting times of the cement compositions produced from these glasses.

Table 11 Glass compositions produced to make cements. Amounts in mol%. NC', Network Connectivity

Name	SiO_2	P_2O_5	CaO	Na_2O	CaF_2	NC'
QMNWKPaG01	50.00	0.00	45.00	5.00	0.00	2.00
QMNWKPaG02	46.00	2.00	46.80	5.20	0.00	2.00
QMNWKPaG03	42.00	4.00	48.60	5.40	0.00	2.00
QMNWKPaG04	38.00	6.00	50.40	5.60	0.00	2.00
QMNWKPaG05	34.00	8.00	52.20	5.80	0.00	2.00
QMNWKPaG06	37.00	6.00	49.50	5.50	2.00	2.00
QMNWKPaG07	36.00	6.00	48.60	5.40	4.00	2.00
QMNWKPaG08	36.80	6.00	49.23	5.47	2.50	2.00
QMNWKPaG09	36.50	6.00	49.05	5.45	3.00	2.00
QMNWKPaG10	36.30	6.00	48.78	5.42	3.50	2.00
QMNWKPaG11	35.80	6.00	48.33	5.37	4.50	2.00
QMNWKPaG13	42.00	4.00	49.00	5.00	0.00	2.00
QMNWKPaG14	42.00	4.00	44.00	10.00	0.00	2.00
QMNWKPaG15	42.00	4.00	39.00	15.00	0.00	2.00
QMNWKPaG16	42.00	4.00	34.00	20.00	0.00	2.00

5.1.2 Glass Production

Glasses in the system SiO_2-P_2O_5-CaO-Na_2O-(CaF_2) were prepared in the melt-quench route (table 11). SiO_2 (Prince Materials Ltd., UK), P_2O_5, $CaCO_3$, Na_2CO_3 and CaF_2 (all Sigma-Aldrich) were melted in a platinum-rhodium (90% Pt, 10% Rh) crucible at a melt temperature of 1480 ˚C for 1 hour in an electric furnace (Lenton EHF 17/3). Batches of 150 g were produced and each glass batch was quenched rapidly in water after the melting period.

5.1.3 Glass Milling

100g of each glass was ground using a vibratory mill (Gy-Ro mill, Glen Creston) for 2 x 7 minutes and sieved (Endecotts, UK) to a particle size below 38 μm.

5.1.4 $Ca(H_2PO_4)_2$ Milling

The $Ca(H_2PO_4)_2$ (Sigma-Aldrich) was prepared by grinding 27 g using a vibratory mill (Gy-Ro mill, Glen Creston) for 4 minutes.

5.1.5 Differential Scanning Calorimetry

Differential scanning calorimetry (DSC) was carried out using a Stanton Redcroft DSC 1500 (Rheometric Scientific, Epsom, UK) to study the glass transition temperature of the glass powders. 50 mg of each glass powder sample was weighed in a platinum crucible and placed onto the DSC stage adjacent the matched platinum crucible with to 50 mg of alumina powder. Samples were ramped from 20-1000℃ at 10ºC/min.

5.2 Cement Powder/Paste

The cement mixture was prepared by mixing the sieved glass powder with the milled $Ca(H_2PO_4)_2$ powder in a ratio to give an overall calcium to phosphorus ratio (Ca/P) of 1.67 (the stoichiometry of apatite). The powders were mixed by hand on a glass slab. In order to produce the cement paste and initiate the cement setting reaction the cement powder was mixed with 2.5% Na_2HPO_4 solution in a liquid to powder ratio (L/P, ml/g) of 0.70. The paste was then mixed by hand with a metal spatula for 30 seconds.

5.2.1 HydroSet

HydroSet was mixed according to the manufacturer's instructions.

5.2.2 Cement Cylinders

The cement paste was filled in cylindrical steel moulds with a height of 6 mm and diameter of 4 mm. The cylinders were ‘over –filled’ and sandwiched between two steel plates. The moulds and plates were then clamped together using a G clamp. The clamp was then placed into a 37°C oven (Borolabs incubator, Borolabs Basingstoke, UK) for 120 minutes. The clamp and plates were then removed and the cements whilst in the moulds were brushed with silicon-carbide paper to ensure a flat surface at each end of the cylinder.

5.2.3 Immersion of Cements

The set cement cylinders were then weighed and height and diameter was measured using a micrometer (Mitutoyo Ltd, Andover, UK) for each cylinder. Each cylinder was then immersed in 10 ml of Tris buffer solution (in 15 ml plastic centrifuge tubes) for either 1 hour, 1 day, 7 days or 28 days. 8 cement cylinders were immersed at each time point for each cement composition for compressive strength measurements. The samples were stored in a 37°C oven for their respective time-points. After being stored for its respective time each cylinder was removed and patted dry, the weight, height and diameter were then measured again.

5.3 Cement Property Characterisation

5.3.1 Setting Time Measurement

The setting time of each cement sample was measured using the Gilmore needle test according to the ISO standard ISO (9917-1:2007(E)). Cement pastes were prepared according to the method outlined, the cement paste was filled into cylindrical moulds (Height 4 mm, Diameter 8 mm) using a

spatula. To measure the initial setting times the ‘lesser’ Gilmore needle (2.12 mm 113.4 g Wt.) was lowered onto the cement surface and left for 5 seconds, the setting time was taken until the needle tip no longer makes an indentation on the cement surface. To measure the final setting time the larger Gilmore needle (1.06 mm dia. 453.6 g Wt.) was used and again the needle is lowered onto the surface of the cement paste and left for 5 seconds, the final setting time was taken when the needle no longer makes an indentation on the cement surface.

5.3.2 Compressive Strength Measurements

Compressive strength was measured using an Instron 5567 mechanical property testing machine (Instron, High Wycome, UK) using a 1kN load cell. Cylindrical specimen after their respective immersion times were placed between two steel plates without drying with a 1 cm square damp filter paper above and below the specimen. Force was applied at a movement rate of 1 mm/min. The test was stopped either automatically by the machine when fracture was detected or when it was evident by eye that fracture had occurred. Eight specimens were tested for each cement composition, for each immersion time.

5.3.3 Inductively Coupled Plasma-Optical Emission Spectrometry

ICP-OES measurements were performed using a Varian Vista-PRO CCD. Samples were diluted by 10 with Tris buffer solution and 69% nitric acid (VWR, Radnor, PA, USA) was added in 5% w/w. Ion concentrations were measured against a range of prepared multi-element standard solutions (Si, Ca, Na, P; VWR, Radnor, PA, USA) of 0.1, 1, 10, 20, 50 and 100 ppm,

prepared with Tris buffer solution to account for ionic strength. A total of four measurements were performed on each cement immersion time point.

5.3.4 Fluoride Measurements

Fluoride-release into Tris buffer was measured using a fluoride-selective electrode (Orion 9609BNWP with Orion pH/ISE meter 710, both Thermo Scientific, Waltham, MA, USA). Calibration was performed using standard solutions of 0.01, 0.1, 1, 10, 100 ppm; prepared using Tris buffer to account for ionic strength from a 1000 ppm F stock solution (VWR, Radnor, PA, USA).

5.4 Cement Phase Analysis

5.4.1 X-ray Powder Diffraction

Powder XRD experiments for the cements were done on Bruker D8-A25-Advance diffractometer operating with the CuKα radiation at 40kV and 40mA. The XRD pattern for the $Ca(H_2PO_4)_2{\cdot}H_2O$ was run on X'Pert Pro PANalytical diffraction system with Cu anode operating at 45kV and 40mA.

5.4.2 Fourier Transform Infrared

Samples were analysed using Fourier-transform infrared spectroscopy (FTIR; Spectrum GX, Perkin Elmer, Waltham, MA, USA; data collected from 4000 to 500 cm^{-1})

5.4.3 Magic Angle Spinning Nuclear Magnetic Resonance

The ^{31}P MAS-NMR experiments were run on Bruker 600MHz spectrometer at the 242.9MHz resonance frequency. The powder samples were packed into 4mm rotor and spun at 11-12kHz. The measurements were done using 60s recycle delay and 85% H_3PO_4 was used to reference the chemical shift

scale. The ^{19}F MAS-NMR experiments were run at the 564.7MHz using a fluorine-free probe in a 2.5 mm rotor spun at 20kHz with 60s delay for the cements and 10s delay for the glass. The ^{19}F chemical shift scale was referenced using 1M NaF solution giving a signal at -120 ppm against CF_3Cl.

5.4.4 Scanning Electron Microscopy

The fracture surface of the cement cylinders were studied under SEM. Specimen stubs were gold coated using an automatic sputter coater. Photomicrographs were taken using a Hitachi S-3400 machine, with the accelerating voltage 20kV, emission current 54mA.

Chapter 6: Glass and $Ca(H_2PO_4)_2$ Characterisation Results and Discussion

6.1 Results

6.1.1 Glass Characterisation

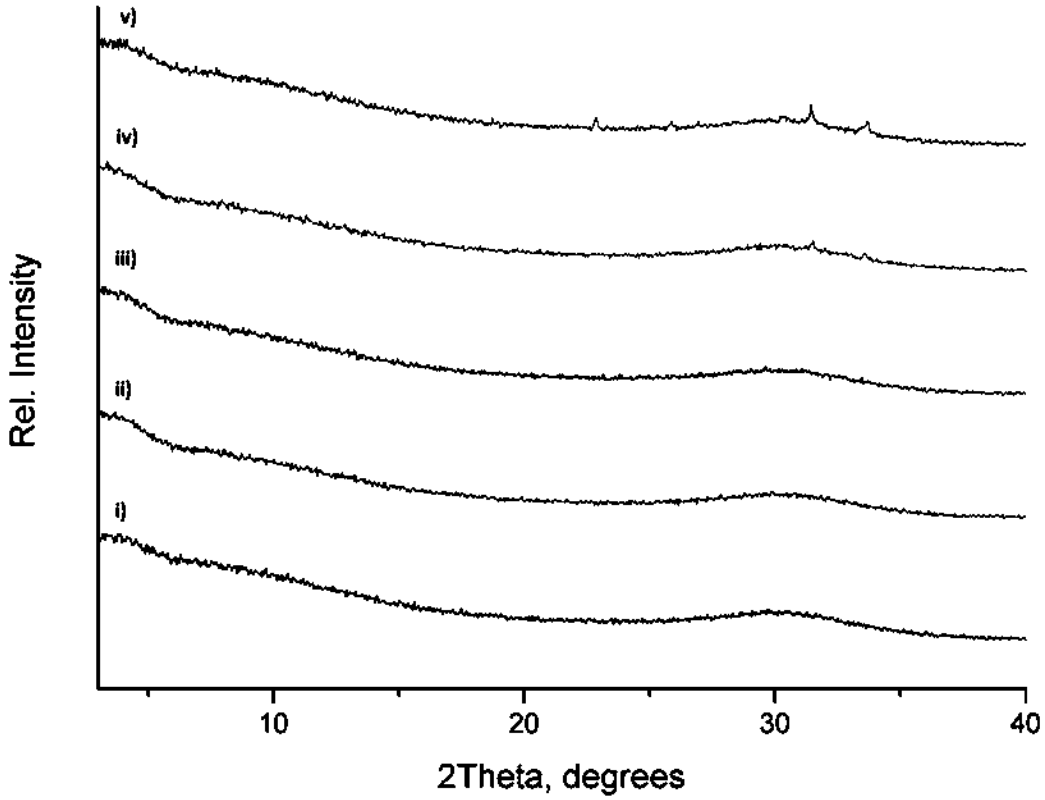

Figure 18 X-ray diffraction patterns of glasses with increasing phosphate content. i) QMNWKPaG01, ii) QMNWKPaG02, iii) QMNWKPaG03, iv) QMNWKPaG04, v) QMNWKPaG05.

Figure 18 shows X-ray diffraction patterns of glasses QMNWKPaG01-05. The X-ray diffraction was performed to confirm the amorphous nature of the glasses. Glass QMNWKPaG01-04 show no clear diffraction lines indicative of crystallisation. Glass QMNWKPaG05 showed indicative lines of crystallisation within the sample.

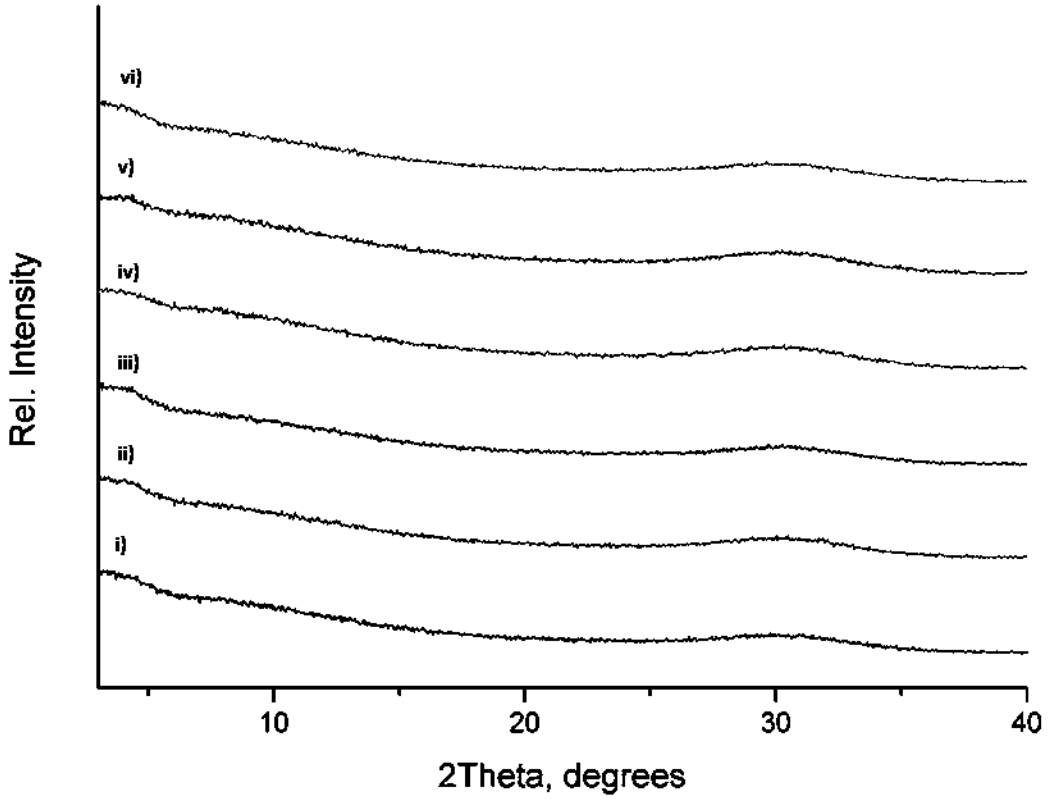

Figure 19 X-ray diffraction patterns of fluoride containing bioactive glass compositions. i) QMNWKPaG06, ii) QMNWKPaG07, iii) QMNWKPaG08, iv) QMNWKPaG09, v) QMNWKPaG10, vi) QMNWKPaG11.

Figure 19 displays X-ray diffraction patterns of glasses produced with increasing fluoride contents. All patterns showed no diffraction lines, confirming the amorphous nature of the glasses produced.

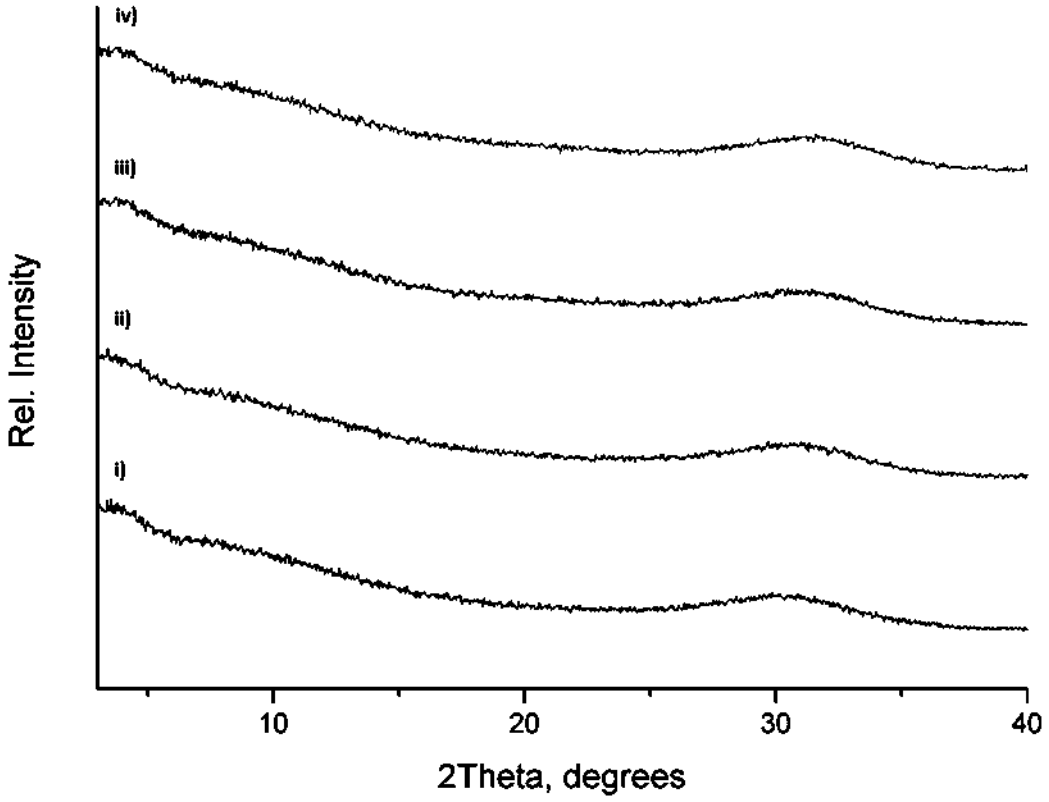

Figure 20 X-ray diffraction patterns of bioactive glass compositions with increasing sodium contents. i) QMNWKPaG13, ii) QMNWKPaG14, iii) QMNWKPaG15, iv) QMNWKPaG16.

Figure 20 displays X-ray diffraction patterns of glasses produced with increasing sodium contents. All patterns showed no diffraction lines, confirming the amorphous nature of the glasses produced.

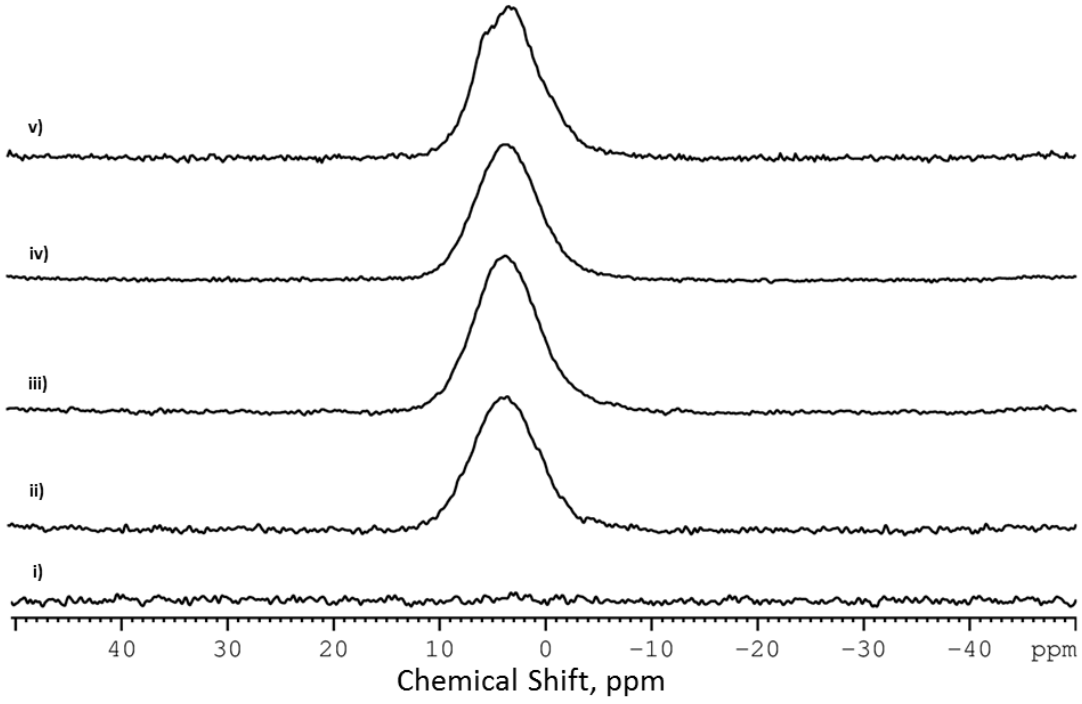

Figure 21 ^{31}P MAS-NMR spectra of glasses with increasing phosphate content. i) QMNWKPaG01, ii) QMNWKPaG02, iii) QMNWKPaG03, iv) QMNWKPaG04, v) QMNWKPaG05.

The ^{31}P MAS-NMR spectra of the glasses with increasing phosphate content showed anticipated results for glasses QMNWKPaG01-04. Glasses QMNWKPaG02-04 show almost identical spectra with one broad chemical shift all at 3.8 ppm indicative of amorphous orthophosphate (Brauer et al., 2009) and without any additional chemical shift which would indicate the presence of crystalline phases. The spectrum of glass QMNWKPaG01 showed no signal as there is no phosphate within the glass composition. QMNWKPaG05 showed expected results, based on the X-ray diffraction pattern, with two peaks at 3.2 and 5.0 ppm indicating possible presence of a phosphate containing crystalline phase.

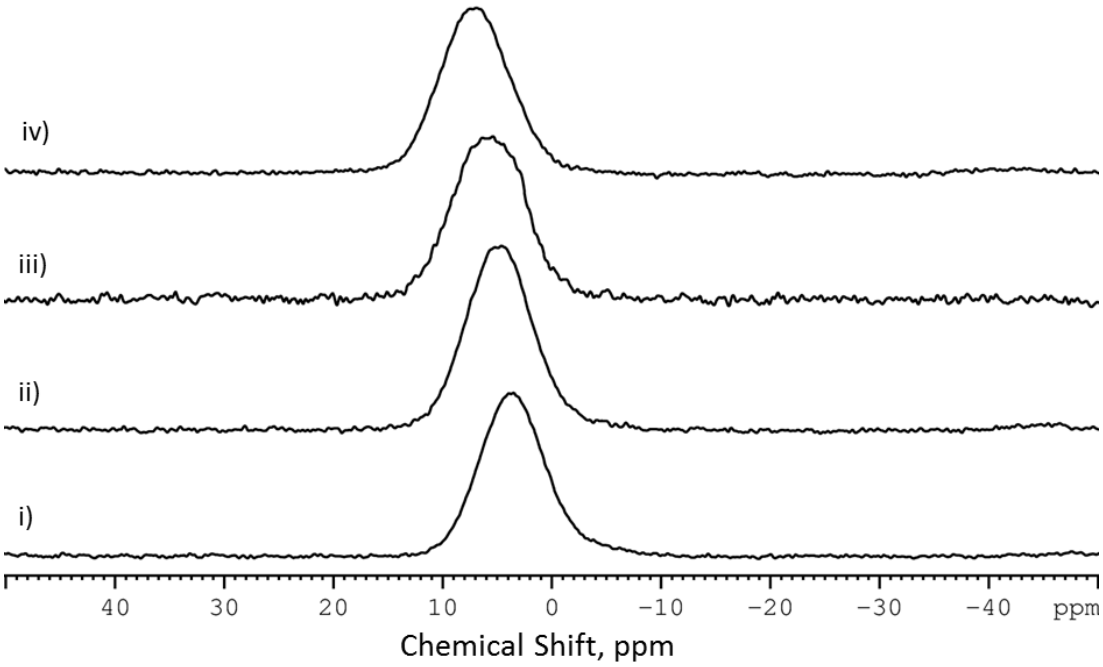

Figure 22 ^{31}P MAS-NMR spectra of bioactive glass compositions with increasing sodium content. i) QMNWKPaG13, ii) QMNWKPaG14, iii) QMNWKPaG15, iv) QMNWKPaG16.

Figure 22 shows ^{31}P MAS-NMR spectra of bioactive glass compositions with increasing sodium content. Each spectrum shows one broad peak, indicative of amorphous orthophosphate. The position shifts to a higher ppm with increasing sodium content, with QMNWKPaG13 a centre at 3.6 ppm; QMNWKPaG14 at 5.0 ppm; QMNWKPaG15 at 5.7 ppm and QMNWKPaG16 at 7.3 ppm.

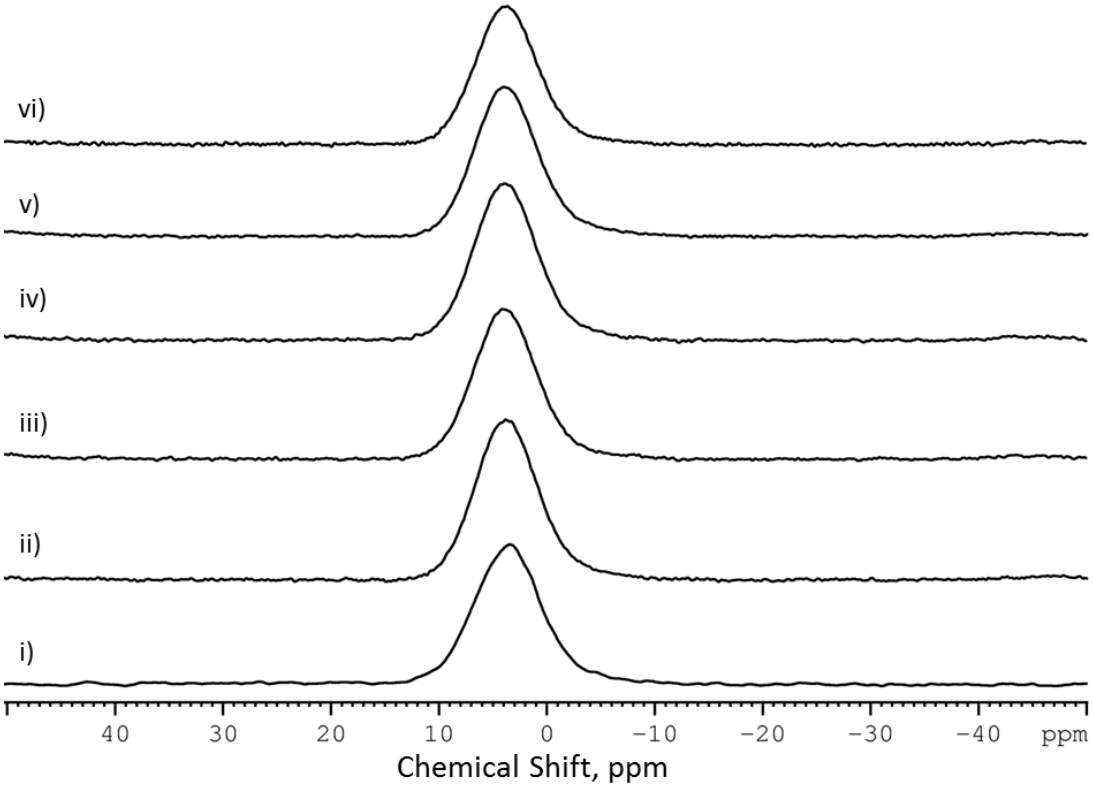

Figure 23 ^{31}P MAS-NMR spectra of fluoride containing bioactive glass compositions. i) QMNWKPaG06, ii) QMNWKPaG07, iii) QMNWKPaG08, iv) QMNWKPaG09, v) QMNWKPaG10, vi) QMNWKPaG11.

Figure 23 shows ^{31}P MAS-NMR spectra of all glasses for the series produced with increasing fluoride contents. All spectra show broad peak at identical positions, 3.8 ppm.

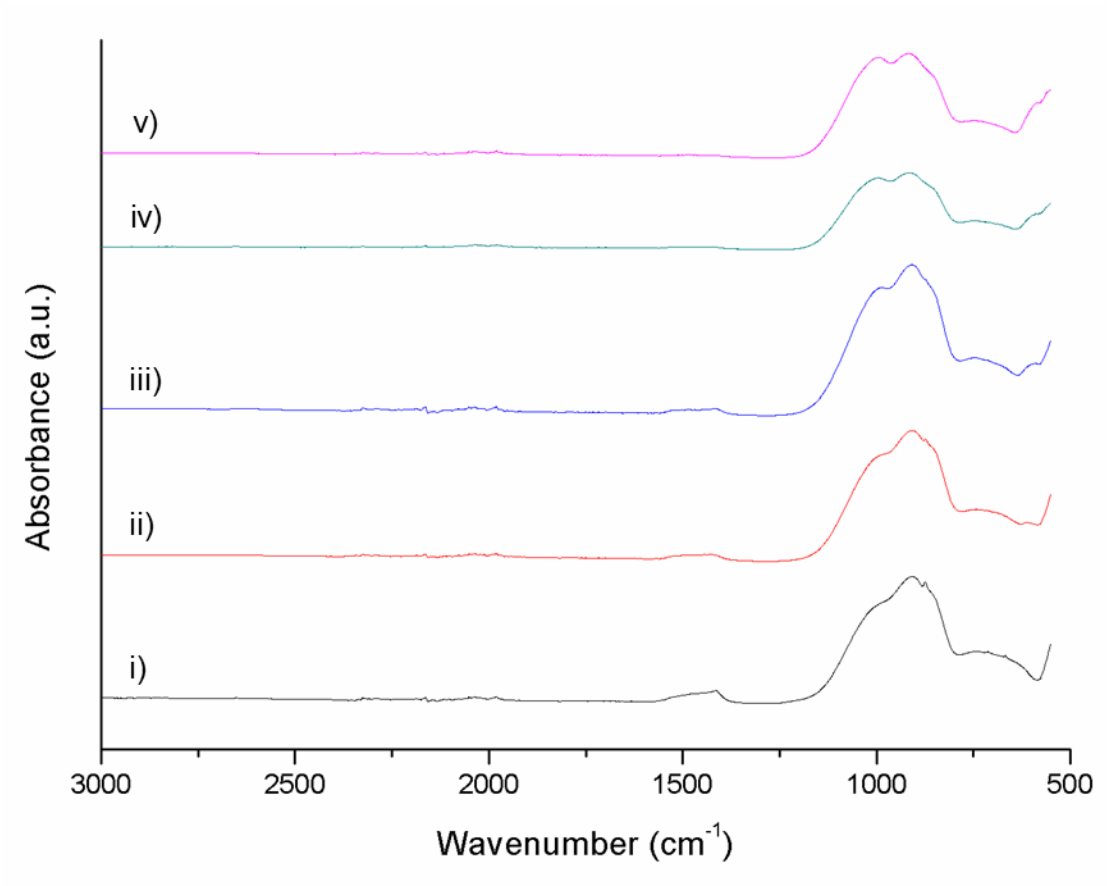

Figure 24 FTIR spectra of glasses with increasing phosphate content. i) QMNWKPaG01, ii) QMNWKPaG02, iii) QMNWKPaG03, iv) QMNWKPaG04, v) QMNWKPaG05.

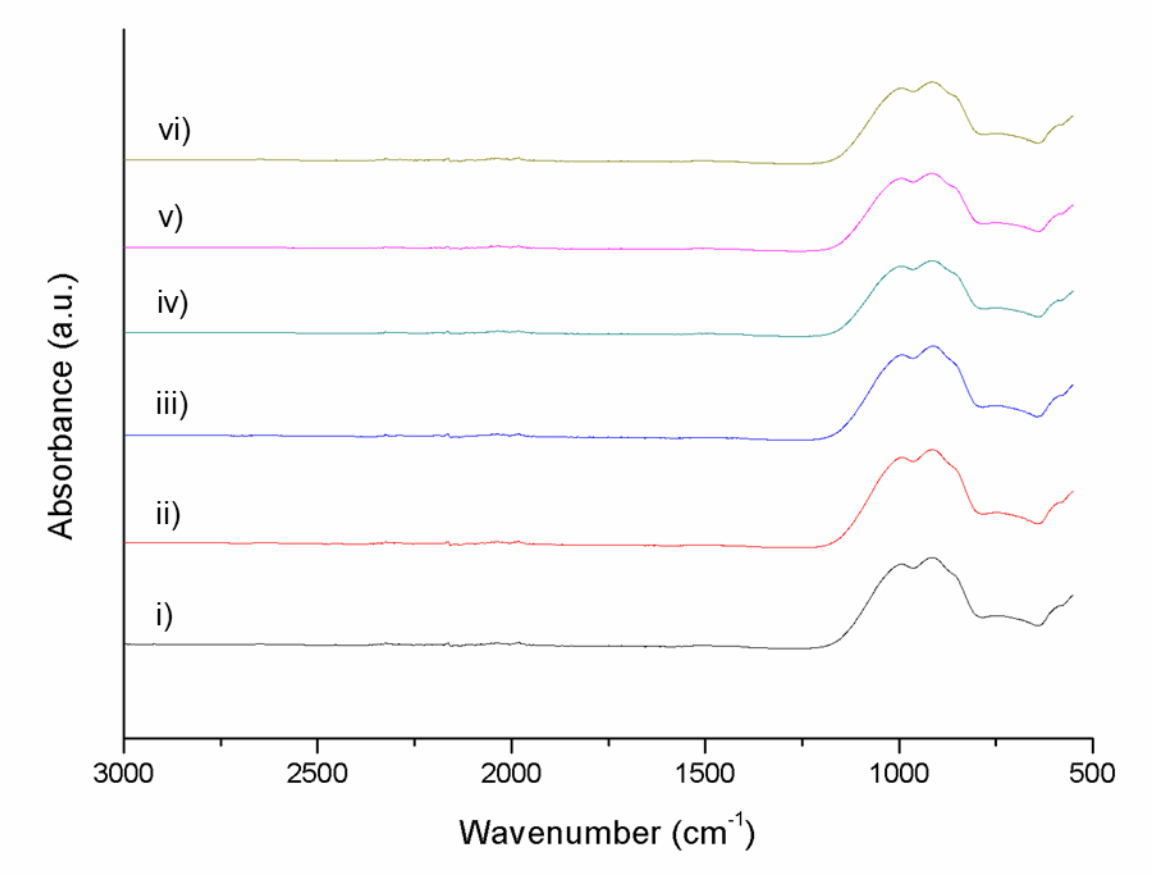

Figure 25 FTIR spectra of fluoride containing bioactive glass compositions. i) QMNWKPaG06, ii) QMNWKPaG07, iii) QMNWKPaG08, iv) QMNWKPaG09, v) QMNWKPaG10, vi) QMNWKPaG11.

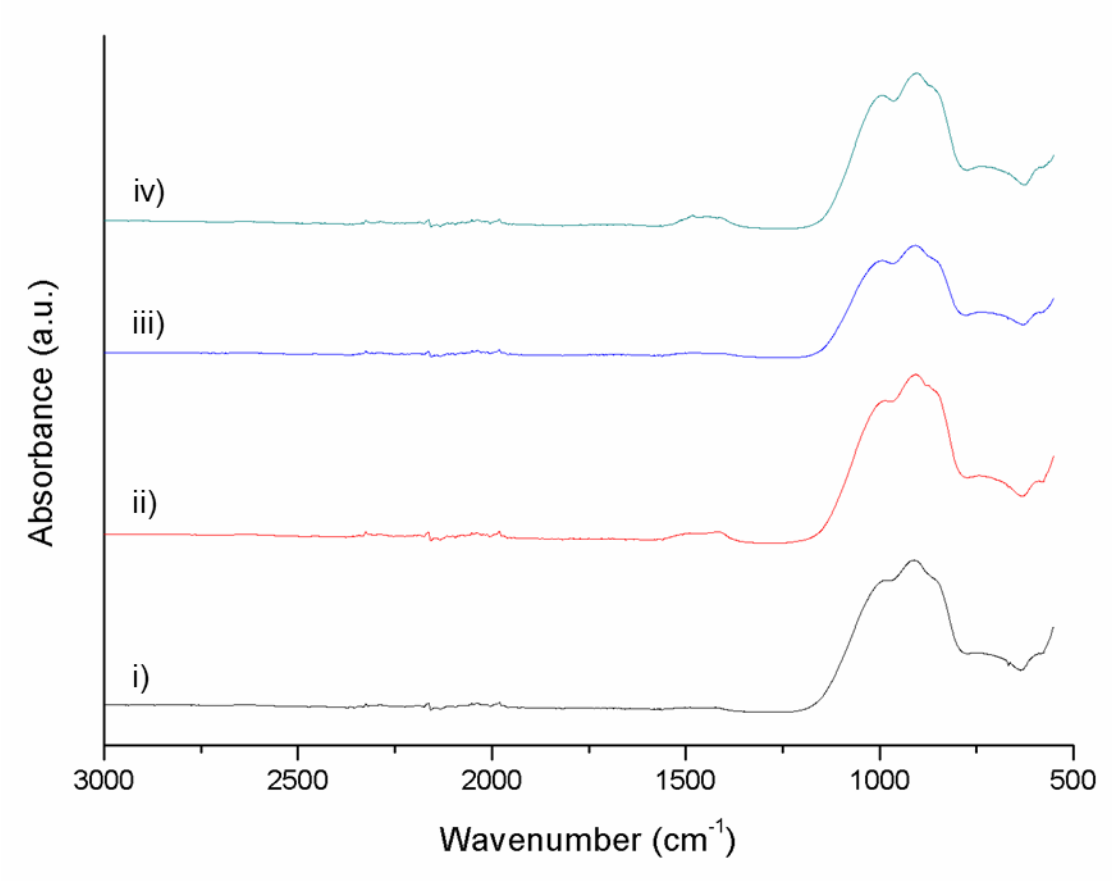

Figure 26 FTIR spectra of bioactive glass compositions with increasing sodium contents. i) QMNWKPaG13, ii) QMNWKPaG14, iii) QMNWKPaG15, iv) QMNWKPaG16.

The FTIR of the bioactive glasses produced in this study show almost identical spectra which are consistent with typical spectra of bioactive glasses. A broad band at ~600 cm^{-1} (on all spectra except QMNWKPaG01) is attributed to amorphous PO_4 groups. Then all spectra also possess bands at 850, 900, 1010 cm^{-1}; which are attributed to being $Si\text{-}O^{-}$ Na^{+}, Si-O- Ca^{2+} and Si-O-Si bonds respectively (Cerruti et al., 2005).

Table 12 Glass transition temperatures of all glass compositions used to make cements

Glass Composition	Glass Transition Temperature (T_g) ºC
QMNWKPaG01	689
QMNWKPaG02	697
QMNWKPaG03	695
QMNWKPaG04	698

QMNWKPaG06	664
QMNWKPaG07	635
QMNWKPaG08	658
QMNWKPaG09	662
QMNWKPaG10	654
QMNWKPaG11	625
QMNWKPaG13	687
QMNWKPaG14	633
QMNWKPaG15	589
QMNWKPaG16	544

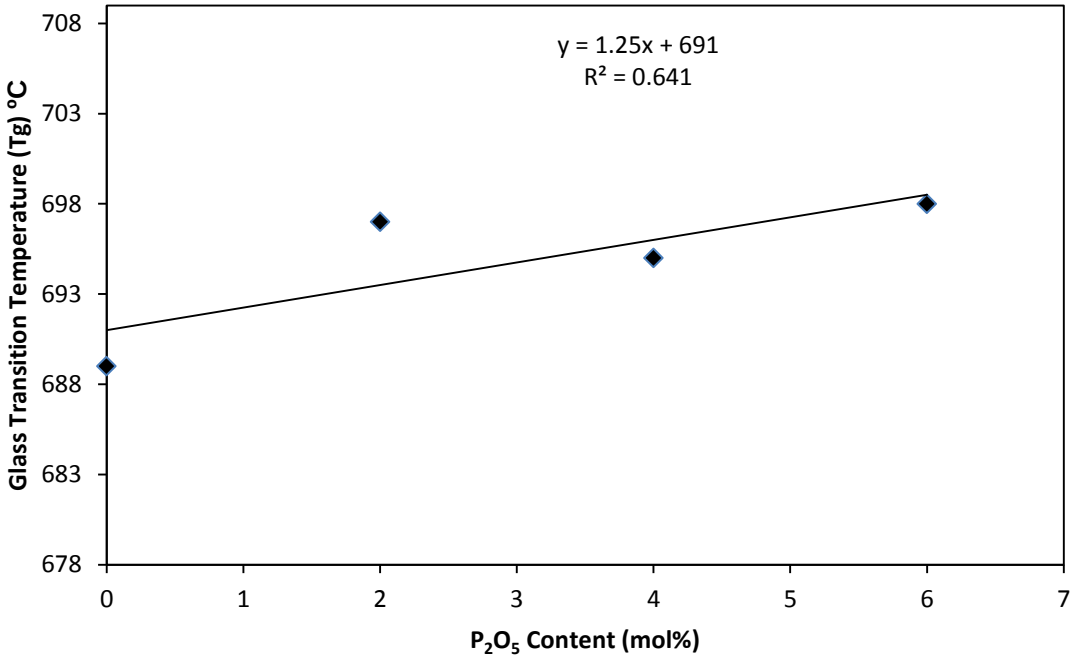

Figure 27 Glass transition temperature of glass compositions QMNWKPaG01-04 plotted against P_2O_5 content. Plotted with line of best fit with correlation coefficient (R^2) and graph equation.

Figure 27 shows the Glass transition temperature of glass compositions QMNWKPaG01-04 plotted against P_2O_5 content. With 0 mol% P2O5 content in the glass the T_g is at its lowest (689 ºC), after this there is a general trend of increasing T_g as the phosphate content is increased, with the 4 and 6 mol% compositions being at 695 and 698 ºC respectively. The 2 mol% composition is perhaps slightly higher than it should be at 697 ºC as it sits slightly above the trend.

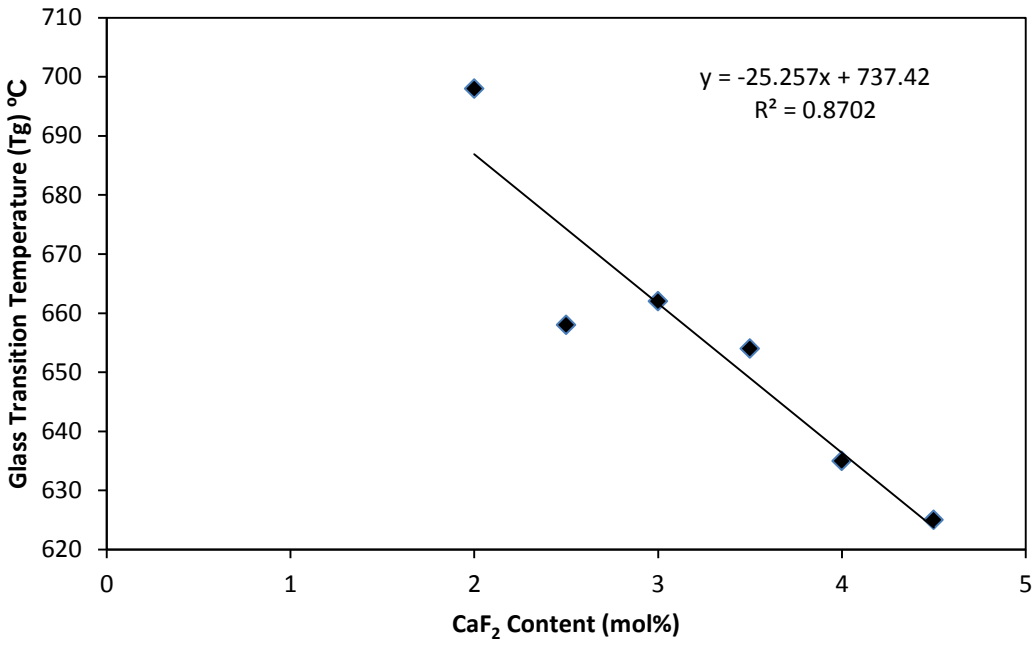

Figure 28 Glass transition temperature of glass compositions QMNWKPaG06-11 plotted against CaF_2 content. Plotted with line of best fit with correlation coefficient (R^2) and graph equation.

Figure 28 shows Glass transition temperature of glass compositions QMNWKPaG06-11 plotted against CaF_2 content. There is a general trend of decreasing Tg as the fluoride content was increased. With 2 mol% CaF_2 the T_g is 698 ºC which decreases to 625 ºC with 4.5 mol%. The 2.5 mol% composition deviates from the general trend being at 658 ºC.

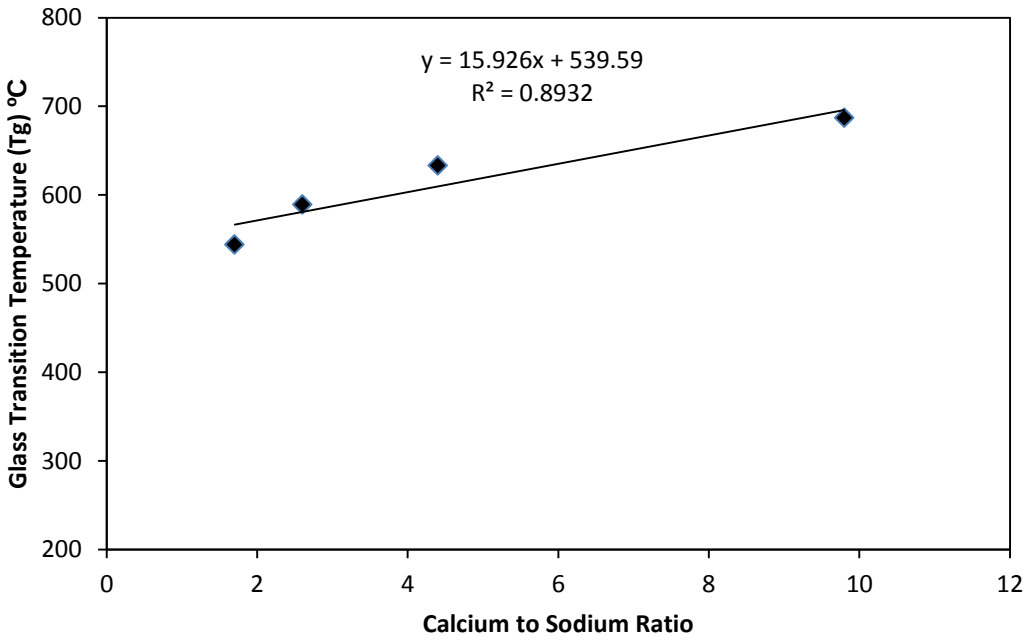

Figure 29 Glass transition temperature of glass compositions QMNWKPaG13-16 plotted against calcium to sodium ratio within the glass composition. Plotted with line of best fit with correlation coefficient (R^2) and graph equation.

Figure 29 shows Glass transition temperature of glass compositions QMNWKPaG13-16 plotted against calcium to sodium ratio within the glass composition. The T_g of each glass rises from 544 to 589 then 633 and finally 687 ºC as the calcium to sodium ratio increases in the glass compositions.

6.1.2 $Ca(H_2PO_4)_2$ Powder Characterisation

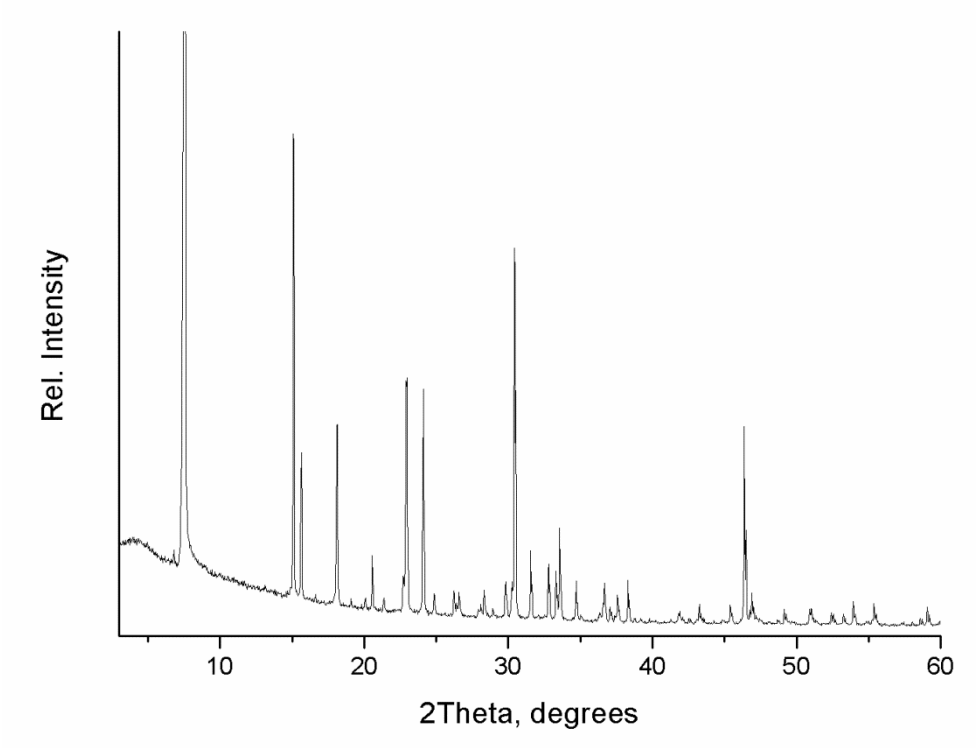

Figure 30 X-ray diffraction pattern of $Ca(H_2PO_4)_2$ powder.

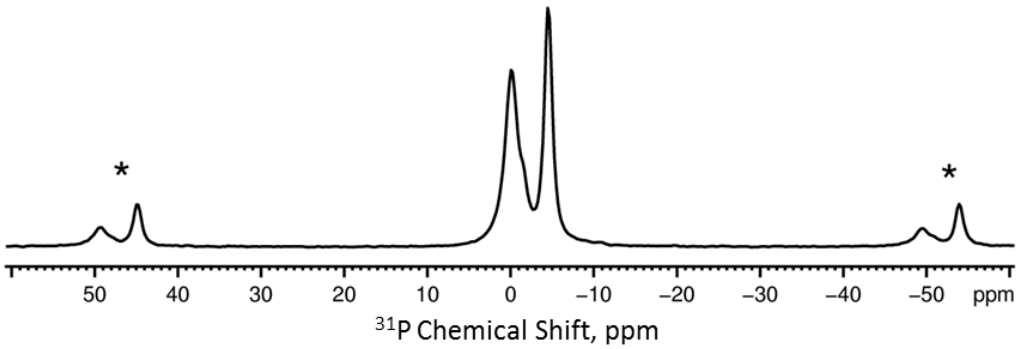

Figure 31 ^{31}P MAS-NMR $Ca(H_2PO_4)_2$ purchased from Sigma-Aldrich. * indicate spinning sidebands.

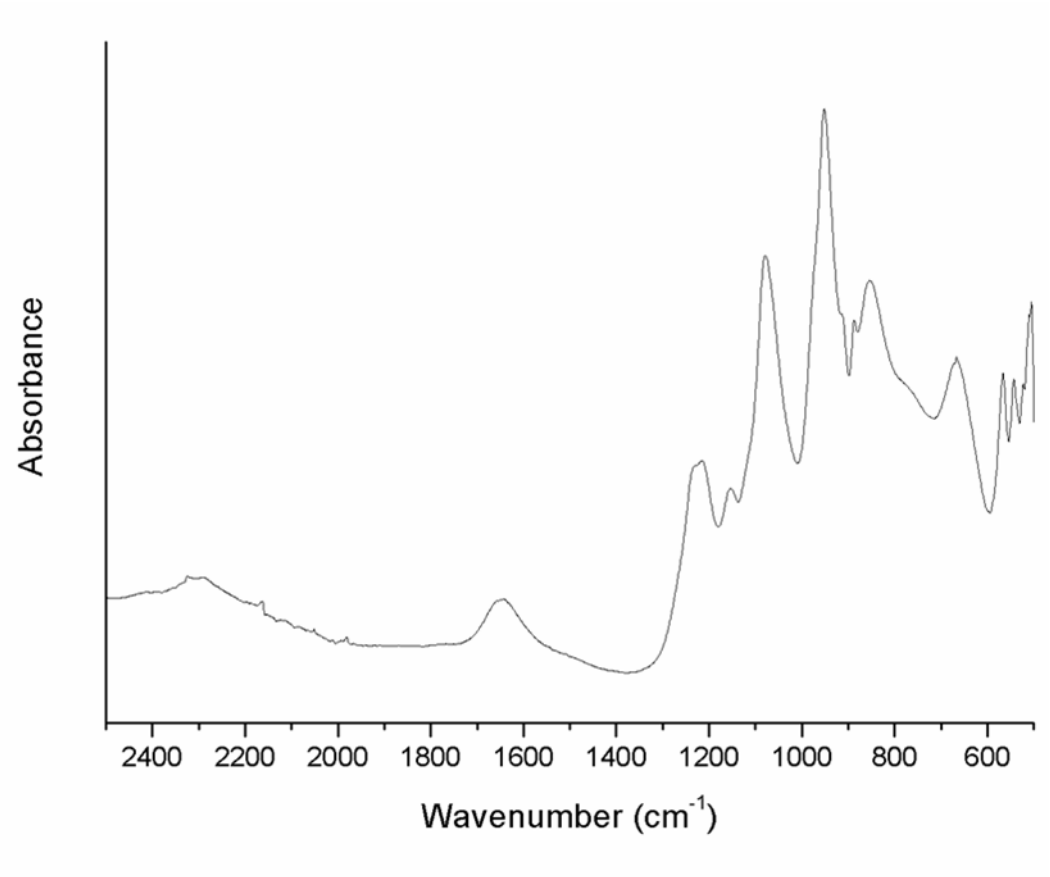

Figure 32 FTIR spectrum of $Ca(H_2PO_4)_2$ powder as purchased from Sigma Aldrich.

The ^{31}P MAS-NMR spectrum (Figure 31) of the $Ca(H_2PO_4)_2$ from Sigma-Aldrich shows the presence of three chemical shifts at -4.6, -1.4 and -0.2 ppm. The diffraction pattern (Figure 30) for the $Ca(H_2PO_4)_2$ powder shows the presence of $Ca(H_2PO_4)_2.H_2O$ only, referenced from ICDD reference code: 00-009-0347. Figure 32 shows FTIR results from the $Ca(H_2PO_4)_2$ starting powder. Bands are present at 1657, 1211, 1168, 1095, 950, 862, 686, 559 and 551 cm^{-1}.

6.2 Discussion

6.2.1 Glass Design & Synthesis

Three series of glasses were designed to investigate the change in glass composition upon the cement properties. The three series investigated addition of P_2O_5, CaF_2 and calcium to sodium ratio. In all glass compositions

the network connectivity was maintained at 2.00 in order to maintain the same Q structure within the glass network. The P_2O_5 series (QMNWKPaG01-05) ranged from 0.00 mol% to 8.00 mol% of P_2O_5 content increasing in 2.00 increments. The analysis of the glasses showed these glasses were amorphous upon production except the 8.00 mol% glass which had crystallinity present, this can be explained as increasing the phosphate content beyond 6.00 mol% has been shown to induce crystallisation (O'Donnell et al., 2009, O'Donnell et al., 2008a).

Table 13 Potential maximum % fluoride substitution of apatite produced through setting reaction of fluoride containing cement compositions. Calculated using total calcium and fluoride amounts in each cement powder mixture.

Cement Composition	% Potential F Substitution
QMNWKPaG06	48
QMNWKPaG07	95
QMNWKPaG08	60
QMNWKPaG09	72
QMNWKPaG10	84
QMNWKPaG11	107

The second series is a series investigating CaF_2 addition into the glass. The 'base' glass was the QMNWKPaG04 composition to which various amounts of CaF_2 was added between 2.5 and 4.5 mol%. The analysis of the glasses showed crystallinity was not present in any of the glass compositions. The amount of fluoride incorporated into each glass was designed so the resultant apatite phase formed in the cement forming reaction had varying levels of fluoride substitution. As Table 13 shows maximum potential fluoride substitution in any apatite produced during the cement forming reaction ranges from just below 50% to just above 100%, provided all fluoride is available for substitution.

The last series was investigated to analyse the effect of calcium to sodium ratio on the cement properties and phases formed during the setting reaction. The initial glasses were all designed with a low sodium content as sodium is not required to form the apatite. It was added in a small fraction however to reduce the melting temperature of the glass. This series was then produced to show if the hypothesis of it not being required was true and also to investigate its effect in general as it could influence the dissolution of the bioactive glass. The QMNWKPaG13 glass was designed and the sodium was substituted for calcium by 5.00 mol% through the series.

After X-ray diffraction analysis of the produced glasses, the glass with the code QMNWKPaG05 was not used to form cements and further study. This decision was taken due to the presence of a number of crystalline diffraction lines on the X-ray diffraction pattern (Figure 19). The presence of a crystalline phase in the produced glass is problematic because crystallinity is uncontrollable as the amount of crystallinity and distribution of crystals could potentially be different between batches giving unpredictability of final glass properties. Following this glass properties may be altered as crystallisation may remove certain components disproportionally. Consequentially this could affect the Q^n structure within the glass, which would in turn influence glass properties like glass dissolution behaviour. Ultimately any change in cement properties from samples produced from this glass may be due to the presence of crystallinity rather than the systematic change through the series.

Whilst making cement pastes and setting them within the moulds all glass compositions successfully set to form a cement block. However cements produced through the reaction of glasses QMNWKPaG01 and QMNWKPaG02 broke apart upon immersion in Tris buffer solution. Consequently these compositions were not studied in immersion.

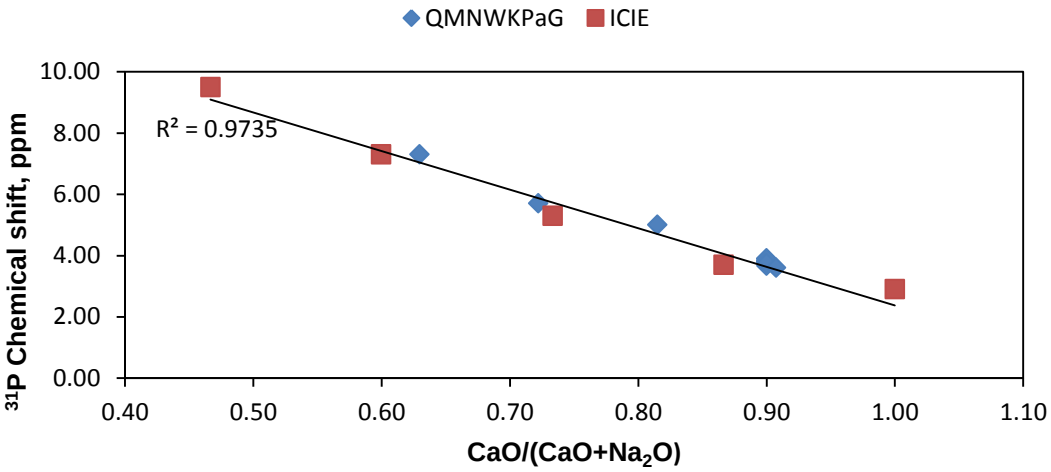

Figure 33 ^{31}P chemical shift position of all glass compositions produced in this study plotted against CaO/(CaO+Na_2O) of the respective glass compositon. Also included are the same values for an ICIE series from (Elgayar et al., 2005). Plotted with line of best fit with correlation coefficient (R^2).

Figure 33 is a plot of the ^{31}P chemical shift of the glasses produced for this project plotted against CaO/(CaO+Na_2O) value. It is known that due to the equal partitioning of sodium and calcium in bioactive glasses an alteration in the ratio of these two components alters the chemical environment of the phosphorus atoms which in turn affects the chemical shift proportionally (Elgayar et al., 2005). The results of this study were compared against another series of similar bioactive glasses and showed an almost identical trend (Elgayar et al., 2005). The reason for this analysis was to provide partial validation that the correct glass composition was produced as it allows

the assessment of the levels of calcium and sodium within the glasses and would identify any glass compositions which did not have their designed amounts.

The glasses with identical $CaO:Na_2O$ showed almost identical positions on the plot. This indicates the correct $CaO:Na_2O$ is present in the glasses made as to what was designed. This is also validated by the close correlation to the comparative ICIE glass series which was a range of bioactive glasses of altering $CaO:Na_2O$ in the glass. Whilst the majority of glasses produced in the project had a fixed $CaO:Na_2O$, three glasses were made with increasing sodium contents which are also plotted on the graph. These results also match the trend seen in the comparative ICIE glass series and have an R^2 of 0.985 giving high confidence that the correct glass compositions were produced.

From previous studies of the phosphate environment in bioactive glasses it is known that the phosphate within the glass exists as an orthophosphate (Brauer et al., 2008). These bioactive glasses are considered to be phase separated between the silicate and phosphate phases and the associated cations that charge balance the phosphate ions are calcium and sodium ions (Elgayar et al., 2005). It is also known that the distribution of calcium and sodium ions is not favoured in either phase. The distribution then matches that which is put in the glass during making. It has also been shown that a change in the ratio of calcium to sodium affects the shielding on the phosphorus atom which in turn affects the chemical shift in the ^{31}P MAS-NMR. The change in chemical shift is proportional to the ratio of calcium and

sodium in the glass (Elgayar et al., 2005). This allows a method of partial validation that the glass compositions have been correctly produced.

6.2.2 $Ca(H_2PO_4)_2$

The analysis of the $Ca(H_2PO_4)_2$ starting powder shows different phases between the two techniques used to analyse the samples. The X-ray diffraction pattern shows only the presence of $Ca(H_2PO_4)_2.H_2O$, whereas the ^{31}P MAS-NMR spectra shows the presence of $Ca(H_2PO_4)_2$ and a small fraction of DCPA ($CaHPO_4$). The discrepancy between these two results may be due to reaction with moisture in the air whilst in storage. The presence of the hydrated form of the calcium phosphate salt ($Ca(H_2PO_4)_2.H_2O$) would affect the expected calcium to phosphorus ratio Ca/P as the reagents were weighed on assumption the reagent was pure $Ca(H_2PO_4)_2$ causing an increase in the overall Ca/P of the cement powder mixture with the presence of either ($Ca(H_2PO_4)_2.H_2O$) or DCPD.6.3 Experimental Cement Compositions

Based on the results from the glass analysis not all compositions were analysed as cement compositions for various reasons previously alluded to. The following section compares all the analysis performed on the cement samples from all glass compositions studied. The cements were split into two distinct series based upon there glass compositions that were studied. These two series being the fluoride containing cement series and the calcium sodium cement series. The fluoride containing cement series contains all glasses that contain fluoride QMNWKPaG06-11 and also glass QMNWKPaG04 which does not contain fluoride but has the ratios of all the other components the same as the fluoride containing compositions thus acting as a fluoride-free ‘base’ glass. The calcium sodium cement series

contains the rest of the cement compositions and have all components the same (silica and phosphate) and only alter the various calcium and sodium contents through the series.

6.4 Glass Structure

6.4.1 Calcium/Sodium Series Glasses

As the calcium content increases within this glass series the glass transition temperature (Tg) was shown to decrease. This would influence the free volume within the glass structure leading to an increase in free volume as the Tg decreases. One would then anticipate this to equate to an alteration of the dissolution behaviour of the glasses upon immersion in solution, With increasing free volume within the glass it would be expected to degrade faster and release Ca^{2+}, Na^{+} and PO_4^{3-} faster than a preceding glass in the series with a lower free volume.

The ^{31}P MAS NMR results show that like results seen previously (Brauer, 2011) the phosphate element in the glass exists as orthophosphate, with calcium and sodium ions acting to charge balance these ions.

6.4.2 Fluoride Containing Glass Series

Similarly to the calcium/sodium glass series there is a change in Tg through the fluoride containing series; as fluoride is increased the Tg decreases. Similarly to the previous series this allows the prediction of the degradation behaviour and ion release of the glasses in question. With the increase in fluoride causing the decrease in Tg, the free volume increases in the compositions as fluoride concentration is increased. From this it would be

predicited that those glasses with increasing fluoride contents will derade faster, releasing their associated ions.

Chapter 7: Calcium/Sodium Glass Cement Series Results & Discussion

7.1 Results

7.1.1 X-ray Diffraction

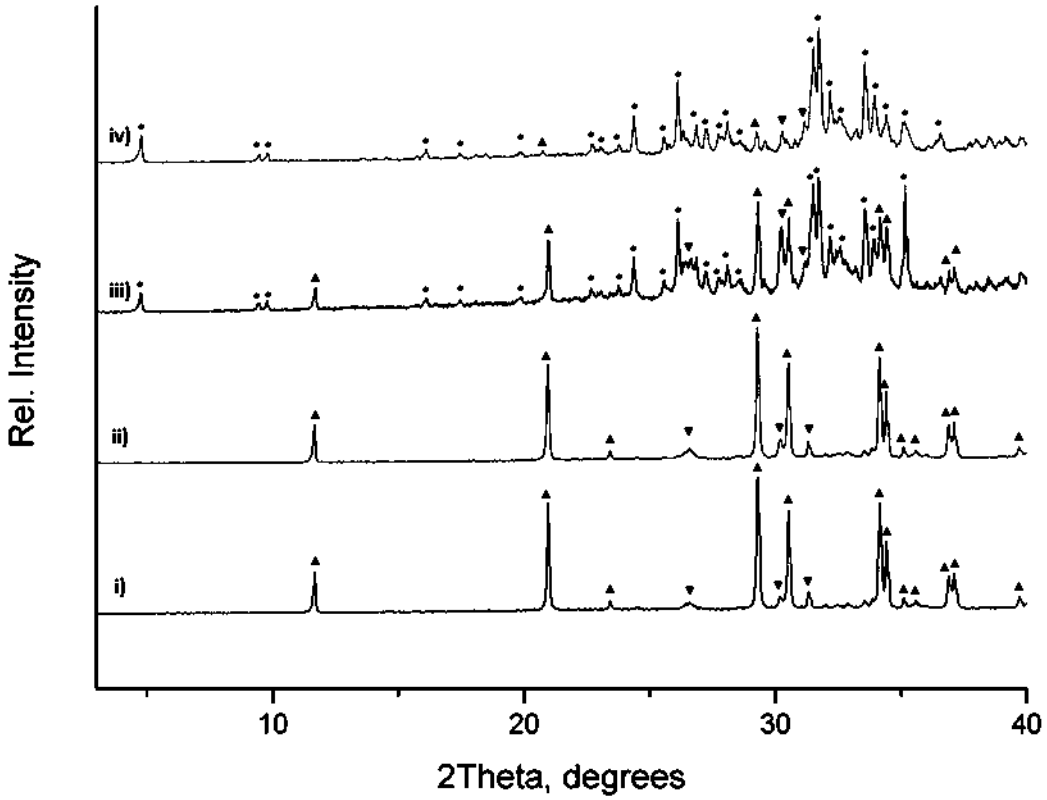

Figure 34 X-ray diffraction patterns of cement composition produced from glass QMNWKPaG03 after immersion in Tris buffer solution for (i) 1 hour, (ii) 1 day, (iii) 7 days and (iv) 28 days. ▲ – DCPD; ▼ – DCPA; ● – Octacalcium Phosphate.

Figure 34 shows the XRD results for cements made from the reaction between $Ca(H_2PO_4)_2$ and QMNWKPaG03 glass powder and immersed in Tris buffer for 1 hour, 1 day, 7 days and 28 days. The one hour pattern has no lines for the $Ca(H_2PO_4)_2$ starting powder, demonstrating it is no longer

present, indicating full dissolution of the salt before one hour[3]. At one hour two phases identifiable on the XRD are DCPD ($CaHPO_4.2H_2O$) and DCPA ($CaHPO_4$). At one day the only phases present are DCPD and DCPA. At 7 days DCPD and DCPA are still present but octacalcium phosphate ($Ca_8(HPO_4)_2(PO_4)_4.5H_2O$, OCP) has also formed. The diffraction peak at 4.7 $^{\circ}2\theta$ is indicative of OCP and is the primary difference between the diffraction patterns of apatite and OCP due to having pseudomorphic crystal structures. At 28 days the DCPD and DCPA are still present on the XRD pattern along with OCP, though the relative intensities of their respective diffraction lines have decreased relative to OCP.

[3] For the starting salt $Ca(H_2PO_4)_2$ is used to describe this as this was purchased from Sigma-Aldrich. However the results from both X-ray diffraction and ^{31}P MAS-NMR disagree with the phase present as either $Ca(H_2PO_4)_2$ or $Ca(H_2PO_4)_2.H_2O$ was identified. The term $Ca(H_2PO_4)_2$ was used though it should be noted that it could be either $Ca(H_2PO_4)_2$ or $Ca(H_2PO_4)_2.H_2O$. Additionally the result written here for the dissolution of the starting salt was the same for all X-ray diffraction salts at one hour.

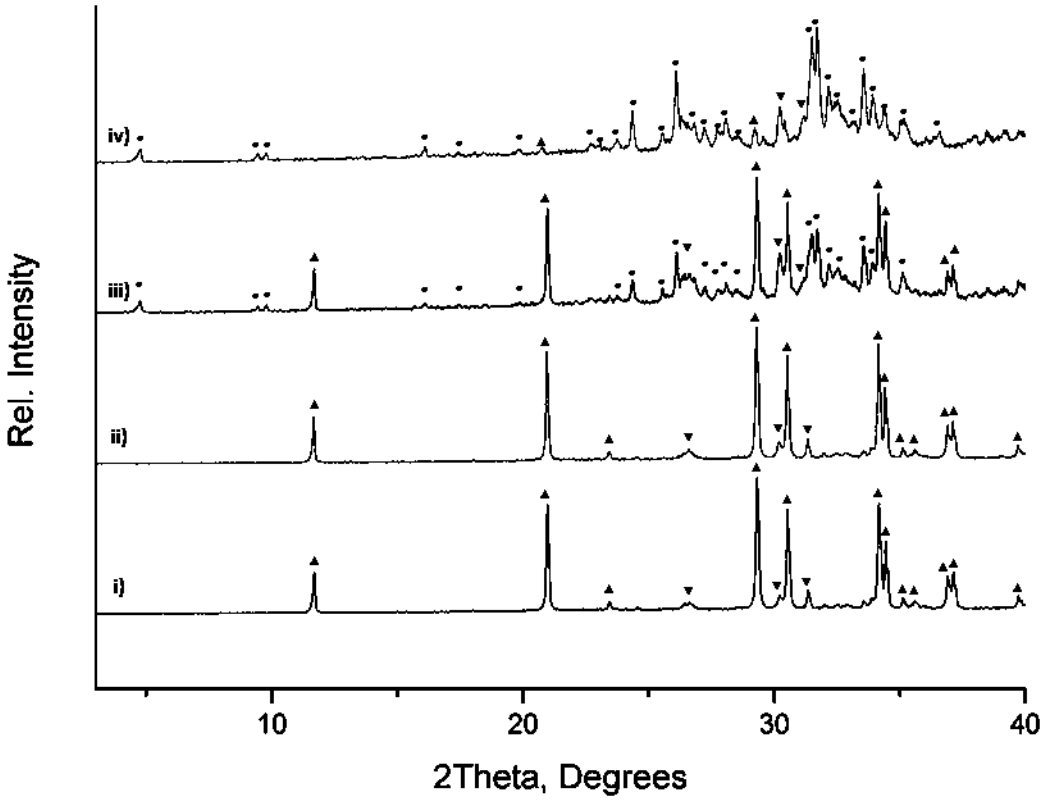

Figure 35 X-ray diffraction patterns of cement composition produced from glass QMNWKPaG13 after immersion in Tris buffer solution for (i) 1 hour, (ii) 1 day, (iii) 7 days and (iv) 28 days. ▲ – DCPD; ▼ – DCPA; ● – Octacalcium Phosphate.

Figure 35 shows the XRD results for QMNWKPaG13 cements at 1 hour, 1 day, 7 days and 28 days. DCPD is the only crystalline phase at one hour immersion. After one day the only crystalline phase present is still DCPD. OCP is formed after 7 days immersion indicated by the peak at 4.7 ˚2θ; DCPD is still present in the cement phase. After 28 days DCPD is no longer present and the crystalline phase is now totally OCP.

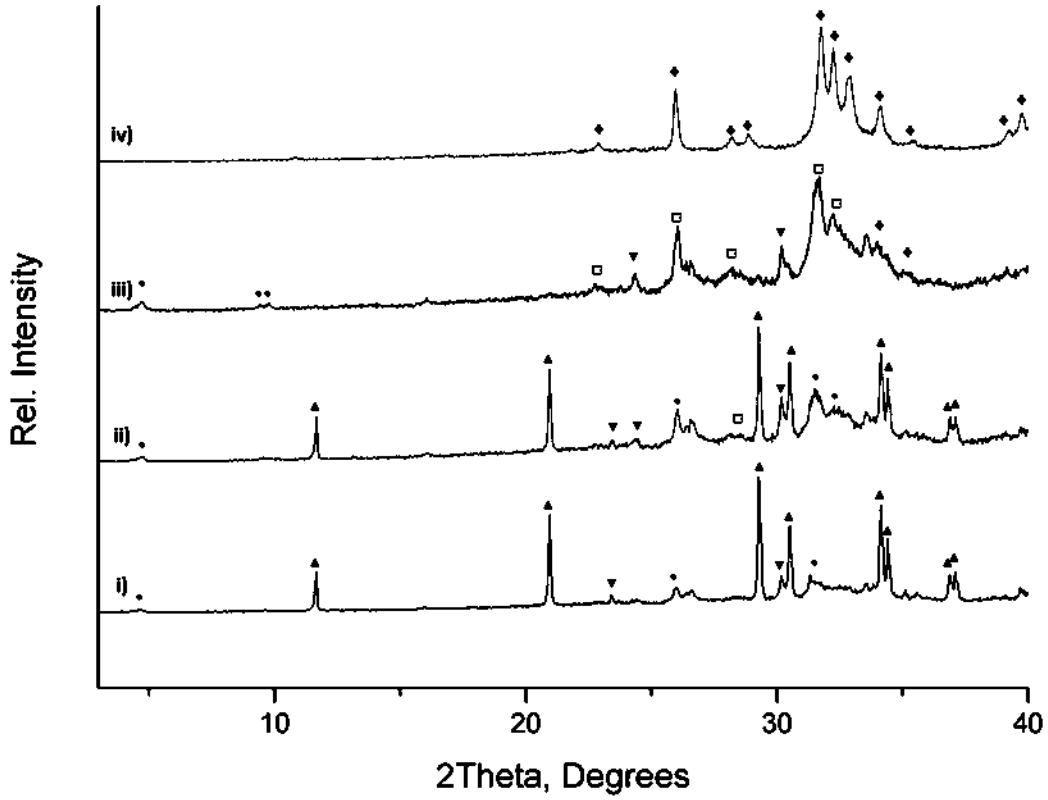

Figure 36 X-ray diffraction patterns of cement composition produced from glass QMNWKPaG14 after immersion in Tris buffer solution for (i) 1 hour, (ii) 1 day, (iii) 7 days and (iv) 28 days. ▲ – DCPD; ▼ – DCPA; ● – Octacalcium Phosphate; □ indistinguishable OCP/Hydroxyapatite.

Figure 36 shows the XRD results for QMNWKPaG14 cements at 1 hour, 1 day, 7 days and 28 days. DCPD is present at one hour as is a phase identified as OCP due to the low intensity broad peak at 4.7 ˚2θ. At one day the OCP peak is slightly more intense potentially indicating an increase in the fraction of the OCP phase; DCPD is again present at this time point. After seven days the DCPD peaks are no longer present indicating it has reacted to OCP, which is also identified. At 28 days the 4.7 ˚2θ diffraction line is absent, indicating the OCP phase is no longer present and that in the cement crystalline phase is apatitic.

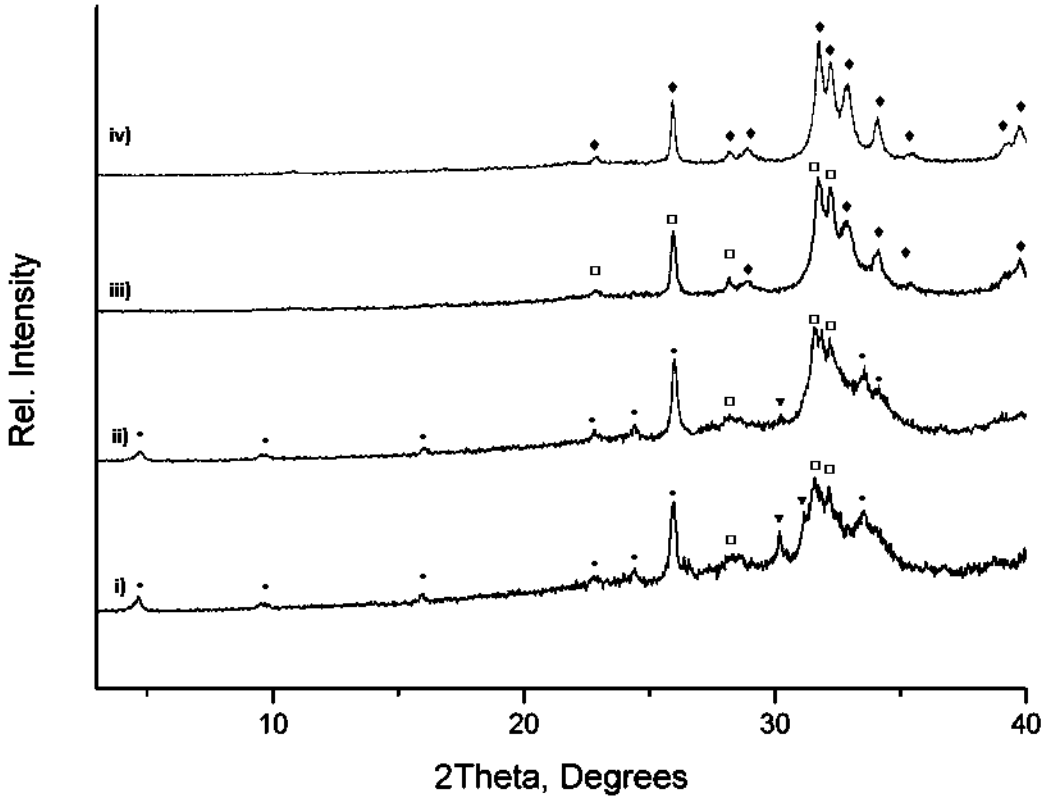

Figure 37 X-ray diffraction patterns of cement composition produced from glass QMNWKPaG15 after immersion in Tris buffer solution for (i) 1 hour, (ii) 1 day, (iii) 7 days and (iv) 28 days. ▲ – DCPD; ▼ – DCPA; ● – Octacalcium Phosphate; □ indistinguishable OCP/Hydroxyapatite; ♦ Apatite.

Figure 37 shows the XRD results for QMNWKPaG15 cements at 1 hour, 1 day, 7 days and 28 days. At one hour DCPD phase is seen as is a phase identified as OCP due to the low intensity peak at 4.7 ˚2θ. At one day the major cement phase is OCP. After seven days the OCP is no longer present, indicated by absence of the the diffraction peak at 4.7 ˚2θ; the cement phase is apatite here. After 28 days in Tris buffer solution the cement phase is apatite.

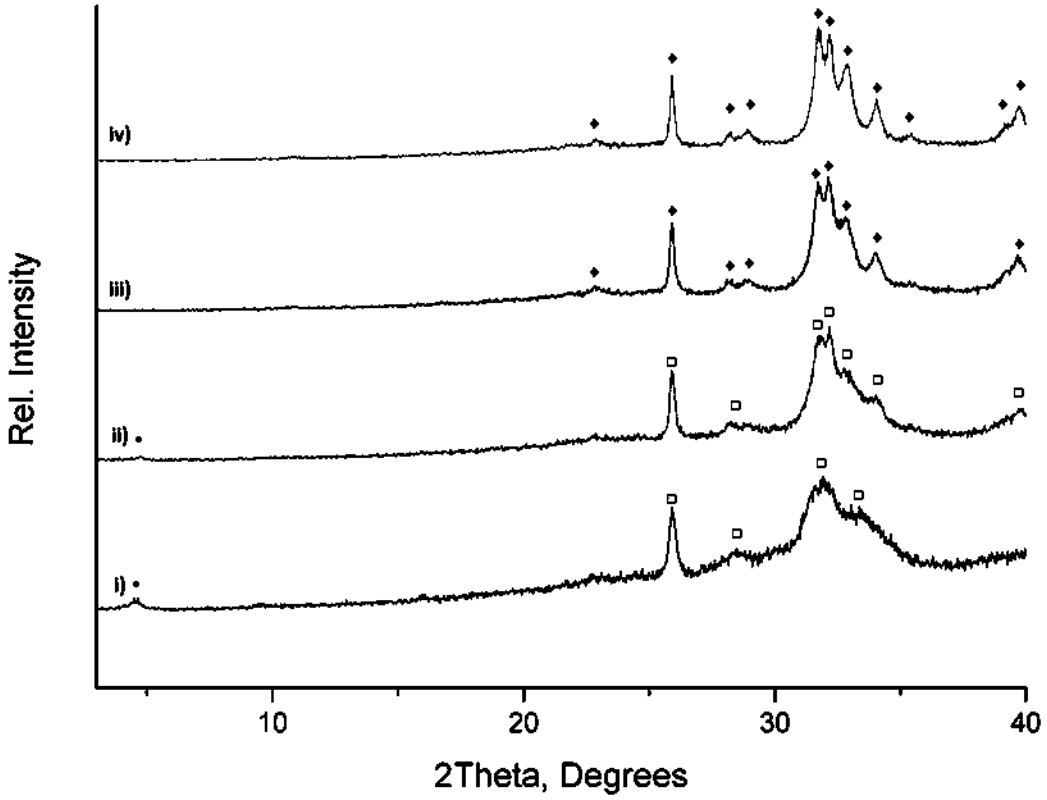

Figure 38 X-ray diffraction patterns of cement composition produced from glass QMNWKPaG16 after immersion in Tris buffer solution for (i) 1 hour, (ii) 1 day, (iii) 7 days and (iv) 28 days. ● – Octacalcium Phosphate; □ indistinguishable OCP/Hydroxyapatite; ♦ Apatite.

Figure 38 shows the XRD results for QMNWKPaG16 cements at 1 hour, 1 day, 7 days and 28 days. At one hour the cement phase is OCP indicated by the peak at 4.7 ˚2θ. At one day this peak is less intense indicating that OCP is transforming to apatite; meaning the cement phase is most likely an OCP and apatite mixture. At both seven days and 28 days the crystalline phase within the cement is apatite.

7.1.2 ^{31}P Magic Angle Spinning Nuclear Magnetic Resonance

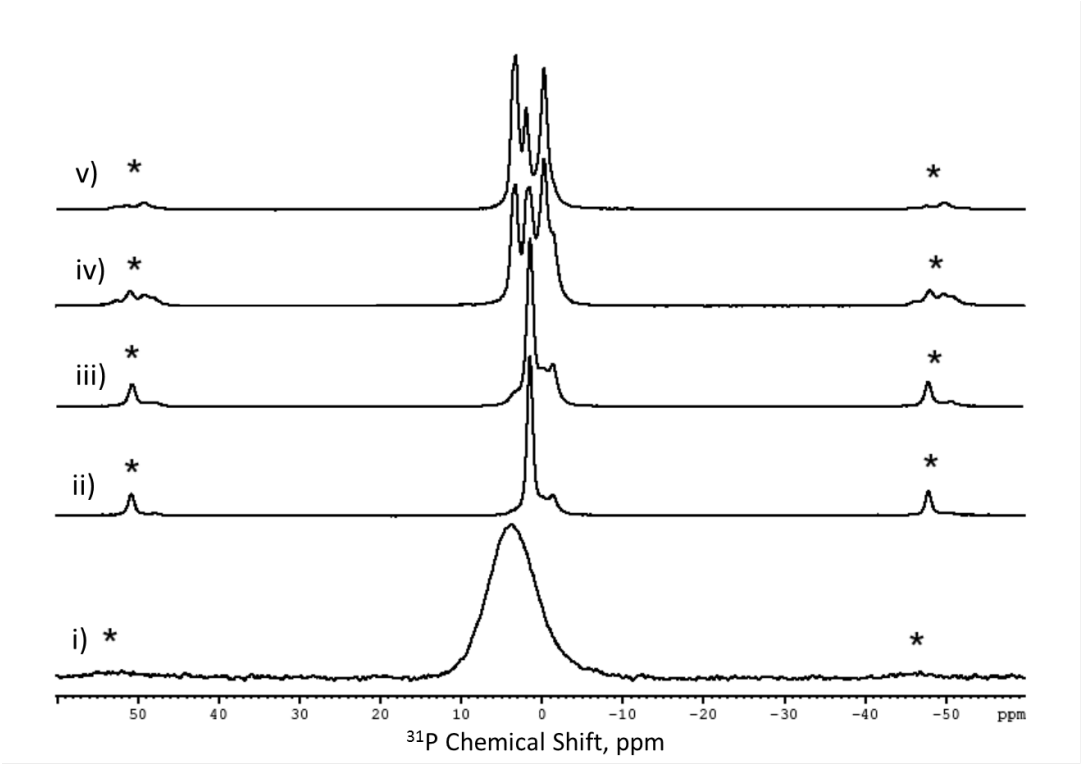

Figure 39 ^{31}P MAS-NMR spectra of the starting glass powder and Tris immersed cement samples in the cement system produced from glass QMNWKPaG03. Showing (i) QMNWKPaG03 initial glass powder; (ii) 1 hour; (iii) 1 day; (iv) 7 days; (v) 28 days.

Figure 39 shows the ^{31}P MAS-NMR results for QMNWKPaG03 glass and QMNWKPaG03 cements at 1 hour, 1 day, 7 days and 28 days. At 1 hour the dominant peak at 1.4 ppm indicates that DCPD is the primary phase. A small fraction of the signal at -1.4 and -0.2 ppm indicates that DCPA is also present, but in a small fraction. At 1 day both DCPD and DCPA are still the only phases in the sample. At 7 days chemical shifts at -0.2, 2.0, 3.2 and 3.6 are present indicative of the formation of OCP as well as resonances indicating DCPD 1.4 ppm and DCPA -1.4 and -0.2 ppm. At 28 days peaks at -0.2, 2.0, 3.2 and 3.6 are present showing the formation of OCP. Resonances indicating DCPD and DCPA are not present, indicating conversion of these phases to OCP.

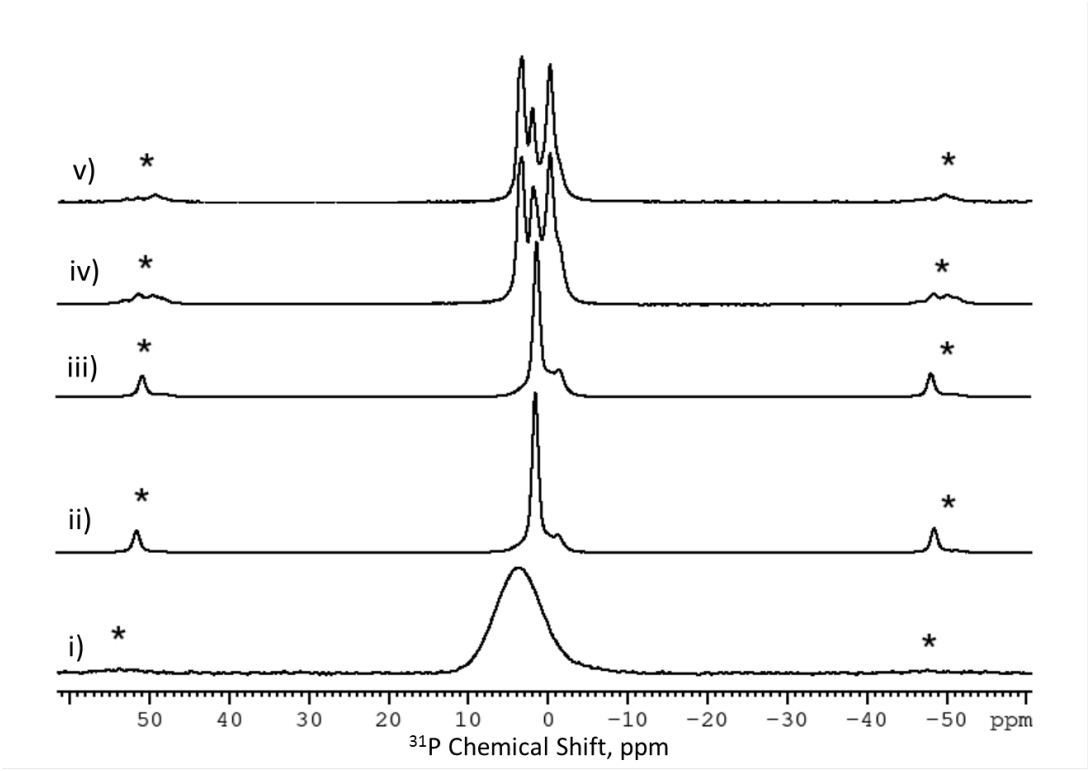

Figure 40 ^{31}P MAS-NMR spectra of the starting glass powder and Tris immersed cement samples in the cement system produced from glass QMNWKPaG13. Showing (i) QMNWKPaG13 initial glass powder; (ii) 1 hour; (iii) 1 day; (iv) 7 days; (v) 28 days.

Figure 40 shows the ^{31}P MAS-NMR results for QMNWKPaG13 glass and QMNWKPaG13 cements at 1 hour, 1 day, 7 days and 28 days. At 1 hour DCPD is the primary phase present at 1.4 ppm, DCPA is also present -1.4 and -0.2 ppm but in a small fraction. At 1 day both DCPD and DCPA are still present. At 7 days chemical shift at -0.2, 2.0, 3.2 and 3.6 are present indicative of the formation of OCP as well as peaks indicating DCPD 1.4 ppm and DCPA -1.4 ppm. At 28 days peaks at -0.2, 2.0, 3.2 and 3.6 are present showing the formation of OCP. Peaks indicating DCPD and DCPA are not present, indicating conversion of these phases to OCP.

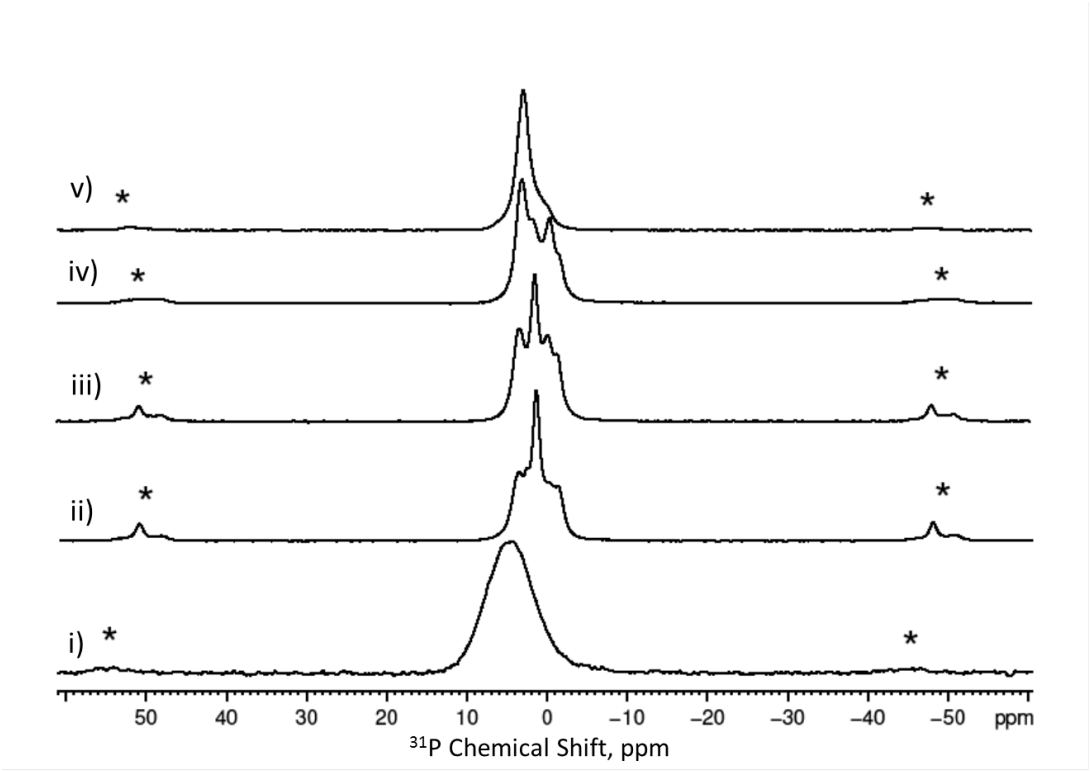

Figure 41 ^{31}P MAS-NMR spectra of the starting glass powder and Tris immersed cement samples in the cement system produced from glass QMNWKPaG14. Showing (i) QMNWKPaG14 initial glass powder; (ii) 1 hour; (iii) 1 day; (iv) 7 days; (v) 28 days.

Figure 41 shows the ^{31}P MAS-NMR results for QMNWKPaG14 glass and QMNWKPaG14 cements at 1 hour, 1 day, 7 days and 28 days. At 1 hour there is a sharp resonance at 1.4 ppm that shows the presence of DCPD; there is a clear resonance at 3.6 ppm and low intensity chemical shift at 3.2 ppm which suggests the presence of OCP but this is not certain as the four OCP peaks, at -0.2, 2.0, 3.2 and 3.6 ppm (Tseng et al., 2004), cannot each easily be distinguished. Also at 1 hour is a shoulder on the left of the broad peaks at -1.4 and -0.2 ppm which suggests the formation of DCPA, consistent with other cement compositions. After 1 day there are four chemical shift at -1.4, -0.2, 1.4 and 3.3 ppm. After 7 days there are chemical shift of OCP at 3.6, 3.2, 2.0, and -0.2 and also a chemical shift at 1.4 of DCPD along with resonances at -1.4 and -0.2 for DCPA. Finally after 28 days

immersion the cement sample there are two chemical shift at 2.9 and -0.2 ppm.

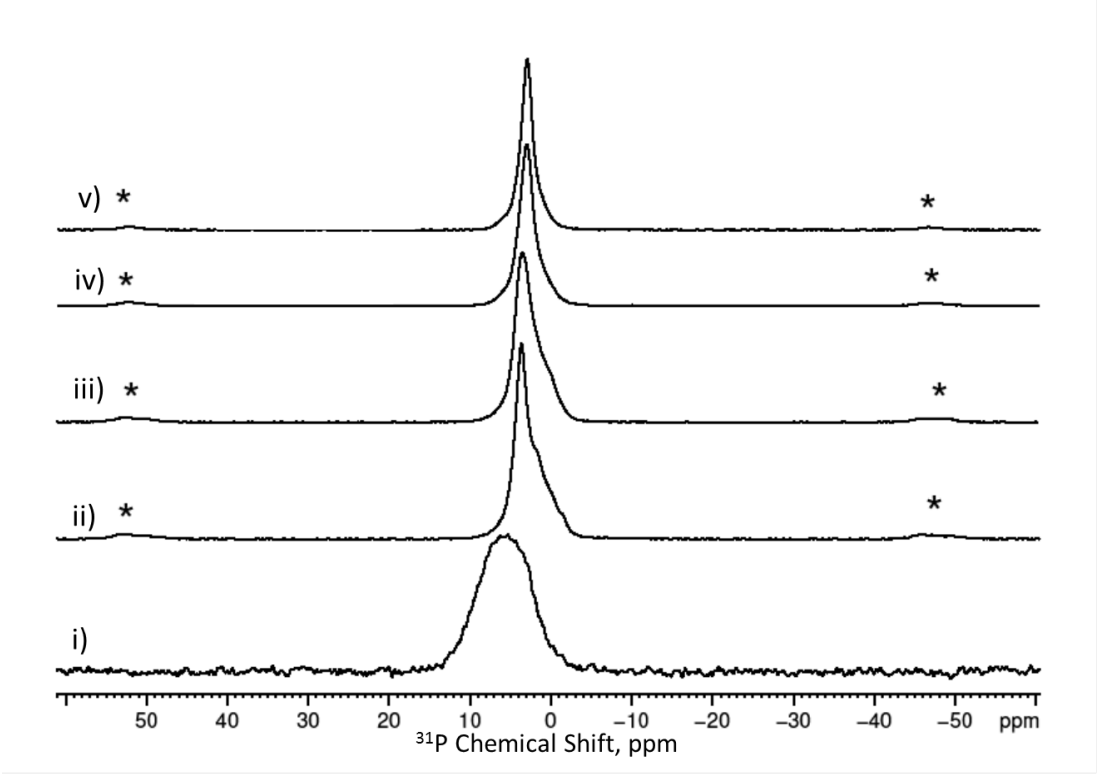

Figure 42 ^{31}P MAS-NMR spectra of the starting glass powder and Tris immersed cement samples in the cement system produced from glass QMNWKPaG15. Showing (i) QMNWKPaG15 initial glass powder; (ii) 1 hour; (iii) 1 day; (iv) 7 days; (v) 28 days.

Figure 42 shows the ^{31}P MAS-NMR results for QMNWKPaG15 glass and QMNWKPaG15 cements at 1 hour, 1 day, 7 days and 28 days. The 1 hour sample has chemical shift at -1.4, -0.2, 2.0 and 3.6 assigned to DCPA (-1.4 and -0.2 ppm), DCPD (2.0 ppm) and apatite (3.6 ppm). The 1 day sample has chemical shift at -0.2, 1.9, and 3.4 ppm of OCP. The 7 and 28 day samples have one resonance at 2.9 ppm assigned to apatite.

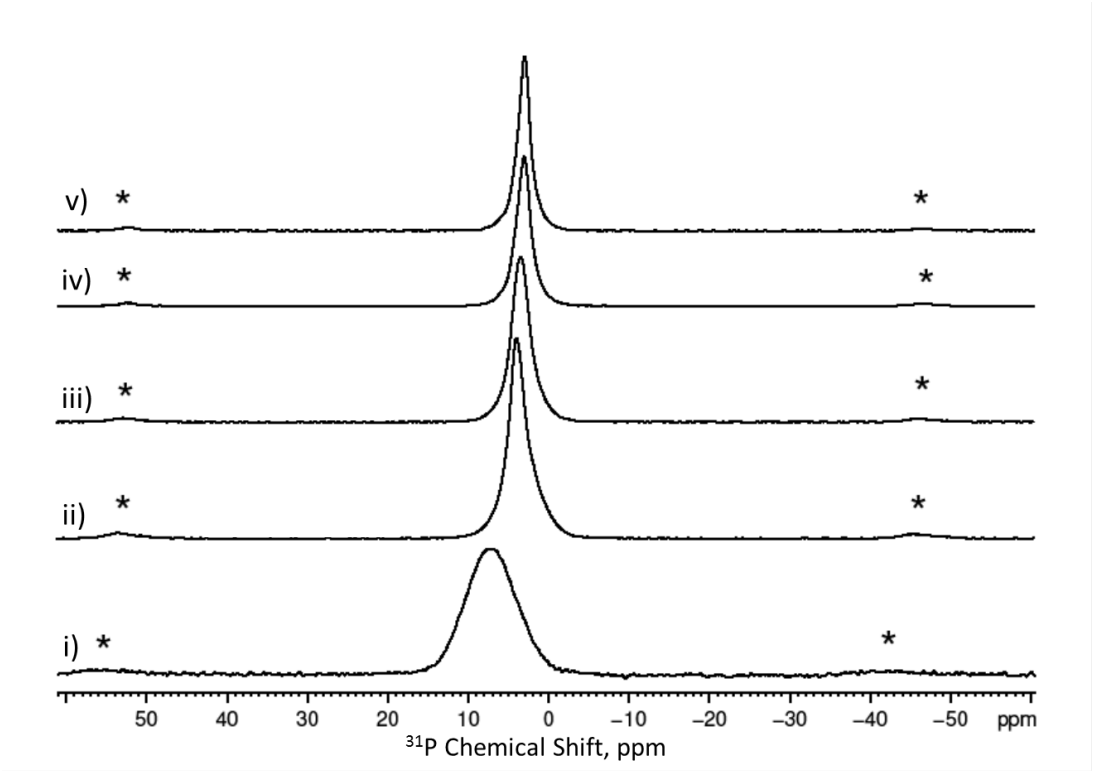

Figure 43 ^{31}P MAS-NMR spectra of the starting glass powder and Tris immersed cement samples in the cement system produced from glass QMNWKPaG16. Showing (i) QMNWKPaG16 initial glass powder; (ii) 1 hour; (iii) 1 day; (iv) 7 days; (v) 28 days.

Figure 43 shows the ^{31}P MAS-NMR results for QMNWKPaG16 glass and QMNWKPaG16 cements at 1 hour, 1 day, 7 days and 28 days. The 1 hour sample has one chemical shift at 4.0 ppm assigned to apatite based on X-ray diffraction results. Similarly the 1 day sample only has one chemical shift at 3.2 ppm assigned to apatite. The 7 and 28 day samples each have one chemical shift at 3.0 ppm assigned, as the 1 day sample, to apatite.

7.1.3 Fourier Transform Infrared Spectroscopy

The following FTIR spectra show the FTIR results of all cement compositions studied. The full spectrum of each sample has been separated so that the scan regions from 500-2000 cm^{-1} for each immersion time are together and the scan regions from 2500-4000 cm^{-1} are together. This was done to make viewing the bands on each spectrum easier. The assignments for each

phase were done using the references identified in the literature review for DCPD (Elliott, 1994), octacalcium phosphate (Fowler et al., 1993) and hydroxyapatite (Elliott, 1994).

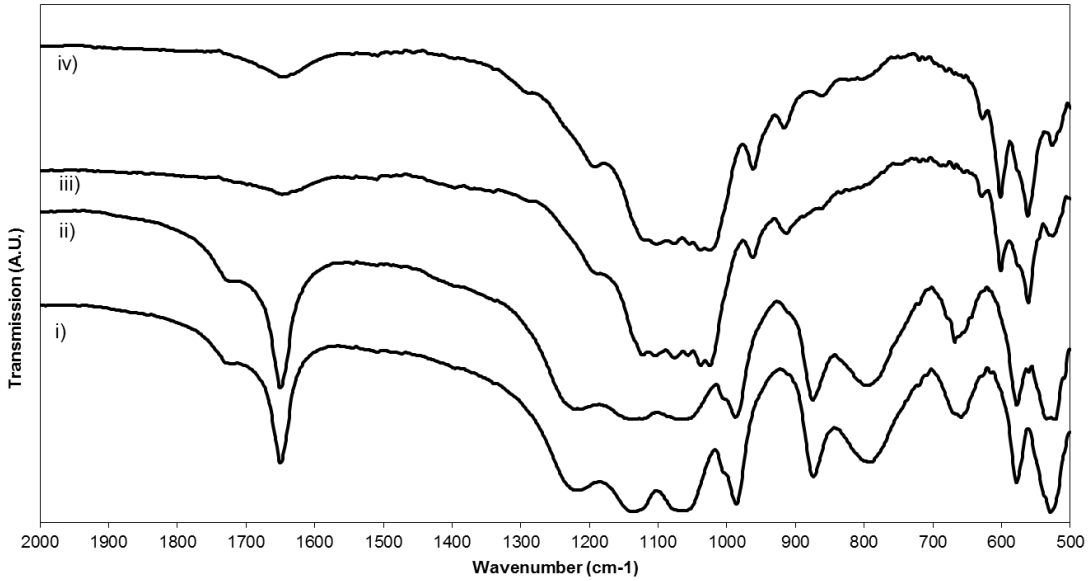

Figure 44 Fourier transform infrared spectra of cement composition QMNWKPaG03 at (i) 1 hour, (ii) 1 day, (iii) 7 days, and (iv) 28 days immersion time in Tris buffer solution, plotted between 500 to 2000 wavenumber cm^{-1}.

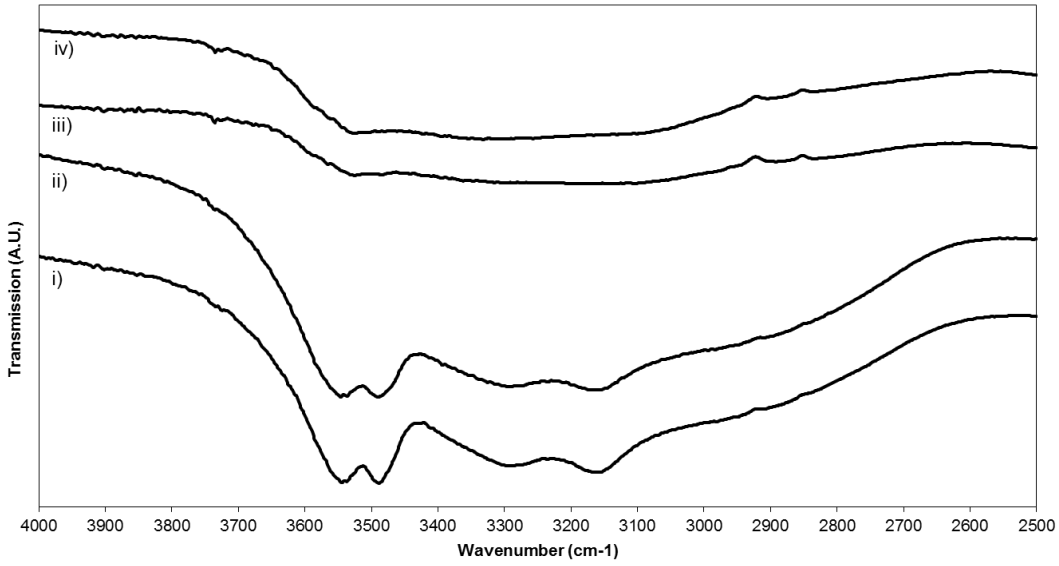

Figure 45 Fourier transform infrared spectra of cement composition QMNWKPaG03 at (i) 1 hour, (ii) 1 day, (iii) 7 days, and (iv) 28 days immersion time in Tris buffer solution, plotted between 2500 to 4000 wavenumber cm^{-1}.

Table 14 FTIR bands and their respective assignments of cement samples produced from glass QMNWKPaG03 after immersion in Tris buffer solution for 1 hour, 1 day, 7 days and 28 days.

Wavenumber (cm^{-1})	Assignment	1 Hour	1 Day	7 Day	28 Day
519	HPO_4 Bending	-	-	√	√
521	PO Bending	√	√	-	-
558	PO_4 Bending	-	-	√	√
574	PO Bending	√	√	√	√
598	PO_4 Bending	-	-	√	√
617	PO_4 Bending	-	-	√	√
649	PO Bending	√	√	-	-
778	H_2O Liberation	√	√	-	-
868	P-O(H) Stretching	√	√	-	-
905	HPO_4(6) [P-(OH)] Stretching	-	-	√	√
956	PO_4 Stretching	-	-	√	√
982	P-O Stretching	√	√	-	-
997	P-O(H) Stretching	√	√	-	-
1048	PO Stretching	√	√	-	-
1123		√	√	-	-
1181	HPO_4 Stretching	-	-	√	√
1207	O-H In-plane Bending	√	√	-	-
1645	H_2O Bending	√	√	√	√
1713	Overtone of 868 band - 2 x 868 = 1736	√	√	-	-
3146	OH Stretching of Water	√	√	-	-
3276	OH Stretching of Water	√	√	-	-
3477	OH Stretching of Water	√	√	-	-
3533	OH Stretching of Water	√	-	-	-

Figures 44 and 45 show the FTIR spectra of cement composition QMNWKPaG03 at 1 hour, 1 day, 7 days and 28 days. At 1 hour and 1 day there are PO bending and stretching bands at 558, 573, 599, 650, and 1050 cm^{-1}. For these two spectra there are also identical bands at 868 and 997 cm^{-1} of P-O(H) Stretching groups. Finally these two spectra have bands denoting the presence of structural water molecules at 1207, 1645, 3146,

3276, 3477 and 3533 cm^{-1}. At 7 days and 28 days the spectra are virtually identical and much reduced compared to the two previous time points. There are PO bending and stretching groups at 558, 587, 598, 617 and 956 cm^{-1}. Additionally there are HPO_4 bending and stretching groups at 518, 848, 910 and 1181 cm^{-1} respectively as well as a H_2O bending band at 1630 cm^{-1}.

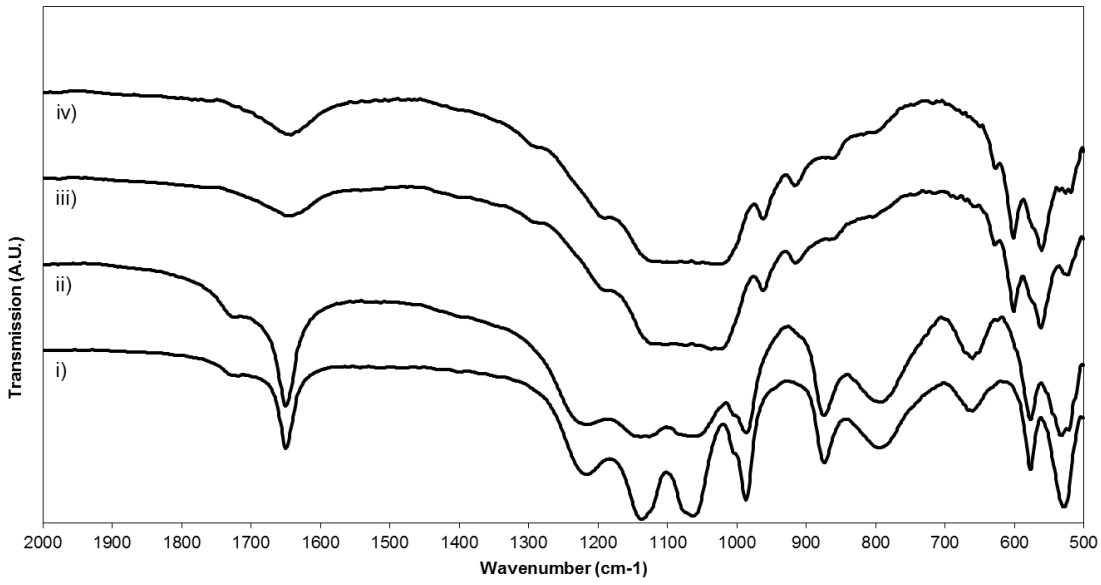

Figure 46 Fourier transform infrared spectra of cement composition QMNWKPaG13 at (i) 1 hour, (ii) 1 day, (iii) 7 days, and (iv) 28 days immersion time in Tris buffer solution, plotted between 500 to 2000 wavenumber cm^{-1}.

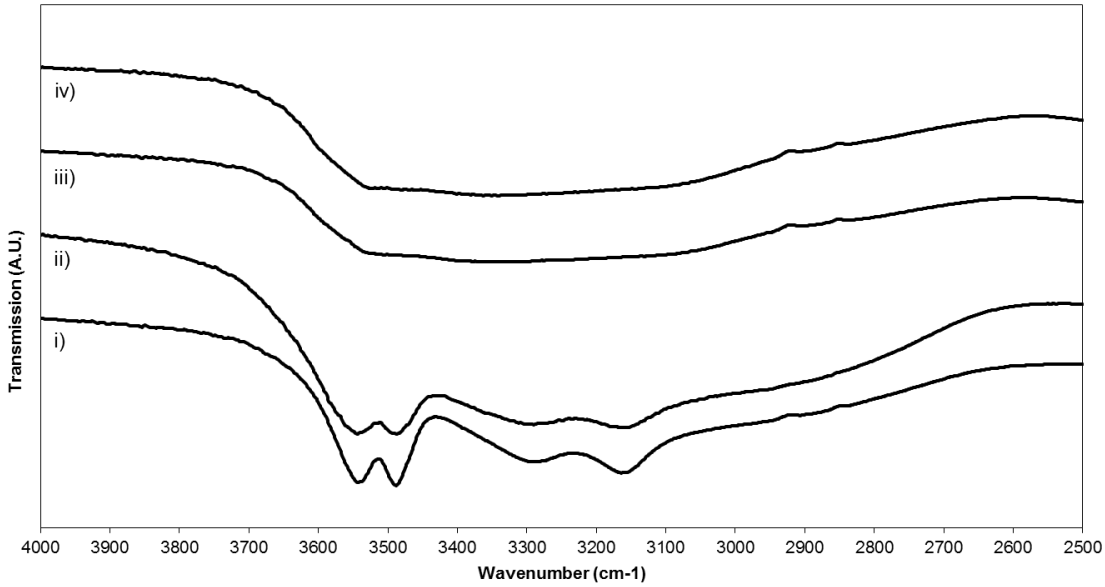

Figure 47 Fourier transform infrared spectra of cement composition QMNWKPaG13 at (i) 1 hour, (ii) 1 day, (iii) 7 days, and (iv) 28 days immersion time in Tris buffer solution, plotted between 2500 to 4000 wavenumber cm^{-1}.

Table 15 FTIR bands and their respective assignments of cement samples produced from glass QMNWKPaG13 after immersion in Tris buffer solution for 1 hour, 1 day, 7 days and 28 days.

Wavenumber (cm^{-1})	Assignment	1 Hour	1 Day	7 Day	28 Day
522	PO Bending	√	√	√	-
558	PO Bending	-	-	√	√
574	PO Bending	√	√	-	-
598	PO Bending	-	-	√	√
615	PO Bending	-	-	√	√
648	PO Bending	√	√	-	-
781	H_2O Liberation	√	√	-	√
851	HPO_4 Stretching	-	-	-	√
868	P-O(H) Stretching	√	√	-	-
905	HPO_4(6) [P-(OH)] Stretching	-	-	√	√
956	PO Stretch	-	-	√	-
983	P-O(H) Stretching	√	√	-	-
994	Unassigned	-	√	-	-
1053	PO Stretching	√	-	-	-
1124	Unassigned	√	-	-	-
1175	HPO_4 Stretch	-	-	√	√
1205	O-H In-plane Bending	√	√	-	-
1283	HPO_4 (OH in-plane bending)	-	-	-	√
1630	H_2O Bending	-	-	√	√
1644	H_2O Bending	√	√	-	-
1714	Overtone of 868 band - 2 x 868 = 1736	√	√	-	-

3150	OH Stretching of Water	√	√	-	-
3274	OH Stretching of Water	√	√	-	-
3479	OH Stretching of Water	√	√	-	-
3531	OH Stretching of Water	√	√	-	-

Figures 46 and 47 show the FTIR spectra of cement composition QMNWKPaG13 at 1 hour, 1 day, 7 days and 28 days. The 1 hour and 1 day spectra have very similar bands present, with PO bending and stretching bands at 520, 574, 648 and 1053 cm^{-1}. These two spectrum also have a P-O(H) stretching band at 868 cm^{-1}. In addition to this there are bands from water molecules at 780, 1205, 1644, 3150, 3274, 3479 and 3531 cm^{-1}. The 7 day and 28 day samples also share similar spectra, with PO bending and stretching bands at 518 (7 day only), 558, 598, 615 and 956 (7 day only) cm^{-1}. There are also bands donating HPO_4 groups in the samples at 850 (28 day only) 905, 1175 and 1283 (28 day only) cm^{-1}. Lastly each spectra has a band at 1630 cm^{-1} from bending in water molecules.

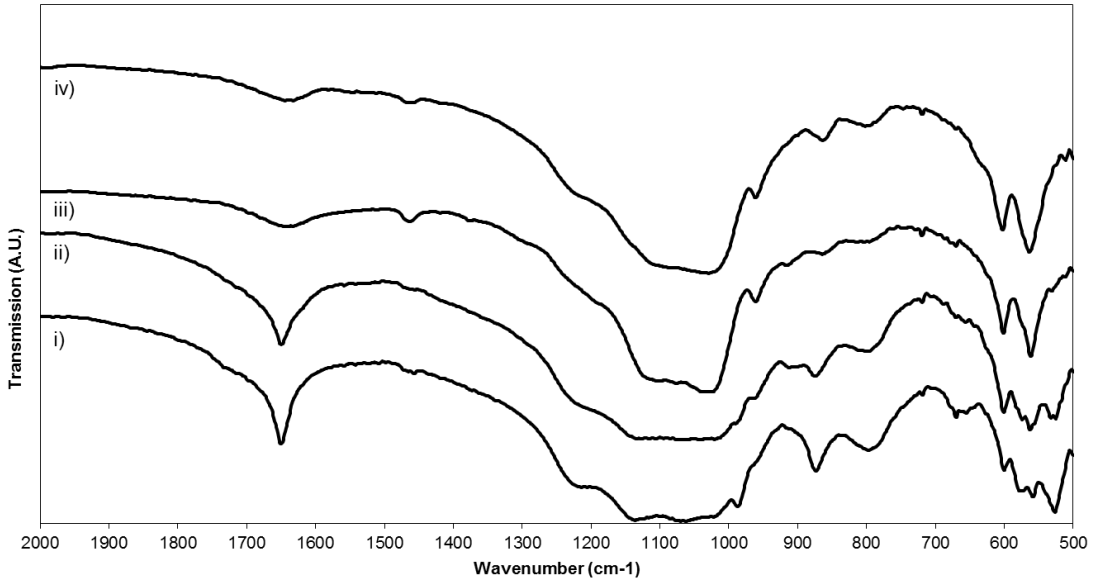

Figure 48 Fourier transform infrared spectra of cement composition QMNWKPaG14 at (i) 1 hour, (ii) 1 day, (iii) 7 days, and (iv) 28 days immersion time in Tris buffer solution, plotted between 500 to 2000 wavenumber cm^{-1}.

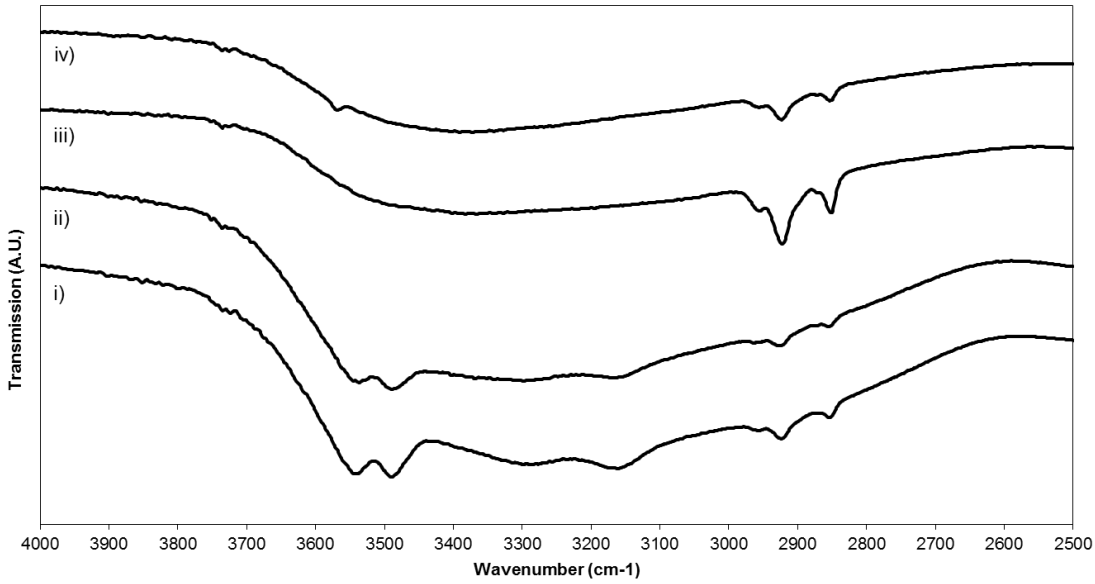

Figure 49 Fourier transform infrared spectra of cement composition QMNWKPaG14 at (i) 1 hour, (ii) 1 day, (iii) 7 days, and (iv) 28 days immersion time in Tris buffer solution, plotted between 2500 to 4000 wavenumber cm^{-1}.

Table 16 FTIR bands and their respective assignments of cement samples produced from glass QMNWKPaG14 after immersion in Tris buffer solution for 1 hour, 1 day, 7 days and 28 days.

Wavenumber (cm^{-1})	Assignment	1 Hour	1 Day	7 Day	28 Day
523	PO Bending	√	√	-	-
553	PO Bending	√	√	√	√
564	PO Bending	√	-	-	-

588	PO Bending	√	-	-	-
595	PO Bending	-	√	√	√
780	H_2O Liberation	√	√	√	√
851	P-O(H) Stretching	-	-	√	√
864	P-O(H) Stretching	√	√	-	-
900	HPO_4(6) [P-(OH)] Stretching	-	-	√	-
953	PO Stretch	-	√	√	√
982	PO Stretch	√	-	-	-
1203	HPO_4(5) [P-(OH)] Stretching	-	-	-	√
1211	O-H In-plane Bending	√	√	-	-
1464	Carbonate	-	√	√	√
1627	H_2O Bending	-	-	√	√
1644	H_2O Bending	√	√	-	-
2844	HPO_4 (OH Stretch)	√	√	√	√
2911	HPO_4 (OH Stretch)	√	√	√	√
2943	HPO_4 (OH Stretch)	√	-	√	√
3148	OH Stretching of Water	√	√	-	-
3477	OH Stretching of Water	√	√	-	-
3530	OH Stretching of Water	√	√	-	-
3556	H-bonded H_2O	-	-	-	√

Figures 48 and 49 show the FTIR spectra of cement composition QMNWKPaG14 at 1 hour, 1 day, 7 days and 28 days. The 1 hour and 1 day spectra have very similar bands present. There are PO bending and stretching bands at 523, 553, 564, 588 and 982 cm^{-1}. In addition to this there are stretching bands from HPO_4 groups at 864, 2844, 2911 and 2943 cm^{-1}. Lastly both spectra contain bands donating the presence of structural water molecules with bands at 780, 1211, 3148, 3477, and 3530 cm^{-1}. The difference between these two spectra is the presence of an additional band at 1464 cm^{-1} on the 1 day spectra which was assigned to being carbonate substitution within an apatite structure. Like the 1 hour and 1 day spectra there are also similarities between the 7 day and 28 days samples. There are PO bending and stretching bands at 557, 597 and 955 cm^{-1}. This is in

addition to stretching bands from HPO_4 groups at 851, 900, 2847, 2915 and 2943 cm^{-1}. Similarly to the 1 day sample there are bands at 1464 cm-1 of carbonate groups within the apatite structure. Lastly the 28 day sample has a H-bonded H_2O group at 3556 cm^{-1}, which indicates the presence of the hydroxy group within the hydroxyapatite structure.

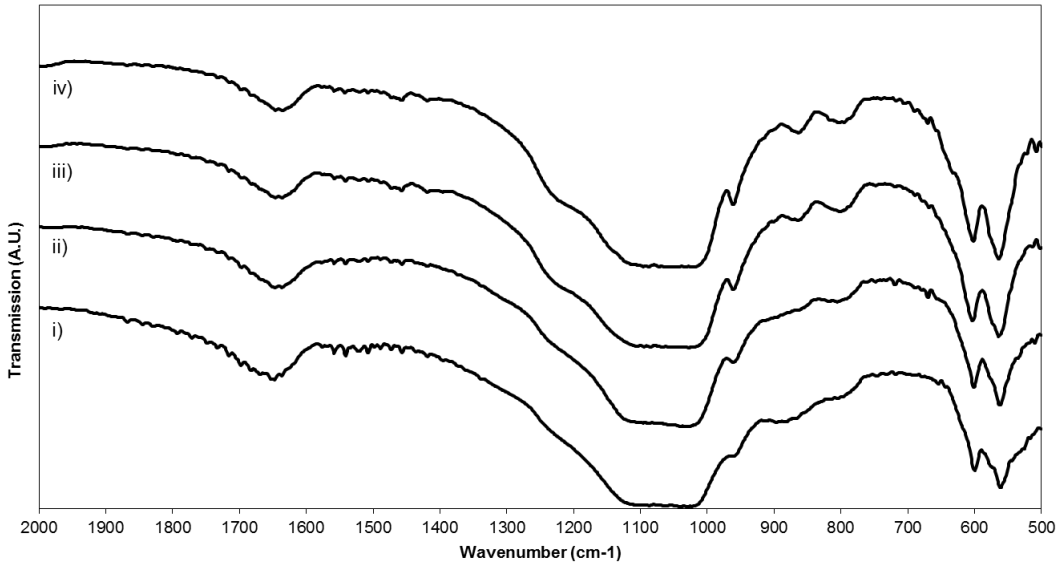

Figure 50 Fourier transform infrared spectra of cement composition QMNWKPaG15 at (i) 1 hour, (ii) 1 day, (iii) 7 days, and (iv) 28 days immersion time in Tris buffer solution, plotted between 500 to 2000 wavenumber cm^{-1}.

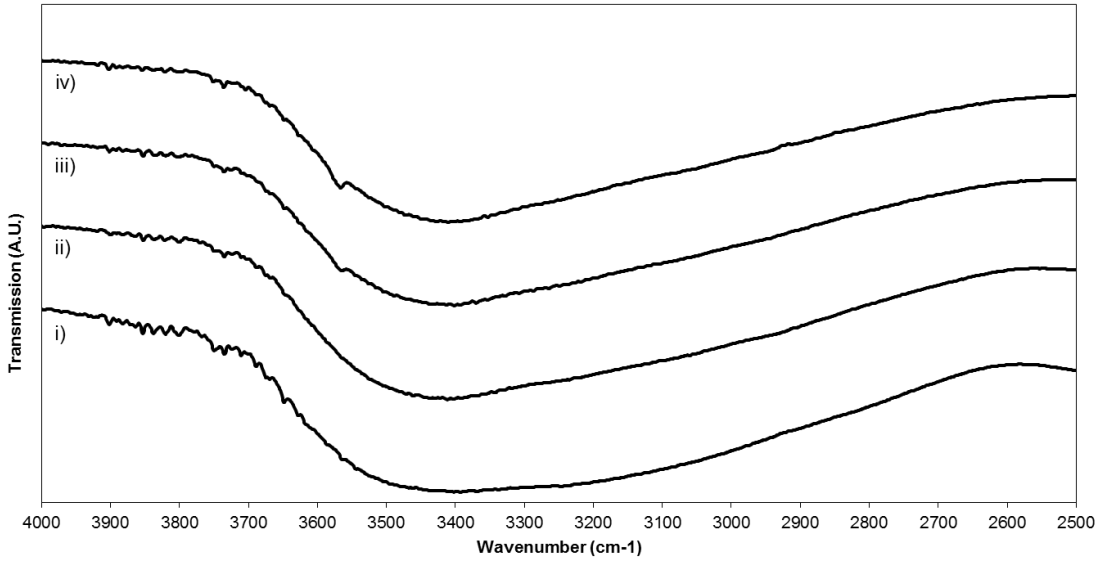

Figure 51 Fourier transform infrared spectra of cement composition QMNWKPaG15 at (i) 1 hour, (ii) 1 day, (iii) 7 days, and (iv) 28 days immersion time in Tris buffer solution, plotted between 2500 to 4000 wavenumber cm^{-1}.

Table 17 FTIR bands and their respective assignments of cement samples produced from glass QMNWKPaG15 after immersion in Tris buffer solution for 1 hour, 1 day, 7 days and 28 days.

Wavenumber (cm^{-1})	Assignment	1 Hour	1 Day	7 Day	28 Day
555	PO Bending	√	√	√	√
594	PO Bending	√	√	√	√
781	H_2O Liberation	√	√	√	√
849	P-O(H) Stretching	-	-	√	√
863	P-O(H) Stretching	√	-	-	-
950	PO Stretch	√	√	√	√
1627	H_2O Bending	-	√	√	√
1638	H_2O Bending	√	-	-	-
3552	H-bonded H_2O	-	-	√	√

Figures 50 and 51 show the FTIR spectra of cement composition QMNWKPaG15 at 1 hour, 1 day, 7 days and 28 days. There are relatively few bands present on these spectra compared to the previous samples. All samples contain PO bending and stretching bands at 555, 594 and 950 cm-1. There are also P-O(H) Stretching bands at 863 cm^{-1} on all spectra, except the 1 day sample. All spectra also have bands from structural water

molecules at 781 and 1638 cm^{-1}. The 7 day and 28 day samples have a H-bonded H_2O band at 3552, which like the QMNWKPaG14 sample is from the hydroxyl groups within the hydroxyapatite structure.

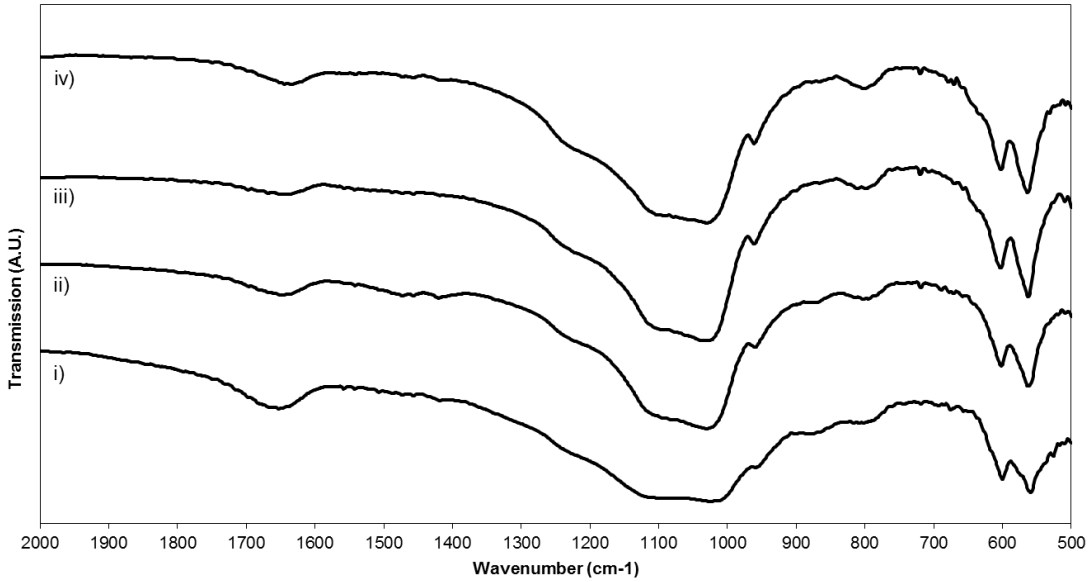

Figure 52 Fourier transform infrared spectra of cement composition QMNWKPaG16 at (i) 1 hour, (ii) 1 day, (iii) 7 days, and (iv) 28 days immersion time in Tris buffer solution, plotted between 500 to 2000 wavenumber cm^{-1}.

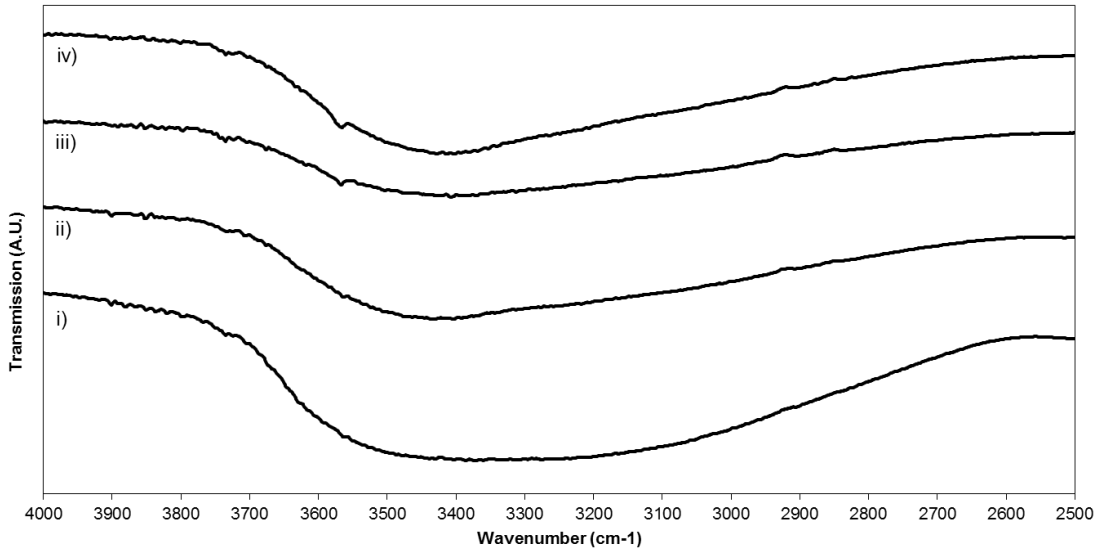

Figure 53 Fourier transform infrared spectra of cement composition QMNWKPaG16 at (i) 1 hour, (ii) 1 day, (iii) 7 days, and (iv) 28 days immersion time in Tris buffer solution, plotted between 2500 to 4000 wavenumber cm^{-1}.

Table 18 FTIR bands and their respective assignments of cement samples produced from glass QMNWKPaG16 after immersion in Tris buffer solution for 1 hour, 1 day, 7 days and 28 days.

Wavenumber (cm^{-1})	Assignment	1 Hour	1 Day	7 Day	28 Day
554	PO Bending	√	√	√	√
595	PO Bending	√	√	√	√
780	H_2O Liberation	√	√	√	√
944	PO Stretch	√	√	√	√
1634	H_2O Bending	-	-	-	√
3554	H-bonded H_2O	-	-	√	√

Figures 52 and 53 show the FTIR spectra of cement composition QMNWKPaG16 at 1 hour, 1 day, 7 days and 28 days. The bands present are almost identical in all spectra. There are PO stretching and bending bands at 554, 595 and 944 cm^{-1}. There are water molecule bands at 780 and 1634 cm^{-1}. The 28 day spectrum also has a H-bonded H_2O bands at 3552 cm^{-1}.

7.1.4 Scanning Electron Microscopy

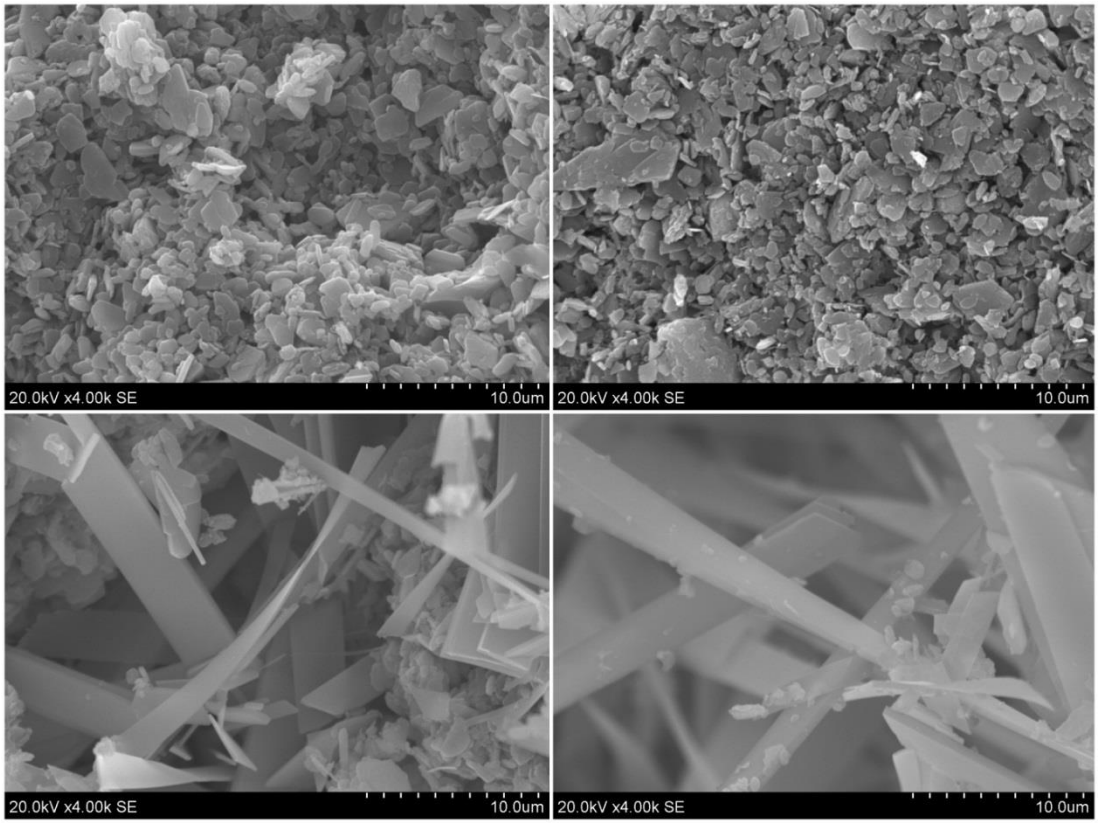

Figure 54 Scanning electron micrographs of QMNWKPaG03 cements at 1 hour (top left), 1 day (top right), 7 days (bottom left) and 28 days (bottom right).

Figure 54 shows the scanning electron micrographs of QMNWKPaG03 cements at 1 hour (top left), 1 day (top right), 7 days (bottom left) and 28 days (bottom right). At 1 hour and 1 day the crystals are small plates that correspond to the morphology of DCPD seen in the literature (Kumar et al., 1999). After 7 days the morphology of the cement is dramatically different with thin ribbon shaped crystals consistent with the morphology of OCP seen elsewhere (Legeros, 1985). The morphology is ribbon like after 28 days again suggesting the persistent presence of OCP (Lai et al., 2010).

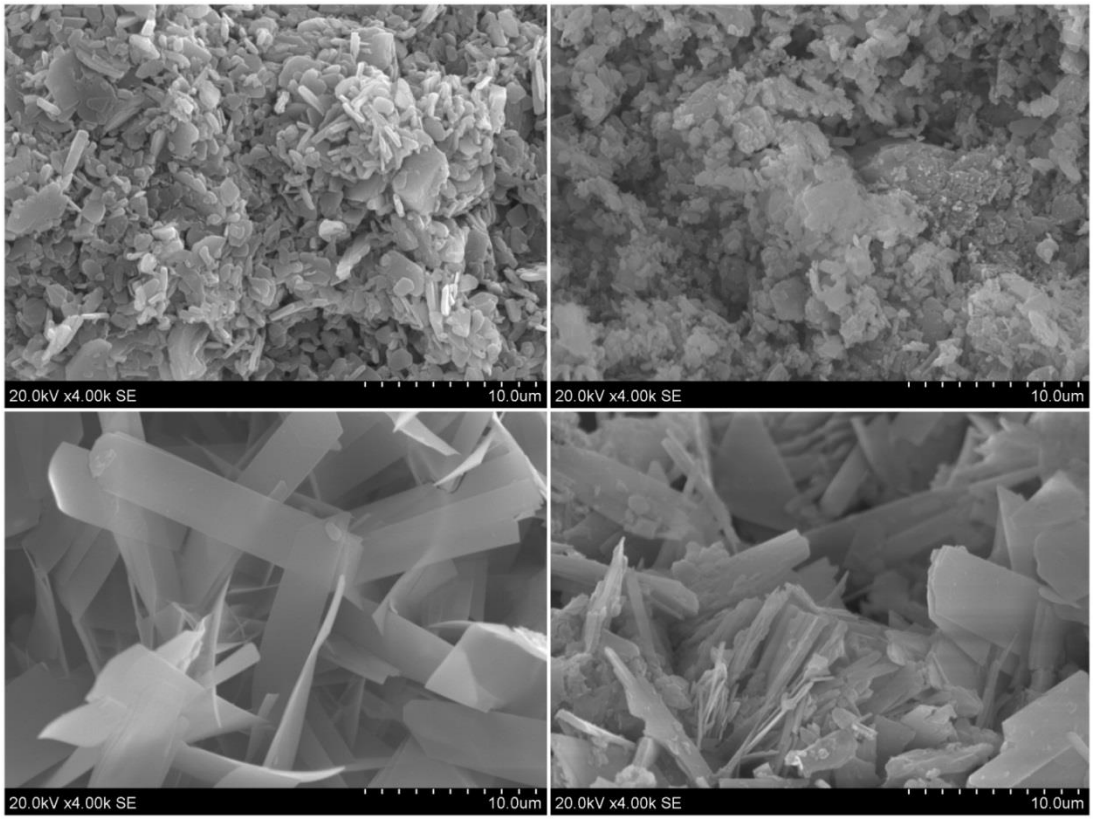

Figure 55 Scanning electron micrographs of QMNWKPaG13 cements at 1 hour (top left), 1 day (top right), 7 days (bottom left) and 28 days (bottom right).

Figure 55 shows the SEM images for QMNWKPaG13 cements at 1 hour, 1 day, 7 days and 28 days. There are two very distinct crystal morphologies existing within this cement. The 1 hour and 1 day samples have plate shaped

crystals, which are indicative of DCPD. The 7 day and 28 day samples seem to have similar microstructures, with distinctive very thin crystals.

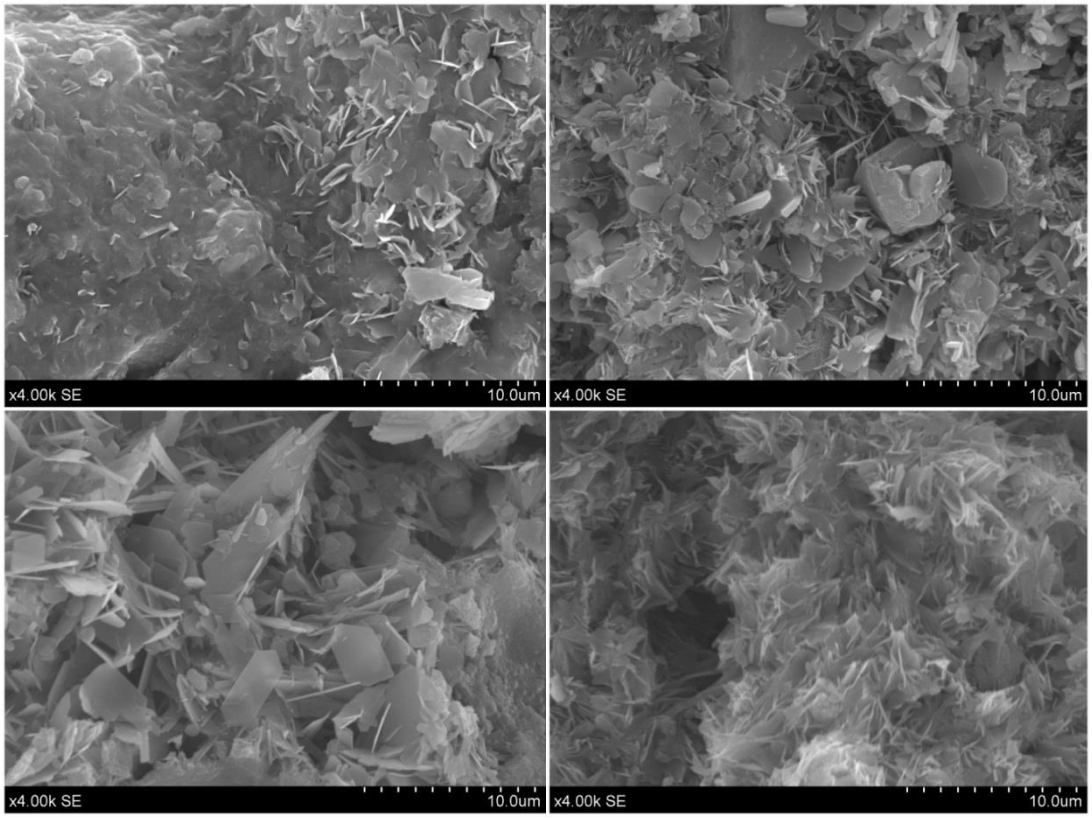

Figure 56 Scanning electron micrographs of QMNWKPaG14 cements at 1 hour (top left), 1 day (top right), 7 days (bottom left) and 28 days (bottom right).

Figure 56 shows the SEM images for QMNWKPaG14 cements at 1 hour, 1 day, 7 days and 28 days. The microstructure in all cements seem to be composed of very similar small plate/ribbon shaped crystals.

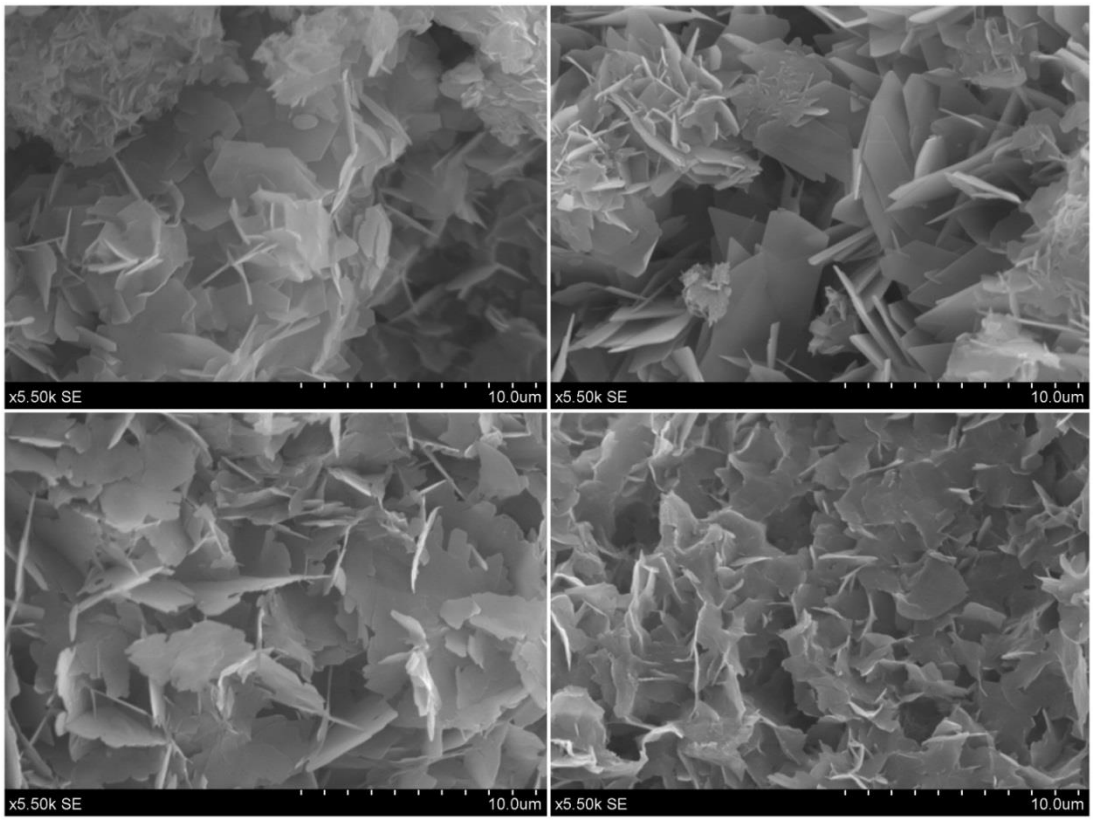

Figure 57 Scanning electron micrographs of QMNWKPaG15 cements at 1 hour (top left), 1 day (top right), 7 days (bottom left) and 28 days (bottom right).

Figure 57 shows the SEM images for QMNWKPaG15 cements at 1 hour, 1 day, 7 days and 28 days. All four time points appear to have similarly shaped crystals, as all are typically very thin. The 1 hour, 7 day and 28 day samples seem to have irregular shaped petal like crystals, whereas the 7 day sample has more ordered ribbon crystals with a few petal shaped crystals interspersed.

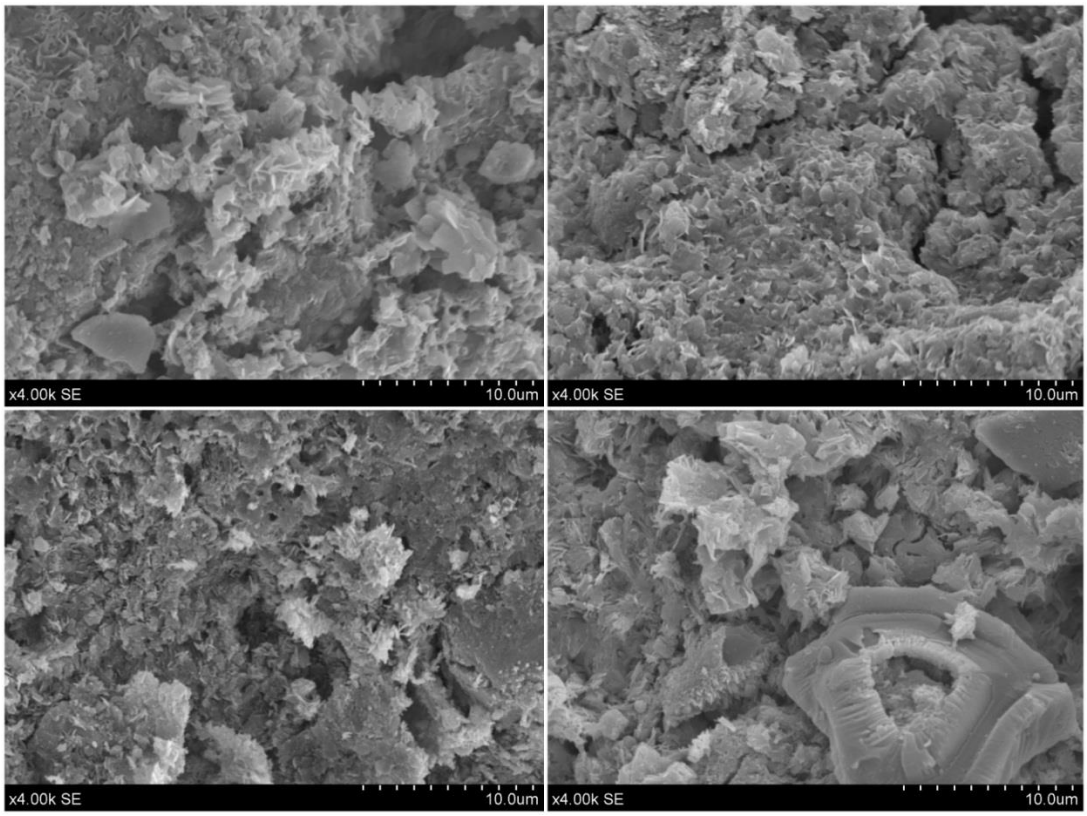

Figure 58 Scanning electron micrographs of QMNWKPaG16 cements at 1 hour (top left), 1 day (top right), 7 days (bottom left) and 28 days (bottom right).

Figure 58 shows the SEM images for QMNWKPaG16 cements at 1 hour, 1 day, 7 days and 28 days. All crystal morphologies at each time point are very similar small thin plate shaped crystals. In the 28 day immersed cement there is a residual glass particle with a reacted core.

7.1.5 Compressive Strength

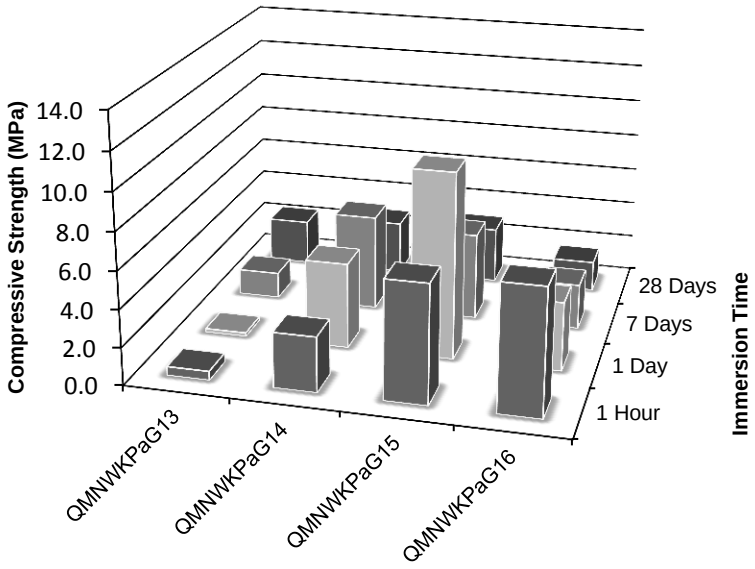

Figure 59 Compressive strength against time of calcium-sodium series cement compositions. plotted in oreder of sodium increase.

Glass Composition	Compressive Strength (MPa)			
	1 Hour	**1 Day**	**7 Days**	**28 Days**
QMNWKPaG03	n/a	n/a	n/a	n/a
QMNWKPaG04	9.65 (±0.55)	12.90 (±1.16)	10.30 (±1.33)	5.67 (±0.94)
QMNWKPaG13	0.47 (±0.09)	0.19 (±0.04)	1.40 (±0.53)	2.44 (±0.40)
QMNWKPaG14	2.94 (±0.42)	4.58 (±0.33)	5.14 (±0.49)	2.86 (±0.67)
QMNWKPaG15	6.29 (±0.38)	9.94 (±0.81)	4.67 (±0.18)	3.02 (±0.45)
QMNWKPaG16	6.72 (±1.00)	3.68 (±0.18)	2.43 (±0.48)	1.63 (±0.21)

The fluorine free samples the QMNWKPaG13 cement samples were unable to give a measurement for compressive strength due to cracking of the cement cylinders during immersion. Compressive strength of the samples ranged from 0.19 to 12.90 MPa.

7.1.6 Setting Time

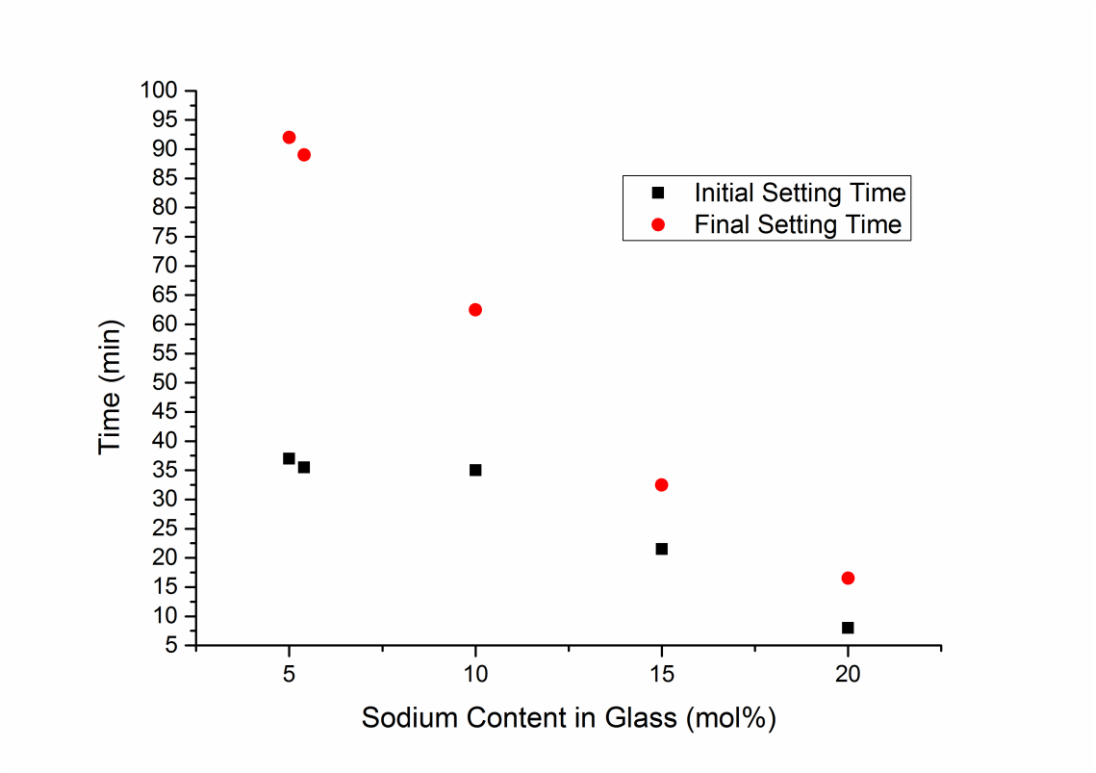

Figure 60 Setting times of Calcium/Sodium cement series of sodium content plotted against time

Table 19 Setting times as measured using Gilmore needle test of cement compositions, showing both initial and final setting times in minutes.

Cement Composition	Initial Setting Time (min)	Final Setting Time (min)
QMNWKPaG03	35.5	89.0
QMNWKPaG13	37.0	92.0
QMNWKPaG14	35.0	62.5
QMNWKPaG15	21.5	32.5
QMNWKPaG16	8.0	16.5

The glass series produced where the calcium to sodium ratio was altered in the base glass showed a clear trend in the setting time with a change in the glass composition. Both the initial and final setting times decreased as the sodium content in the glass powder was increased. In the lowest sodium glasses (QMNWKPaG03 & 13) the initial setting times are 35.5 and 37

minutes and the final setting times are 89 and 92 minutes respectively. The QMNWKPaG14 composition has a similar initial setting time as the two glasses with lower sodium contents of 35 minutes, but has a decreased final setting time of 62.5 minutes. As the sodium is increased in the last two compositions (QMNWKPaG15 & 16) both the initial and final setting times decreased.

7.1.7 Ion Release

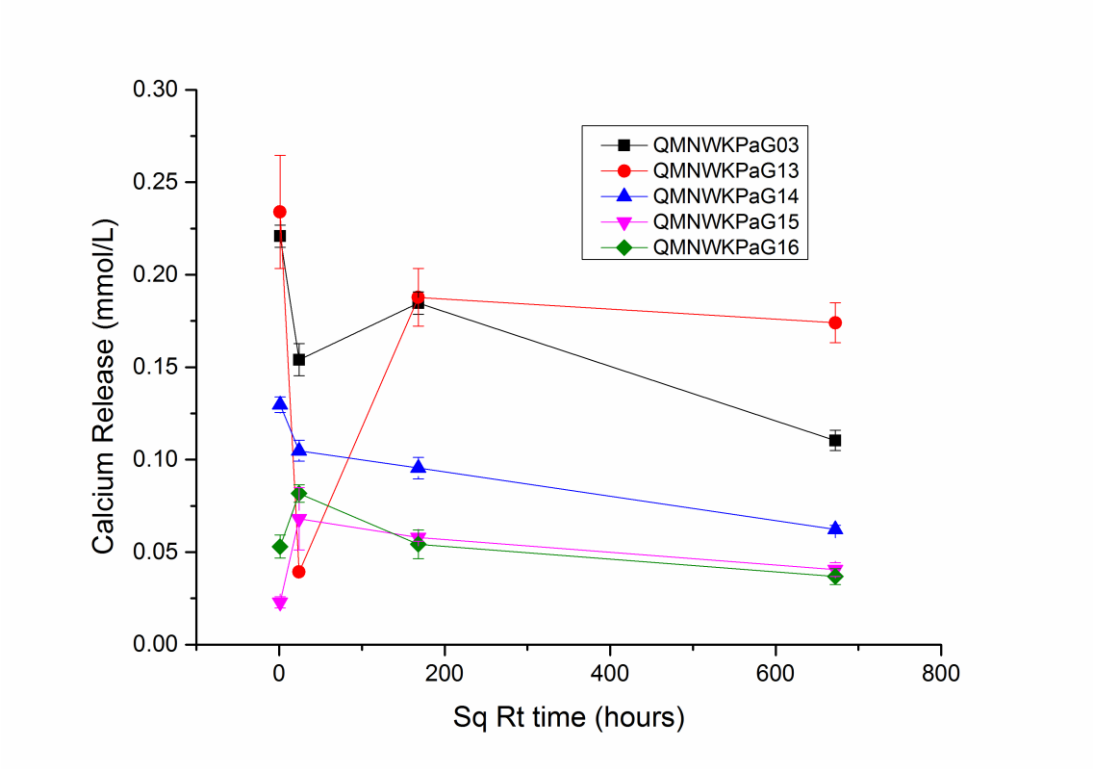

Figure 61 Calcium release (millimole per litre, mmol/L) from immersed cement cylinders (n=4) plotted against square root of immersion time (hours) for all calcium/sodium cement compositions from immersion for 1 hour, 1 day, 7 days, 28 days. (Error Bars = Standard Deviation).

Table 20 Calcium release (millimole per litre, mmol/L) from immersed cement cylinders (n=4) for all cement compositions from immersion for 1 hour, 1 day, 7 days, 28 days. (Standard Deviation).

Cement Composition	Calcium Release (mmol/L)			
	1 Hour	1 Day	7 Days	28 Days
QMNWKPaG03	0.22 (±0.00)	0.15 (±0.00)	0.18 (±0.00)	0.11 (±0.00)
QMNWKPaG13	0.23 (±0.03)	0.04 (±0.00)	0.19 (±0.01)	0.17 (±0.01)
QMNWKPaG14	0.13 (±0.00)	0.10 (±0.00)	0.10 (±0.00)	0.06 (±0.00)

QMNWKPaG15	0.02 (±0.00)	0.07 (±0.01)	0.06 (±0.00)	0.04 (±0.00)
QMNWKPaG16	0.05 (±0.00)	0.08 (±0.00)	0.05 (±0.00)	0.04 (±0.00)

The calcium release shows very similar levels of calcium release from the cement for most of the different cement compositions. At 1 hour the majority of the compositions have between 0.02 and 0.23 mmol/L calcium release. At 1 day the majority of calcium release for the cement compositions is between 0.04 and 0.15 mmol/L. At 7 days the majority of the calcium release is between 0.05 and 0.19 mmol/L. After 28 days calcium release is relatively low, ranging between 0.02 and 0.06 mmol/L for all compositions except compositions QNMWKPaG03 and 13 which have releases of 0.11 and 0.17 mmol/L.

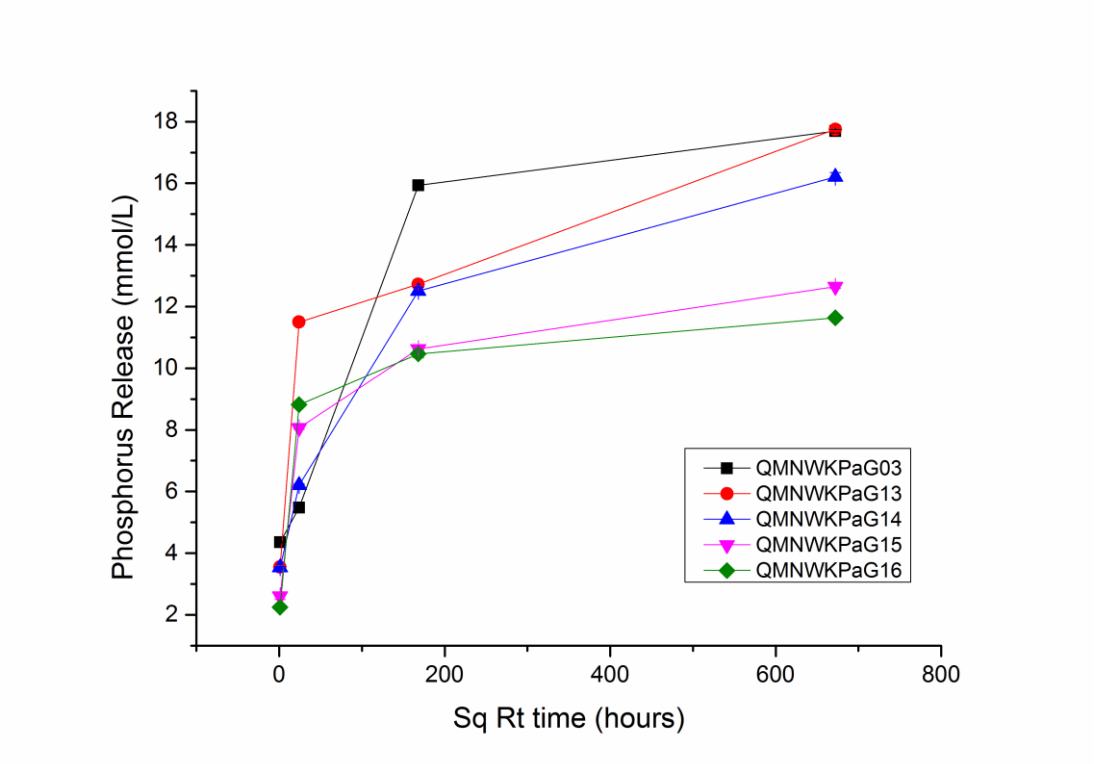

Figure 62 Phosphorus release (millimole per litre, mmol/L) from immersed cement cylinders (n=4) plotted against square root of immersion time (hours) for all calcium/sodium cement compositions from immersion for 1 hour, 1 day, 7 days, 28 days. (Error Bars = Standard Deviation).

Table 21 Phosphorus release (millimole per litre, mmol/L) from immersed cement cylinders (n=4) for all cement compositions from immersion for 1 hour, 1 day, 7 days, 28 days. (Standard Deviation).

Cement Composition	Phosphorus Release (mmol/L)			
	1 Hour	1 Day	7 Days	28 Days
QMNWKPaG03	4.35 (±0.02)	5.48 (±0.03)	15.94 (±0.11)	17.69 (±0.05)
QMNWKPaG13	3.55 (±0.04)	11.50 (±0.01)	12.73 (±0.04)	17.75 (±0.06)
QMNWKPaG14	3.54 (±0.02)	6.21 (±0.03)	12.51 (±0.12)	16.21 (±0.14)
QMNWKPaG15	2.61 (±0.11)	8.06 (±0.04)	10.63 (±0.03)	12.65 (±0.06)
QMNWKPaG16	2.25 (±0.03)	8.82 (±0.05)	10.46 (±0.11)	11.64 (±0.05)

At 1 hour the phosphorus release is between 2.25 and 4.35 mmol/L for all cement compositions. After 1 day the amount of phosphorus in solution for all compositions has risen to between 5.48 and 11.50 mmol/L. After 7 days the phosphorus in solution has increased a smaller amount to be between 10.46 and 15.94 mmol/L for all cement compositions. At 28 days there is a fairly high distribution of the various phosphorus release rates. The release distribution is high with all compositions being between 11.64 and 17.69 mmol/L.

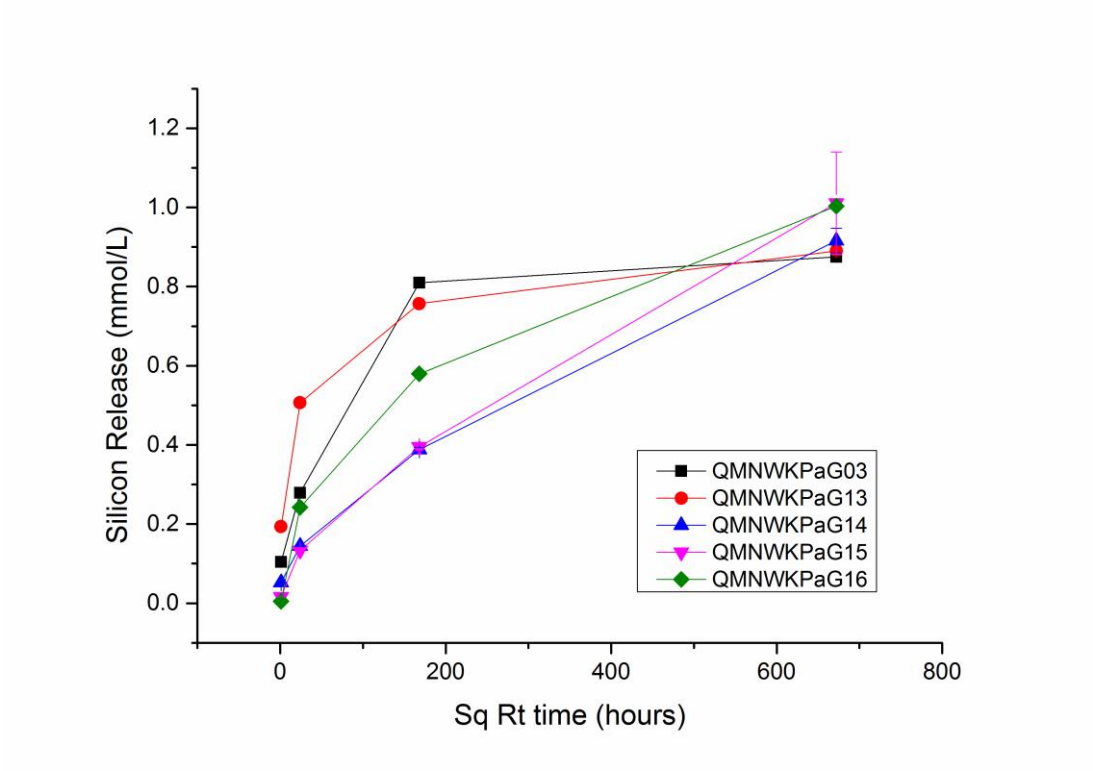

Figure 63 Silicon release (millimole per litre, mmol/L) from immersed cement cylinders (n=4) plotted against square root of immersion time (hours) for all calcium/sodium cement compositions from immersion for 1 hour, 1 day, 7 days, 28 days. (Error Bars = Standard Deviation).

Table 22 Silicon release (millimole per litre, mmol/L) from immersed cement cylinders (n=4) for all cement compositions from immersion for 1 hour, 1 day, 7 days, 28 days. (Standard Deviation).

Cement Composition	Silicon Release (mmol/L)			
	1 Hour	1 Day	7 Days	28 Days
QMNWKPaG03	0.10 (±0.00)	0.28 (±0.00)	0.81 (±0.00)	0.88 (±0.00)
QMNWKPaG13	0.19 (±0.00)	0.51 (±0.00)	0.76 (±0.00)	0.89 (±0.00)
QMNWKPaG14	0.05 (±0.00)	0.14 (±0.00)	0.39 (±0.00)	0.92 (±0.03)
QMNWKPaG15	0.02 (±0.00)	0.13 (±0.00)	0.40 (±0.00)	1.01 (±0.12)
QMNWKPaG16	0.00 (±0.00)	0.24 (±0.00)	0.58 (±0.00)	1.00 (±0.00)

The silicon release shows a constant increase in silicon release for all cement compositions that shows no noticeable differences for the different series. At 1 hour there is the lowest silicon release of between 0.00 and 0.19 mmol/L, which increases to between 0.13 and 0.51 mmol/L after 1 day. Then at 7 days the amount in solution is further increased to between 0.39 and

0.81 mmol/L. There is again another increase in silicon release after 28 days to between 0.88 and 1.01 mmol/L.

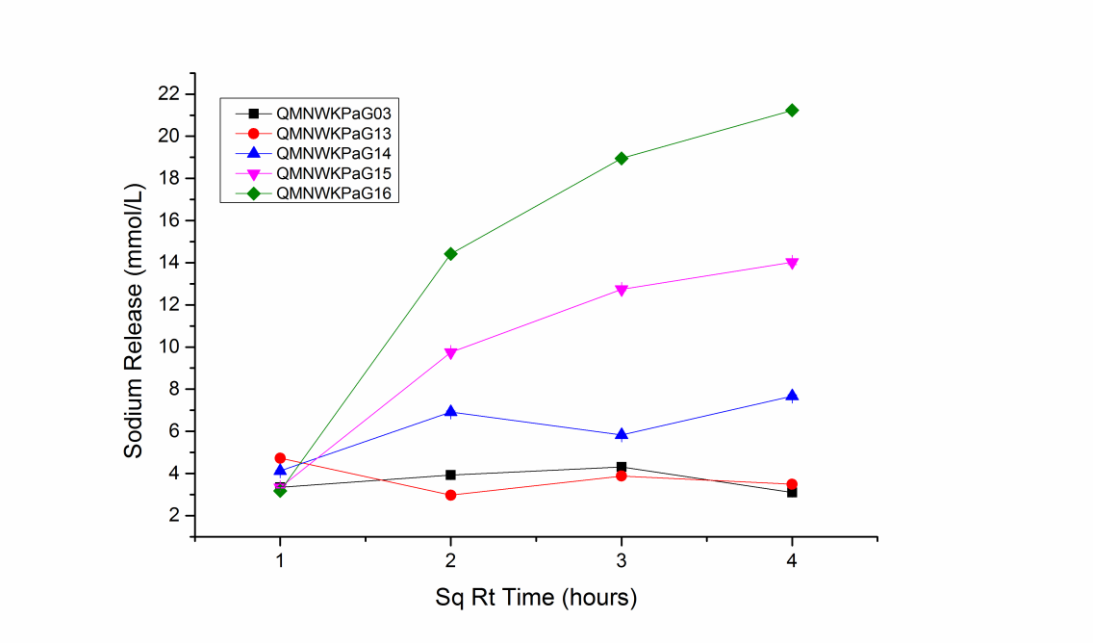

Figure 64 Sodium release (millimole per litre, mmol/L) from immersed cement cylinders (n=4) plotted against square root of immersion time (hours) for all calcium/sodium cement compositions from immersion for 1 hour, 1 day, 7 days, 28 days. (Error Bars = Standard Deviation).

Table 23 Sodium release (millimole per litre, mmol/L) from immersed cement cylinders (n=4) for all cement compositions from immersion for 1 hour, 1 day, 7 days, 28 days. (Standard Deviation).

Cement Composition	Sodium Release (mmol/L)			
	1 Hour	1 Day	7 Days	28 Days
QMNWKPaG03	3.35 (±0.00)	3.92 (±0.02)	4.31 (±0.00)	3.10 (±0.03)
QMNWKPaG13	4.73 (±0.01)	2.97 (±0.03)	3.88 (±0.03)	3.49 (±0.00)
QMNWKPaG14	4.12 (±0.03)	6.92 (±0.04)	5.83 (±0.02)	7.68 (±0.05)
QMNWKPaG15	3.33 (±0.01)	9.74 (±0.02)	12.74 (±0.06)	14.02 (±0.10)
QMNWKPaG16	3.18 (±0.02)	14.42 (±0.06)	18.95 (±0.08)	21.23 (±0.11)

Cement compositions QMNWKPaG03 and 13 have very similar levels of sodium release at all time points studied, with release levels between 2.97 and 4.73 mmol/L. compositions QMNWKPaG14-16 show higher levels of sodium release after 1 hour compared to the other cement compositions. At 1 day the release of sodium from cements QMNWKPaG14-16 was 6.92,

9.74 and 14.42 mmol/L respectively. After 7 days the QMNWKPaG14 composition has decreased slightly to 5.83 mmol/L whilst the QMNWKPaG15 and 16 compositions have increased to 12.74 and 18.95 mmol/L. then at 28 days all three compositions have increased to 7.68, 14.02 and 21.23 mmol/L respectively.

7.2 Discussion

7.2.1 Cement Phase Analysis

QMNWKPaG03 and QMNWKPaG13

Due to the high similarity of both the QMNKWPaG03 and QMNWKPaG13 glass compositions and their analytical results, the following discussion refers to both glass compositions.

1 hour

The ^{31}P MAS-NMR showed the cement phases as being predominantly DCPD with an intense chemical shift a 1.4 ppm. The peak at -1.4 ppm indicated the presence of DCPA within each cement phase; this was probably from the $Ca(H_2PO_4)_2$ starting powder, which was confirmed to contain DCPA as an impurity, rather than the DCPA being formed in the cement setting reaction. The X-ray diffraction confirmed this finding, with the majority of the diffraction lines matching that of DCPD and three relatively low intensity diffraction lines matching DCPA. The FTIR is strongly indicative of the presence of DCPD with a PO bending peak, OH stretching in water peaks (3146, 3276, 3477 and 3533 cm^{-1}), and PO stretching peaks (865, 997 and 1123 cm^{-1}) being especially indicative. DCPA cannot be easily distinguished on the FTIR spectra given its low fraction of the cement.

1 day

The spectroscopy for the 1 day cement very much matches that of the 1 hour sample. The ^{31}P MAS-NMR shows the intense DCPD chemical shift at 1.4 ppm and a smaller less intense chemical shift of DCPA at -1.4 ppm. There were small chemical shifts at 0 ppm which has not been assigned to a specific phase. The X-ray diffraction pattern is similar to the 1 hour pattern with three DCPA diffraction lines of low intensity compared to the more numerous DCPD lines. The FTIR follows a similar trend to the XRD and NMR with the spectra similar to that of the 1 hour samples. There are distinguishing DCPD peaks at 520 (PO bending), 995 (P-O(H) stretching) and 3141, 3477 & 3531 cm^{-1} (all OH stretching in water).

7 day

There is a dramatic change in the cement phases between the 1 day and 7 day samples. The ^{31}P MAS-NMR spectra show four clear chemical shift at 3.6, 3.2, 1.8, -0.2 ppm, which account for the six phosphorus atoms within the OCP structure; the 1.8 ppm OCP chemical shift has a shoulder at 1.4 ppm which was assigned to DCPD. Additionally there is a small chemical shift at -1.4 ppm which is remaining DCPA in the sample. The NMR interpretation is matched on the X-ray diffraction pattern. OCP and apatite share very similar diffraction patterns due to their pseudomorphic crystal structure; the only three additional diffraction peaks (4.6, 9.4 and 9.7 $^{\circ}2\theta$) exist on the OCP diffraction pattern which do not exist on the apatite diffraction pattern. The 7 day XRD pattern has these three diffraction peaks indicative of OCP, showing the presence of OCP. The XRD gives

confirmation of the presence of both DCPD and DCPA. On the FTIR spectra the OH stretching in water peaks typical of DCPD are not discernible; indicating at least that the DCPD has become a much lower fraction of the cement phase compared to 1 day.

28 day

At 28 days the ^{31}P MAS-NMR clearly shows the four chemical shifts at 3.6, 3.2, 1.8, -0.2 ppm, indicative of OCP. There is also a very small shoulder at -1.4 ppm which indicates a very small fraction of DCPA present. The X-ray diffraction shows the presence of OCP with indicative diffraction lines at 4.6, 9.4 and 9.7 ˚2θ. There are also low intensity peaks of both DCPD and DCPA. DCPD was not detected on the ^{31}P MAS-NMR whereas the DCPA was; the reason for this is due to its low fraction it would have a low intensity and it would be under the 1.8 ppm chemical shift of OCP and would not be seen as a shoulder due to surrounding OCP chemical shift of OCP. The FTIR matches that of the 7 day sample; there are clearly indicative peaks of OCP primarily HPO_4 bending and stretching peaks. Again there are no clear OH water stretching bands which would clearly indicate DCPD.

QMNWKPaG14

1 hour

At 1 hour there was an intense shift at 1.4 ppm showing the presence of DCPD. This is consistent with both the FTIR and XRD results where there are typical diffraction lines for DCPD at 21 ˚2θ and FTIR bands at 523, 3150, 3475, 3530 cm^{-1} typical of DCPD. The XRD and NMR results also clearly show that octacalcium phosphate is present but in a smaller fraction

compared to the DCPD by the relative intensities shown. DCPA is also present in this sample; evident on the MAS-NMR spectrum as a shoulder at -1.4 ppm and on the XRD by a number of indicative diffraction lines.

1 day

The 1 day sample shows that whilst the same phases are present as in the 1 hour samples the relative amounts of each has changed. The MAS-NMR spectrum shows an increase in the relative amount of octacalcium phosphate present which would be caused by dissolution of the DCPD phase and precipitation of the octacalcium phosphate phase from the ions which originally made up the DCPD. DCPA is still present in the cement sample at 1 day. However it is difficult to distinguish whether there has been a change in its amount within the cement sample because it exists as a non-resolved shoulder on the NMR spectrum.

7 days

The 7 day cement sample has OCP, apatite and DCPA present. The X-ray diffraction pattern shows that DCPD in no longer present in the cement phase as the typical diffraction lines are not present. Octacalcium phosphate is distinguished on both the XRD and NMR with diffraction lines at 4.7, 9.3 and 9.8 $^{\circ}2\theta$ and chemical shift at 3.6, 3.2, 2.0 and -0.2 ppm. Apatite is deemed as being evident from the NMR results as there is a chemical shift at 2.9 ppm present. It is difficult to distinguish if apatite is present just from the XRD as the diffraction patterns of octacalcium phosphate and apatite are hard to distinguish between. The FTIR also indicates the presence of apatite

formation from bands at 1465 cm^{-1} which shows the presence of carbonate substitution in apatite.

28 days

The NMR of the 28 day sample has an intense chemical shift of apatite at 2.9 ppm, there is also a shoulder present to the right of this resonance at approximately 0 ppm which is difficult to assign. The X-ray diffraction has diffraction lines only for apatite and no other crystalline phase is present in detectable amounts. The FTIR has bands of HPO_4 groups at 2845, 2915 and 2945 cm^{-1} usually found in octacalcium phosphate. This then most likely indicates that octacalcium phosphate is present but in quantities where the indicative 4.7 $^{\circ}2\theta$ line is not detectable. Again carbonate substitution in the apatite is detected on the FTIR. Also present on the FTIR is a band at 3555 cm^{-1} that is of the OH group within the apatite structure. Concluding then the apatite formed after 28 day immersion of this cement composition is a carbonate-substituted hydroxyapatite.

QMNWKPaG15

1 hour

At one hour the X-ray diffraction showed the presence of octacalcium phosphate, with a diffraction line at 4.7 degrees 2 theta. The ^{31}P MAS-NMR results agreed with this finding as there were chemical shift at 3.6, 2.0 and -0.2 ppm. There is also DCPA present which was shown on both the X-ray diffraction and ^{31}P MAS-NMR. It is difficult to distinguish whether hydroxyapatite is present also; the X-ray diffraction presents a fairly low intensity diffraction line at 4.7 degrees 2 theta which in the reference pattern

for octacalcium phosphate is typically the most intense line. This result coupled with the more intense lines around 32 degrees 2 theta suggest the sample may be a mixture of both octacalcium phosphate and an apatite species. A typical 2.8 ppm chemical shift for apatite could not be clearly identified on the ^{31}P MAS-NMR but due to the high intensity of the 3.6 ppm chemical shift it may just be a low intensity resonance which is masked by more intense chemical shift. The FTIR does not have many bands, but does have two at 555 and 594 cm^{-1} which are crystalline calcium phosphate and could be either apatite or octacalcium phosphate. There is also a band at 863 cm^{-1} which was assigned to being a P-O(H) stretching bond on octacalcium phosphate.

1 day

The one day sample showed the continued presence of octacalcium phosphate, identifiable from the X-ray diffraction. The ^{31}P MAS-NMR spectrum has an intense chemical shift at 3.4 ppm and a small shoulder at -0.2 ppm. Similarly to the 1 hour sample it is difficult to easily conclude whether hydroxyapatite is also present. The typical ^{31}P MAS-NMR chemical shift for octacalcium phosphate were not easily identifiable as there are only two chemical shift and without the X-ray diffraction it would be difficult to reliably conclude the presence of octacalcium phosphate. Another point to notice is the disappearance of DCPA from the ^{31}P MAS-NMR but it was noticeable on the X-ray diffraction. This may be due to different cement samples being analysed, and this was a variation between the two.

7 days

The ^{31}P MAS-NMR and X-ray diffraction both show the presence of apatite. A chemical shift at 2.9 ppm on the NMR spectrum and typical apatite diffraction lines on the X-ray diffraction. The DCPA is not identifiable on either the NMR or X-ray diffraction.

28 days

Between the 7 day sample and the 28 day sample there is little change in the cement phase. The ^{31}P MAS-NMR spectrum has one chemical shift at 2.9 ppm of apatite and the X-ray diffraction.

QMNWKPaG16

1 hour

The 1 hour sample is difficult to interpret. The X-ray diffraction pattern shows a mixture of octacalcium phosphate and apatite, this was interpreted from the low intensity 4.7 degree 2 theta diffraction line for octacalcium phosphate relative to the more intense hydroxyapatite/octacalcium phosphate diffraction lines. The ^{31}P MAS-NMR is more difficult to interpret; there is one intense chemical shift at 4.0 ppm. Apatite normally gives a diffraction line at 2.9 ppm, it is also known that sodium will shift phosphorus signals to higher chemical shift so it may be the case that a sodium substituted apatite has formed as this glass has the highest sodium content of all the glasses used to make the cements.

1 day

The 1 day sample shows a predominantly apatite cement phase with a small diffraction line at 4.7 degree 2 theta on the X-ray diffraction pattern. The ^{31}P MAS-NMR spectrum has one chemical shift at 3.3 ppm. If the hypothesis for

sodium substitution is true then this shift would indicate sodium was being replaced in the apatite crystal by calcium. This can be explained through the higher solubility of a sodium substituted apatite which under equilibrium would reprecipitate to a sodium free apatite.

7 days

The 7 days sample shows a monophasic apatite cement phase the X-ray diffraction has typical diffraction lines of apatite and the ^{31}P MAS-NMR has one chemical shift at 3.0 ppm, which was assigned to being an apatite phase.

28 days

Similarly to the 7 day sample the cement phase only consists of apatite. The X-ray diffraction has only lines for apatite and the ^{31}P MAS-NMR has only one chemical shift at 2.9 ppm of apatite.

7.2.2 Effect of Glass Structure Upon Dissolution

Characterisation and analysis of the glass structure showed a number of structural changes throughout the series which could potentially be impacting upon glass dissolution and eventual phase formation and cement evolution. Specifically the increase in free volume, intimated by Tg changes, as calcium is increased through the series. Increase in the free volume would equate to a more degradable glass. Within the context of the cement setting reaction it would be anticipated that faster depredation of these glasses would lead to the earlier formation of more calcium rich species. This is because the glass contributes a large proportion of the calcium in the overall cement setting reaction and releasing this faster is likely to increase the amount of calcium

available for reaction, changing the stoichiometry of the reaction, favouring a more calcium rich species to form.

This idea is supported in the results seen here as that when you go ‘up’ the series the analysis of the cement phase formed shows the formation of initial phases at 1 hour that are more calcium rich. The QMNWKPaG13 and 03 glasses show the initial formation of brusihte (Ca/P = 1.00) compared to QMNWKPaG15 which has a higher calcium content and forms primarily octacalcium phosphate (Ca/P = 1.33), the QMNWKPaG16 composition forms hydroxyapatite (Ca/P = 1.67) at 1 hour. Whilst the data does indeed support the idea that the changes in the free volume induce faster glass degradation and changes in cement phase shown here it cannot be for definite. This is because as well as the Tg changing though the series the cement formulation is also subject to change throughout this series.

As the sodium content decreases down the series the amount of calcium coming from the glass part of the cement formulation decrease. To maintain the overall Ca/P ratio in the cements the glass:salt ration changes through the series. Descending the series the glass content of the overall cement formulation decrease and the amount of salt increases. This could potentially have a large effect upon the cement setting chemistry due to the probably change in the pH of the cement setting reaction. Whilst this may affect the dissolution of the glass it will also reduce the pH of the cement reaction solution possibly inducing the formation of the more acidic stable calcium phosphate phases, like brushite.

7.2.3 Compressive Strength

The compressive strength for the cements with increasing sodium content at 1 hour show a clear trend of increasing compressive strength when sodium is increased. This is caused by the change in phase that is exhibited in the early setting of the cements. In the low sodium content glasses the initial cement phase is DCPD and as you move up the series the propensity for the formation of OCP increases and mixed DCPD/OCP cement phases form as the sodium content is increased until the last glass in the series where the cement phase is a mixture of OCP and apatite. Like in the fluoride cements the presence of the weaker DCPD phase the compressive strengths are decreased when a high proportion of the cement phase is DCPD.

Another trend exhibited in this cement series is a decrease in compressive strength after 1 day. Additionally there is a greater decrease in the compressive strength as the sodium content is increased in the glass used to produce the cement. The decrease is believed to be due to release of silicon, sodium and phosphorus into the Tris solution during immersion. This release causes porosity in the cement cylinder which decreases the compressive strength as there is a linear relationship in cements between porosity and compressive strength. The glasses are affected disproportionately as more sodium is in the glass used to make the cement the larger the drop in compressive strength. This is because the proportion of glass powder used to make theses cement compositions increases as sodium content is increased meaning there is a higher proportion of silicon and sodium ions making up the cement. When these ions are released into solution this

causes greater porosity as you move up the series causing a larger decrease in compressive strength.

An interesting point to notice is that the initial cement reaction appears to have a large effect on the cement strength at later time points. The alteration in initial phase was attributed to being the cause of the different strength at 1 hour and 1 day but if this is the case then why do the QMNWKPaG03 and QMNWKPaG13 cements not achieve higher compressive strengths when they convert to octacalcium phosphate at 7 days.

With respect to clinical performance compressive strength is an important property to optimise. Whilst these materials are not currently used for load bearing applications they should be sufficiently strong to prevent deformation and remain coherent. Additionally bone cement which is too strong can be disadvantageous as it can lead to atypical force distribution (which can cause adjacent bone fracture) and stress shielding causing unwarranted resorption of bone. An ideal material will match the compressive strength of the bone into which it is implanted. Given trabecular bone has a compressive strength between 8 and 13 MPa, a compressive strength around this value would be sufficient for good clinical performance for most applications[4].

It should be noted that the compressive strength values should only be interpreted as a way of comparing the different cement compositions rather than values that are applicable to in-vivo performance. Many factors will affect the strength on the cement in-vivo including amount of cement,

[4] Stronger cement compositions may be required for specific applications, especially when the cement is bridging a gap in bone (i.e. cranial defects) rather than filling a cavernous bone void.

morphology of implant site, mineralisation of cement after implantation, location of implant site, surrounding bone density and osseointegration as these factors will affect the force distribution.

7.2.4 Setting Time

The setting time results show clear trends between glass composition and the measured setting time. The fluoride free cement compositions show a decrease in setting time as the sodium content is increased in the glass. The gradual decrease is witnessed for both the initial and final setting times. A factor which causes this is the change in phase exhibited by the cements during setting as sodium content is increased in the glass. In these cement system the DCPD phase which forms initially transforms to octacalcium phosphate at different rates depending upon the sodium content, with a higher sodium content giving a faster transition rate. It is known that DCPD forming cements have lower compressive strengths than octacalcium phosphate/hydroxyapatite cements (Dorozhkin, 2008). Given the Gilmore needle test relies on the strength of the cement to determine the setting time then a weaker cement is likely to have a longer setting time as a more substantial proportion of the bulk cement phase would have had to have formed of a weaker (DCPD) cement phase to resist the Gilmore needle sufficiently compared to a stronger cement phase. Therefore as the higher sodium content cements form octacalcium phosphate/hydroxyapatite at earlier time points they are able to resist both Gilmore needles at earlier time points.

It is difficult to discern a reliable assessment of the effect of P_2O_5 content in the glass on the setting time of the cement because there are only two cement compositions where the only component altered is P_2O_5. The figure below shows the comparison between these two compositions with 4.00 and 6.00 mol% P_2O_5. There clearly shows a dramatic change in setting time, with the high phosphate glass giving a much reduced setting time. This is most likely cement phase related as QMNWKPaG03 forms DCPD initially whereas the QMNKWPaG04 composition forms an OCP/hydroxyapatite cement phase rapidly. It cannot be predicted from these results whether phosphate content affects the glass dissolution which caused the alteration in phases or whether it is the alteration in glass powder/$Ca(H_2PO_4)_2$.

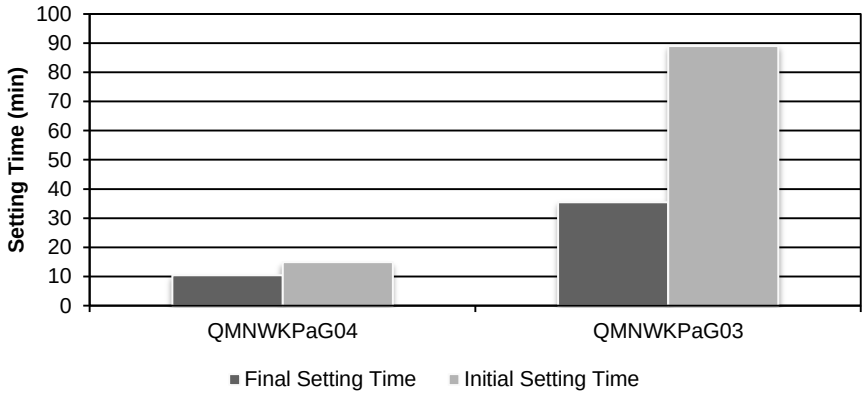

Figure 65 Initial and final setting times of the cement series with increasing phosphate content

7.2.4 Ion Release

The silicon release followed a fairly conspicuous trend, with silicon content in the solution increasing with immersion time. This is related to the hydrolysis of the residual silicate chains which are hydrolysed over a period of time, releasing soluble silicon species into solution.

The sodium release follows a glass composition trend; at 1 hour the sodium release from all glass compositions is approximately equal. At 1 day QMNWKPaG03 and 13 had very similar sodium release levels (and sodium contents in the glass), however, cements where glass QNMWKPaG14-16 were used the sodium levels are proportionally higher. This trend continues at both 7 and 28 days.. This trend is because these glass compositions contain more sodium than the others; additionally more glass is used to make the cement powder relative to the calcium phosphate salt. The increase in sodium in glass compositions combined with the presence of more glass means there is more sodium present in the cement available for release.

The calcium release does not show any obvious trends between glass compositions. The initial release remains fairly constant after the first measurement which means that no calcium is being release during the immersion time and none is being consumed by the cement during the immersion either. It should be noted also that the calcium levels in the solution are relatively low when compared to the phosphorus release.

The phosphorus release data gives a clear trend for all glass compositions; with concentration in solution increasing over time. There does not appear any obvious trend between the different glass compositions in the release rate or amount released. This shows that phosphorus is continually released this may be due to the conversion of relatively phosphate rich calcium phosphate species that initially form and convert to species where phosphate

is less relative to calcium values. This transformation retains the calcium but the phosphate is released into solution, causing the results witnessed here.

Chapter 8: Fluoride Glass Cement Series Results & Discussion

8.1 Results

8.1.1 X-ray Diffraction

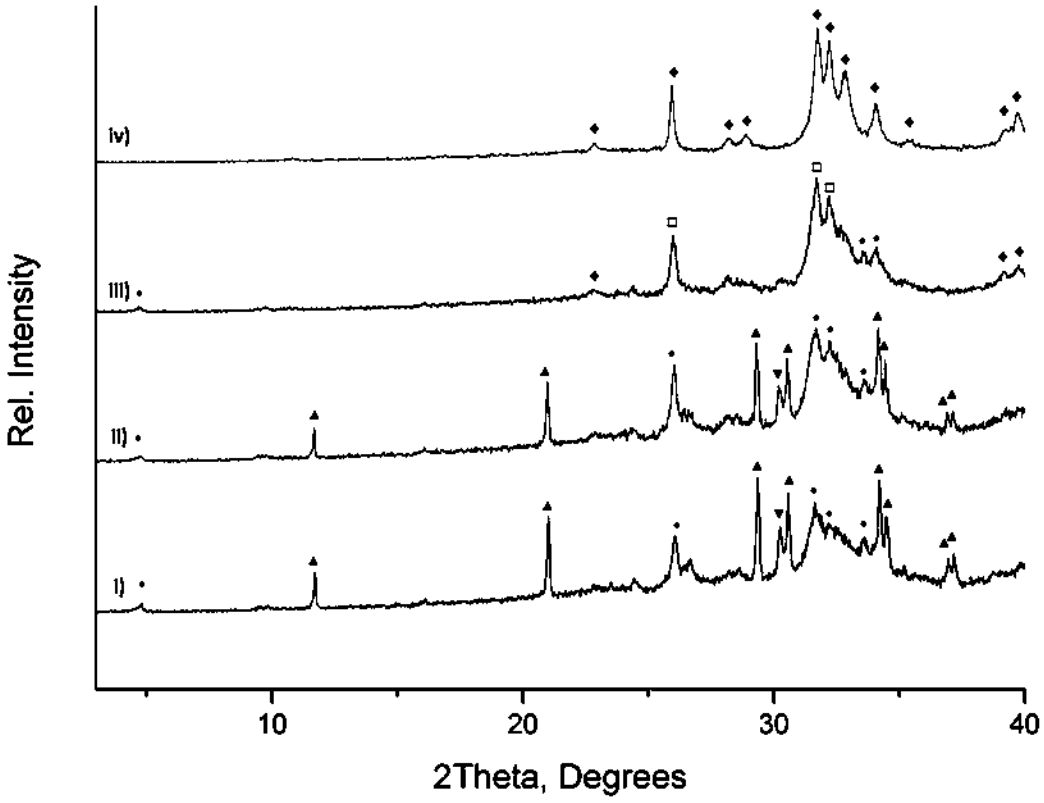

Figure 66 X-ray diffraction patterns of cement composition produced from glass QMNWKPaG04 after immersion in Tris buffer solution for (i) 1 hour, (ii) 1 day, (iii) 7 days and (iv) 28 days. ▲ – DCPD; ▼ – DCPA; ● – Octacalcium Phosphate; □ indistinguishable OCP/Hydroxyapatite; ♦ Apatite.

Figure 66 shows the XRD results for $Ca(H_2PO_4)_2$ and QMNWKPaG04 cements at 1 hour, 1 day, 7 days and 28 days. At one hour and one day the cement is biphasic, consisting of DCPD and OCP. The 4.7 ˚2θ line is small and broad, typically this line is the most intense on the diffraction pattern of OCP. Considering the low intensity of this line relative to the other OCP lines in this sample and that apatite shares these remaining diffraction lines with

OCP, it could be that there is a mixture of both OCP and apatite. After seven days a number of peaks are no longer present for instance the line at 11.67 ˚2θ, thus, DCPD is no longer present. At 28 days the peak at 4.7 ˚2θ of OCP is very low in intensity; it is likely that apatite and OCP are present with OCP in small quantities though other techniques are needed to confirm this.

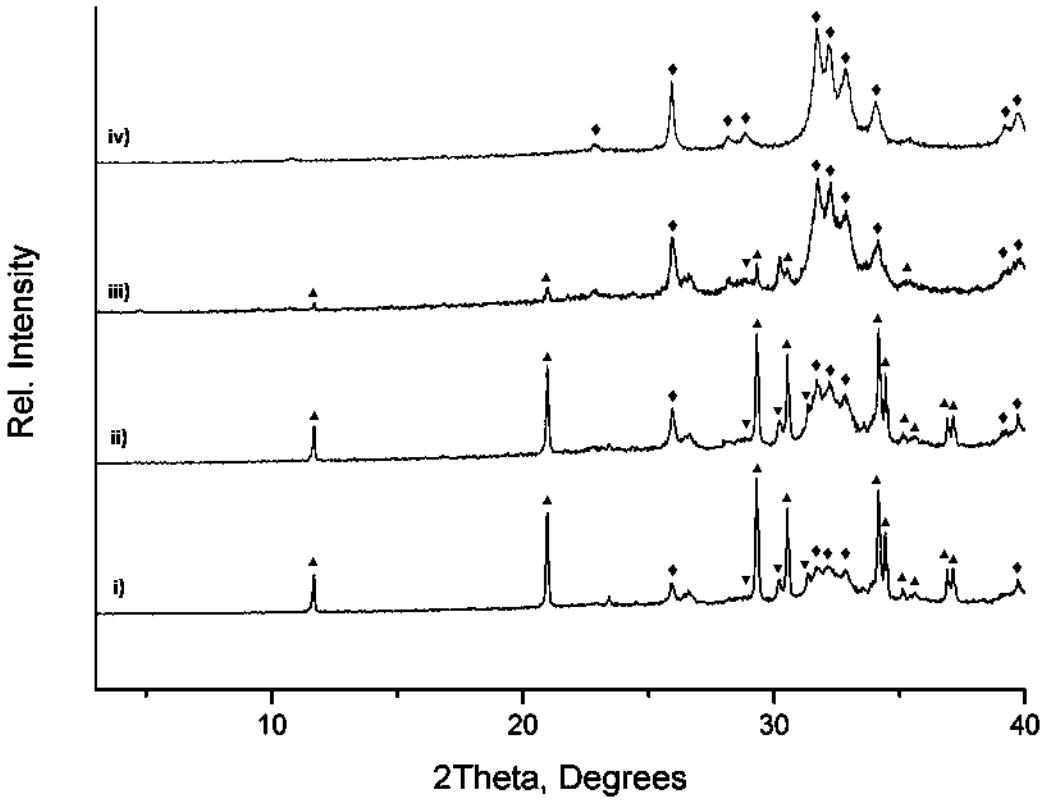

Figure 67 X-ray diffraction patterns of cement composition produced from glass QMNWKPaG06 after immersion in Tris buffer solution for (i) 1 hour, (ii) 1 day, (iii) 7 days and (iv) 28 days. ▲ – DCPD; ▼ – DCPA; ♦ Apatite.

Figure 67 shows the XRD results for QMNWKPaG06 cements at 1 hour, 1 day, 7 days and 28 days. This composition is fluoride containing and at one hour DCPD is present as well as an apatite[5] phase but the appearance of the

[5] The phase is deemed apatite for simplicity. The phase could be hydroxyapatite, fluorohydroxyapatite or fluorapatite as this composition contains fluoride. X-ray diffraction

apatite phase suggests low crystallinity due to the broadness of the peaks. At one day the same phases are present except the intensity of the apatite peaks has increased compared to one hour; indicating the DCPD is transforming to apatite. At seven days a small line is present at 11.67 ˚2θ indicating a small fraction of DCPD present but the majority of the crystalline phase is apatitic. The diffraction pattern of the 28 day cement shows the presence of apatite; DCPD is no longer present.

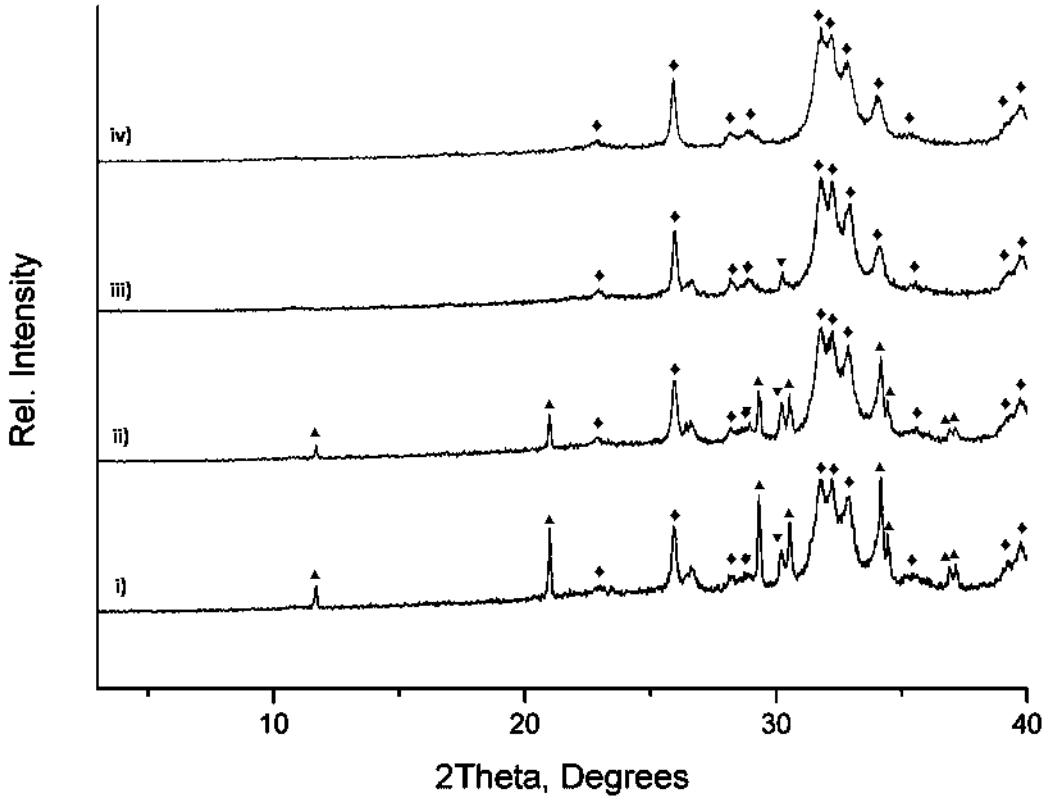

Figure 68 X-ray diffraction patterns of cement composition produced from glass QMNWKPaG07 after immersion in Tris buffer solution for (i) 1 hour, (ii) 1 day, (iii) 7 days and (iv) 28 days. ▲ – DCPD; ▼ – DCPA; ♦ Apatite.

Figure 68 shows the XRD results for QMNWKPaG07 cements at 1 hour, 1 day, 7 days and 28 days. At one hour the main crystalline phase is apatite, DCPD is present in a small fraction of the total crystalline phase. After one

cannot be used to differentiate between these phases consequently the term apatite has been used.

day the diffraction pattern is similar although there is a slight reduction in the intensity of the DCPD peaks. After seven days the DCPD is no longer present; only apatite is present. After 28 days the cement phase is apatite.

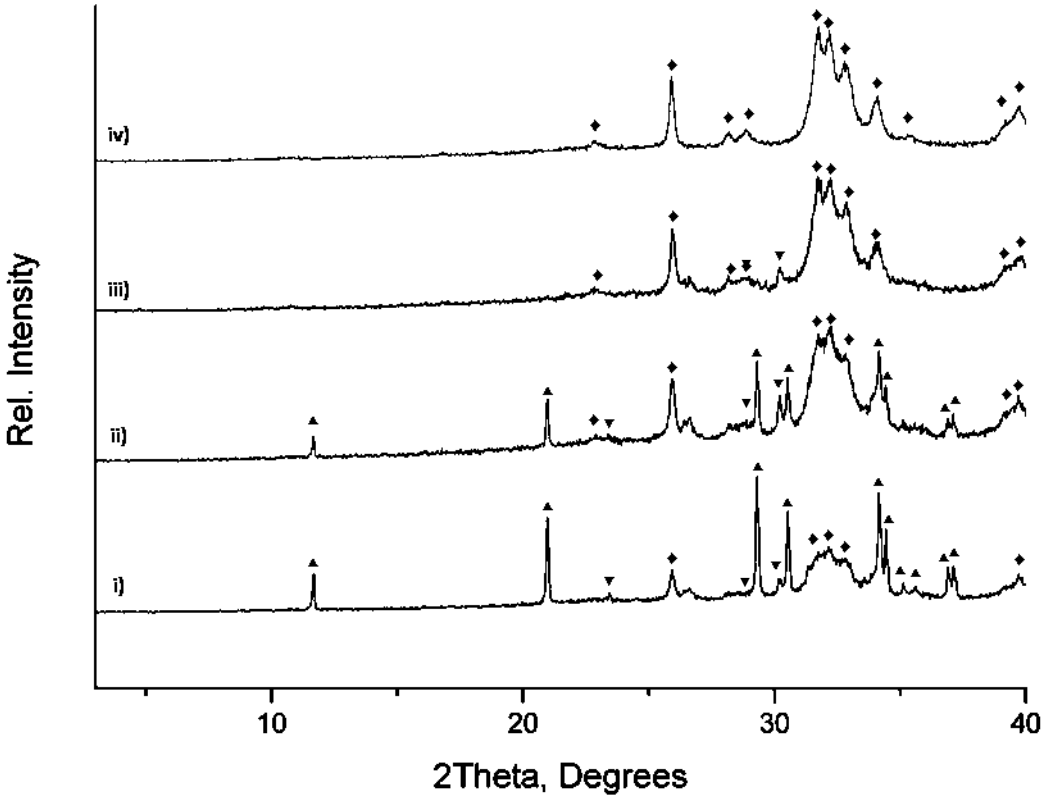

Figure 69 X-ray diffraction patterns of cement composition produced from glass QMNWKPaG08 after immersion in Tris buffer solution for (i) 1 hour, (ii) 1 day, (iii) 7 days and (iv) 28 days. ▲ – DCPD; ▼ – DCPA; ♦ Apatite.

The X-ray diffraction results for cements QMNWKPaG07-10 (Figures 68, 69, 70, 71) were identical with respect to the phases present at each time point. Therefore, for figure descriptions for each please see Figure 68 above.

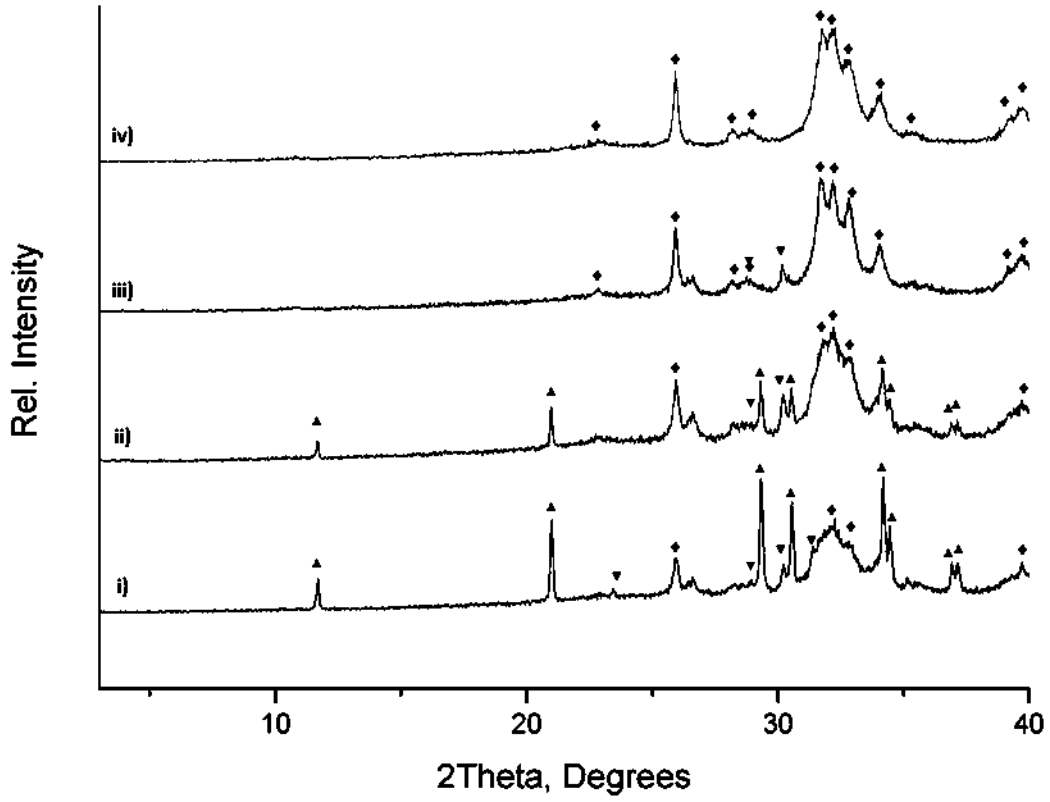

Figure 70 X-ray diffraction patterns of cement composition produced from glass QMNWKPaG09 after immersion in Tris buffer solution for (i) 1 hour, (ii) 1 day, (iii) 7 days and (iv) 28 days. ▲ – DCPD; ▼ – DCPA; ♦ Apatite.

The X-ray diffraction results for cements QMNWKPaG07-10 (Figures 68, 69, 70, 71) were identical with respect to the phases present at each time point. Therefore, for figure descriptions for each please see Figure 68 above.

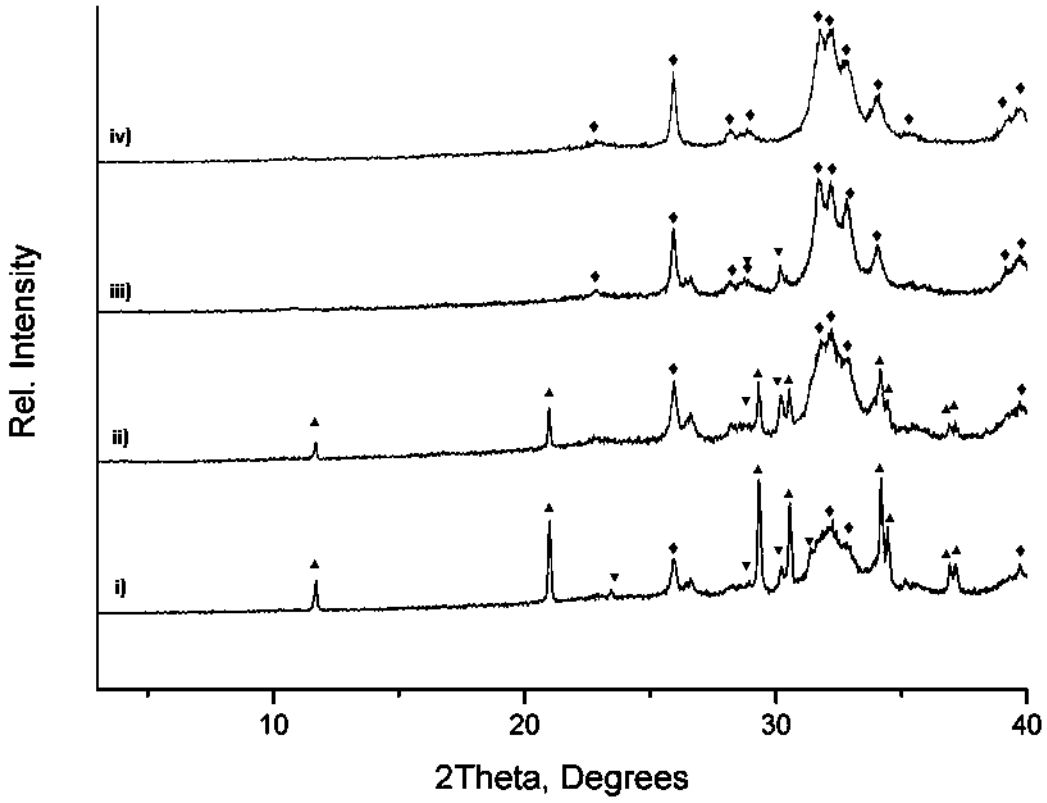

Figure 71 X-ray diffraction patterns of cement composition produced from glass QMNWKPaG10 after immersion in Tris buffer solution for (i) 1 hour, (ii) 1 day, (iii) 7 days and (iv) 28 days. ▲ – DCPD; ▼ – DCPA; ♦ Apatite.

The X-ray diffraction results for cements QMNWKPaG07-10 (Figures 68, 69, 70, 71) were identical with respect to the phases present at each time point. Therefore, for figure descriptions for each please see Figure 66 above.

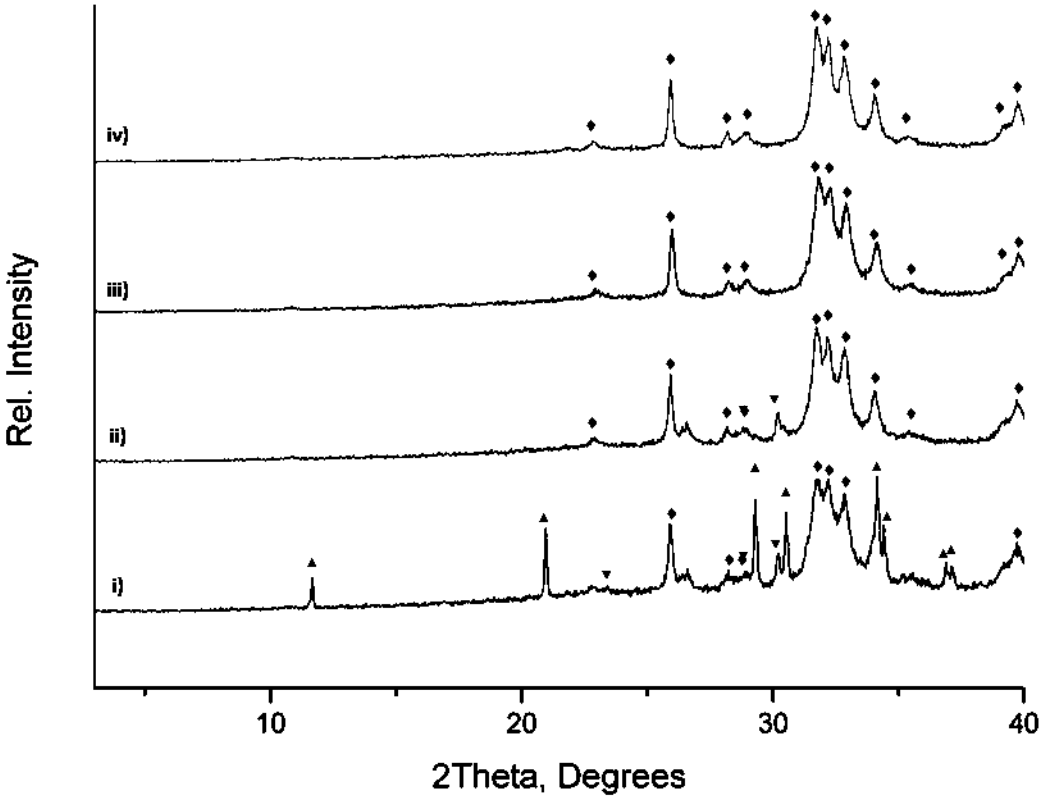

Figure 72 X-ray diffraction patterns of cement composition produced from glass QMNWKPaG11 after immersion in Tris buffer solution for (i) 1 hour, (ii) 1 day, (iii) 7 days and (iv) 28 days. ▲ – DCPD; ▼ – DCPA; ♦ Apatite.

Figure 72 shows the XRD results for QMNWKPaG11 cements at 1 hour, 1 day, 7 days and 28 days. At one hour the main crystalline phase is apatite, DCPD is present in a small fraction of the total crystalline content. After one day the DCPD is not present, the crystalline phase primarily consists of apatite. The patterns for 7 days and 28 days show the crystalline cement phase is apatite.

8.1.2 Magic Angle Spinning Nuclear Magnetic Resonance

8.1.2.1 ^{31}P MAS-NMR

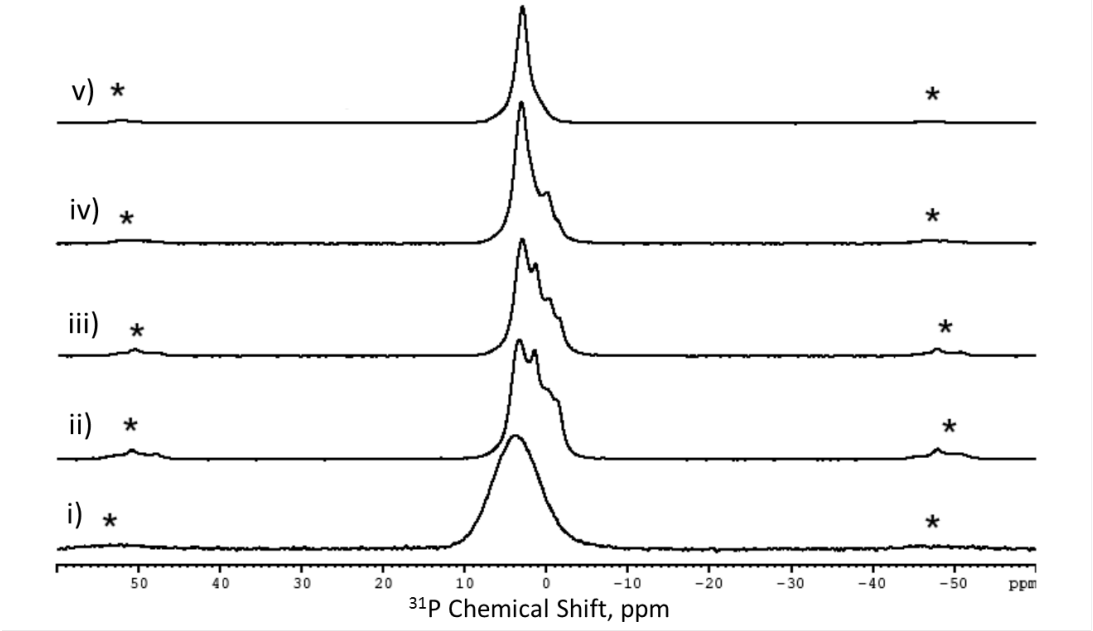

Figure 73 ^{31}P MAS-NMR spectra of the starting glass powder and Tris immersed cement samples in the cement system produced from glass QMNWKPaG04. Showing (i) QMNWKPaG04 initial glass powder; (ii) 1 hour; (iii) 1 day; (iv) 7 days; (v) 28 days.

Figure 73 shows the ^{31}P MAS-NMR results for QMNWKPaG04 glass and QMNWKPaG04 cements at 1 hour, 1 day, 7 days and 28 days. At 1 hour there are chemical shift at -1.4, -0.2, 1.4 and 3.3 ppm. The 1 day sample has chemical shift at -1.4, -0.2, 1.4, and 3.1 ppm. The 1 hour and 1 day spectra show identical phases present with DCPA (-1.4 and -0.2 ppm), DCPD (1.4 ppm) and apatite (3,1 ppm). The 7 day sample has chemical shift at -1.4, -0.2, 2.0 and 3.1 ppm, this shows the same phases present at the 1 hour and 1 day samples (DCPD, DCPA and Apatite). The 2.0 ppm peak appears as a shoulder on the 3.1 ppm peak, this was attributed to DCPD and appears at 2.0 ppm rather than 1.4 ppm due to it being a shoulder on the 3.1 ppm peak

which makes it appear at a higher chemical shift. The 28 day sample has a chemical shift at 2.9 ppm, which was assigned as apatite.

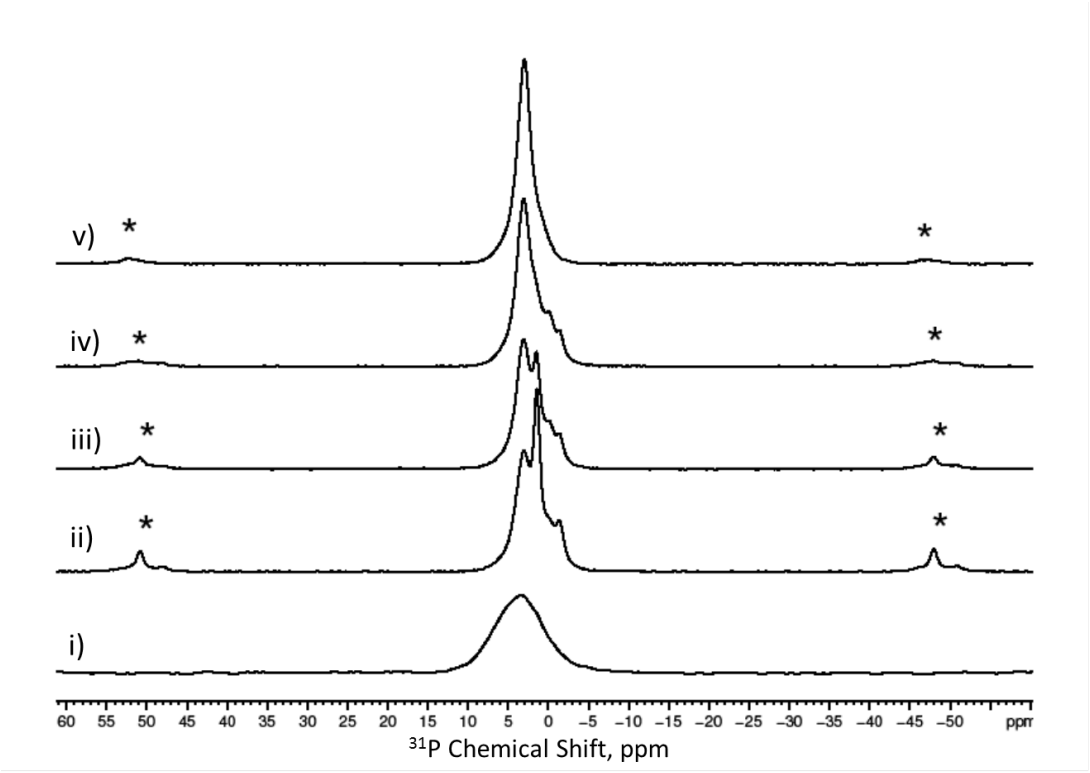

Figure 74 ^{31}P MAS-NMR spectra of the starting glass powder and Tris immersed cement samples in the cement system produced from glass QMNWKPaG06. Showing (i) QMNWKPaG06 initial glass powder; (ii) 1 hour; (iii) 1 day; (iv) 7 days; (v) 28 days.

Figure 74 shows the ^{31}P MAS-NMR results for PaG06 glass and PaG06 cements at 1 hour, 1 day, 7 days and 28 days. At 1 hour the NMR spectra identifies the cement phase formed in the initial reaction, showing the presence of an apatite phase at 2.9 ppm, DCPD at 1.4 ppm and DCPA at --1.4 and -0.2 ppm. At one day the same phases are present except the DCPD has decreased its amount compared to the apatite phase. At 7 days apatite is the primary cement phase, with a small shoulder on the right side of this peak indicating a small residual amount of DCPD. The -0.2 ppm peak is still present as well as a peak at -1.4 ppm showing the presence of DCPA. At 28

days apatite 2.9 ppm is the prominent phase with a small shoulder on the right side indicating another phase though this is unidentifiable.

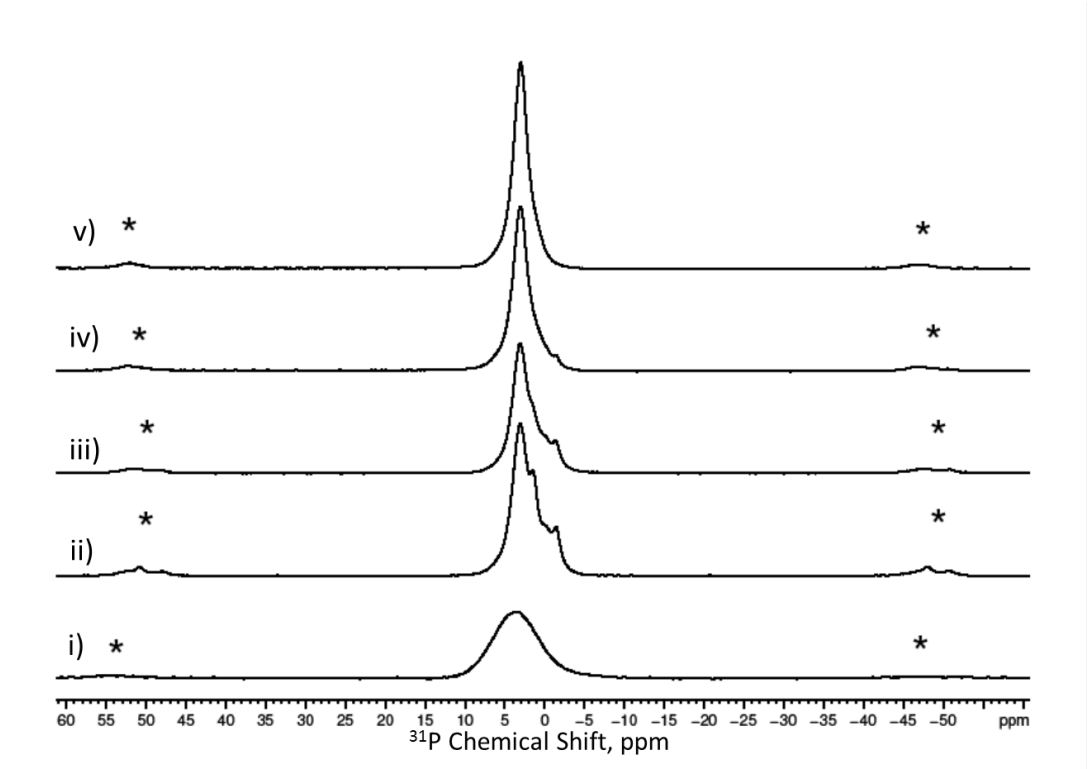

Figure 75 ^{31}P MAS-NMR spectra of the starting glass powder and Tris immersed cement samples in the cement system produced from glass QMNWKPaG07. Showing (i) QMNWKPaG07 initial glass powder; (ii) 1 hour; (iii) 1 day; (iv) 7 days; (v) 28 days.

Figure 75 shows the ^{31}P MAS-NMR results for QMNWKPaG07 glass and QMNWKPaG07 cements at 1 hour, 1 day, 7 days and 28 days. . At 1 hour the NMR spectra identifies the cement phase formed in the initial reaction, showing the presence of an apatite phase at 2.9 ppm, DCPD at 1.4 ppm and DCPA at -1.4 and -0.2 ppm. At one day the same phases are present except the DCPD has decreased its amount compared to the apatite phase, appearing as a shoulder on the right of the apatite peak. After 7 days immersion apatite is the predominant phase with a peak at 2.9 ppm; DCPA -

1.4 and -0.2ppm is also present in small quantities. At 28 days the phosphorus in the cement phase is completely apatitic, 2.9 ppm.

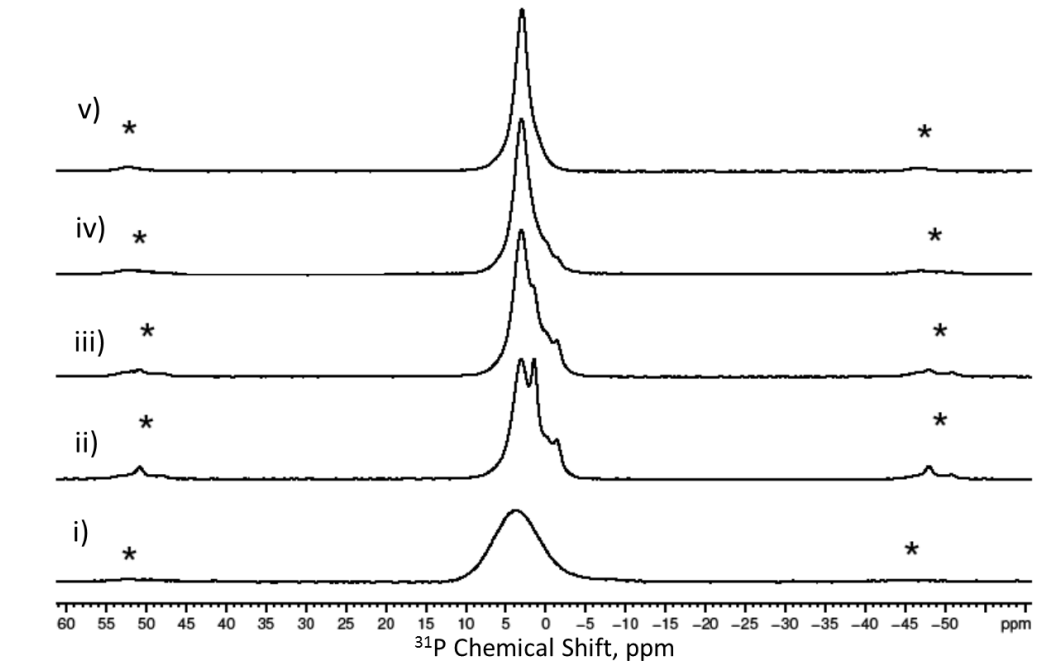

Figure 76 ^{31}P MAS-NMR spectra of the starting glass powder and Tris immersed cement samples in the cement system produced from glass QMNWKPaG08. Showing (i) QMNWKPaG08 initial glass powder; (ii) 1 hour; (iii) 1 day; (iv) 7 days; (v) 28 days.

Figure 76 shows the ^{31}P MAS-NMR results for QMNWKPaG08 glass and QMNWKPaG08 cements at 1 hour, 1 day, 7 days and 28 days. At 1 hour the NMR spectra identifies the cement phase formed in the initial reaction, showing the presence of an apatite phase at 2.9 ppm, DCPD at 1.4 ppm and DCPA at -1.4 and -0.2 ppm. At one day there are peaks at -1.4, -0.2, 1.4 and 2.9 ppm indicating the same phases are present except the DCPD has decreased its amount compared to the apatite phase, appearing as a shoulder on the right of the apatite peak. After 7 days immersion apatite is the predominant phase with a peak at 2.9 ppm; DCPA -1.4 and -0.2 ppm is

also present in small quantities. At 28 days the phosphorus in the cement phase is completely apatitic, 2.9 ppm.

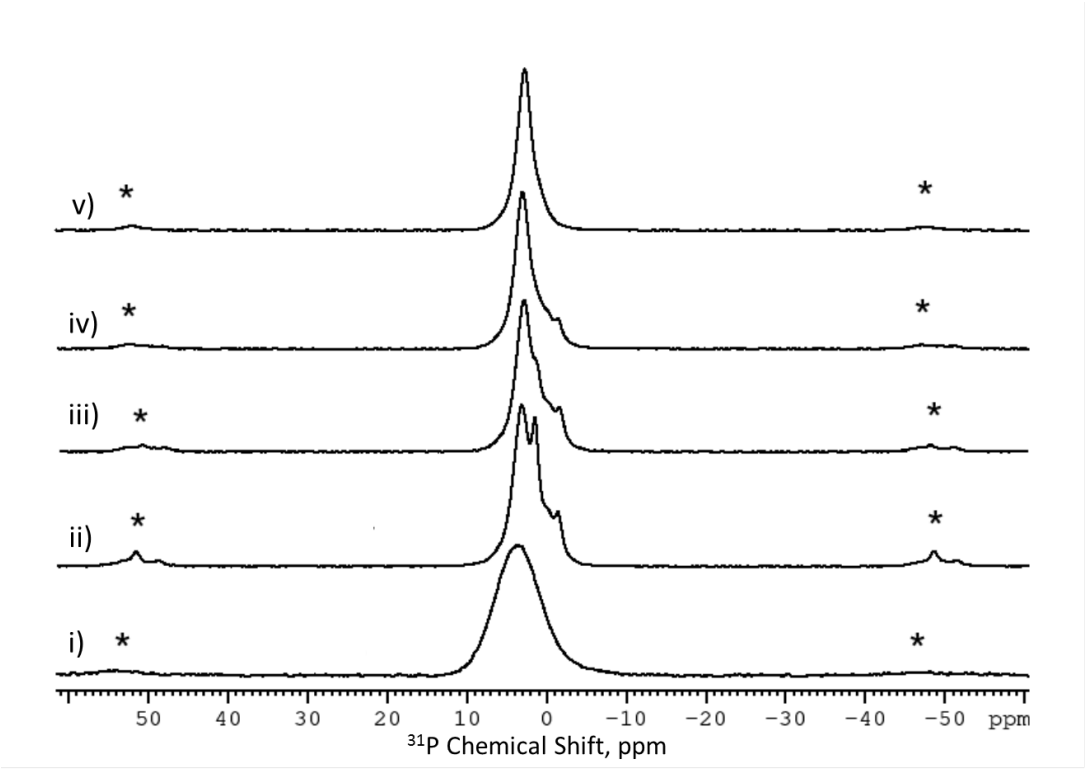

Figure 77 ^{31}P MAS-NMR spectra of the starting glass powder and Tris immersed cement samples in the cement system produced from glass QMNWKPaG09. Showing (i) QMNWKPaG09 initial glass powder; (ii) 1 hour; (iii) 1 day; (iv) 7 days; (v) 28 days.

Figure 77 shows the ^{31}P MAS-NMR results for QMNWKPaG09 glass and QMNWKPaG09 cements at 1 hour, 1 day, 7 days and 28 days. At 1 hour the NMR spectra identifies the cement phase formed in the initial reaction, showing the presence of an apatite phase at 2.9 ppm, DCPD at 1.4 ppm and DCPA at -1.4 and -0.2 ppm. At one day the same phases are present except the DCPD has decreased its amount compared to the apatite phase, appearing as a shoulder on the right of the apatite peak. After 7 days immersion apatite is the predominant phase with a peak at 2.9 ppm; DCPA -

1.4 and -0.2 ppm is also present in small quantities. At 28 days the phosphorus in the cement phase is completely apatitic, 2.9 ppm.

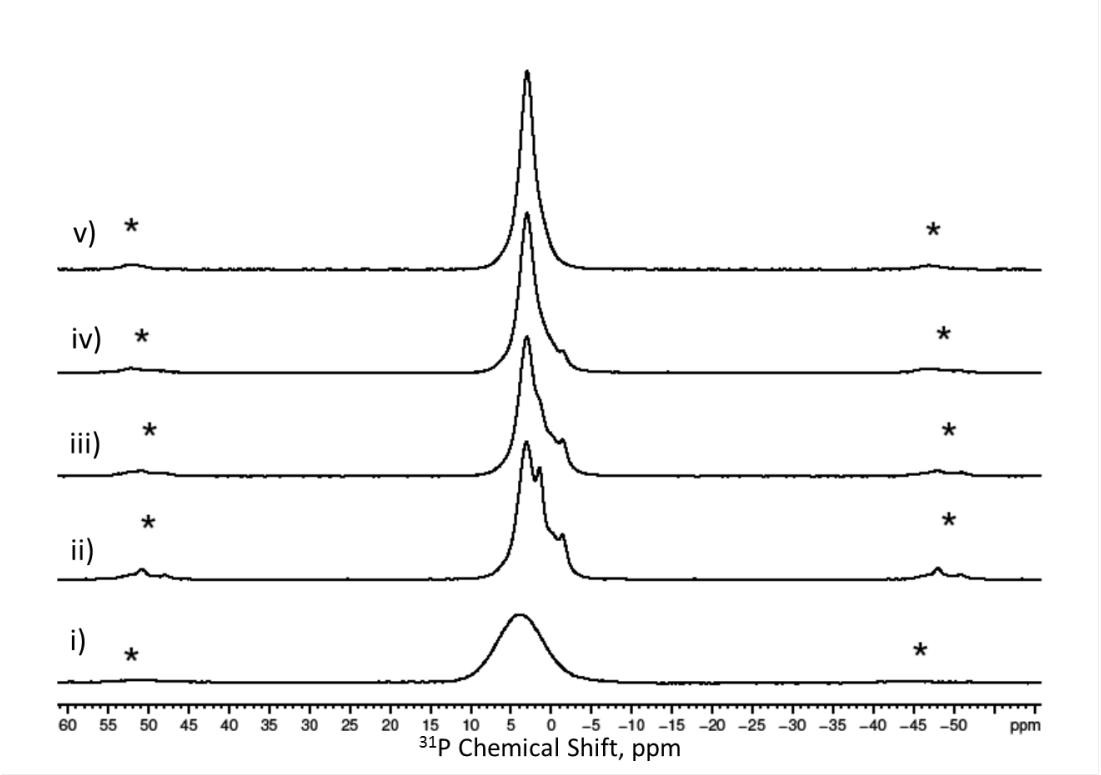

Figure 78 ^{31}P MAS-NMR spectra of the starting glass powder and Tris immersed cement samples in the cement system produced from glass QMNWKPaG10. Showing (i) QMNWKPaG10 initial glass powder; (ii) 1 hour; (iii) 1 day; (iv) 7 days; (v) 28 days.

The ^{31}P MAS-NMR results for cement compositions QMNWKPaG09-11 are identical in the presence of various peaks. For results description of Figure 78 and Figure 79 see the description after Figure 76.

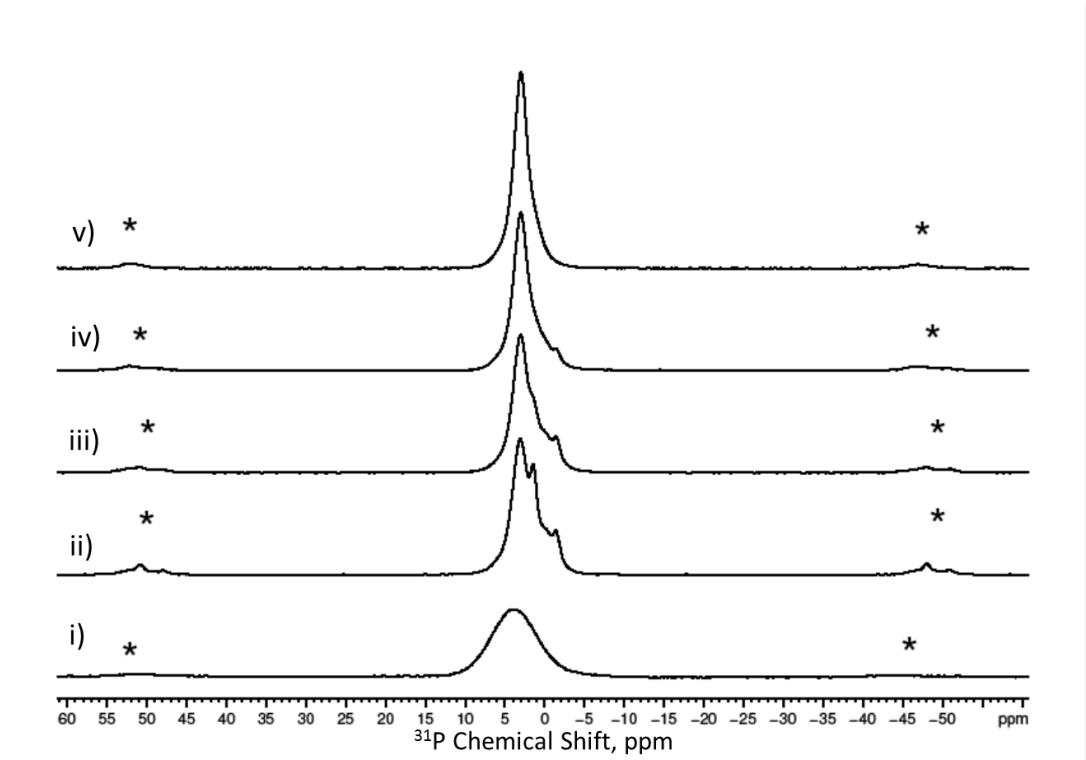

Figure 79 ^{31}P MAS-NMR spectra of the starting glass powder and Tris immersed cement samples in the cement system produced from glass QMNWKPaG11. Showing (i) QMNWKPaG11 initial glass powder; (ii) 1 hour; (iii) 1 day; (iv) 7 days; (v) 28 days.

The ^{31}P MAS-NMR results for cement compositions QMNWKPaG09-11 are identical in the presence of various peaks. For results description of Figure 78 and Figure 79 see the description after Figure 76.

8.1.2.2 ^{19}F MAS-NMR

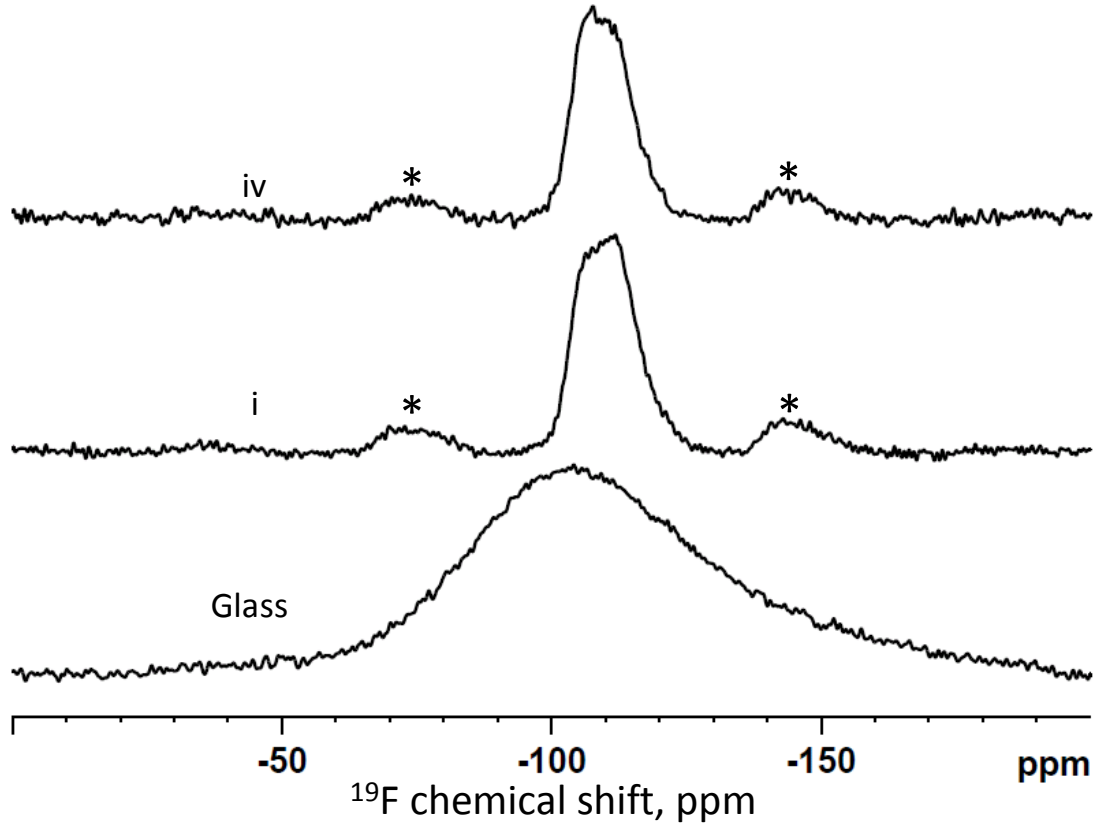

Figure 80 ^{19}F MAS-NMR of glass QMNWKPaG10 and i) 1 hour and iv) 28 days immersion in Tris buffer solution.

The ^{19}F MAS-NMR spectra for QMNWKPaG10 (CaF_2 3.50 mol%) cement compositions at 1 hour and 28 days including the glass are shown in Figure 78. The glass shows a very broad chemical shift with its highest point at approximately -104 ppm. The 1 hour and 28 day samples show at least two peaks very close to each other in the same positions in each spectrum at -106 and -108 ppm. There is a slight change in the relative intensity between the two bands at -106 and -108 ppm, with the -108 ppm peak being slightly more intense at 1 hour, whereas at 28 days this is reversed.

8.1.3 Fourier Transform Infrared

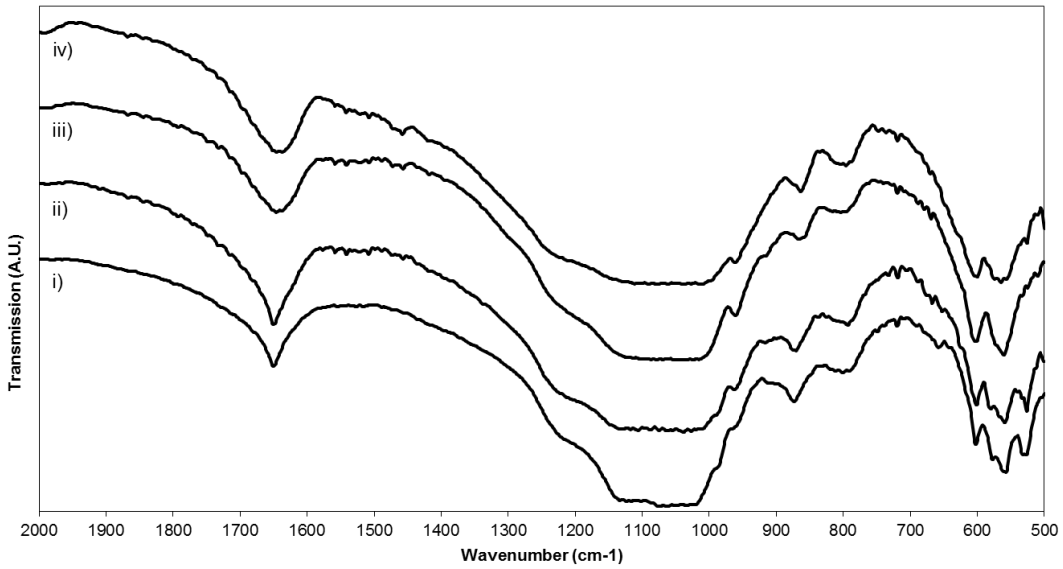

Figure 81 Fourier transform infrared spectra of cement composition QMNWKPaG04 at (i) 1 hour, (ii) 1 day, (iii) 7 days, and (iv) 28 days immersion time in Tris buffer solution, plotted between 500 to 2000 wavenumber cm^{-1}.

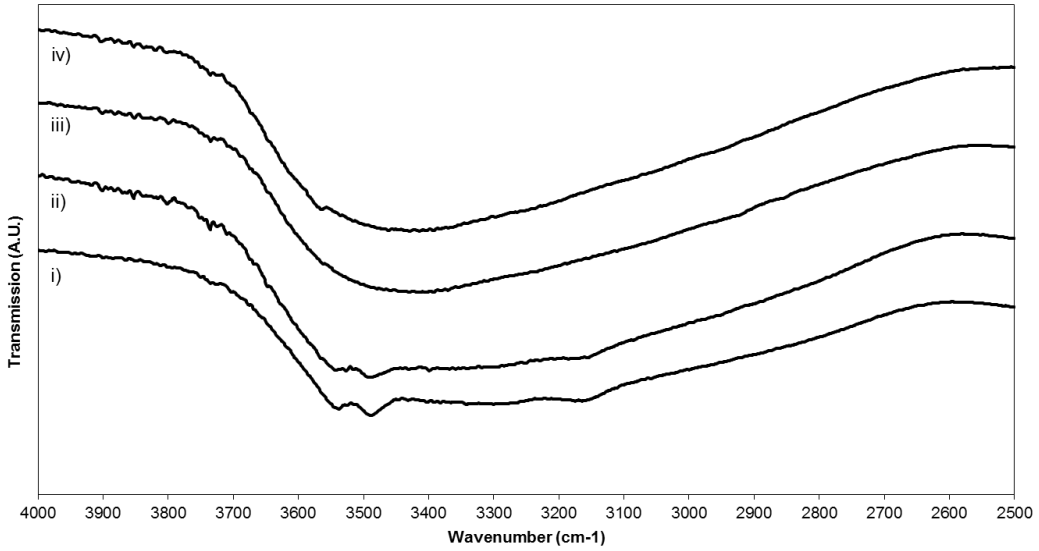

Figure 82 Fourier transform infrared spectra of cement composition QMNWKPaG04 at (i) 1 hour, (ii) 1 day, (iii) 7 days, and (iv) 28 days immersion time in Tris buffer solution, plotted between 2500 to 4000 wavenumber cm^{-1}.

Table 24 FTIR bands and their respective assignments of cement samples produced from glass QMNWKPaG04 after immersion in Tris buffer solution for 1 hour, 1 day, 7 days and 28 days.

Wavenumber (cm^{-1})	Assignment	1 Hour	1 Day	7 Day	28 Day
523	PO Bending	√	√	-	-
554	PO Bending	√	√	√	√
566	PO Bending	√	√	-	-

596	PO Bending	√	√	√	√
781	H_2O Liberation	√	√	√	√
854	HPO_4(5) [P-(OH)] Stretching	-	-	√	√
865	P-O(H) Stretching	√	√	-	-
954	PO_4 Stretching	√	√	√	√
982	P-O Stretching	√	-	-	-
1213	O-H In-plane Bending	√	√		
1643	H_2O Bending	√	√	√	√
3148	OH Stretching of Water	√	-	-	-
3473	OH Stretching of Water	√	√	-	-
3528	OH Stretching of Water	√	√	-	-
3554	H-bonded H_2O	-	-	-	√

Figures 81 and 82 show the FTIR spectra of cement composition QMNWKPaG04 at 1 hour, 1 day, 7 days and 28 days. The spectra at 1 hour and 1 day are similar in which bands they have present with PO bond bending and stretching bands at 524, 554, 566, 596, 954 and 982 (1 hour only) cm^{-1}. At 865 cm^{-1} both spectra have a band donating P-O(H) Stretching groups. Lastly there are bands showing water molecules at 781, 1643, 3148 (1 hour only), 3473 and 3528 cm^{-1}. Similarly to the 1 hour and 1 day spectra the 7 day and 28 day samples also have similar bands. PO bending and stretching bands are present at 555, 597 and 954 cm^{-1}, with a P-O(H) Stretching band at 855 cm^{-1}. Structural water molecules give bands at 785, 784 and 1630 cm^{-1}, with the 28 day sample having a H-bonded H_2O band at 3554 cm^{-1}.

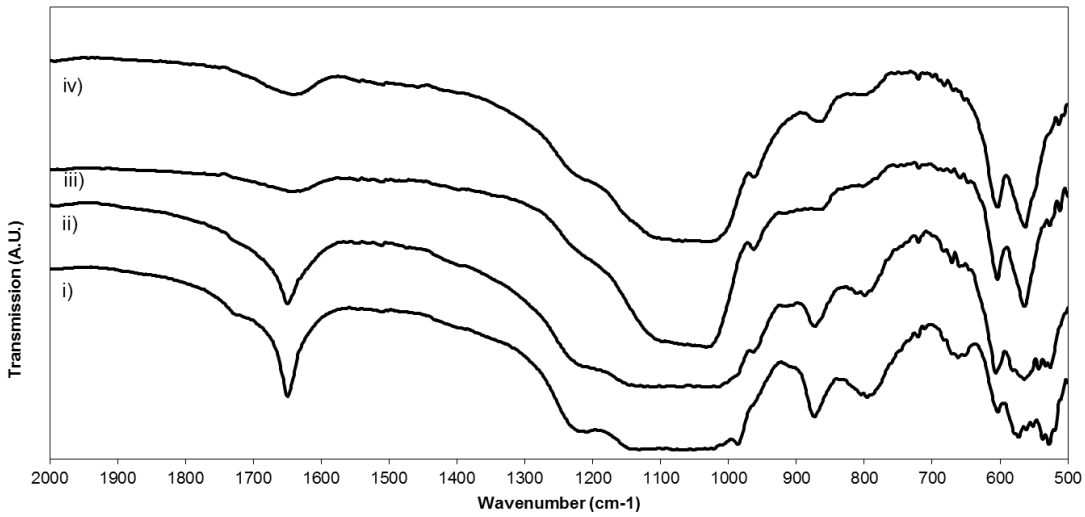

Figure 83 Fourier transform infrared spectra of cement composition QMNWKPaG06 at (i) 1 hour, (ii) 1 day, (iii) 7 days, and (iv) 28 days immersion time in Tris buffer solution, plotted between 500 to 2000 wavenumber cm^{-1}.

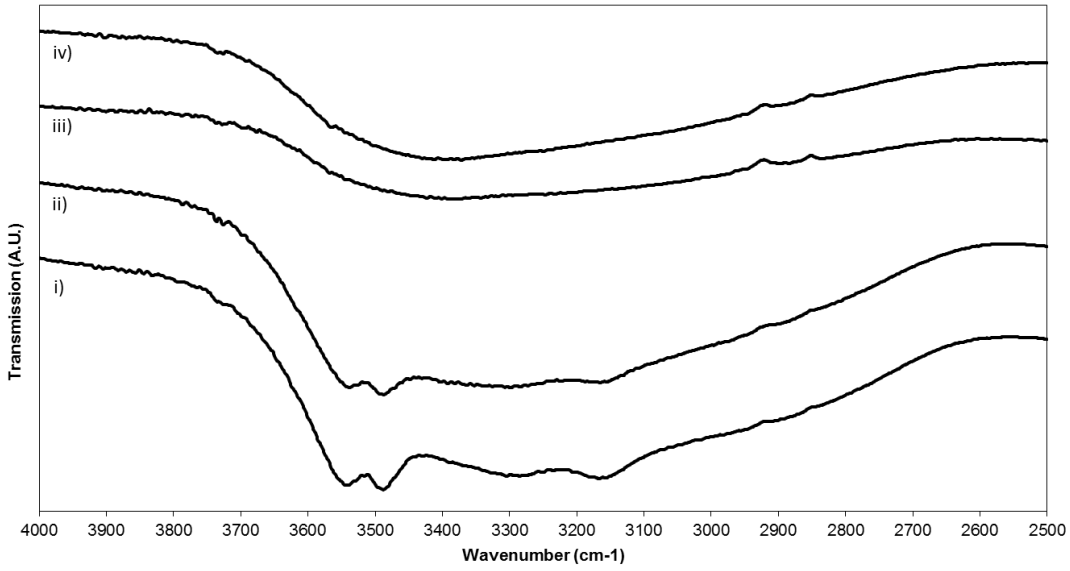

Figure 84 Fourier transform infrared spectra of cement composition QMNWKPaG06 at (i) 1 hour, (ii) 1 day, (iii) 7 days, and (iv) 28 days immersion time in Tris buffer solution, plotted between 2500 to 4000 wavenumber cm^{-1}.

Table 25 FTIR bands and their respective assignments of cement samples produced from glass QMNWKPaG06 after immersion in Tris buffer solution for 1 hour, 1 day, 7 days and 28 days.

Wavenumber (cm^{-1})	Assignment	1 Hour	1 Day	7 Day	28 Day
524	PO Bending	√	√	-	-
561	PO Bending	√	√	√	√
599	PO Bending	√	√	√	√
649	H_2O Liberation	√	√	-	-

781	H_2O Liberation	√	√		√
852	P-O(H) Stretching	-	-	√	√
866	P-O(H) Stretching	-	-	√	√
953	PO_4 Stretching	-	-	-	-
980	P-O Stretching	√	-	-	-
1205	O-H In-plane Bending	√	√	√	√
1628	H_2O Bending	-	-	√	√
1645	H_2O Bending	√	√	-	-
1714	Overtone of 866 band - 2 x 866 = 1732	√	√	-	-
3150	OH Stretching of Water	√	√	-	-
3476	OH Stretching of Water	√	√	-	-
3531	OH Stretching of Water	√	√	-	-

Figures 83 and 84 show the FTIR spectra of cement composition QMNWKPaG06 at 1 hour, 1 day, 7 days and 28 days. At 1 hour and 1 day there are PO bending and stretching bands at 524, 561, 599 and 980 cm^{-1}. In addition there is a P-O(H) stretching band at 866 cm^{-1}. Finally bands from water molecules are present at 649 (1 hour only), 781, 3150, 3476 and 3531 cm^{-1}. The 7 day and 28 day samples have PO bending and stretching bands at 561, 600, 653 and 953 cm^{-1}, with a P-O(H) Stretching band at 852 cm^{-1}. Similarly to the 1 hour and 1 day samples there are structural water molecules present at 1628 1209 and, in the 28 day sample, at 787 cm^{-1}.

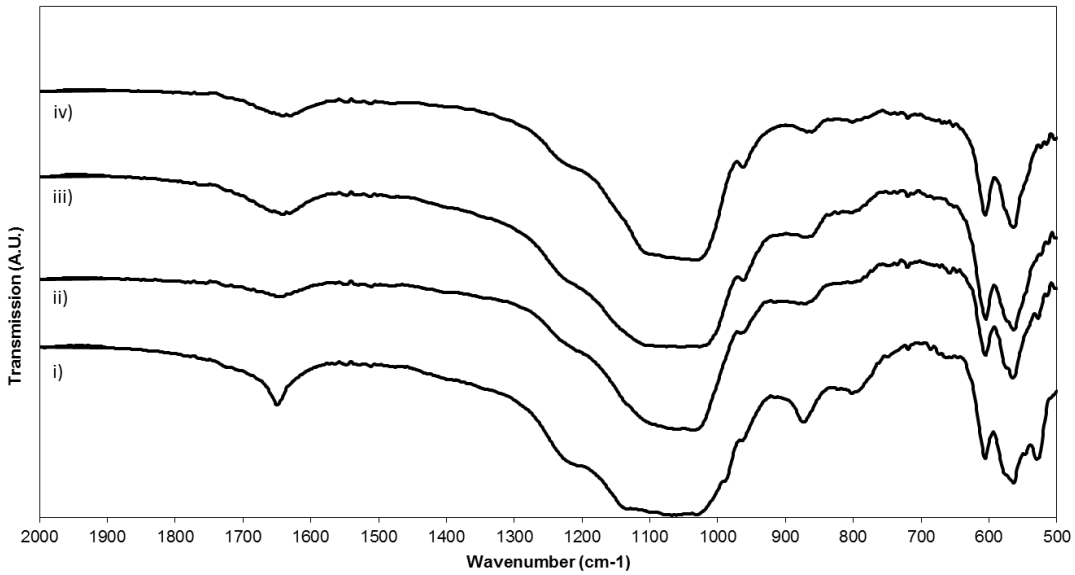

Figure 85 Fourier transform infrared spectra of cement composition QMNWKPaG07 at (i) 1 hour, (ii) 1 day, (iii) 7 days, and (iv) 28 days immersion time in Tris buffer solution, plotted between 500 to 2000 wavenumber cm^{-1}.

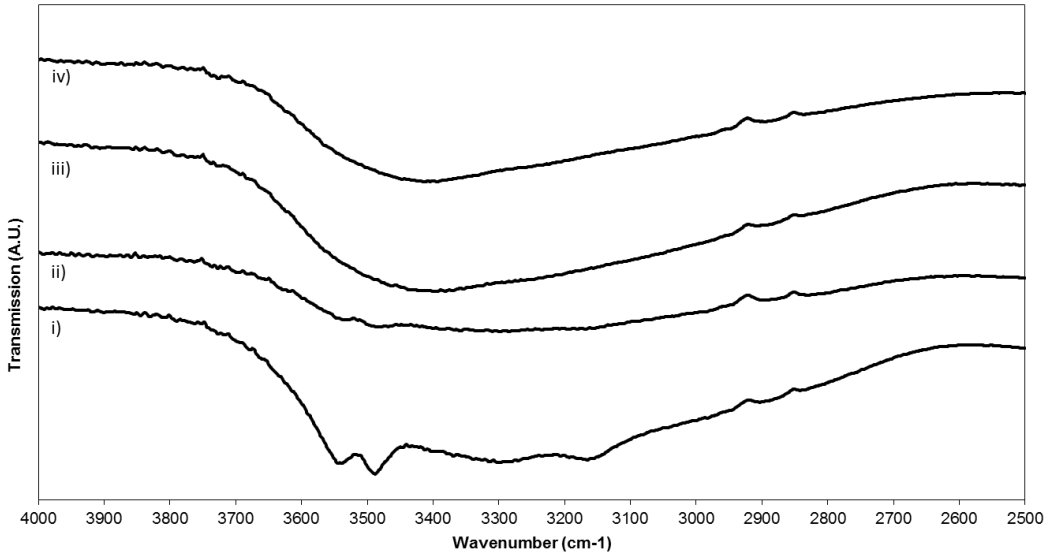

Figure 86 Fourier transform infrared spectra of cement composition QMNWKPaG07 at (i) 1 hour, (ii) 1 day, (iii) 7 days, and (iv) 28 days immersion time in Tris buffer solution, plotted between 2500 to 4000 wavenumber cm^{-1}.

Table 26 FTIR bands and their respective assignments of cement samples produced from glass QMNWKPaG07 after immersion in Tris buffer solution for 1 hour, 1 day, 7 days and 28 days.

Wavenumber (cm^{-1})	Assignment	1 Hour	1 Day	7 Day	28 Day
524	PO Bending	√	-	-	-
559	PO Bending	√	√	√	√
564	PO Bending	√	√	√	-
600	PO Bending	√	√	√	√

785	H_2O Liberation	√	√	√	√
854	P-O(H) Stretching	-	-	√	√
858	P-O(H) Stretching		√	-	-
866	P-O(H) Stretching	√	-	-	-
955	PO_4 Stretching	√	√	√	√
983	P-O Stretching	√	-	-	-
1207	O-H In-plane Bending	√	√	√	√
1630	H_2O Bending	-	√	√	√
1641	H_2O Bending	√	-	-	-
3148	OH Stretching of Water	√	-	-	-
3478	OH Stretching of Water	√	√	-	-
3530	OH Stretching of Water	√	√	-	-

Figures 85 and 86 show the FTIR spectra of cement composition QMNWKPaG07 at 1 hour, 1 day, 7 days and 28 days. At 1 hour and 1 day the PO bending and stretching bands are similar being at 559, 567, 601 and 955 cm^{-1}, the 1 hour sample has an additional band at 524 cm^{-1}. Each sample also has also a P-O(H) Stretching band at 864 cm^{-1}. Lastly there are structural water molecules present at 785, 1207, 1641, 3148, 3478 and 3530 cm^{-1}. The 7 day and 28 day samples are similar having PO bending and stretching bands at 559, 567 (7 day only), 600and 955 cm^{-1}. Similarly to the 1 hour and 1 day samples there are structural water molecules at 784, 1211 and 1627 cm^{-1}.

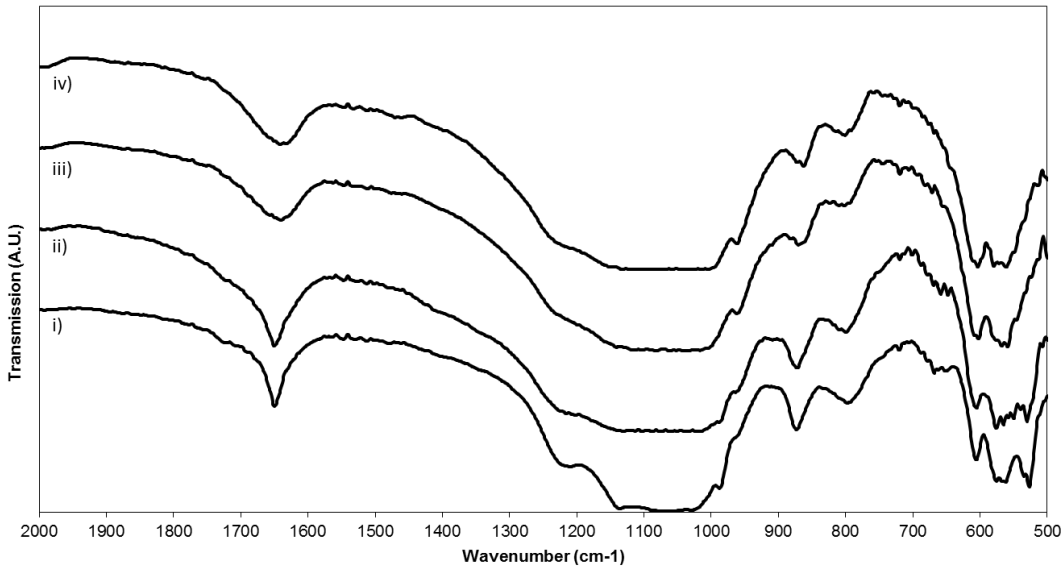

Figure 87 Fourier transform infrared spectra of cement composition QMNWKPaG08 at (i) 1 hour, (ii) 1 day, (iii) 7 days, and (iv) 28 days immersion time in Tris buffer solution, plotted between 500 to 2000 wavenumber cm^{-1}.

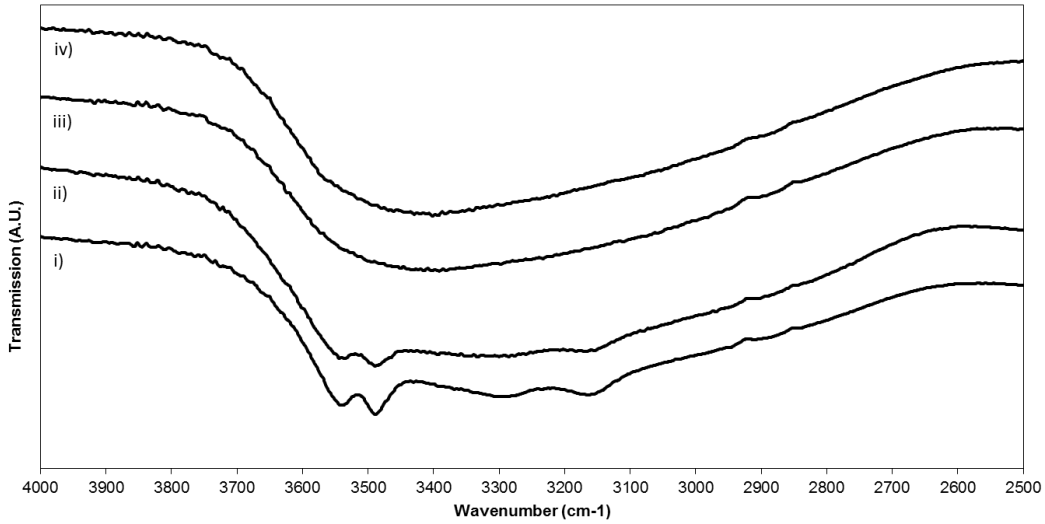

Figure 88 Fourier transform infrared spectra of cement composition QMNWKPaG08 at (i) 1 hour, (ii) 1 day, (iii) 7 days, and (iv) 28 days immersion time in Tris buffer solution, plotted between 2500 to 4000 wavenumber cm^{-1}.

Table 27 FTIR bands and their respective assignments of cement samples produced from glass QMNWKPaG08 after immersion in Tris buffer solution for 1 hour, 1 day, 7 days and 28 days.

Wavenumber (cm^{-1})	Assignment	1 Hour	1 Day	7 Day	28 Day
523	PO Bending	√	√	-	-
557	PO Bending	√	√	√	√
600	PO Bending	√	√	√	√
784	H2O Liberation	√	√	√	√
866	P-O(H) Stretching	√	√	√	√

955	P-O Stretching	√	√	√	√
982	P-O Stretching	√	-	-	-
1205	O-H In-plane Bending	√	√	√	√
1627	H2O Bending	-	-	√	√
1644	H2O Bending	√	√	-	-
3144	OH Stretching of Water	√	√	-	-
3280	OH Stretching of Water	√	-	-	-
3477	OH Stretching of Water	√	√	-	-
3527	OH Stretching of Water	√	√	-	-

Figures 87 and 88 show the FTIR spectra of cement composition QMNWKPaG08 at 1 hour, 1 day, 7 days and 28 days. At 1 hour and 1 day the samples share similar spectra, with PO bending and stretching bands at 523, 557, 600, 955 and 982 (1 hour only) cm^{-1}, in addition there is also a P-O(H) Stretching band at 866 cm^{-1} on both spectra. Bands from water molecules bands exist at 784, 1205, 1644, 3144, 3280 (1 hour only), 3477 and 3527 cm^{-1}. At 7 days and 28 days there are less bands compared to the previous immersion time points and like previous samples the two spectra have almost identical bands present. There are PO bending and stretching bands in both spectra at 555, 598 and 953 cm^{-1}. Similarly to the 1 hour and 1 day samples there is a P-O(H) Stretching band at 856 cm^{-1}. There are also three bands from water molecules at 788, 1217, 1627 cm^{-1}.

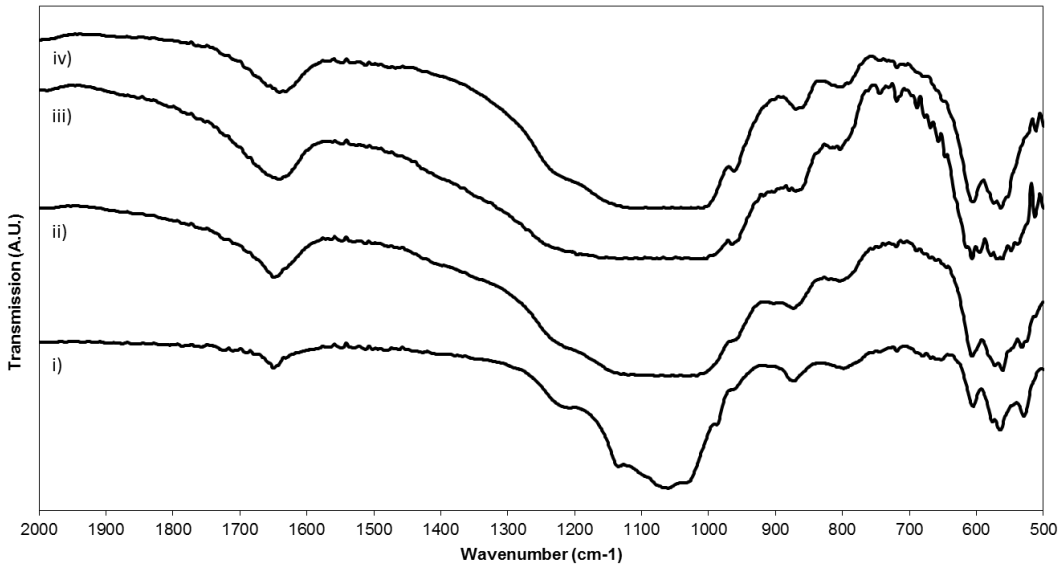

Figure 89 Fourier transform infrared spectra of cement composition QMNWKPaG09 at (i) 1 hour, (ii) 1 day, (iii) 7 days, and (iv) 28 days immersion time in Tris buffer solution, plotted between 500 to 2000 wavenumber cm^{-1}.

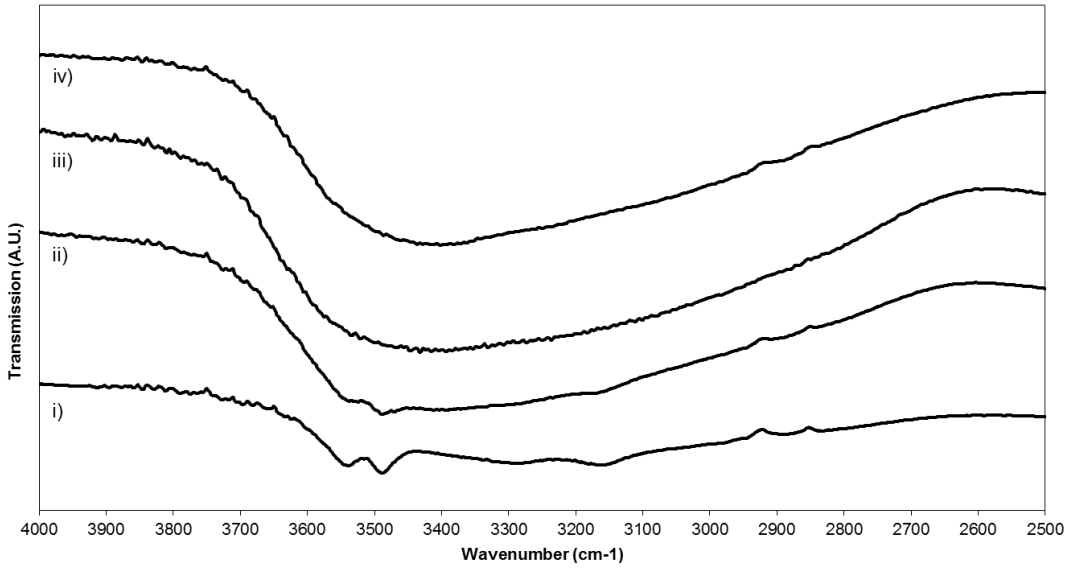

Figure 90 Fourier transform infrared spectra of cement composition QMNWKPaG09 at (i) 1 hour, (ii) 1 day, (iii) 7 days, and (iv) 28 days immersion time in Tris buffer solution, plotted between 2500 to 4000 wavenumber cm^{-1}.

Table 28 FTIR bands and their respective assignments of cement samples produced from glass QMNWKPaG09 after immersion in Tris buffer solution for 1 hour, 1 day, 7 days and 28 days.

Wavenumber (cm^{-1})	Assignment	1 Hour	1 Day	7 Day	28 Day
524	PO Bending	√	√	-	-
559	PO Bending	√	√	√	√
566	PO Bending	√	√	-	-
599	PO Bending	√	√	√	√

786	H_2O Liberation	√	√	√	√
862	P-O(H) Stretching	√	√	√	√
950	P-O Stretching	√	√	√	√
982	P-O Stretching	√	-	-	-
1123	PO Stretching	√	-	-	-
1211	O-H In-plane Bending	√	√		√
1638	H_2O Bending	√	√	√	√
3141	OH Stretching of Water	√	-	-	-
3477	OH Stretching of Water	√	√	-	-
3531	OH Stretching of Water	√	√	-	-

Figures 89 and 90 show the FTIR spectra of cement composition QMNWKPaG09 at 1 hour, 1 day, 7 days and 28 days. The 1 hour and 1 day spectra share similarities in having PO bending bands at 524, 559, 566, 599 cm^{-1} and a PO stretching band at 950 cm^{-1}. The 1 hour sample has additional PO stretching bands at 982 and 1123 cm^{-1}, which the 1 day sample does not have. In addition to the phosphate groups both spectra also have bands of water molecules at 786, 1638, 3141 (1 hour only), 3477, 3531 cm^{-1}. The 7 day and 28 day samples have relatively few bands on the spectra. There are PO bending and stretching bands at 555, 592 and 953 cm^{-1} as well as a P-O(H) Stretching band at 853 cm^{-1}. There are also some water molecule bands at 781, 1217 (28 day only) and 1625 cm^{-1}.

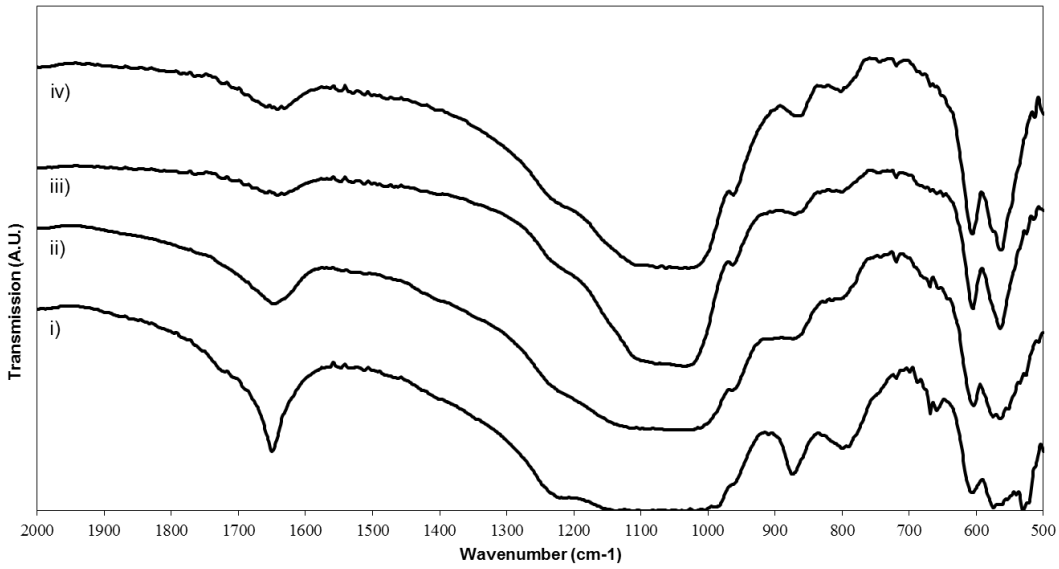

Figure 91 Fourier transform infrared spectra of cement composition QMNWKPaG10 at (i) 1 hour, (ii) 1 day, (iii) 7 days, and (iv) 28 days immersion time in Tris buffer solution, plotted between 500 to 2000 wavenumber cm^{-1}.

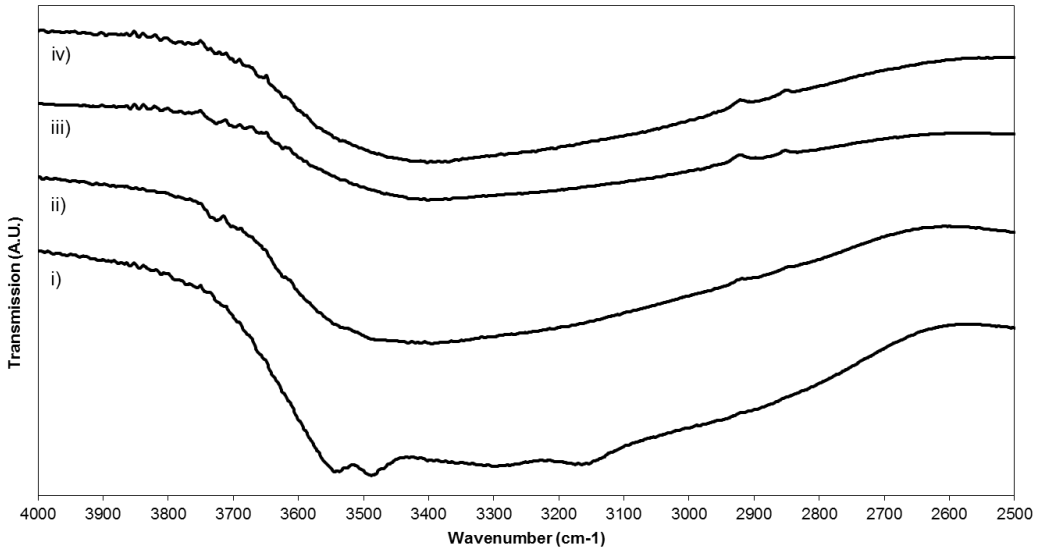

Figure 92 Fourier transform infrared spectra of cement composition QMNWKPaG10 at (i) 1 hour, (ii) 1 day, (iii) 7 days, and (iv) 28 days immersion time in Tris buffer solution, plotted between 2500 to 4000 wavenumber cm^{-1}.

Table 29 FTIR bands and their respective assignments of cement samples produced from glass QMNWKPaG10 after immersion in Tris buffer solution for 1 hour, 1 day, 7 days and 28 days.

Wavenumber (cm^{-1})	Assignment	1 Hour	1 Day	7 Day	28 Day
519	PO Bending	√	-	-	-
553	PO Bending	√	√	-	-
560	PO Bending	-	-	√	√
595	PO Bending	√	√	-	-
601	PO Bending	-	-	√	√

650	H_2O Liberation	√	-	-	-
784	H_2O Liberation	√	√	√	√
865	P-O(H) Stretching	√	√	√	√
955	P-O Stretching	-	-	√	√
1203	O-H In-plane Bending	-	-	√	√
1219	O-H In-plane Bending	√	√	-	-
1627	H_2O Bending	-	-	√	√
1644	H_2O Bending	√	√		
1703	Overtone of 865 band - 2 x 865 = 1730	√	-	-	-
3144	OH Stretching of Water	√	-	-	-
3285	OH Stretching of Water	√	-	-	-
3473	OH Stretching of Water	√	-	-	-
3531	OH Stretching of Water	√	-	-	-

Figures 91 and 92 show the FTIR spectra of cement composition QMNWKPaG10 at 1 hour, 1 day, 7 days and 28 days. The 1 hour sample has PO bending and stretching bands at 519, 553 and 595 cm^{-1}, with a P-O(H) Stretching band at 865 cm^{-1}. The 1 day, 7 day and 28 day samples share all the same bands. There are PO bending and stretching bands at 553, 598 and 953 cm^{-1}, with a P-O(H) Stretching band at 855 cm^{-1}. Lastly there are bands from water molecules at 790, 1219 and 1636 cm^{-1}.

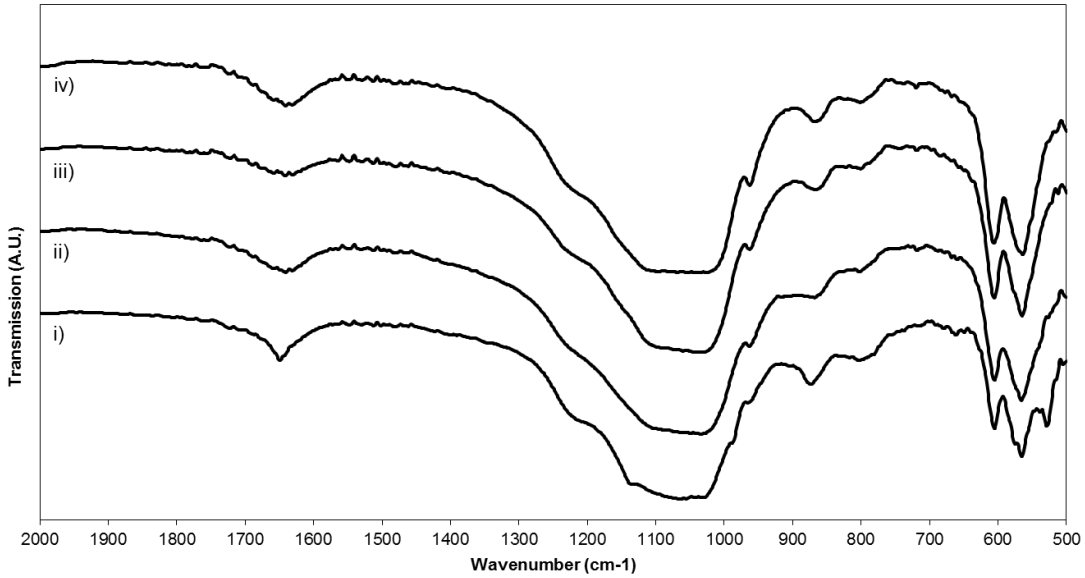

Figure 93 Fourier transform infrared spectra of cement composition QMNWKPaG11 at (i) 1 hour, (ii) 1 day, (iii) 7 days, and (iv) 28 days immersion time in Tris buffer solution, plotted between 500 to 2000 wavenumber cm^{-1}.

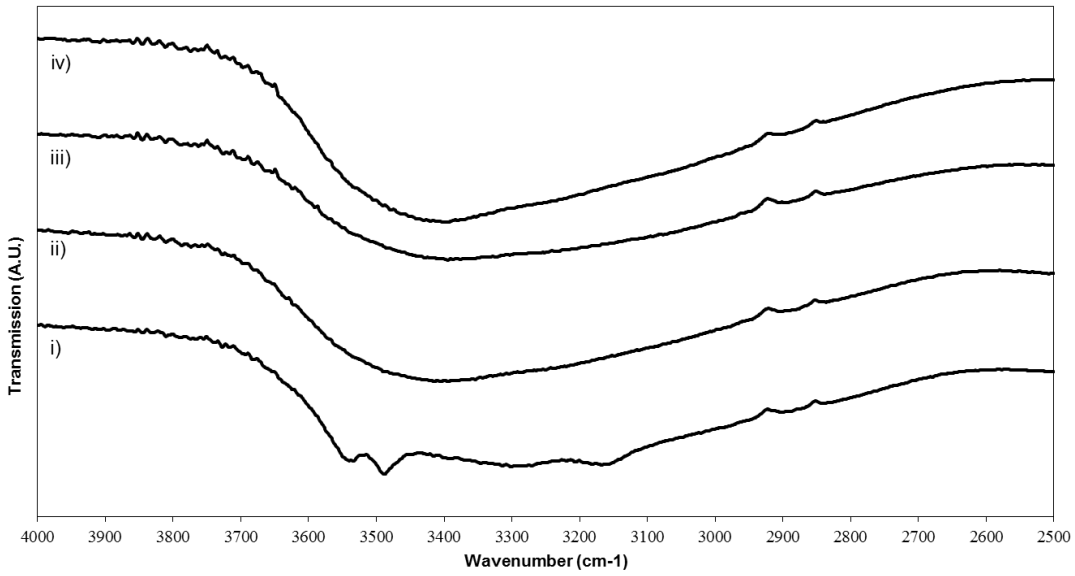

Figure 94 Fourier transform infrared spectra of cement composition QMNWKPaG11 at (i) 1 hour, (ii) 1 day, (iii) 7 days, and (iv) 28 days immersion time in Tris buffer solution, plotted between 2500 to 4000 wavenumber cm^{-1}.

Table 30 FTIR bands and their respective assignments of cement samples produced from glass QMNWKPaG11 after immersion in Tris buffer solution for 1 hour, 1 day, 7 days and 28 days.

Wavenumber (cm^{-1})	Assignment	1 Hour	1 Day	7 Day	28 Day
525	PO Bending	√	-	-	-
562	PO Bending	√	√	√	√
567	PO Bending	√	-	-	-
601	PO Bending	√	√	√	√

781	H_2O Liberation	√	-	-	√
862	P-O(H) Stretching	√	√	√	√
954	P-O Stretching	√	√	√	√
983	P-O(H) Stretching	√	-	-	-
1199	O-H In-plane Bending	√	-	-	-
1211	O-H In-plane Bending	-	√	√	√
1625	H_2O Bending	-	√	√	√
1638	H_2O Bending	√	-	-	-
3144	OH Stretching of Water	√	-	-	-
3475	OH Stretching of Water	√	-	-	-
3530	OH Stretching of Water	√	-	-	-

Figures 93 and 94 show the FTIR spectra of cement composition QMNWKPaG11 at 1 hour, 1 day, 7 days and 28 days. At 1 hour there are PO bending and stretching bands at 525, 562, 567, 601 and 954 cm^{-1}, in addition to P-O(H) Stretching bands at 862 and 983 cm^{-1}. Lastly the 1 hour spectrum has water molecule bands at 781, 1199, 1638, 3144, 3475 and 3530 cm^{-1}. The 1 day, 7 day and 28 day spectra are broadly similar in the bands they each possess. There are PO bending and stretching bands at 561, 601 and 957 cm^{-1}, with a P-O(H) Stretching band at 854 cm^{-1}. There are also water molecule bands at 788 (28 day only), 1207 and 1630 cm^{-1}.

8.1.4 Scanning Electron Microscopy

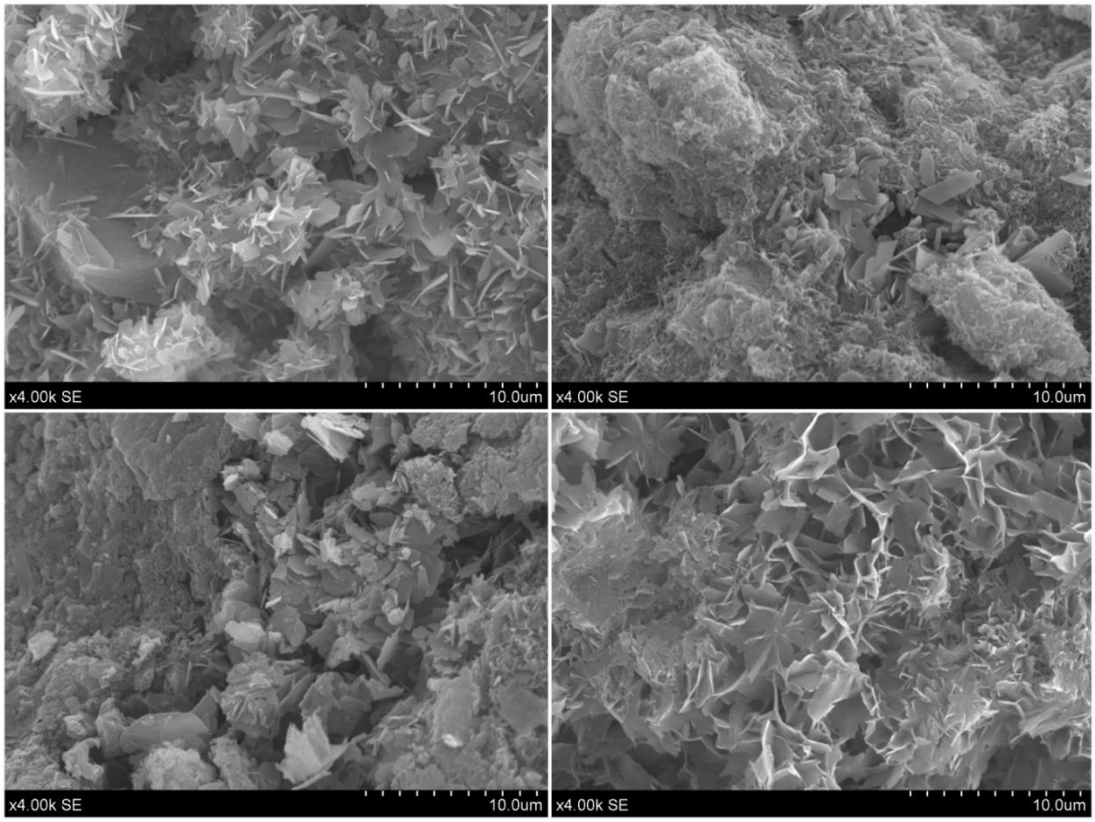

Figure 95 Scanning electron micrographs of QMNWKPaG04 cements at 1 hour (top left), 1 day (top right), 7 days (bottom left) and 28 days (bottom right).

Figure 95 shows the SEM images for QMNWKPaG04 cements at 1 hour, 1 day, 7 days and 28 days. At 1 hour the cement shows small plate shaped crystals with a high degree of interlocking; these were attributed to being apatite or OCP which displays this morphology. The image of the cement at 1 day shows what appear to be apatite/OCP crystals inside a bulk cement phase. The 7 day sample demonstrates plate like crystals. After 28 days immersion there are many interlocked irregular petal shaped crystals.

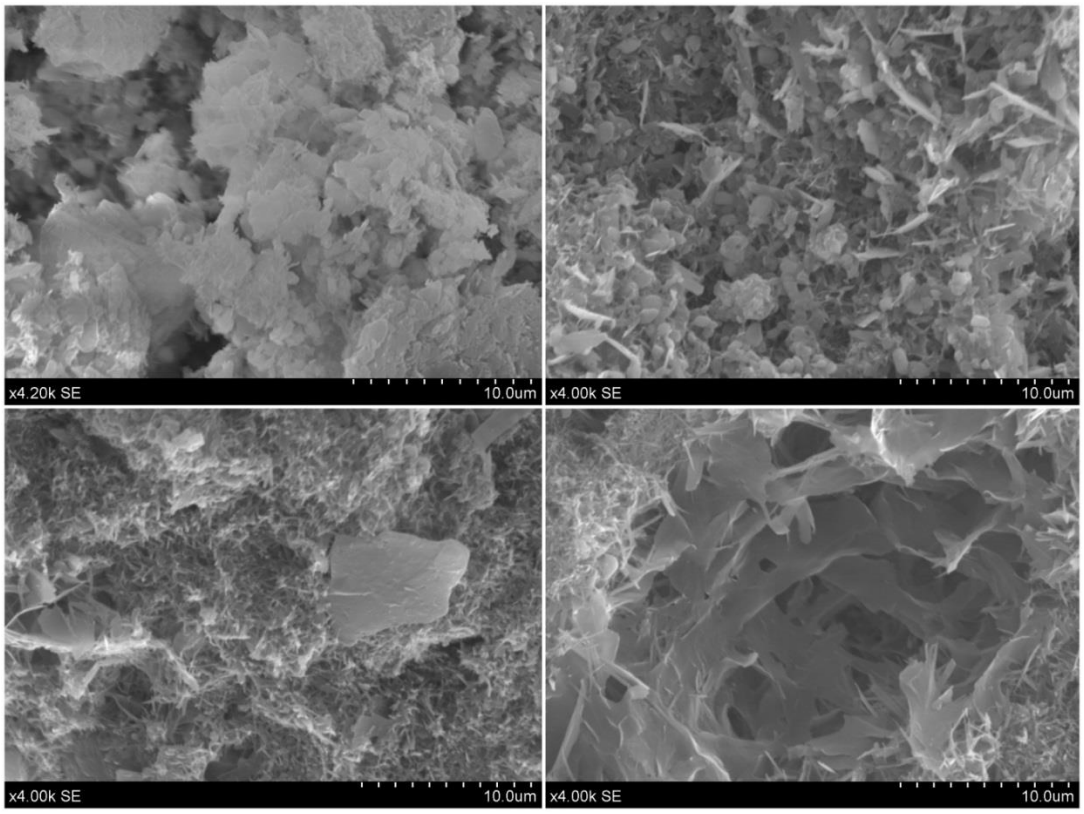

Figure 96 Scanning electron micrographs of QMNWKPaG06 cements at 1 hour (top left), 1 day (top right), 7 days (bottom left) and 28 days (bottom right).

Figure 96 shows the SEM images for QMNWKPaG06 cements at 1 hour, 1 day, 7 days and 28 days. The 1 hour sample shows clustered collections of small crystals. The 1 day sample shows a collection of three types of crystal morphology; ribbon morphology, round plates and needle crystals. The 7 day sample shows the majority of the crystals have a small needle morphology but there is also present a few ribbon shaped crystals. The centre of the image shows a glass particle is present. The 28 day sample has many needle shaped crystals on the edge of the image whereas the centre has a network of irregular shaped, thin crystals.

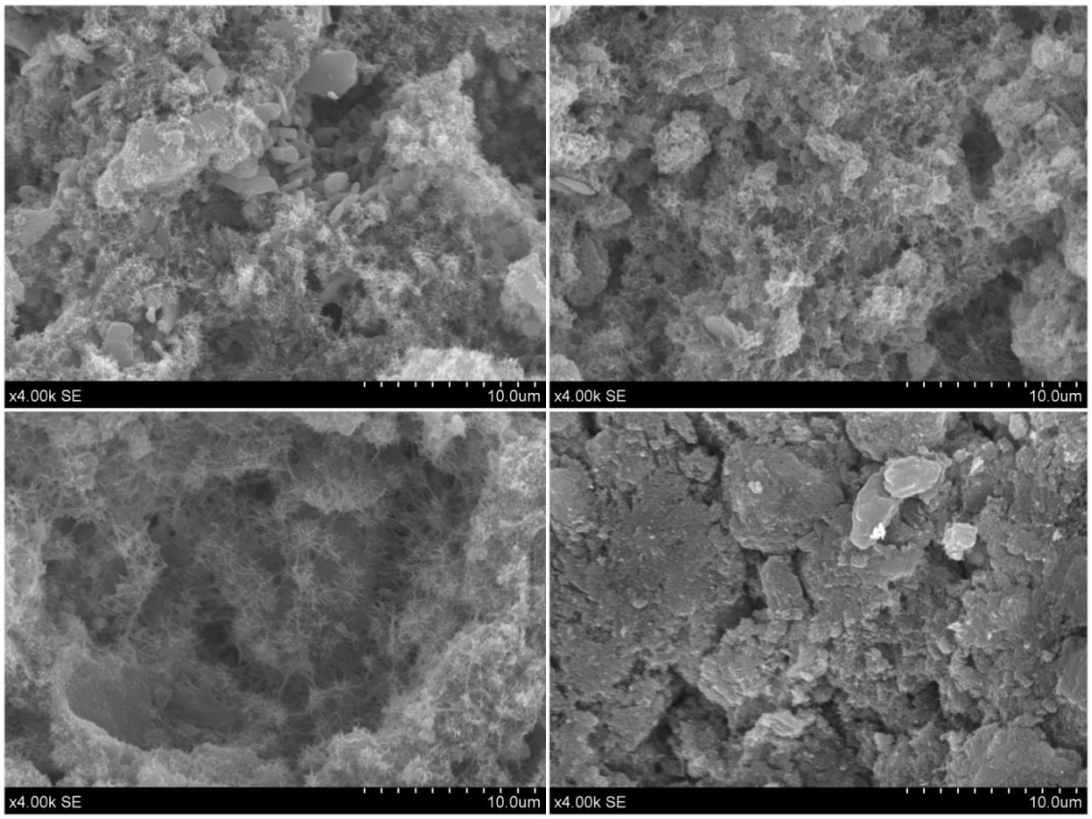

Figure 97 Scanning electron micrographs of QMNWKPaG07 cements at 1 hour (top left), 1 day (top right), 7 days (bottom left) and 28 days (bottom right).

Figure 97 shows the SEM images for QMNWKPaG07 cements at 1 hour, 1 day, 7 days and 28 days. The 1 hour sample shows two crystal morphologies relatively thick plated shaped crystals and very small needle like crystals. At 1 day and 7 days the morphology is entirely needle like. At 28 days the individual crystal is difficult to distinguish and only the bulk cement phase can be seen.

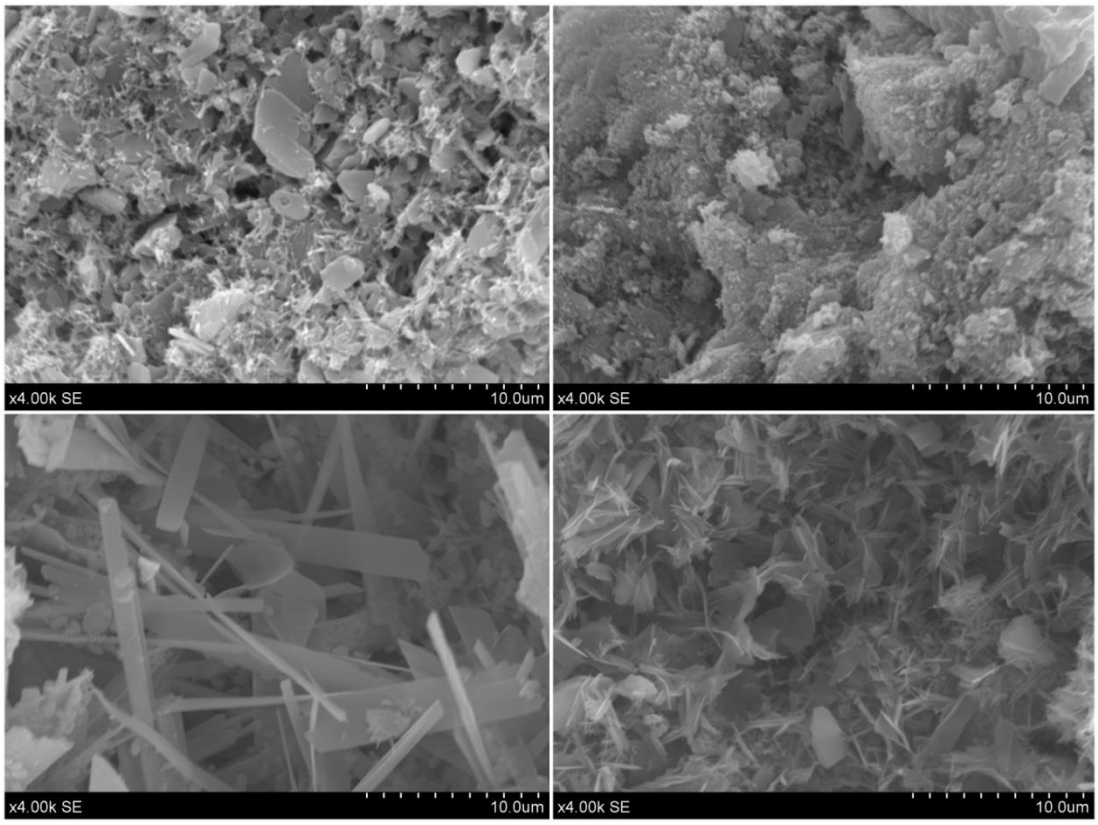

Figure 98 Scanning electron micrographs of QMNWKPaG08 cements at 1 hour (top left), 1 day (top right), 7 days (bottom left) and 28 days (bottom right).

Figure 98 shows the SEM images for QMNWKPaG08 cements at 1 hour, 1 day, 7 days and 28 days. The 1 hour sample shows a mixture of relatively small needle crystals and larger plate shaped crystals. At 1 day individual crystal cannot be easily distinguished most likely due to their very small size. There is a dramatic change in morphology in the 7 day sample, where the cement morphology exists as large ribbons and rods. The 28 day sample has a mixture of needle and plate morphologies.

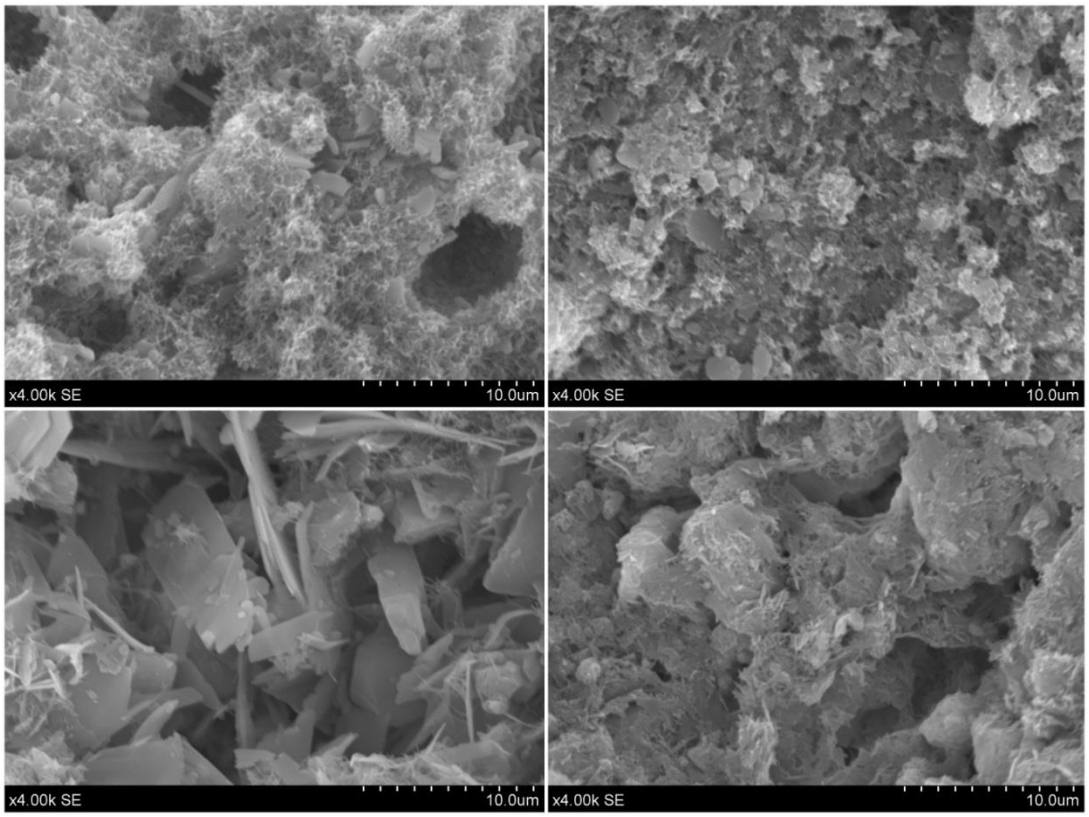

Figure 99 Scanning electron micrographs of QMNWKPaG09 cements at 1 hour (top left), 1 day (top right), 7 days (bottom left) and 28 days (bottom right).

Figure 99 shows the SEM images for QMNWKPaG09 cements at 1 hour, 1 day, 7 days and 28 days. At 1 hour the cement has two predominant morphologies, needles and small relatively thick plates. After 1 day the cement morphology shows a needle shape. The 7 day sample shows a majority of plate shaped crystals with some needles interdispersed. At 28 days the cement phase is primarily made up of a needle morphology.

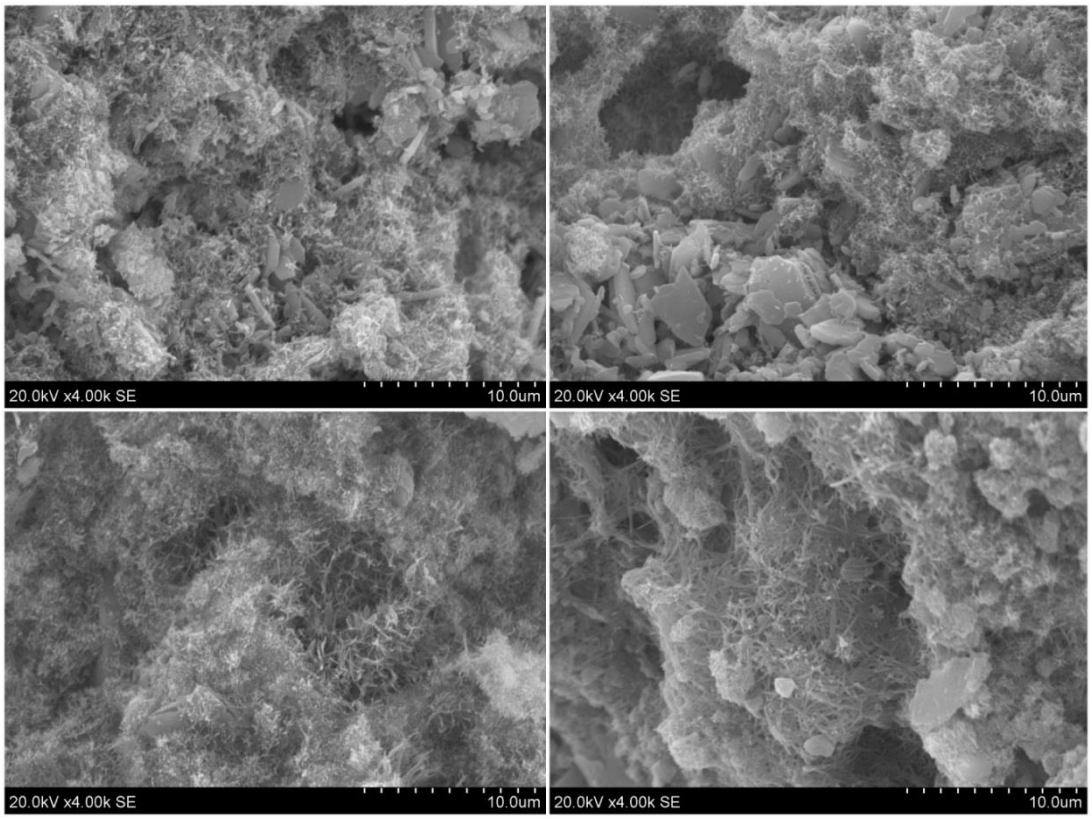

Figure 100 Scanning electron micrographs of QMNWKPaG10 cements at 1 hour (top left), 1 day (top right), 7 days (bottom left) and 28 days (bottom right).

Figure 100 shows the SEM images for QMNWKPaG10 cements at 1 hour, 1 day, 7 days and 28 days. At 1 hour the crystal morphology is a mixture of both needle and plate shaped crystals. The morphology is much the same at 1 day. The crystal morphology in the 7 day and 28 day samples is also very similar; there is a monophasic crystal morphology with all crystals having a needle shape.

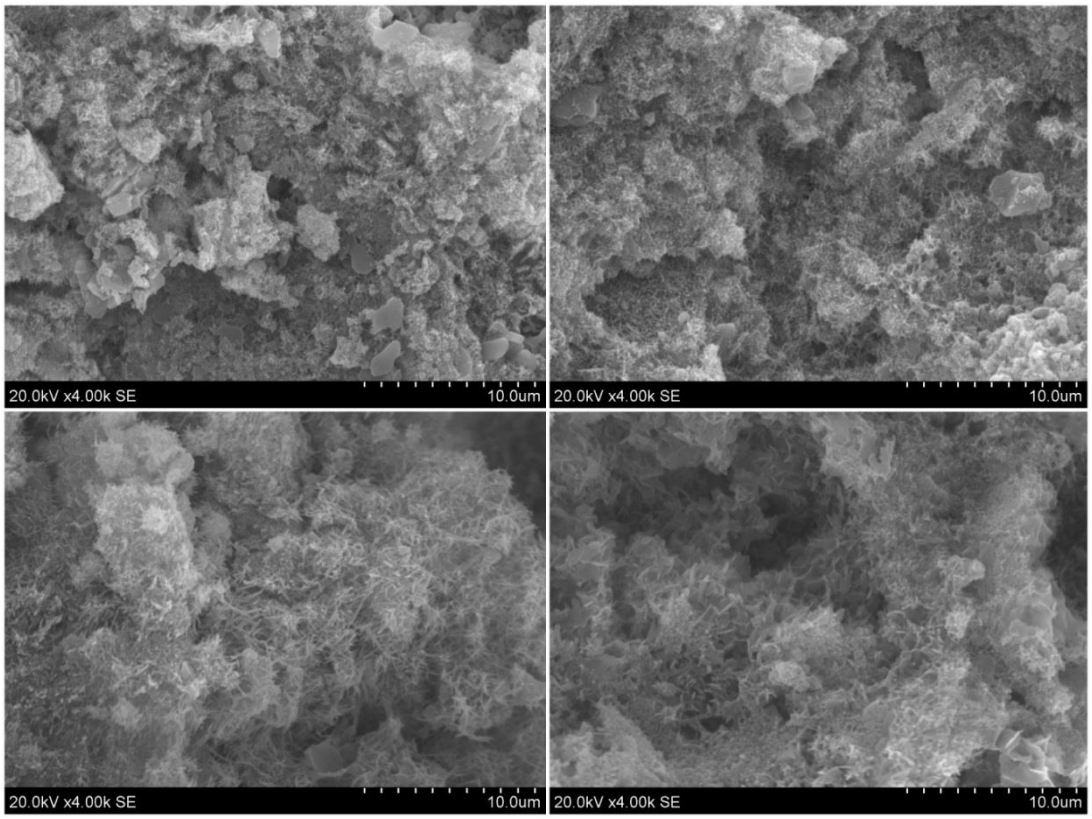

Figure 101 Scanning electron micrographs of QMNWKPaG11 cements at 1 hour (top left), 1 day (top right), 7 days (bottom left) and 28 days (bottom right).

Figure 101 shows the SEM images for QMNWKPaG11 cements at 1 hour, 1 day, 7 days and 28 days. The morphology in all four images is very similar as they all predominantly have small needle-like morphologies. Over the immersion time there does appear to be a growth of the crystals and in the one hour sample there are a very few number of plate like crystals.

8.1.5 Compressive Strength

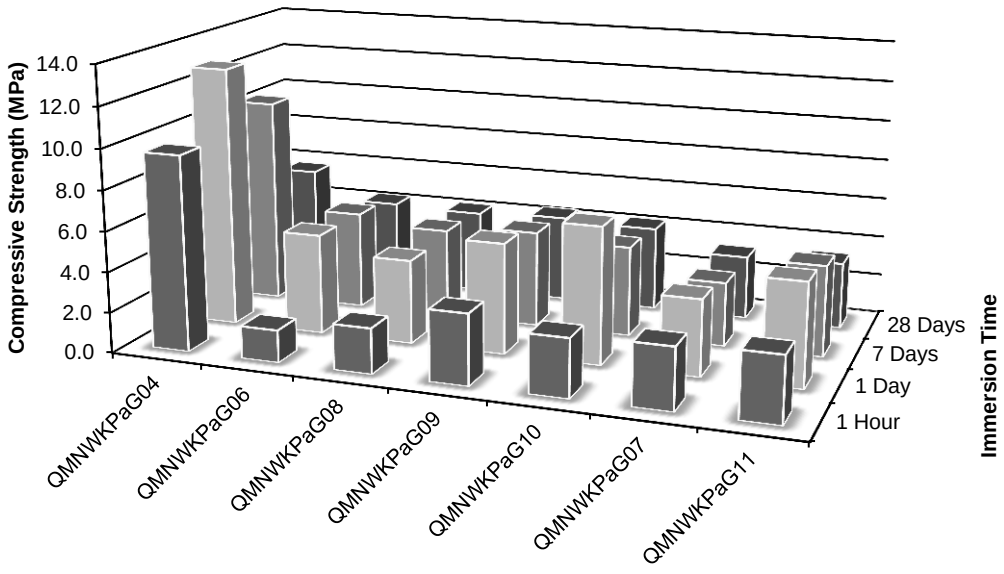

Figure 102 The compressive strength (MPa) of the fluoride containing cement series along with the equivalent fluorine-free glass composition.

Glass Composition	Compressive Strength (MPa)			
	1 Hour	1 Day	7 Days	28 Days
QMNWKPaG04	9.65 (±0.55)	12.90 (±1.16)	10.30 (±1.33)	5.67 (±0.94)
QMNWKPaG06	1.60 (±0.30)	4.98 (±0.53)	4.88 (±0.39)	4.28 (±0.61)
QMNWKPaG08	2.24 (±0.76)	4.17 (±0.72)	4.44 (±1.11)	4.18 (±0.55)
QMNWKPaG09	3.48 (±0.43)	5.48 (±0.99)	4.78 (±0.45)	4.35 (±0.64)
QMNWKPaG10	2.87 (±0.79)	6.76 (±0.39)	4.49 (±0.64)	4.21 (±0.68)
QMNWKPaG07	3.03 (±0.43)	3.77 (±0.69)	3.18 (±1.06)	3.18 (±0.54)
QMNWKPaG11	3.22 (±0.45)	5.10 (±0.52)	4.51 (±1.02)	3.31 (±0.56)

All of the fluorine containing cement samples showed increases in compressive strength compared to the 1 hour samples for each composition. The maximum compressive strength for cement samples containing fluoride was 6.76 MPa for the QMNWKPaG10 at 1 day. With the lowest being 1.60 for the QMNWKPaG06 composition at 1 hour. The fluorine free sample (QMNWKPaG04) had higher compressive strengths than those containing fluoride, ranging from 5.67 to 12.90 MPa.

8.1.6 Setting Time

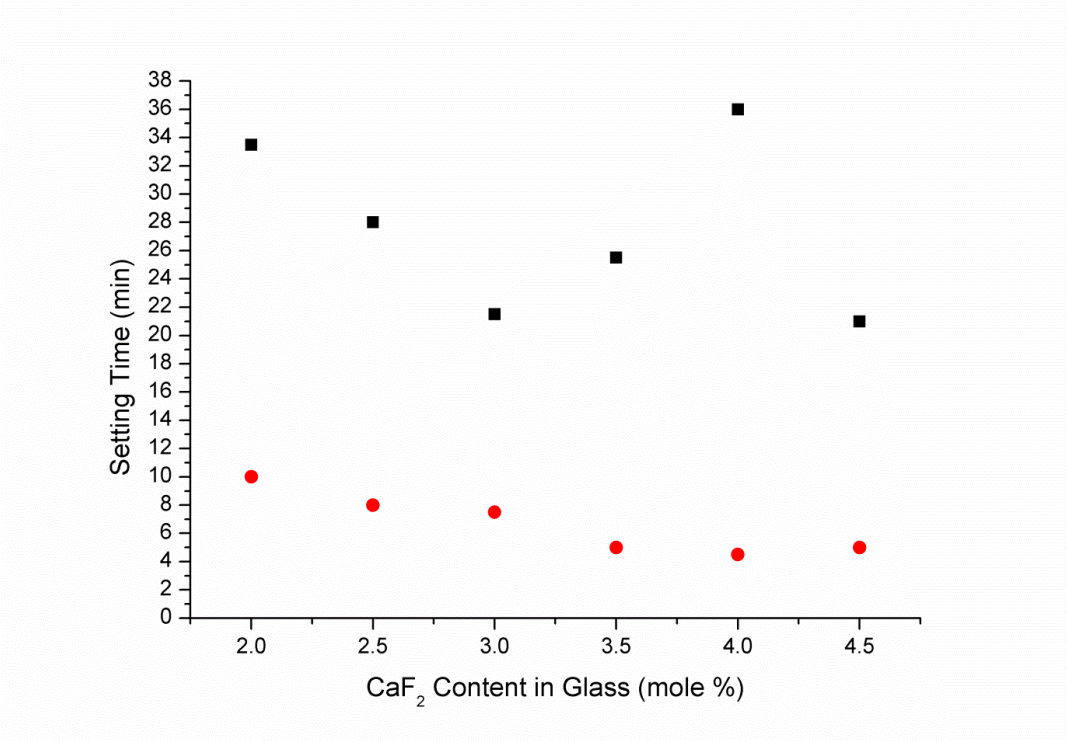

Figure 103 Initial and final setting times (minutes) against CaF_2 content in glass (mol%) of fluoride containing cement compositions

Table 31 Setting times as measured using Gilmore needle test of cement compositions, showing both initial and final setting times in minutes.

Cement Composition	Initial Setting Time (min)	Final Setting Time (min)
QMNWKPaG04	10.5	15.0
QMNWKPaG06	10.0	33.5
QMNWKPaG08	8.0	28.0
QMNWKPaG09	7.5	21.5
QMNWKPaG10	5.0	25.5
QMNWKPaG07	4.5	36.0
QMNWKPaG11	5.0	21.0

The fluoride containing cement series shows a gradual decrease in initial setting time as the fluoride concentration is increased, decreasing from 10 minutes (QMNWKPaG06) to 5 minutes (QMNWKPaG11). The final setting time from this series shows a slight trend of decreasing setting time with

increasing fluoride content; however the QMNWKPaG07 composition deviates from this trend with a final setting time of 36 minutes whilst the others in this series are between 21 and 33.5 minutes. The comparative glass composition without fluoride (QMNWKPaG04) has an initial setting time of 10.5 minutes and a final setting time of 15 minutes.

8.1.7 Ion Release

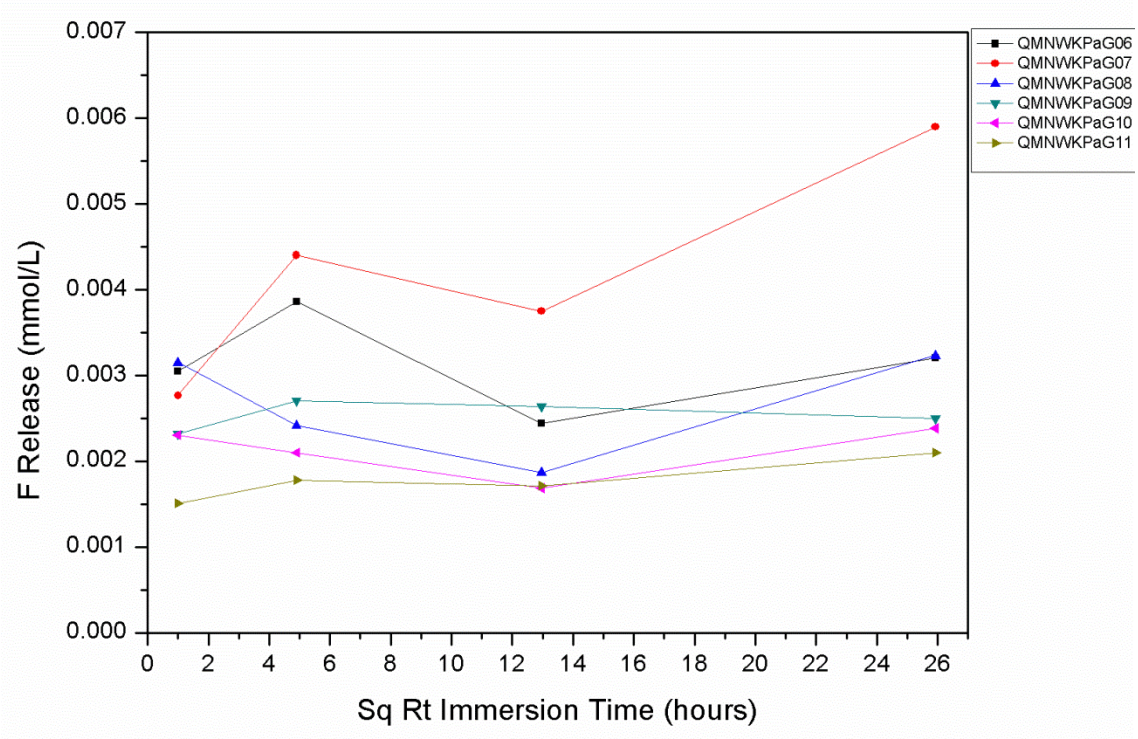

Figure 104 Fluoride release (millimole per litre, mmol/L) from immersed cement cylinders (n=4) plotted against square root of immersion time (hours) for all fluoride containing cement compositions from immersion for 1 hour, 1 day, 7 days, 28 days. (Error Bars = Standard Deviation).

Table 32 Fluoride release (millimole per litre, mmol/L) from immersed cement cylinders (n=4) for fluoride containing cement compositions from immersion for 1 hour, 1 day, 7 days, 28 days.

Cement Composition	Fluoride Release (mmol/L)			
	1 Hour	1 Day	7 Days	28 Days
QMNWKPaG06	0.0030	0.0039	0.0024	0.0032
QMNWKPaG07	0.0028	0.0044	0.0037	0.0059
QMNWKPaG08	0.0032	0.0024	0.0019	0.0032
QMNWKPaG09	0.0023	0.0027	0.0026	0.0025
QMNWKPaG10	0.0023	0.0021	0.0017	0.0024
QMNWKPaG11	0.0015	0.0018	0.0017	0.0021

The fluoride release measurements from the fluoride containing cement compositions show variable release at 1 hour, with fluoride release ranging from 0.0015 and 0.0030 mmol/L. At one hour the fluoride concentrations in the immersion solutions change with some compositions increasing and others decreasing, the range of fluoride release being between 0.0018 and 0.0044 mmol/L. At 7 days there is an apparent decrease in fluoride concentration in solution for all compositions compared to 7 days, with fluoride release levels between 0.0017 and 0.0037 mmol/L. After 28 days the fluoride release has increased compared to the 7 day levels to between 0.0021 and 0.0059 mmol/L.

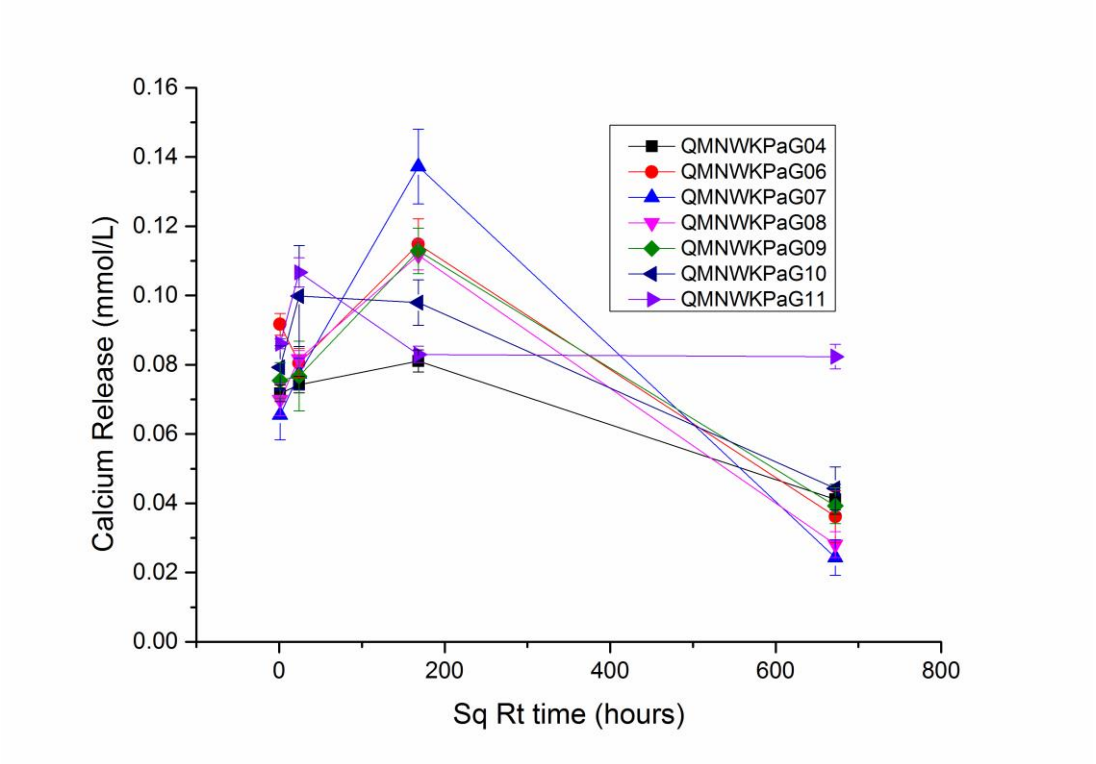

Figure 105 Calcium release (millimole per litre, mmol/L) from immersed cement cylinders (n=4) plotted against square root of immersion time (hours) for all fluoride containing cement compositions from immersion for 1 hour, 1 day, 7 days, 28 days. (Error Bars = Standard Deviation).

Table 33 Calcium release (millimole per litre, mmol/L) from immersed cement cylinders (n=4) for all cement compositions from immersion for 1 hour, 1 day, 7 days, 28 days. (Standard Deviation).

Cement Composition	Calcium Release (mmol/L)			
	1 Hour	1 Day	7 Days	28 Days
QMNWKPaG04	0.07 (±0.00)	0.07 (±0.00)	0.08 (±0.00)	0.04 (±0.00)
QMNWKPaG06	0.09 (±0.00)	0.08 (±0.00)	0.11 (±0.00)	0.04 (±0.00)
QMNWKPaG07	0.07 (±0.00)	0.08 (±0.00)	0.14 (±0.01)	0.02 (±0.00)
QMNWKPaG08	0.07 (±0.00)	0.08 (±0.00)	0.11 (±0.00)	0.03 (±0.00)
QMNWKPaG09	0.08 (±0.00)	0.08 (±0.01)	0.11 (±0.00)	0.04 (±0.00)
QMNWKPaG10	0.08 (±0.00)	0.10 (±0.01)	0.10 (±0.00)	0.04 (±0.00)
QMNWKPaG11	0.09 (±0.00)	0.11 (±0.00)	0.08 (±0.00)	0.08 (±0.00)

The calcium release shows very similar levels of calcium release from the cement for most of the different cement compositions. At 1 hour the majority of the compositions have between 0.07 and 0.09 mmol/L calcium release. At 1 day the majority of calcium release for the cement compositions is between 0.07 and 0.11 mmol/L. At 7 days the majority of the calcium release is between 0.08 and 0.11 mmol/L. After 28 days calcium release is relatively low, ranging between 0.02 and 0.06 mmol/L for all compositions.

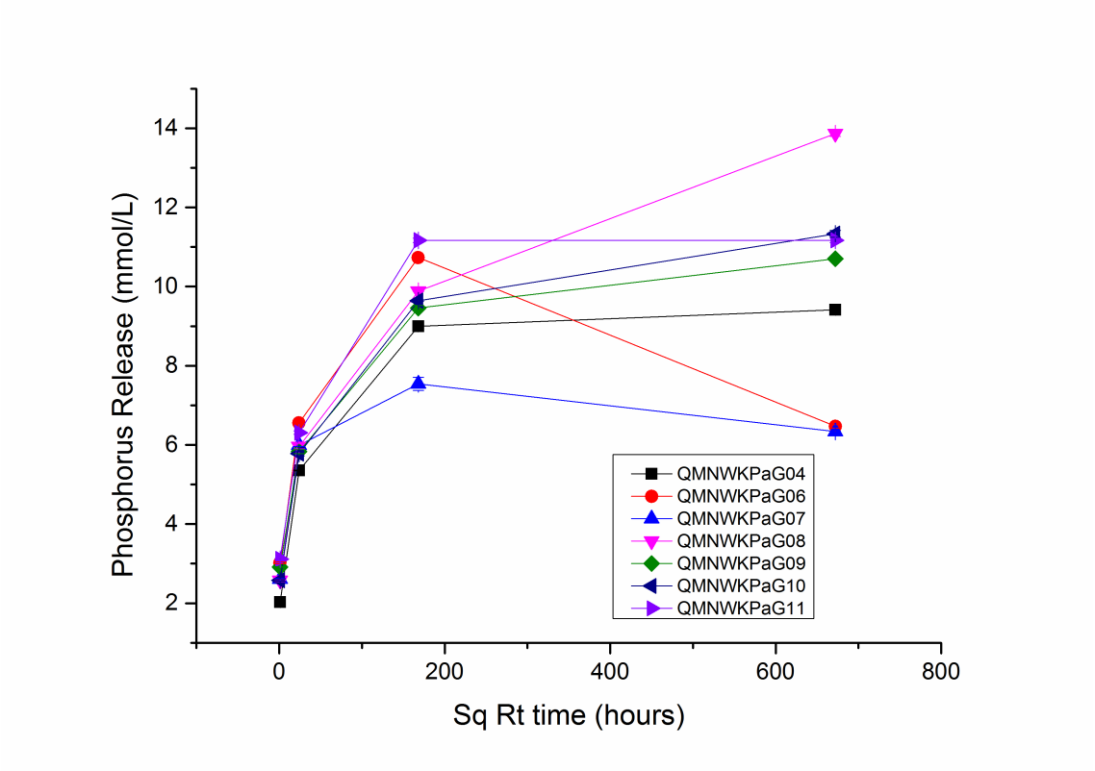

Figure 106 Phosphorus release (millimole per litre, mmol/L) from immersed cement cylinders (n=4) plotted against square root of immersion time (hours) for all fluoride containing cement compositions from immersion for 1 hour, 1 day, 7 days, 28 days. (Error Bars = Standard Deviation).

Table 34 Phosphorus release (millimole per litre, mmol/L) from immersed cement cylinders (n=4) for all cement compositions from immersion for 1 hour, 1 day, 7 days, 28 days. (Standard Deviation).

Cement Composition	Phosphorus Release (mmol/L)			
	1 Hour	1 Day	7 Days	28 Days
QMNWKPaG04	2.03 (±0.03)	5.36 (±0.00)	9.00 (±0.04)	9.41 (±0.01)
QMNWKPaG06	3.02 (±0.02)	6.56 (±0.03)	10.74 (±0.02)	6.47 (±0.04)
QMNWKPaG07	2.61 (±0.01)	5.99 (±0.03)	7.54 (±0.16)	6.34 (±0.01)
QMNWKPaG08	2.58 (±0.02)	5.96 (±0.06)	9.89 (±0.02)	13.87 (±0.07)
QMNWKPaG09	2.92 (±0.00)	5.83 (±0.05)	9.46 (±0.06)	10.71 (±0.00)
QMNWKPaG10	2.58 (±0.02)	5.78 (±0.05)	9.64 (±0.01)	11.33 (±0.08)
QMNWKPaG11	3.12 (±0.01)	6.31 (±0.04)	11.17 (±0.05)	11.17 (±0.05)

At 1 hour the phosphorus release is between 2.03 and 3.12 mmol/L for all cement compositions. After 1 day the amount of phosphorus in solution for all compositions has risen to between 5.36 and 6.56 mmol/L. After 7 days the phosphorus in solution has increased a smaller amount to be between 7.54

and 11.17 mmol/L for all cement compositions. At 28 days there is a fairly high distribution of the various phosphorus release rates. The release distribution is high with all compositions being between 6.34 and 11.33 mmol/L.

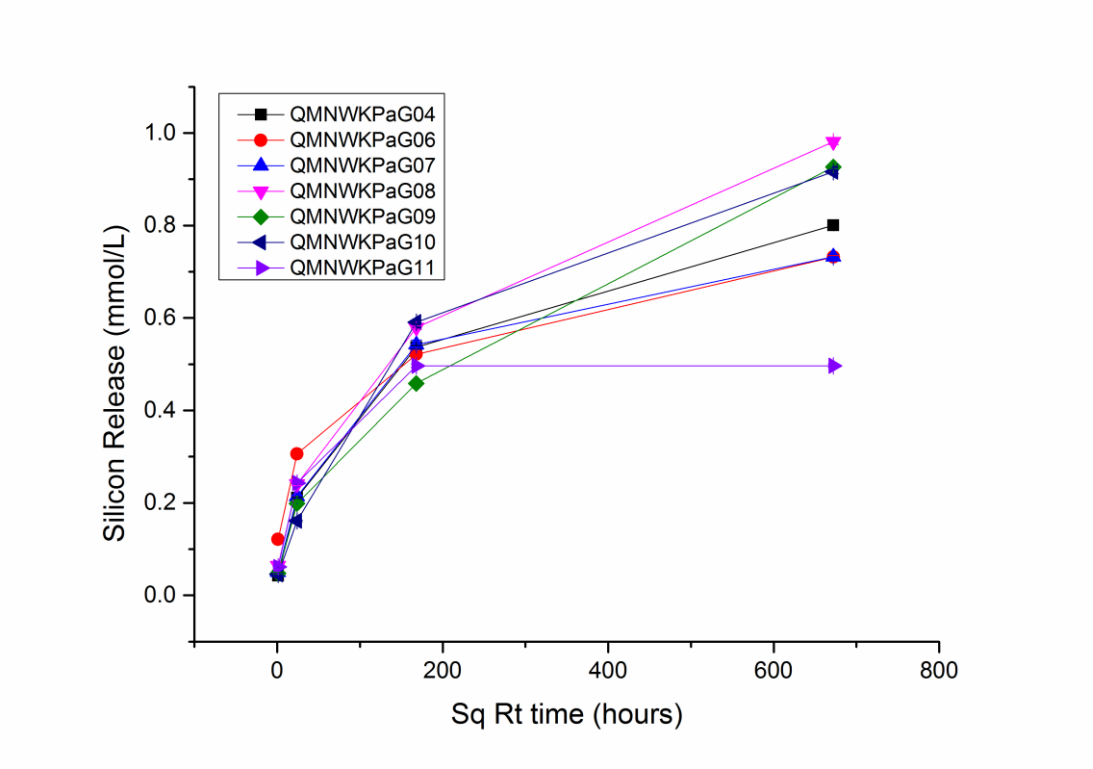

Figure 107 Silicon release (millimole per litre, mmol/L) from immersed cement cylinders (n=4) plotted against square root of immersion time (hours) for all fluoride containing cement compositions from immersion for 1 hour, 1 day, 7 days, 28 days. (Error Bars = Standard Deviation).

Table 35 Silicon release (millimole per litre, mmol/L) from immersed cement cylinders (n=4) for all cement compositions from immersion for 1 hour, 1 day, 7 days, 28 days. (Standard Deviation).

Cement Composition	Silicon Release (mmol/L)			
	1 Hour	1 Day	7 Days	28 Days
QMNWKPaG04	0.04 (±0.00)	0.21 (±0.00)	0.54 (±0.00)	0.80 (±0.00)
QMNWKPaG06	0.12 (±0.00)	0.31 (±0.00)	0.52 (±0.00)	0.73 (±0.00)
QMNWKPaG07	0.05 (±0.00)	0.21 (±0.00)	0.54 (±0.01)	0.73 (±0.00)
QMNWKPaG08	0.06 (±0.00)	0.24 (±0.00)	0.58 (±0.00)	0.98 (±0.00)
QMNWKPaG09	0.05 (±0.00)	0.20 (±0.00)	0.46 (±0.00)	0.93 (±0.00)
QMNWKPaG10	0.05 (±0.00)	0.16 (±0.00)	0.59 (±0.00)	0.92 (±0.00)
QMNWKPaG11	0.06 (±0.00)	0.24 (±0.00)	0.50 (±0.00)	0.50 (±0.00)

The silicon release shows a constant increase in silicon release for all cement compositions that shows no noticeable differences for the different series. At 1 hour there is the lowest silicon release of between 0.04 and 0.12 mmol/L, which increases to between 0.16 and 0.31 mmol/L after 1 day. Then at 7 days the amount in solution is further increased to between 0.46 and 0.58 mmol/L. There is again another increase in silicon release after 28 days to between 0.73 and 0.98 mmol/L.

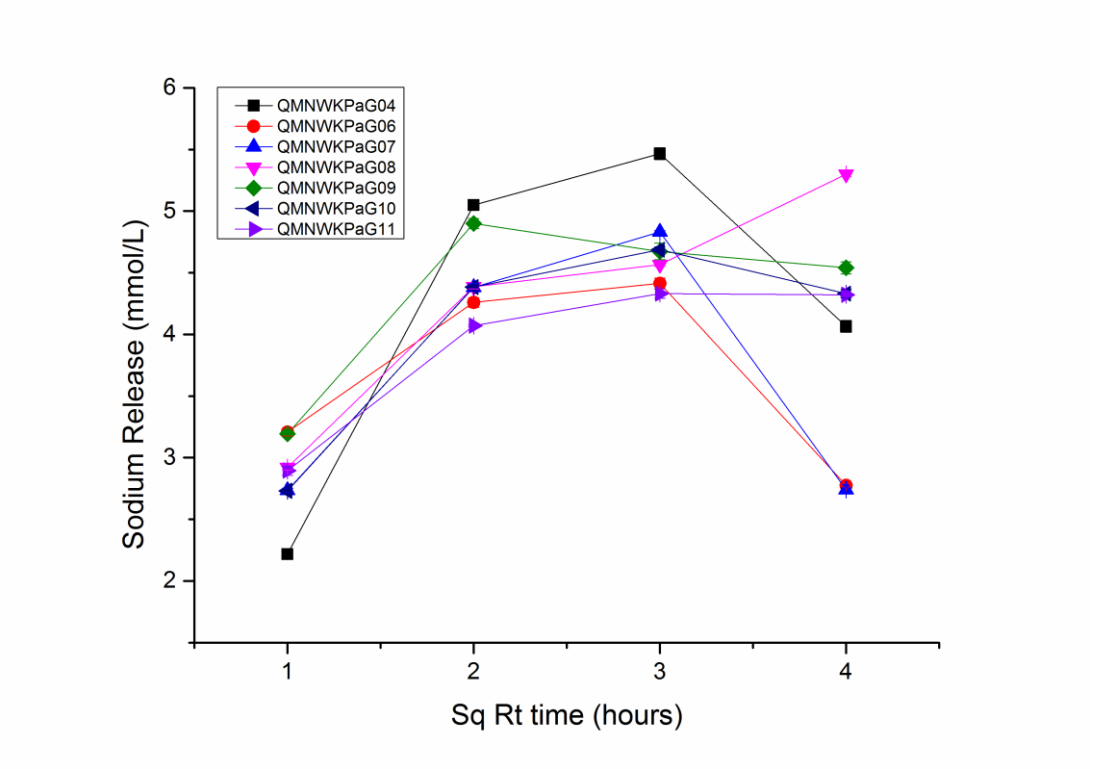

Figure 108 Sodium release (millimole per litre, mmol/L) from immersed cement cylinders (n=4) plotted against square root of immersion time (hours) for all fluoride containing cement compositions from immersion for 1 hour, 1 day, 7 days, 28 days. (Error Bars = Standard Deviation).

Table 36 Sodium release (millimole per litre, mmol/L) from immersed cement cylinders (n=4) for all cement compositions from immersion for 1 hour, 1 day, 7 days, 28 days. (Standard Deviation).

Cement Composition	Sodium Release (mmol/L)			
	1 Hour	1 Day	7 Days	28 Days
QMNWKPaG04	2.22 (±0.00)	5.05 (±0.03)	5.47 (±0.04)	4.07 (±0.04)
QMNWKPaG06	3.21 (±0.03)	4.26 (±0.03)	4.41 (±0.04)	2.78 (±0.01)
QMNWKPaG07	2.73 (±0.01)	4.38 (±0.03)	4.83 (±0.01)	2.74 (±0.01)

QMNWKPaG08	2.92 (±0.02)	4.39 (±0.01)	4.57 (±0.01)	5.30 (±0.01)
QMNWKPaG09	3.19 (±0.00)	4.90 (±0.04)	4.67 (±0.06)	4.54 (±0.04)
QMNWKPaG10	2.73 (±0.01)	4.38 (±0.02)	4.69 (±0.02)	4.33 (±0.03)
QMNWKPaG11	2.90 (±0.03)	4.07 (±0.00)	4.33 (±0.03)	4.32 (±0.01)

Cement compositions in the fluoride containing cement compositions all have very similar levels of sodium release at all time points studied, with release levels between 2.22 and 5.47 mmol/L.

8.2 Discussion

8.2.1 Cement Phase Analysis

8.2.1.1 QMNWKPaG04

1 hour

What is clearly evident form the ^{31}P MAS-NMR and X-ray diffraction is that at one hour both the glass and $Ca(H_2PO_4)_2$ starting reagents have reacted and are no longer present. With respect to the cement phase the ^{31}P MAS-NMR shows chemical shifts at 3.3, 1.4, -0.2, -1.4 ppm. The 1.4 and -1.4 ppm shifts are easily assignable to DCPD and DCPA respectively the 3.3 and -0.2 ppm are less easily assigned. OCP has chemical shifts at 3.6, 3.2, 1.8, and -0.2 ppm, this spectrum is crowded with reasonably broad chemical shifts which causes convergence of peaks. Given the XRD has diffraction lines showing the presence of OCP, the -0.2 ppm shift is that from OCP and the 3.3 ppm shift may be the 3.6 and 3.2 ppm OCP shifts but converged into one peak. The XRD indicates the formation of OCP, DCPD and DCPA, with DCPA being only a small fraction due to the low intensity of the diffraction lines. Referring to the FTIR, there are clear OH stretching water bands present at 3148, 3473 and 3528 cm^{-1}. There are a number of PO bending and stretching bands present, bands at 555 and 600 cm^{-1} (PO bending) are

indicative of either OCP or apatite, due to apatite not being clearly present of the NMR these have been assigned to being part of the OCP structure.

1 day

At 1 day the 31P MAS-NMR spectrum is similar to the 1 hour sample. There are four distinguishable chemical shifts at 3.1, 1.4, -0.2, and -1.4 ppm. The 1.4 and -1.4 ppm shifts are easily assigned to being DCPD and DCPA; similarly to the 1 hour sample the last two shifts (3.1 and -0.2 ppm) are more difficult to easily assign, but again due to the presence of OCP diffraction lines on the XRD these were assigned to showing the presence of OCP. The 3.1 ppm shift like the 1 hour sample is most likely a mixture of the 3.6 and 3.2 ppm shifts of OCP. Compared to the 1 hour sample the position of this shift has changed from 3.3 to 3.1 ppm. The reason for this is perhaps the formation of an apatite phase at 2.8 ppm, where all three shifts are present together and existing as 'one' shift. Given the 4.6 $^{\circ}2\theta$ diffraction line of OCP is so weak on the diffraction pattern for this cement this could indicate that both OCP and apatite are present. The XRD has diffraction lines indicative of both DCPD and DCPA, consistent with the NMR results. The FTIR spectra have PO bond bending bands at 555 and 600 cm^{-1}, which indicates the presence of OCP, apatite or a mixture of the two. Bands at 3480 and 3530 cm^{-1} showing OH stretching of water indicate that DCPD is present.

7 days

The ^{31}P MAS-NMR spectrum has two clearly noticeable chemical shifts at -0.2 ppm and 3.1 ppm; the 3.1 ppm shift not being symmetrical, having low intensity shoulders either side of the main shift at 3.1 ppm. Given the XRD

has an OCP diffraction line at 4.6 ˚2θ it could be assumed that the 'shoulders' on the shift at 3.1 ppm are the OCP shifts at 3.6 and 1.8 ppm; consequentially the presence of an apatite shift (2.8 ppm) cannot be discounted. There are numerous broad diffraction lines for OCP, apatite or a mixture of the two. Conspicuously there is an absence of any clear lines donating the presence of either DCPD or DCPA. Whilst DCPA has been found on the ^{31}P MAS-NMR spectrum (a shift at -1.4 ppm) it most likely not detected on XRD as it is too low a fraction of the cement phase to be detectable. The FTIR spectra have two PO bond bending bands at 555 and 600 cm^{-1} indicating either OCP or apatite. It is noticeable that there is an absence of a HPO_4 bond bending band and 520 cm^{-1} that is of OCP and there a few of the HPO_4 bond bending and stretching bands as would be expected in a pure OCP sample (although one HPO_4 bond stretching band is at 855 cm^{-1}). The spectroscopic results then conclude to the cement phase as being a mixture of DCPA, OCP and apatite; the DCPD in this cement sample appears to have formed either an apatite/OCP phase between 1 day and 7 days.

28 days

The ^{31}P MAS-NMR of the 28 day sample shows one main chemical shift at 2.9 ppm and two less intense shoulder peaks at 5.5 and 0.8 ppm. The 2.9 ppm shift was assigned to hydroxyapatite as the XRD shows a monophasic apatite cement phase. The 5.5 ppm shift was assigned to being unprotonated surface phosphates and the 0.8 ppm chemical shift protonated surface phosphates, confirmed by (Kolmas and Kolodziejski, 2012) to be

present in synthesised hydroxyapatite. The FTIR spectra agrees with this assignment, as well as having bands indicative of apatite there is also a band at 855 cm^{-1} assigned as a HPO_4 stretching bond; fitting the 0.8 ppm shift assignment of protonated phosphate groups.

8.2.1.2 Fluoride containing compositions

Glasses QMNWKPaG06-11 have increasing levels of fluoride incorporation from 2.5-4.5 mol%. ^{31}P and ^{19}F MAS-NMR, X-ray diffraction, and FTIR spectroscopic techniques were used to identify the cement phases investigated in the setting reaction and phase evolution during immersion in Tris buffer solution. The ^{31}P MAS-NMR was run on all samples and showed the presence at 1 hour in all samples of DCPD (1.4 ppm), DCPA (-0.2 & -1.4 ppm) and an apatite (2.9 ppm) phase. This assignment is supported in X-ray diffraction where characteristic diffraction lines were assigned on the 1 hour diffraction patterns for all fluoride containing cements. The FTIR results also support this assignment as typical apatite bands (crystalline orthophosphate) were identified at approximately 560 and 600 cm^{-1}. Additionally DCPD was identified through the assignment of bands at 520 (PO bending), 3150, 3475 and 3530 cm^{-1} (all OH stretch in water) which all belong to DCPD.

Between 1 hour and 28 days a phase evolution process occurs with both the DCPD and DCPA phase initially present undergoing dissolution then precipitation to apatite. The rate of this transformation occurs at a different rate for the different glass compositions with different fluoride amounts. With higher fluoride content the rate of this dissolution occurs at a faster rate. For instance, after 7 days in the cement QMNWKPaG11, the highest fluoride

content cement, has only apatite present; identified clearly on the X-ray diffraction and ^{31}P MAS-NMR. Comparatively in all other samples at this time only DCPA is present. Similarly after one day all cement samples contain a mixture of DCPD, DCPA and apatite with the exception of QMNWKPaG11 which contains only apatite and DCPA. After 28 days all of the cement samples show monophasic apatite cement phases. The ^{31}P MAS-NMR results show one peak in all samples at 28 days immersion at 2.9 ppm, assigned as apatite. All of the X-ray diffraction results are in conclusion with this result as they also show only diffraction lines for apatite. The FTIR result again back this up by the presence of apatite bands at 560 and 600 cm^{-1}.

One observation that can be made is the apparent decrease in the relative intensity of the different phases through this cement series at the same time point. Addition of more fluoride in the glass composition causes an increase in the rapidity of the formation of the apatite phase and a decrease of the DCPD phase. Although this rate of transformation may be related to the amount of apatite formed before 1 hour immersion, as it is evident (from the ^{31}P MAS-NMR) that more apatite is present at 1 hour immersion as fluoride content is increased. Normally deconvolution can be used to quantify the relative intensities of the phases present in a sample. This was not done here however due to the low resolution of the respective peaks within the sample, which render any deconvolution highly inaccurate.

^{19}F MAS-NMR was only performed on the 1 hour and 28 day samples of cements produced through a reaction from the QMNWKPaG10 glass. The spectra confirmed the formation of a fluoride containing apatite phase. The

spectra do however suggest that the apatite formed is a fluoridated apatite rather than fluorapatite; meaning that the phase formed is a Fluorohydroxyapatite ($Ca_{10}(PO_4)_6(OH)_{2-x}F_x$) rather than a pure stoichiometric fluorapatite ($Ca_{10}(PO_4)_6F_2$). This result was drawn from the position of the peaks indicating fluoride within the apatite structure. Braun & Jana showed that the position of the fluorine chemical shifts in apatite with hydroxyl content. Stoichiometric fluorapatite has a peak position of -101 ppm, it was shown that as hydroxyl content increases (and fluoride content decreases) the position of the chemical shift becomes more negative. The QMNWKPaG08 cement samples show two peaks at approximately -106 and -108 ppm respectively. The -106 ppm peak is attributed to being a low fluoride substituted fluorohydroxyapatite species and the -108 ppm peak is attributed to a CaF_2 species given this is where crystalline CaF_2 gives a resonance. Comparing the 1 hour sample with the 28 day sample there is a slight increase in the relative intensity of the fluorohydroxyapatite species compared to the CaF_2 in the 28 day sample. The difference between the glass spectrum and the cement spectra show the fluoride has changed environment through the cement setting reaction and subsequent immersion. Whilst without analysing all the other samples one cannot conclude with certainty that all other samples follow this same trend it is highly likely given the similarity in properties that this series has. Given this the apatite within the fluoride containing cement samples will hereby be referred to as fluoridated apatite.

8.2.2 Effect of Glass Structure Upon Dissolution

As with the calcium/sodium cement series with the glasses produced there is a change in the glass structure through the series. As well as the addition of CaF_2 through the series there is also witnessed an increase in the free volume. As mentioned previously this would likely equate to a more soluble glass that would release its constituent ions at a faster rate as the free volume increased. This is supported in the results at a higher fraction of apatite is witnessed in the cements at 1 hour with increasing levels of CaF_2. This supports the idea that free volume increases also equates to a more rapidly dissolving glass because the glass element of the cement produces a higher ratio of the overall calcium content of the cement; meaning that a cement phase with a higher calcium content (hydroxyapatite over brushite) forming preferentially indicates more calcium in solution.

Unlike in the calcium/sodium cement series, where a similar trend could not be definitively concluded due to changes in cement composition through the series, the results here can be more reliably attributed to changes in glass structure. This is because unlike in the previous series the glass:salt ratio does not change, so the only change between the cement compositions in the alteration in glass composition rather than the amount there.

8.2.3 Compressive Strength

The fluorine-free cement (QMNWKPaG04) compared with all the fluorine containing cements shows a higher compressive strength, with the QMNWKPaG04 (see Figure 100) composition having a compressive strength at 1 hour of 9.65 MPa and the highest fluoride-containing composition being 3.48 MPa. As is visible in the figure above this is a general trend at all time

points, except arguably the 28 day sample which is only marginally higher in the fluorine–free sample compared to those containing fluoride. The cause of this is related to the crystallite size and morphology. The cement strength is determined by interlocking of the cement phase crystallites. The ability to interlock and strength of interlocking is related to the crystallite size and shape. In Portland cement the length of the crystallite affects the strength of the sample and the strong cement has larger crystallites (provided other factors are constant). The SEM results show that the QMNWKPaG04 (fluoride-free) cement composition has much larger plate-like crystallites (figure 109) that are considerably larger that the small needle-like crystallites in the fluoride containing cements. When comparing the cements with differing fluoride contents there does not appear to be a clear trend in compressive strength and fluoride content. This means that addition of fluoride in these levels causes a decrease in compressive strength that is not proportional to fluoride content.

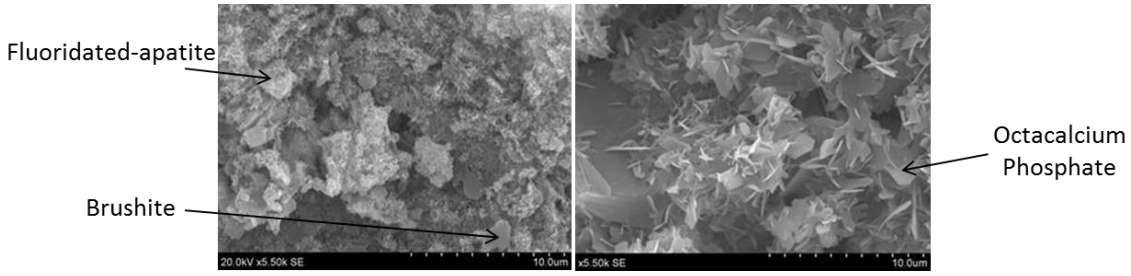

Figure 109 QMNWKPaG11 1 Hour (right), QMNWKPaG04 1 Hour (left)

8.2.4 Setting Time

The fluoride containing cements have a trend when the fluoride content is changed. As fluoride content in the glass is increase the length of the initial

setting time decreases (Figure 103). The final setting times also show a general trend for decreasing the setting time as fluoride content in the cement is increased. There is a probable anomalous result for the QMNWKPaG07 cement with 4.00 mol% CaF_2. The cause of this trend is probably similar to that causing the difference in the fluoride free cements, albeit with different phases. The 1 hour immersion data shows that with increasing fluoride in the cement the proportion of apatitic cement phase to DCPD cement phase increases (Figure 113). As the stronger apatite phase forms the ability to resist the Gilmore needle increases leading to shorter setting times as the fluoride concentration is increased and apatite phase forms at a faster rate. It is also important to note that this change can be directly attributed to change in glass composition rather than change in glass powder/$Ca(H_2PO_4)_2$ ratio because this ratio in the fluoride cement series is constant. Comparing the addition of fluoride with a cement composition which contains no fluoride but all other components are in the same ratios the results show that fluoride dramatically decreases the final setting time but has less of an effect on the initial setting time. The QMNWKPaG04 (fluoride-free) composition has an initial setting time of 10.5 minutes and a final setting time of 19 minutes, whilst the initial setting times for the fluoride containing cements are between 10 and 5 minutes and final setting time between 22 and 36 minutes. The cause of this difference again most likely lies in the rapidity at which the cement phase forms. It could be that the easier to nucleate fluoridated apatite phase forms rapidly (without immersion in Tris), meaning the cement is able to resist the Gilmore needle at a much earlier time point; though further experimentation would be required to confirm this.

8.2.5 Ion Release

The fluoride release data showed that release was very low, with the fluoride release levels not surpassing 0.006 mmol/L in any cement compositions. This shows the majority of the fluoride remains within the cement mass. Its exact location (i.e. in cement phase or as precipitated CaF_2) is unclear. The ^{19}F MAS-NMR suggested the fluorine is split between the apatite cement phase and a precipitated CaF_2 phase. This is not unexpected as there is a strong thermodynamic drive for the fluoride to be incorporated into the apatite structure.

The sodium shows similar levels in all compositions. This was related to the glass design where the sodium content in all of these glass compositions was kept constant; this coupled with the glass fraction of the cement powder is maintained at a similar level for all of these cement compositions caused the sodium release to be approximately constant.

The calcium release does not show any obvious trends between glass compositions. The initial release remains fairly constant after the first measurement which means that no calcium is being release during the immersion time and none is being consumed by the cement during the immersion either. It should be noted also that the calcium levels in the solution are relatively low when compared to the phosphorus release.

The silicon release followed a fairly conspicuous trend, with silicon content in the solution increasing with immersion time. This is related to the hydrolysis of the residual silicate chains which are hydrolysed over a period of time, releasing soluble silicon species into solution.

The phosphorus release data gives a clear trend for all glass compositions; with concentration in solution increasing over time. There does not appear any obvious trend between the different glass compositions in the release rate or amount released. This shows that phosphorus is continually released this may be due to the conversion of relatively phosphate rich calcium phosphate species that initially form and convert to species where phosphate is less relative to calcium values. This transformation retains the calcium but the phosphate is released into solution, causing the results witnessed here.

Chapter 9: HydroSet™ Results and Discussion

9.1 Results

9.1.1 X-ray Diffraction

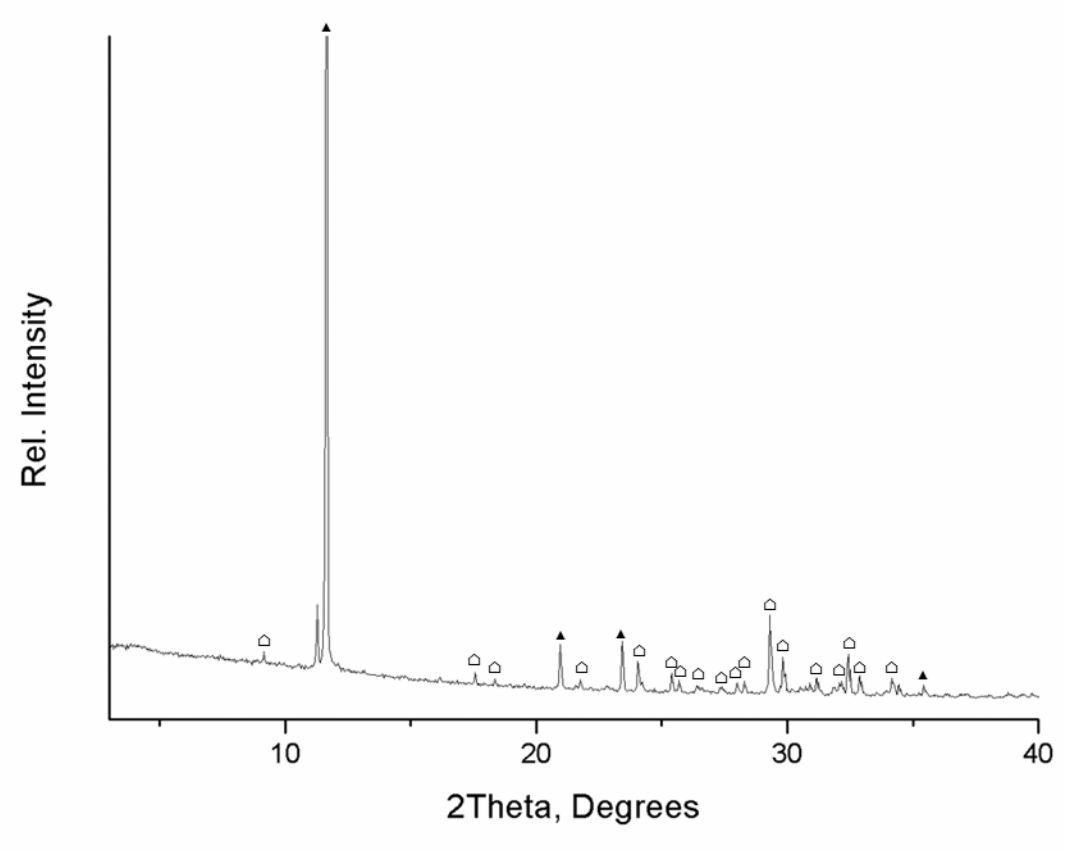

Figure 110 X-ray Diffraction pattern of HydroSet™ Starting powder. ▲ - DCPD; ⌂ - tetracalcium phosphate.

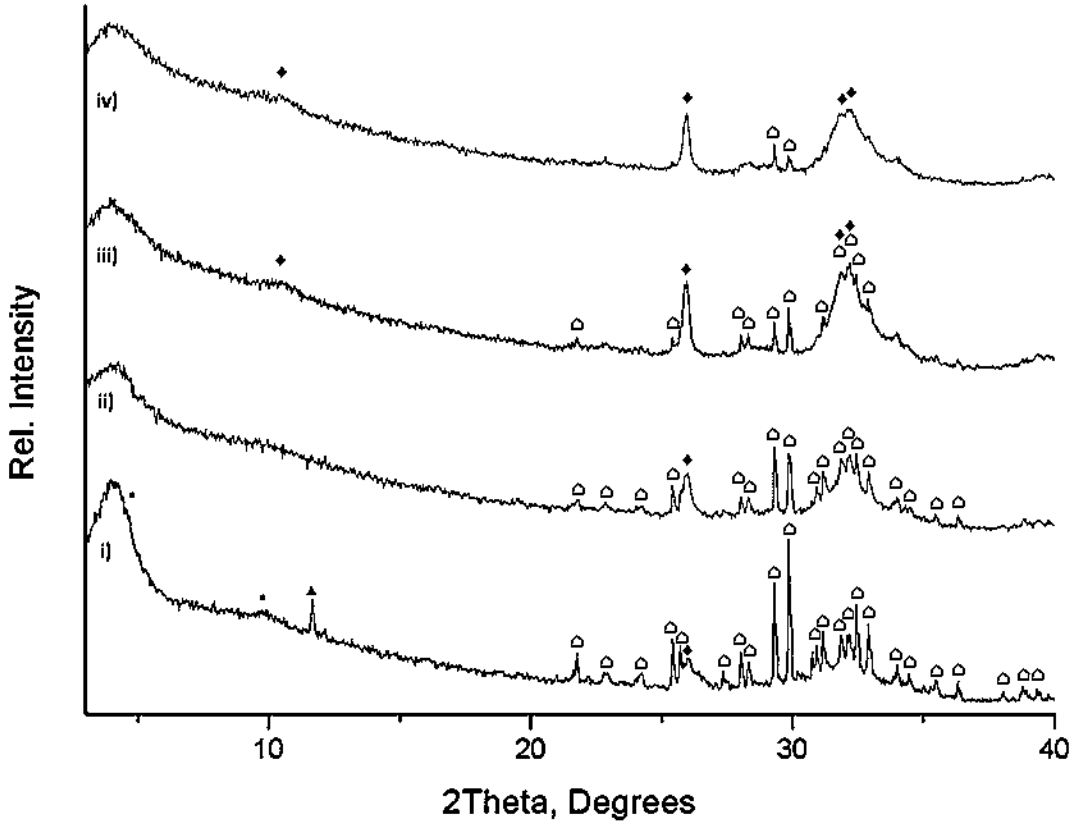

Figure 111 X-ray diffraction pattern of HydroSet™ cement cylinders after i) 1 hour, ii) 1 day, iii) 7 days and iv) 28 days immersion in Tris buffer soltution. ● – Octacalcium Phosphate; ♦ Apatite; ⌂ - tetracalcium phosphate; ▲DCPD.

Figure 110 and Figure 111 show the X-ray diffraction patterns of the HydroSet™ starting powder and the immersed HydroSet™ specimen after 1 hour, 1 day, 7 days and 28 days. The pattern of the starting materials shows both DCPD and tetracalcium phosphate ($Ca_4(PO_4)_2O$) within the sample. In the one hour pattern tetracalcium phosphate, DCPD and a small fraction of octacalcium phosphate were all identified within the sample. For all other immersion time points the octacalcium phosphate and DCPD phases were not identified and instead hydroxyapatite and tetracalcium phosphate were the cement phases, with the fraction of tetracalcium phosphate decreasing in relative intensity within the sample.

The identification of octacalcium phosphate is not as clear as in some of the synthesised experimental cements and one could argue that it is perhaps not present. The propensity of OCP to hydrolyse to hydroxyapatite has been discussed extensively previously. Why OCP is given as being present in these samples is due to the higher intensity broad line below 5 °2θ at 1 hour compared to the longer immersion times; which is in addition to the low intensity line at 9.5[6] °2θ at 1 hour which switch to approximately 10.8 degrees two theta for the subsequent samples. This switch from an OCP diffraction line 9.5 °2θ to an apatite one at 10.8 °2θ is noticeable and taken as evidence supporting OCP formation.

9.1.2 ^{31}P MAS-NMR

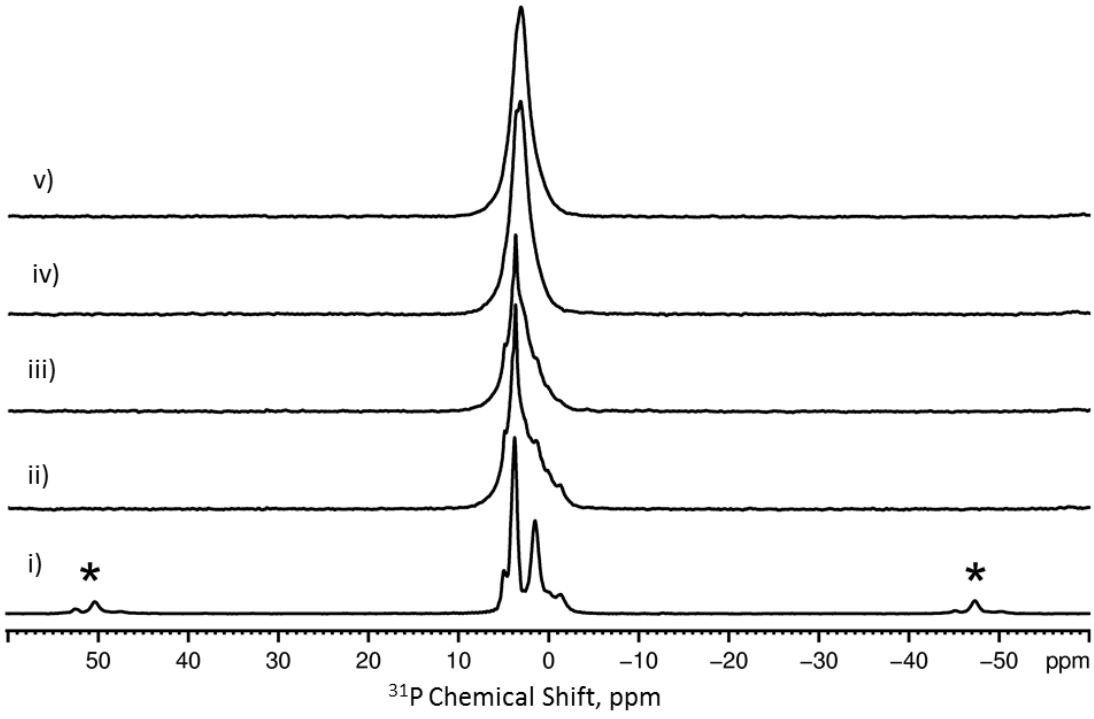

Figure 112 ^{31}P MAS-NMR spectra of HydroSet™ showing i) starting powder, ii) 1 hour immersion, iii) 1 day immersion, iv) 7 days immersion and v) 28 days immersion.

[6] The broad diffraction line at 9.5 °2 θ is believed to be a combination of two lines in OCP which are found at 9.3 and 9.7 °2 θ .

Figure 112 shows the ^{31}P MAS-NMR for the HydroSet™ cement after immersion in Tris buffer solution. The starting powder sample has six peaks at -1.4, -0.1, 1.4, 2.8, 3.7 and 4.9 ppm. The 1 hour sample has chemical shifts at -1.4, -0.2, 0.2, 1.4, 2.0, 2.7, 3.7, 4.0 and 4.9 ppm. The 1 day sample has chemical shift at 0.0, 1.4, 2.0, 2.7, 3.7, 4.0 and 4.9 ppm. The 7 day sample has chemical shift at 3.1 and 3.6 ppm. The 28 day sample has chemical shift at 3.1 and 3.6 ppm.

The spectral results of HydroSet™ show that this cement system is an OCP/HAP forming calcium phosphate cement. The ^{31}P MAS-NMR and X-ray diffraction of the starting materials show that the phases present are DCPD, tetracalcium phosphate and DCPA. The DCPA was identified only on the ^{31}P MAS-NMR and not on the X-ray diffraction by chemical shift at -1.4 and -0.2 ppm.

After 1 hour in Tris buffer solution the X-ray diffraction shows the presence of DCPD, tetracalcium phosphate and octacalcium phosphate. The ^{31}P MAS-NMR (Figure 112) for this sample is more complicated and difficult to interpret. The tetra calcium phosphate is clearly still present, as can be identified by the peaks at 3.8 and 4.8 ppm. This is true also for DCPD where a peak at 1.4 ppm is present. The peaks at -1.4 and -0.2 ppm show a small fraction of DCPA is still present in the cement phase from the starting materials. At one hour there is also octacalcium phosphate present. This was identified on the X-ray diffraction from low intensity lines at 4.7 and 9.8 degrees 2 theta. The ^{31}P MAS-NMR is slightly more difficult to identify OCP due to the large number of peaks at similar chemical shifts. Strong evidence

of OCP on the ^{31}P MAS-NMR spectra is a peak at 3.6 ppm which would be expected if OCP was present. The other chemical shift for OCP at 3.3, 2.0 and -0.2 ppm are more difficult to identify due to the higher number of signals between -1.4 and 5.0 ppm from a number of calcium phosphate phases.

The X-ray diffraction shows that on the 1 day, 7 day and 28 day samples the same two phases are present, tetracalcium phosphate and hydroxyapatite. The only apparent change is the relative intensities of the two phases appear to change; the tetracalcium phosphate decreases in relative intensity whereas the hydroxyapatite increases in its relative intensity. The ^{31}P MAS-NMR results show that at 1 hour tetracalcium phosphate is present with peaks at 3.8 and 5.0 ppm. There is a fairly broad shoulder at 2.8 ppm suggesting hydroxyapatite is present, as well as a peak at 1.4 ppm suggesting a small fraction of DCPD is present. There are also several peaks at 3.6, 2.0 and -0.2 ppm showing that OCP is present. The 7 day ^{31}P MAS-NMR spectrum has a peak at 3.0 ppm of hydroxyapatite and two additional peaks at 3.7 and 4.9 ppm of tetra calcium phosphate. The 28 day sample has a main peak at 2.9 ppm (hydroxyapatite), a shoulder at 3.7 ppm and a very small shoulder at 4.9 ppm (tetracalcium phosphate).

9.1.3 Compressive Strength

Glass Composition	**Compressive Strength (MPa)**			
	1 Hour	**1 Day**	**7 Days**	**28 Days**
HydroSet™	14.24	25.43	13.58	25.12

HydroSet™ has higher values compared to the experimental compositions, the values ranged from 13.58 to 25.43 MPa.

9.1.4 Setting Time

Cement Composition	Initial Setting Time (min)	Final Setting Time (min)
HydroSet™	6	30

The initial setting time of the HydroSet sample was 6 min and the final setting time was 30 min.

9.2 Discussion

9.2.1 Cement Phase Analysis

The spectral results of HydroSet™ show that this cement system is an OCP/HAP forming calcium phosphate cement. The ^{31}P MAS-NMR and X-ray diffraction of the starting materials show that the phases present are DCPD, tetracalcium phosphate and DCPA. The DCPA was identified only on the ^{31}P MAS-NMR and not on the X-ray diffraction by chemical shift at -1.4 and -0.2 ppm.

After 1 hour in Tris buffer solution the XRD shows the presence of DCPD, tetracalcium phosphate and octacalcium phosphate. The ^{31}P MAS-NMR (Figure 112) for this sample is more complicated and difficult to interpret. The tetracalcium phosphate is clearly still present, as can be identified by the peaks at 3.8 and 4.8 ppm. This is true also for DCPD where a peak at 1.4 ppm is present. The peaks at -1.4 and -0.2 ppm show a small fraction of DCPA is still present in the cement phase from the starting materials. At one hour there is also OCP present. This was identified on the X-ray diffraction from low intensity lines at 4.7 and 9.8 degrees 2 theta. The ^{31}P MAS-NMR is slightly more difficult to identify OCP due to the large number of peaks at similar chemical shifts. Strong evidence of OCP on the ^{31}P MAS-NMR

spectra is a peak at 3.6 ppm which would be expected if OCP was present. The other chemical shift for OCP at 3.3, 2.0 and -0.2 ppm are more difficult to identify due to the higher number of signals between -1.4 and 5.0 ppm from a number of calcium phosphate phases.

The X-ray diffraction shows that on the 1 day, 7 day and 28 day samples the same two phases are present, tetracalcium phosphate and hydroxyapatite. The only apparent change is the relative intensities of the two phases appear to change; the tetracalcium phosphate decreases in relative intensity whereas the hydroxyapatite increases in its relative intensity. The ^{31}P MAS-NMR results show that at 1 hour tetracalcium phosphate is present with peaks at 3.8 and 5.0 ppm. There is a fairly broad shoulder at 2.8 ppm suggesting hydroxyapatite is present, as well as a peak at 1.4 ppm suggesting a small fraction of DCPD is present. There are also several peaks at 3.6, 2.0 and -0.2 ppm showing that OCP is present. The 7 day ^{31}P MAS-NMR spectrum has a peak at 3.0 ppm of hydroxyapatite and two additional peaks at 3.7 and 4.9 ppm of tetra calcium phosphate. The 28 day sample has a main peak at 2.9 ppm (hydroxyapatite), a shoulder at 3.7 ppm and a very small shoulder at 4.9 ppm (tetracalcium phosphate).

9.2.2 Compressive Strength

9.2.3 Setting Time

Stryker, the manufacturers of HydroSet™ state that HydroSet™ has an initial setting time of 4.5 minutes and a final setting time of 8.5 minutes (Co, 2010) whereas the results using the Gilmore needle test give an initial setting time of 6 minutes and final setting time of 30 minutes. Thus difference is because

the manufacturers use a different method to measure the initial and final setting times when developing HydroSet™. This highlights that setting time is a difficult thing to assess and measure and especially apply this to a clinically meaningful context. There is no figure of acceptable and not acceptable setting times rather the assessment should be does this set well enough in-vivo to allow the clinician to easily implant it and to not cause any negative effects in-vivo such as washout or disfigurement.

Chapter 10: Overall Discussion

10.1 General Comments and Trends of Experimental Cements

Table 37 Summary of major cement phases formed in each cement formulation at each immersion time point. DCPD = dicalcium phosphate dihydrate (Red), OCP = octacalcium phosphate (Green), HAP = hydroxyapatite (Purple), AP = apatite[7] (Blue), FAP = fluoridated apatite (Black).

Cement Composition	Immersion Time			
	1 Hour	1 Day	7 Days	28 Days
	Calcium/Sodium Series			
HydroSet™	DCPD/OCP	DCPD/OCP/ HAP	HAP	HAP
QMNWKPaG13	DCPD	DCPD	DCPD /OCP	OCP
QMNWKPaG03	DCPD	DCPD	DCPD /OCP	OCP
QMNWKPaG14	DCPD /OCP	DCPD /OCP	OCP	OCP/HAP
QMNWKPaG15	OCP	OCP	AP	AP
QMNWKPaG16	OCP/AP	OCP/AP	AP	AP
	CaF_2 Series			
QMNWKPaG04	DCPD /OCP	DCPD /OCP	OCP/AP	AP
QMNWKPaG06	DCPD /AP	DCPD /AP	DCPD /AP	AP
QMNWKPaG08	DCPD/FAP	DCPD /AP	AP	FAP
QMNWKPaG09	DCPD /AP	DCPD /AP	AP	AP
QMNWKPaG10	DCPD /AP	DCPD /AP	AP	AP
QMNWKPaG07	DCPD /AP	DCPD /AP	AP	AP
QMNWKPaG11	DCPD /AP	AP	AP	AP

The results presented here demonstrate the use and value gained from using multiple techniques to characterise not only the setting reaction of calcium phosphate cements, but also in the characterisation of calcium phosphates in general. The value was most obvious when characterising the octacalcium phosphate, due to the similarity in the crystal structure of apatite and octacalcium phosphate it can be very difficult to differentiate between these two phases via X-ray diffraction. As mentioned previously this is due to

[7] HAP and AP were used respectively for hydroxyapatite and apatite in order to specify when the prensence of hydroxyl ions in the apatite structure. Usually confirmed using FTIR.

these two phases possessing indistinguishable diffraction patterns above 10 ˚2θ. When performing X-ray diffraction on calcium phosphate systems it is advisable to run from at least 3 ˚2θ in order to be able to detect the 4.7 ˚2θ diffraction line which is a diffraction line present in octacalcium phosphate but not in apatite. However, whilst this procedure was performed on these cement systems it still could have led to mischaracterisation of the exact cement phase. This is because whilst the presence of the 4.7 ˚2θ diffraction line does show that octacalcium phosphate is present it does not tell you whether apatite is not present as there could be present a mixture of the two phases. It could be partially deciphered by looking at the relative intensities of the diffraction lines because the 4.7 ˚2θ diffraction line is the most intense line on octacalcium phosphate, one could argue that a relatively intense 4.7 ˚2θ line would indicate that the cement phase is in the vast majority octacalcium phosphate with only maybe a small fraction of apatite. The results here demonstrate that this cannot be assumed; for instance, in the X-ray diffraction pattern of the 28 day QMNWKPaG03 cement the diffraction lines around 31˚2θ are much more intense than the diffraction line at 4.7 ˚2θ which could lead one to assume the octacalcium phosphate is present but as a small fraction of the cement phase. However the ^{31}P MAS-NMR showed that the cement phase was virtually completely octacalcium phosphate and that there was not apatite detectable.

Further to this the multiple technique characterisation of calcium phosphates proved valuable in fully characterising the cement phases, especially when the cement phase is primarily apatite. The 28 day QMNWKPaG14 cement

sample demonstrates this aptly. The X-ray diffraction shows that apatite is present which is in agreement with the ^{31}P MAS-NMR results. The FTIR was able to demonstrate the presence of the hydroxyl group in the apatite structure and the presence of carbonate substitution, enabling the characterisation of this cement phase as being carbonate substituted hydroxyapatite.

All of the spectral results show that both the starting reagents have dissolved within 1 hour for all cement compositions. The ^{31}P MAS-NMR spectra show that the $Ca(H_2PO_4)_2$ and the phosphate content of the glass has degraded before one hour to form the cement phase. This is due to the high solubility of both the $Ca(H_2PO_4)_2$ salt phase and the bioactive glass. This differs from the HydroSet™ setting reaction where the starting reagents of undergo complete dissolution between 7 days and 28 days.

The ^{19}F MAS-NMR could only be run on one cement sample, the QMNWKPaG08. It confirmed the presence of a CaF_2 species and a fluoridated apatite species. Stoichiometric fluorapatite ($Ca_{10}(PO_4)_6F_2$) gives a chemical shift at -101 ppm. It has been shown previously that non-stoichiometric fluorapatite causes a shift in the position of the chemical shift on the ^{19}F MAS-NMR spectra proportionally to fluoride content.

10.2 Calcium-sodium Cement Compositions (QMNWKPaG03 & 13-16

10.2.1 Summary

In all the cement compositions there is a clear reaction pathway; in the fluoride-free cement compositions this being DCPD > octacalcium phosphate > hydroxyapatite and the fluoride containing series being DCPD > apatite.

The change in glass composition clearly causes the rate at which this reaction pathway progresses to change. The slowest rate of this transition occurs in the QMNWKPaG03 and QMNWKPaG13 cement compositions where the DCPD to octacalcium phosphate transition occurs between 1 day and 7 days and the octacalcium phosphate to hydroxyapatite transition is not witnessed within 28 days. Whereas the fastest transition occurs in QMNWKPaG16 cement composition, at 1 hour the cement phase is a mixture of apatite and octacalcium phosphate, with hydroxyapatite being the major phase. The cement has already passed though the DCPD step within an hour. There is also a noticeable shift as the sodium content of the glass is increased, as more sodium is in the glass composition the rate of phase evolution increases.

The cause of this can be speculated upon and may be due to the combination of a number of factors. (1) The increase in sodium content has been shown to cause an increase in pH (Wallace et al., 1999). This affect could be translated into the cement system causing those cements to more rapidly increase pH after the initial acidity created by the dissolution of the $Ca(H_2PO_4)_2$, causing a faster transition to a pH outside that of the stability range of DCPD thus causing a faster transition to octacalcium

phosphate/apatite. (2) As the sodium is increased in the glass composition the amount of $Ca(H_2PO_4)_2$ salt added to maintain the overall calcium to phosphorus ratio in the cement powder is decreased. A decrease in salt quantity would reduce the acidity of the reaction environment when the salt dissolves, the cement would then reach a pH outside the stability range of DCPD.

10.2.2 Proposed Setting Reaction

(1) $Ca(H_2PO_4)_2 + 2H_2O \rightarrow CaHPO_4.2H_2O + H_3PO_4$

(2) $H_3PO_4 \rightarrow 3H^+ + PO_4^{3-}$

(3a) $2(Si\text{-}O)Ca + 2H^+ \rightarrow 2SiOH + Ca^{2+}$

(3b) $R\text{-}(Si\text{-}O)Na + H^+ \rightarrow R\text{-}SiOH + Na^+$

(4) $10CaHPO_4.2H_2O \rightarrow Ca_8(HPO_4)_2(PO_4)_4.5H_2O + 2Ca^{2+} + 4H_2PO_4^- + 15H_2O$

(5) $Ca_8(HPO_4)_2(PO_4)_4.5H_2O + 2(OH)^- + 2Ca^{2+} \rightarrow Ca_{10}(PO_4)_6(OH)_2 + 5H_2O + 2H^+$

(1) All the spectroscopic techniques show that within 1 hour the $Ca(H_2PO_4)_2$ starting reagent has completely dissolved and the primary cement phase is DCPD ($CaHPO_4.2H_2O$). This is particularly evident on in the QMNWKPaG03 1 hour cement composition where the FTIR, MAS-NMR and XRD all show an almost pure DCPD cement phase. This is due to the high solubility of $Ca(H_2PO_4)_2$, which once the 2.5% Na_2HPO_4 solution is added immediately dissolves, creating an acidic reaction environment. The H^+, Ca^{2+} and PO_4^{3-} ions released after the dissolution then precipitate the DCPD phase, which according to calcium phosphate solubility diagrams is favoured due to the high acidity of the reaction solution (Elliott, 1994).

(2-3) Steps 2-3 are related stages and step three is induced by step two. Step two is partially simplified as the H_3PO_4 species would most likely exist as a number of protonated phosphate species of varying degrees between completely deprotonated to completely protonated with any deprotonated hydrogen ions being in the reaction solution. Steps 3a and 3b refer to degradation of the glass which is induced by the acidity of the solution. Ion exchange occurs between the calcium and sodium ions and the protons in solution. This causes the release of calcium and sodium ions into the reaction solution and creation of silanol groups (Si-OH) on the silicate chains (Hench, 1993). Another likely consequence of the ion exchange process is an increase in pH due to the consumption of protons in solution. This idea is applied from the original and widely accepted Hench mechanism of glass dissolution (Hench, 1993).

(4) Once the pH of the reaction environment begins to increase caused by the ion exchange process and after the immersion in Tris buffer, a phase transition process is initiated. The DCPD undergoes a dissolution/precipitation process after which octacalcium phosphate precipitates. It is most likely a contribution of two processes which induce this transformation. (1) Change in pH causes DCPD to leave its pH stability range and (2) there is a thermodynamic drive to form a more thermodynamically stable phase (Elliott, 1994). The point at which this process begins to occur and the rate at which it happens is shown to alter between cement compositions.

(5) The octacalcium phosphate phase over time is transformed to a hydroxyapatite phase. This is a thermodynamically driven process as hydroxyapatite is more thermodynamically stable than octacalcium phosphate (Fernandez et al., 1999a). It is strongly believed that the transformation of octacalcium to hydroxyapatite proceeds via a solid state phase transition rather than dissolution/precipitation as in DCPD to octacalcium phosphate transition (Tseng et al., 2006, Aue et al., 1984).

10.3 Fluoride Containing Cement Compositions

10.3.1 Summary

The fluoride containing glasses produced cements followed the same reaction pathway as each other. The presence of DCPA was most likely introduced as an impurity from the $Ca(H_2PO_4)_2$, which was shown to be present in the NMR. In all cement compositions with fluorine the reaction follows the same pathway (evolution of phase); in the initial cement reaction (0-60 min) DCPD and fluoridated-apatite are formed. Subsequently the DCPD phase undergoes a hydrolysis reaction to form apatite; this is evident on the NMR where the intensity of the DCPD chemical shift decreases relative to the apatite shift (Figure 111). The DCPA generally persists until after the DCPD has been hydrolysed and like DCPD it will be hydrolysed also to an apatite phase.

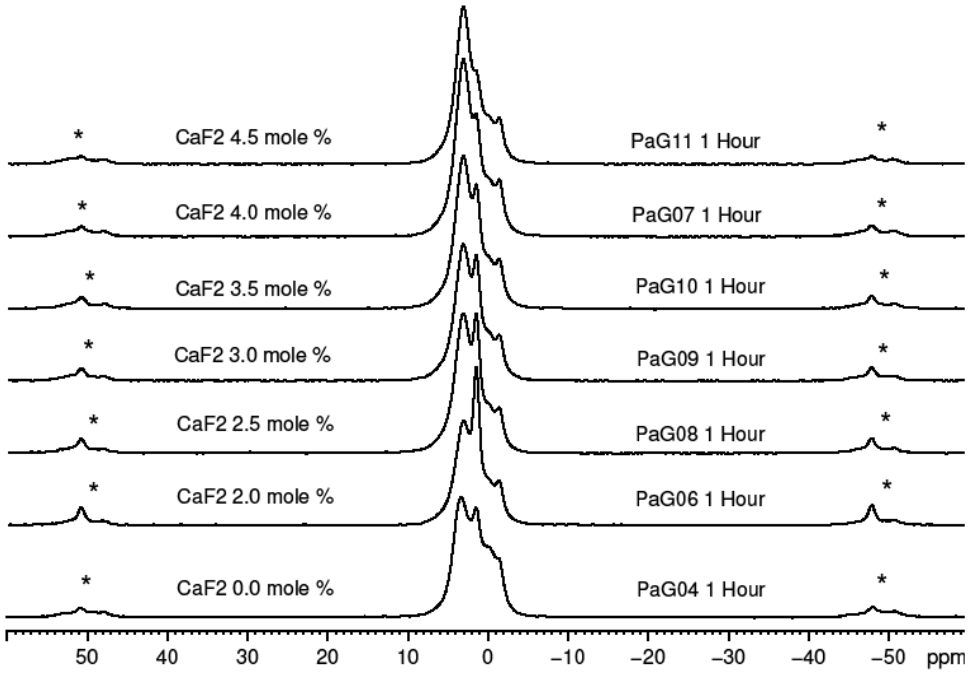

Figure 113 ^{31}P MAS-NMR spectra of series of fluoride containing cement compositions plotted in order of increasing CaF_2 (mol%) in the glass used to produce the cement, ranging from 2.5-4.5 mol% CaF_2 and 0 mol% CaF_2.

An evident trend in the fluoride containing series is the effect on the cement setting reaction of the fluoride content, whilst the amount of DCPA appears unaffected (due to it being an impurity in the starting material) the ratio of DCPD and apatite phase alters depending upon fluoride concentration. As is visible in Figure 113, as the concentration of fluoride increases the fraction of DCPD decreases.

10.3.2 Proposed Setting Reaction

(1) $Ca(H_2PO_4)_2 + 2H_2O \rightarrow CaHPO_4.2H_2O + H_3PO_4$

(2) $H_3PO_4 \rightarrow 3H^+ + PO_4^{3-}$

(3a) $2(Si\text{-}O)Ca + 2H^+ \rightarrow 2SiOH + Ca^{2+}$

(3b) $(Si\text{-}O)Na + H^+ \rightarrow SiOH + Na^+$

(4) $Ca^{2+} + (PO_4)^{3-} + (OH)^- + F^- \rightarrow Ca_{10}(PO_4)_6(OH)_{2-x}F_x$

(5) $6CaHPO_4.2H_2O + 2\text{-}x(OH)^- + xF^- + 4Ca^{2+} \rightarrow Ca_{10}(PO_4)_6(OH)_{2-x}F_x + 5H_2O + 6H^+$

(1-3) The initial cement setting mechanism in the fluoride containing cements is believed to follow the same initial steps as in the fluoride-free cements (and is explained in detail there). Essentially this details the dissolution of the $Ca(H_2PO_4)_2$ and glass starting reagents to release the calcium phosphate phase forming ions. Additionally the formation of DCPD occurs during these stages.

(4) In step four the reaction pathway deviates from that of the fluoride-free cements. The cements show the direct precipitation of a fluoridated apatite, rather than an octacalcium phosphate phase. Indeed, whilst octacalcium phosphate is identified in at least one time point for every cement composition not containing fluoride in cement compositions containing fluoride octacalcium phosphate was not identified at any time point

(5) The DCPD formed in the initial dissolution of the $Ca(H_2PO_4)_2$ dissolves and precipitates to a fluoridated apatite. For most of the compositions this occurred between 1 day and 7 days apart from the cement with the lowest fluoride concentration, which transformed completely between 7 days and 28 days.

10.4 HydroSet™

10.4.1 Summary

Both the X-ray diffraction and ^{31}P MAS-NMR for the studied HydroSet™ are somewhat difficult to interpret given the complexity of the results caused by the presence of many phases. The X-ray diffraction and ^{31}P MAS-NMR

results agree the cements form octacalcium phosphate and hydroxyapatite during the cement setting reaction, with the octacalcium phosphate transforming to hydroxyapatite with 28 days in Tris buffer solution. The starting materials remain unreacted inside the cement cylinder for a considerably longer period than the cement developed in this project. Whilst the DCPD fully dissolves between 1 day and 7 days the tetracalcium phosphate is still present at 28 days.

One interesting result is the amount of time the tetracalcium phosphate takes to fully react to form the cement phase. The two starting reagents are added together in an overall calcium to phosphorus ratio of 1.67 to favour apatite formation (Clarkin et al., 2009). This could be due to the relative particle sizes of the two starting reagents or lack of water penetrating the cement cylinder causing the dissolution of the tetracalcium phosphate and precipitation of the cement phase, as it has been shown particle size can have a large influence on the reactivity of starting components in calcium phosphate cements (Ishikawa et al., 1995).

Traditionally it was believed that during the setting of HydroSet™ the cement phase formed was hydroxyapatite (Clarkin et al., 2009). The results show here that the cement setting reaction additionally forms octacalcium phosphate. It is not known from these results if the octacalcium phosphate forms as a precursor to the hydroxyapatite formation, as it does in the novel cement compositions developed, or if it only forms as well as the hydroxyapatite.

10.4.2 Setting Reaction

1. $2CaHPO_4.2H_2O + 2Ca_4(PO_4)_2O + H_2O \rightarrow Ca_8(HPO_4)_2(PO_4)_4.5H_2O + 2Ca^{2+} + 2(OH)^-$
2. $Ca_8(HPO_4)_2(PO_4)_4.5H_2O + 2Ca^{2+} + 2(OH)^- \rightarrow Ca_{10}(PO_4)_6(OH)_2 + 2H^+ + 5H_2O$

10.5 Crystal Morphology

The results from the scanning electron microscopy showed a range of crystal morphologies which appeared to follow a number of trends that correlated with the spectral analysis of the cement samples. There were generally four crystal morphologies visible in the cement phases; although there was some slight differences in the exact dimensions of each of the morphologies. The four morphologies identified were needles, ribbons, plates and irregular petals.

1. Needles – The needle morphology was only seen in the cements where fluoride was added and the cement phase was apatitic. Figure 114 shows a representative image of this morphology. As can be seen the crystals are very small but relatively long in one direction. It is thought that the phase of these crystallites is a fluoridate-apatite. Fluorapatite or fluoride containing apatite is known to take this needle morphology and its occurrence here agrees with this interpretation.

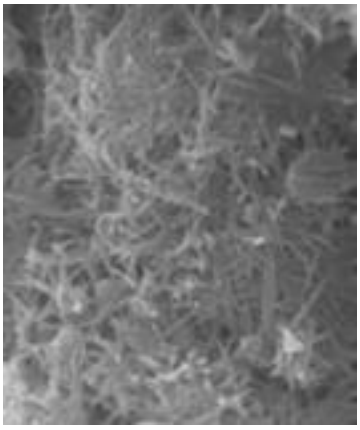

Figure 114 Typical needle morphology witnessed on the SEM images of the calcium phosphate cements.

2. Ribbons – ribbon morphology was observed in cement compositions where octacalcium phosphate was present or had been previously formed. The ribbons were generally large >30 μm in their longest direction. The ribbons are displayed in Figure 115. The cause of this morphology is outlined in the following section.

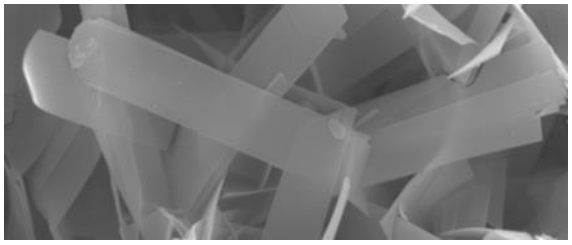

Figure 115 Typical ribbon morphology witnessed on the SEM images of the calcium phosphate cements.

3. Plates – Figure 116 shows the plate morphology seen in some of the cements. This morphology is attributed to being DCPD crystallites because it is only witnessed in the cements where DCPD is identified using the spectroscopy, this is emphasised in the QMNWKPaG03 cement composition at 1 hour and 1 day.

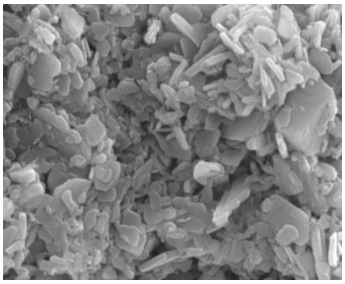

Figure 116 Typical plate morphology witnessed on the SEM images of the calcium phosphate cements.

4. Irregular Petals – there was a distinctive irregular petal morphology seen in some of the cement compositions at generally longer time points of immersion. As seen in Figure 117 the crystals have irregular shaped boarders but are very thin. It is believed that these crystals are predominantly apatite that has undergone phase transition from octacalcium phosphate crystals. This would account for the thin nature of the crystal that is driven by the structure of the octacalcium phosphate. Continual growth during the immersion period causes the irregular shape observed as the crystals.

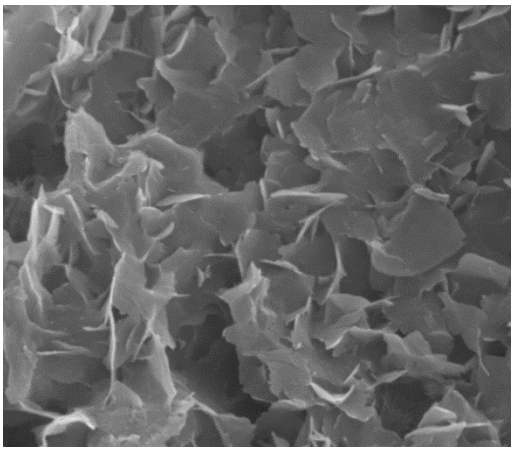

Figure 117 Typical irregular plate morphology witnessed on the SEM images of the calcium phosphate cements.

10.5.1 Octacalcium Phosphate

In the SEM images it is evident that the OCP crystallites take a ribbon-like morphology. This ‘ribbon’ or ‘plate’ morphology is not unique in this study

and is in fact a common trend for OCP. It is believed this is caused by the octacalcium phosphate structure having the lowest overall interfacial energy compared to any other potential morphology. In 1878 Gibbs theorised that a crystal (or droplet) will arrange itself in an orientation of low surface (or interfacial) energy that minimises Gibbs free energy (Gibbs, 1957). This was defined as:

$$\Delta G_i = \sum_j \gamma_j O_j \quad (13)$$

Where γ_j represents the surface energy per unit area of the jth face and O_j is the area of said face. ΔG_i represents the difference in energy between a real crystal composed of i molecules with a surface, and a similar configuration of i molecules located inside an infinitely large crystal. This quantity is therefore the energy associated with the surface. The conclusion can then be drawn that the equilibrium shape of the crystallite will be that which minimises the value of ΔG_i. Succinctly put, where possible thermodynamics will induce a crystallite morphology that maximises the surface area of low interfacial energy surfaces and minimises the surface area of high interfacial energy ones. Further to this the Gibbs-Wulff theorem proposes that the length of a vector drawn from the centre of a crystal to the crystal face h_j will be proportional to its surface energy γ_j (Strickland-Constable, 1968).

$$h_j = \lambda_{\gamma j} \quad (14)$$

The vector 'h_j' is the height of the *j*th face, and is drawn from the centre of the crystal to the chosen face.

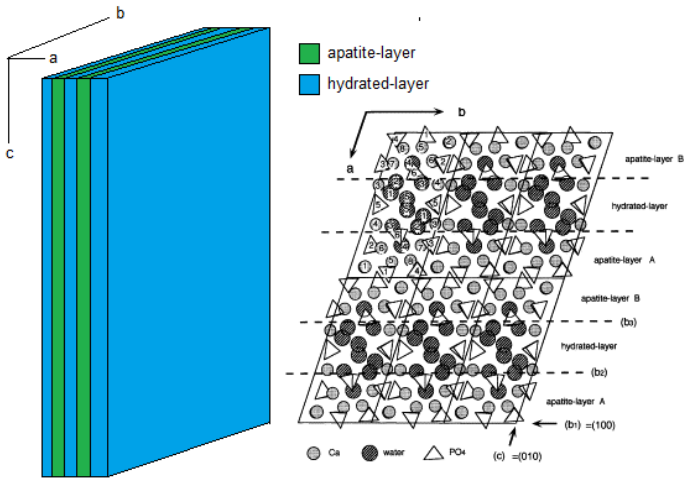

Figure 118 Representative images of atom arrangement in octacalcium phosphate crystal structure (right) and layer ordering and morphology of octacalcium phosphate crystallites.

If this idea is applied to the morphology of the octacalcium phosphate crystals seen on the SEM then it explains the morphology witnessed. The octacalcium phosphate crystal consists of two layers; an apatite-layer and a water-layer. The 'a' axis of an octacalcium phosphate crystallite is made of alternating apatite-layer and water-layers. Comparing the composition of the apatite and hydrated layers in the OCP crystal structure the apatite layer is made of six Ca^{2+} ions, two phosphate ions and one water molecule; the water layer consists of two Ca^{2+} ions, one phosphate ion and four water molecules, with the remaining three phosphates are located in the junction between the two layers (Brown, 1962). Due to the difference in the composition of these two layers it is thought that they will have different interfacial energies. Due to the high water content of the hydrated layer, the H_2O molecules would induce hydrogen bonding between the crystal and surrounding aqueous solution and there would have a slightly higher affinity between the hydrated layer and the solution compared to the apatite layer

and the same solution. This would equate to a lower interfacial energy on the water layer compared to the apatite layer. Thermodynamics would then favour the increase in the proportion of lower interfacial energy surface in order to reduce free energy. In this instance the face of the b-c axis on the OCP crystal would be increased causing the ribbon (or sometimes plate) morphology.

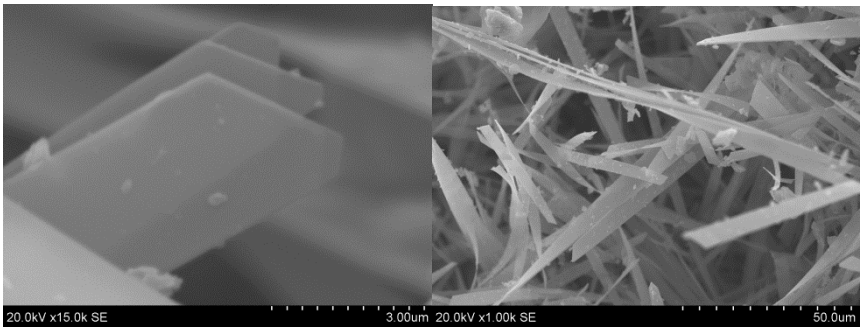

Figure 119 Scanning eletron micrographs of cement compositions showing typical octacalcium phosphate morphology

10.5.2 Fluoridated Apatite

The SEM images show a clear morphology difference between different cement phases. A particularly noticeable difference is between the hydroxyapatite/octacalcium phosphate and fluoridated-apatite cement phases. The hydroxyapatite/octacalcium phosphate crystallite morphology in the fluorine-free cement compositions has a ribbon or plate morphology (Figure 119) whilst the fluoridated-apatite shows a small needle morphology. The potential causes of the needle morphology is that the fluoridate-apatite has not passed through the OCP precursor phase like the hydroxyapatite has, so the thermodynamic drive to increase the face area corresponding to the octacalcium phosphate water layer has not occurred.

10.6 Phase Transition in Cement Evolution

10.6.1 Dicalcium Phosphate Dihydrate-Octacalcium Phosphate-Hydroxyapatite

According to thermodynamic theory one would expect for hydroxyapatite to form preferentially to octacalcium phosphate due to it having a lower solubility because of its higher stability and being more thermodynamically stable than octacalcium phosphate. However, in the incidence of the fluorine-free cement compositions it is clear that octacalcium phosphate forms as an intermediary to hydroxyapatite formation. It is known that octacalcium phosphate both nucleates and grows easier than hydroxyapatite (Elliott, 1994). This indicates that the reaction is a kinetically determined process as opposed to a thermodynamically determined one. According to the Ostwald-Lussac law of stages, in a system where a number of crystalline phases can potentially form, the phase with the most kinetically favourable phase will form preferentially over any phase with a higher nucleation energy barrier (De Yoreo and Vekilov, 2003). Then the phase will pass through any potential metastable intermediary phases until the most stable phase is formed.

A contributor to the high energy of formation of hydroxyapatite is the relative lack of hydroxyl ions in the solution given the reaction occurs in an acidic environment meaning the available concentration of hydroxyl ions is very low. Given hydroxyl ions make up part of the hydroxyapatite structure the chance of them being readily available for nucleation is relatively low. Octacalcium phosphate on the other hand does not have hydroxyl ions within its structure and actually possesses protonated phosphate groups. Another

factor contributing to the favourable formation of octacalcium phosphate is the structural water molecules in the crystal structure which would contribute to lowering the interfacial energy of the octacalcium phosphate crystallites.

The Ostwald-Lussac law of stages also applies to understanding why DCPD forms preferentially to DCPA; as DCPA is a more stable and less soluble, as such, thermodynamically one would expect DCPA to form preferentially (Elliott, 1994, Gibbs, 1957). As with the octacalcium phosphate the cause of this is most likely due to the kinetics of the nucleation of the DCPD phase. The formula of DCPD ($CaHPO_4.2H_2O$) and DCPA ($CaHPO_4$) show that the only difference is two structural water molecules in the DCPD structure. These water molecules are likely to lower the interfacial energy in DCPD nuclei which is likely to be reflected in a lower nucleation energy barrier.

There is a slight deviation in the reaction pathway from the Ostwald-Lussac law of stages as after the DCPD forms one would expect DCPA to form except in the fluorine free composition the reaction goes from DCPD to OCP and in the fluorine containing compositions the reaction goes from DCPD to apatite. The cause of this is perhaps pH related as during the initial setting when the DCPD is initially formed the reactions conditions are highly acidic in the region of the stability of DCPD and DCPA.

10.6.2 Dicalcium Phosphate Dihydrate -Fluoridated Apatite

These results show that in an acidic environment the nucleation of fluorapatite is more kinetically favourable than the formation of octacalcium phosphate. This conclusion was drawn from a number of the results gained from the studies performed. Firstly the ^{31}P MAS-NMR and XRD confirmed

that in all of the fluoride containing cement compositions a fluoridated apatite was formed in all instances, whereas in the fluoride free cement compositions octacalcium phosphate was identified in at least one time point in all compositions. Secondly in the SEM images show a difference in the size and number of crystallites between the fluoride containing and fluoride-free samples. In general the fluorine containing cement compositions had small (<10 μm length) crystallites that were more numerous than the generally larger crystallites (>20 μm) in the fluorine free cement compositions.

Explaining the reaction mechanism requires applying both kinetics and thermodynamics the process. There are three potential reasons for the formation of apatite preferentially to OCP in the fluoride containing cements.

(1) Fluorapatite has a lower energy barrier to nucleation than octacalcium phosphate, this idea is supported by the large number of small crystallites witnessed on the SEM. Fluorapatite is a more thermodynamically stable phase than OCP but the reaction pathway is a kinetically driven process, following the Ostwald-Lussac law (De Yoreo and Vekilov, 2003). OCP is less thermodynamically stable than hydroxyapatite but the nucleation of it is more kinetically favourable it does not mean than less thermodynamically stable phases are always more kinetically favourable in formation. It is believed that a more soluble (and less stable) phase is likely to have a lower nucleation energy than a less soluble phase. The SEM support this idea in that

the apatite cement phase is a high number of small needle-like crystals.

(2) Apatites (including hydroxyl, fluoro and any mixtures of the two) have lower nucleation energies than OCP and the reason apatite does not form directly in the fluorine free cement compositions is the lack of hydroxyl ions in the acidic cement forming reaction environment. This is in contrast to the first idea which suggests that only fluorapatite has a lower nucleation energy.

(3) OCP may in actual fact form in the fluoride containing cements though the transition from OCP to fluorapatite occurs before the first time point studied. There is evidence showing that addition of fluoride to a OCP containing solution does increase the rate of OCP to apatite formation but this theory is slightly affected by the fact there is a clear difference in both the number and size of crystallites. If OCP was still an intermediary phase then you would expect the nuclei to form at the same rate and grow to the same size as those crystallites without fluoride because the nucleation barrier for OCP formation should not change through fluoride presence. This is not the case however as the crystallites in the fluoride containing cements are smaller and more numerous than the fluoride free OCP crystallites. Another point against this idea is that in OCP to apatite transition the resultant crystallite morphology of the apatite is the same as the morphology (plate-like) of the initial OCP formed. This is because the transition between these two species is via solid state phase transition rather than dissolution and precipitation (Tseng et al., 2006). However, in the

SEM images for the fluoride containing cements the morphology of the apatite cement phase is small needle-like crystals.

At least all three explanations are possible, however of these ideas theory one is probably the most likely as it fits with the results and nothing obviously contradicts it. Further experimentation should be conducted to confirm this is the case.

10.7 Comparisons and Differences with Existing Calcium Phosphate Cements

Comparing the novel cements developed through this project, with conventional CPCs, shows a series of similarities and differences in their properties and behaviour. These novel cements are related in that they are calcium phosphate forming cement phases.

A difference from traditional calcium phosphates is the use of glass as a reactive precursor which releases ions for the cement setting reaction. Whist previously bioactive glasses have been added to calcium phosphate cements, there role was only as a bioactive filler designed to improve biocompatibility of the cement (Renno et al., 2013). This is a similar approach to other biomaterials which have had bioactive glass added to them as a filling agent (Li et al., 2013). The use of glass gives contrasting properties to traditional CPC's; these results demonstrate the potential to control various properties of the cements produced. Traditional calcium phosphate cements can only be manipulated through changes in particle size, ratios of components or through the addition of accelerants or retarders. The reason for this is that salts are fixed in their stoichiometry and solubility

whereas glasses can have these properties altered through composition changes. It was shown here that the setting time, compressive strength, and cement phase could all be altered through changes in the glass composition. This is due to the high variability in potential glass composition which enables the alteration of

A difference witnessed with these cements is the extension in setting times of DCPD forming cement compositions without the use of retardants. Unworkable setting times (1-3 mins) initially hampered the clinical use of DCPD forming calcium phosphate cements (Tamimi et al., 2012). The short setting times did not allow adequate time for the cement to be mixed the injected into the implanted site and moulded to the desirable shape. Consequently efforts were taken to extend these times to those more acceptable and various retardants were added to delay the setting reactions. Magnesium and pyrophosphate have both been added as retardants to DCPD cements[8]. With the addition of additives one must consider the potential negative in-vivo consequences of their addition. Pyrophosphates are known to have biological effects, specifically have been known to cause bisphosphonate related osteonecrosis of the jaw (BRONJ), when used to treat osteoporosis; and both magnesium and pyrophosphates have been shown to influence apatite mineralisation in vitro. Therefore it is advantageous to limit the number of potential additional components in any cement formulation.

[8] Additionally the use of these components has also been used to inhibit the transformation of Brushite to apatite in-vivo, with the aim of increasing resorption rates.

Compressive strengths are difficult to judge and compare as porosity affects strength proportionally (Guo et al., 2009). Whilst the compressive strengths presented here are perhaps lower than those previously reported for calcium phosphate cements (which have maximum values of approximately 25-30 MPa), it should be mentioned of the effect liquid to powder ratio (L/P) has upon cement strength. The L/P in the initial reaction has a high effect upon the porosity of the resultant cement. Typically apatite forming calcium phosphate cements have L/P of 0.3 – 0.4, however due to the high solubility of the two starting reagents causes the need for the high L/P (0f 0.7) to produce a cement with sufficient rheology for the cement to be injectable.

Silicon incorporation (and release) in the cement composition also has a number of benefits. Aqueous Si has been shown to enhance osteoblast proliferation, differentiation and collagen production and to have dose dependent effects on osteoclast cells under in vitro conditions (Reffitt et al., 2003). Whilst there are developed calcium phosphate bone substitute materials incorporating silicon into their formulation, currently there are no known examples of silicon incorporation into calcium phosphate cements.

Octacalcium phosphate forming calcium phosphate cements have been reported previously (Honda et al., 2009) but not as extensively as if octacalcium phosphate is a precursor species to hydroxyapatite as has previously been suggested. Although this may have just been due to difficulty in identification as it has been shown here that the previously believed directly hydroxyapatite forming HydroSet™ actually forms octacalcium phosphate during early time points. In addition, as the HydroSet™ starting

reagents are identical to those originally formulated in CPCs (and is commonly used in commercial examples) it is likely that many other CPC formulations also form OCP but it has not been identified. Octacalcium phosphate has been shown to enhance bone formation in-vivo (Suzuki et al., 2006, Anada et al., 2008) and also have a positive impact on cell proliferation (Morimoto et al., 2012).

Chapter 11: Conclusions

- It was shown that it is possible to form a calcium phosphate cement where one of the starting reagents is a silicate based bioactive glass.

- Bioactive glass plays a crucial role in the formation of the cement phase through the release of calcium and phosphate ions. It was possible to form a cement which had both clinically acceptable setting times and compressive strengths.

- It was shown through investigation of numerous glass compositions that glass composition has an effect upon cement properties, specifically the setting time and compressive strength. Alterations in setting times was mainly due to alteration in the cement phase induced by either change in glass composition or alteration in glass/$Ca(H_2PO_4)_2$ ratio.

- The sodium and calcium ratio within the glass composition had a large effect upon cement properties. As the sodium content was increased the setting time decreased which was attributed to the change in cement phase the alteration in glass composition induced.

- It was hypothesised that fluorapatite cements would be stronger due to much longer crystallites in the C-axis (known to occur in fluorapatite) (Elliott, 1994) leading to a higher degree of interlocking of

the fluorapatite cement phase than conventional hydroxyapatite cements, however, this was not the result found.

- The addition of fluoride caused a higher degree of nucleation leading to small but more numerous crystallites than the fluoride-free cement compositions. It was confirmed in one composition that fluorapatite had been formed and it is likely to be present in the other compositions (but should be confirmed). However the large increase in the number of crystallites in the fluoride samples coupled with their small size is likely to cause an increase in solubility due to an increase in surface area.

- The presence of fluoride inhibited the formation of octacalcium phosphate. In all cement compositions where fluoride was **not** present octacalcium phosphate was always identified in at least one time point whereas when fluoride was present in the cement compositions octacalcium phosphate was not identified in any cement compositions at any time points. This was attributed to the fluoride offering a different reaction route and the cement setting reaction forming a fluoridated apatite rather than octacalcium phosphate.

Chapter 12: Future Work

There are a number of potential routes which could be explored following the completion of this project to further progress this project. Essentially the future work could be categorised as either (1) further understanding the chemistry of the cements outlined in the above piece of work or (2) improved the cement properties and tailor compositions for particular in-vivo applications.

An immediate task to be conducted would be to perform ^{19}F MAS-NMR analysis on all fluoride containing cement compositions in order to confirm the strongly suspected formation of a fluoridated apatite cement phase.

Studying the dissolution profile of the glasses in solution would also provide much information that would help interpret the results seen here. These studies would involve immersion of each glass in a buffered solution like Tris buffer, in a similar fashion to what has been performed previously (Brauer 2011). Ion release measurements can then be conducted to measure rate of release of the respective ions.

Porosity measurements would be an important property to measure. The scale and size of the porosity is an important factor in the performance of these materials in-vivo. High porosity and large pore interconnect size allows cellular penetration and neovascularisation. An ideal method for measuring this would be to use mercury intrusion porosimetry which measures the pore interconnect size[9].

[9] This was attempted with 8 x 12 mm cylindrical specimen. However the instrumentation was unable to reach a sufficient strength vacuum to perform the measurement.

Another property to measure would be the particle size of the glass powders. Whilst care was taken to perform identical methods to produce the glass powders there may still be some differences induce by change in glass composition therefore it would be desirable to confirm this. This could be measured by using a particle size analyser which would give the particle size distributions within the glass sample. The particle size of the $Ca(H_2PO_4)_2$ powder is not known and it would also be advisable to measure this. This would have to be done in an ethanol solution due to the high solubility of this salt.

It would also be worthwhile to produce cements with strontium; there are lots of examples in the literature where strontium has been incorporated into traditional calcium phosphate cements. Bioactive glasses have been shown to readily incorporate strontium and have been shown to release it in solution. Strontium has also been shown to have a beneficial effect on osteoblast and osteoclast cells (Gentleman et al., 2010). Additionally strontium would cause the cements to be more radiopaque than pure calcium cements, allowing their resorption to be tracked via X-rays.

In this study the cement cylinders were immersed into Tris buffer solution, this was partly for simplicity as Tris buffer solution does not contain many ions which could influence the cement phase evolution. However, body fluid is a much more complex mixture of numerous different ions which could all affect the setting reaction, cement phase evolution and the cement phase itself. Therefore it would be interesting to study the effect upon cement properties of cement cylinders immersed into different solutions; possible

solutions could be simulated body fluid, physiological-like solution and phosphate buffered saline. All of these solutions have been used previously to immerse calcium phosphate cements.

References

ABERG, J., HENRIKSSON, H. B., ENGQVIST, H., PALMQUIST, A., BRANTSING, C., LINDAHL, A., THOMSEN, P. & BRISBY, H. 2012. Biocompatibility and resorption of a radiopaque premixed calcium phosphate cement. *Journal of Biomedical Materials Research Part A,* 100A**,** 1269-1278.

ABRAHAM, F. F. 1968. A Reexamination of Homogeneous Nucleation Theory - Thermodynamic Aspects. *Journal of the Atmospheric Sciences,* 25**,** 47-&.

ALBEE, F. H. 1920. Studies in Bone Growth: Triple Calcium Phosphate as a Stimulus to Osteogenesis. *Ann Surg,* 71**,** 32-9.

ALKHRAISAT, M. H., MARINO, F. T., RODRIGUEZ, C. R., JEREZ, L. B. & CABARCOS, E. L. 2008. Combined effect of strontium and pyrophosphate on the properties of brushite cements. *Acta Biomaterialia,* 4**,** 664-70.

ALVES, H. L. R., DOS SANTOS, L. A. & BERGMANN, C. P. 2008. Injectability evaluation of tricalcium phosphate bone cement. *Journal of Materials Science-Materials in Medicine,* 19**,** 2241-2246.

ANAC, C. 1992. *Performance Assessment For Alkali Silica Reaction,* *http://homepage.tudelft.nl/n89v3/Page4.html* [Online]. Delft, Netherlands: Delft University of Technology. Available: http://homepage.tudelft.nl/n89v3/Page4.html [Accessed 31/03/2014 2014].

ANADA, T., KUMAGAI, T., HONDA, Y., MASUDA, T., KAMIJO, R., KAMAKURA, S., YOSHIHARA, N., KURIYAGAWA, T., SHIMAUCHI, H. & SUZUKI, O. 2008. Dose-dependent osteogenic effect of octacalcium phosphate on mouse bone marrow stromal cells. *Tissue Engineering Part A,* 14**,** 965-978.

APELT, D., THEISS, F., EL-WARRAK, A. O., ZLINSZKY, K., BETTSCHART-WOLFISBERGER, R., BOHNER, M., MATTER, S., AUER, J. A. & VON RECHENBERG, B. 2004. In vivo behavior of three different injectable hydraulic calcium phosphate cements. *Biomaterials,* 25**,** 1439-1451.

AUE, W. P., ROUFOSSE, A. H., GLIMCHER, M. J. & GRIFFIN, R. G. 1984. Solid-state phosphorus-31 nuclear magnetic resonance studies of synthetic solid phases of calcium phosphate: potential models of bone mineral. *Biochemistry,* 23**,** 6110-4.

AZAMI, M., JALILIFIROOZINEZHAD, S., MOZAFARI, M. & RABIEE, M. 2011. Synthesis and solubility of calcium fluoride/hydroxy-fluorapatite nanocrystals for dental applications. *Ceramics International,* 37**,** 2007-2014.

BEST, B. 1990. *Physical Parameters of Cooling in Cryonics* [Online]. Ben Best Publications. Available: http://www.benbest.com/ [Accessed 31/03/2014 2014].

BOANINI, E., PANZAVOLTA, S., RUBINI, K., GANDOLFI, M. & BIGI, A. 2010. Effect of strontium and gelatin on the reactivity of alpha-tricalcium phosphate. *Acta Biomaterialia,* 6**,** 936-942.

BOHNER, M. 2000. Calcium orthophosphates in medicine: from ceramics to calcium phosphate cements. *Injury-International Journal of the Care of the Injured,* 31**,** S37-S47.

BOHNER, M. 2001. Physical and chemical aspects of calcium phosphates used in spinal surgery. *European Spine Journal,* 10**,** S114-S121.

BOHNER, M. & GBURECK, U. 2008. Thermal reactions of brushite cements. *Journal of Biomedical Materials Research Part B-Applied Biomaterials,* 84B**,** 375-385.

BOHNER, M., GBURECK, U. & BARRALET, J. E. 2005. Technological issues for the development of more efficient calcium phosphate bone cements: A critical assessment. *Biomaterials,* 26**,** 6423-6429.

BOHNER, M., MALSY, A. K., CAMIRE, C. L. & GBURECK, U. 2006. Combining particle size distribution and isothermal calorimetry data to determine the reaction kinetics of alpha-tricalcium phosphate-water mixtures. *Acta Biomaterialia,* 2**,** 343-348.

BOHNER, M., VANLANDUYT, P., MERKLE, H. P. & LEMAITRE, J. 1997. Composition effects on the pH of a hydraulic calcium phosphate cement. *Journal of Materials Science-Materials in Medicine,* 8**,** 675-681.

BOUDEVILLE, P., ROMIEU, G., GARRIC, X., MUNIER, S. & VERT, M. 2010. Calcium-strontium mixed phosphate as novel injectable and radio-opaque hydraulic cement. *Acta Biomaterialia,* 6**,** 3208-3215.

BOUDEVILLE, P., SERRAJ, S., LELOUP, J. M., MARGERIT, J., PAUVERT, B. & TEROL, A. 1999. Physical properties and self-setting mechanism of calcium phosphate cements from calcium bis-dihydrogenophosphate monohydrate and calcium oxide. *Journal of Materials Science-Materials in Medicine,* 10**,** 99-109.

BRAUER, D. S., KARPUKHINA, N., LAW, R. V. & HILL, R. G. 2009. Structure of fluoride-containing bioactive glasses. *Journal of Materials Chemistry,* 19**,** 5629-5636.

BRAUER, D. S., KARPUKHINA, N., O'DONNELL, M. D., LAW, R. V. & HILL, R. G. 2010a. Fluoride-containing bioactive glasses: effect of glass design and structure on degradation, pH and apatite formation in simulated body fluid. *Acta Biomaterialia,* 6**,** 3275-82.

BRAUER, D. S., KARPUKHINA, N., O'DONNELL, M. D., LAW, R. V. & HILL, R. G. 2010b. Fluoride-containing bioactive glasses: Effect of glass design and structure on degradation, pH and apatite formation in simulated body fluid. *Acta Biomaterialia,* 6**,** 3275-3282.

BRAUER, D. S., KARPUKHINA, N., SEAH, D., LAW, R. V. & HILL, R. G. 2008. Fluoride-containing bioactive glasses. *Glass - the Challenge for the 21st Century,* 39-40**,** 299-304.

BRAUER, D. S., KARPULTHINA, N., O'DONNELL, M. D., LAW, R. V. & HILL, R. G. 2010c. Fluoride-containing bioactive glasses: Effect of glass design and structure on degradation, pH and apatite formation in simulated body fluid. *Acta Biomaterialia,* 6**,** 3275-3282.

BRAUER, R. G. H. D. S. 2011. Predicting the bioactivity of glasses using the network connectivity or split netork models. *Journal of Non-Crystalline Solids,* 357**,** 3.

BRAUN, M., HARTMANN, P. & JANA, C. 1995. F-19 and P-31 Nmr-Spectroscopy of Calcium Apatites. *Journal of Materials Science-Materials in Medicine,* 6**,** 150-154.
BROWN, W. E. 1962. Octacalcium Phosphate and Hydroxyapatite: Crystal Structure of Octacalcium Phosphate. *Nature,* 196**,** 3.
BRUNNER, T. J., GRASS, R. N., BOHNER, M. & STARK, W. J. 2007. Effect of particle size, crystal phase and crystallinity on the reactivity of tricalcium phosphate cements for bone reconstruction. *Journal of Materials Chemistry,* 17**,** 4072-4078.
BURLET, N. & REGINSTER, J. Y. 2006. Strontium ranelate - The first dual acting treatment for postmenopausal osteoporosis. *Clinical Orthopaedics and Related Research***,** 55-60.
CANALIS, E., HOTT, M., DELOFFRE, P., TSOUDEROS, Y. & MARIE, P. J. 1996. The divalent strontium salt S12911 enhances bone cell replication and bone formation in vitro. *Bone,* 18**,** 517-23.
CAZALBOU, S., COMBES, C., EICHERT, D. & REY, C. 2004. Adaptative physico-chemistry of bio-related calcium phosphates. *Journal of Materials Chemistry,* 14**,** 2148-2153.
CERRUTI, M., GREENSPAN, D. & POWERS, K. 2005. Effect of pH and ionic strength on the reactivity of Bioglass((R)) 45S5. *Biomaterials,* 26**,** 1665-1674.
CHOW, L. C. 2000. Calcium phosphate cements: Chemistry, properties, and applications. *Mineralization in Natural and Synthetic Biomaterials,* 599**,** 27-37

364.
CHOW, L. C. 2009. Next generation calcium phosphate-based biomaterials. *Dental Materials Journal,* 28**,** 1-10.
CHOW, L. C. & BROWN, W. E. 1973. Reaction of Dicalcium Phosphate Dihydrate with Fluoride. *Journal of Dental Research,* 52**,** 1220-1227.
CHRISTIE, J. K., PEDONE, A., MENZIANI, M. C. & TILOCCA, A. 2011. Fluorine Environment in Bioactive Glasses: ab Initio Molecular Dynamics Simulations. *Journal of Physical Chemistry B,* 115**,** 2038-2045.
CHUNG, T. M., WANG, T. C., HO, R. M., SUN, Y. S. & KO, B. T. 2010. Polymeric Crystallization under Nanoscale 2D Spatial Confinement. *Macromolecules,* 43**,** 6237-6240.
CICEK, G., AKSOY, E. A., DURUCAN, C. & HASIRCI, N. 2011. Alpha-tricalcium phosphate (alpha-TCP): solid state synthesis from different calcium precursors and the hydraulic reactivity. *Journal of Materials Science-Materials in Medicine,* 22**,** 809-817.
CLARKIN, O. M., BOYD, D., MADIGAN, S. & TOWLER, M. R. 2009. Comparison of an experimental bone cement with a commercial control, Hydroset (TM). *Journal of Materials Science-Materials in Medicine,* 20**,** 1563-1570.
CO, S. L. G. 2010. HydroSet: Injectable HA Bone Substitute. Instruction for Use. Kalamazoo: Stryker.
COLEMAN, N. J. A. N., J. W. 2013. *Glass Bones,* http://www.rsc.org/education/eic/issues/2006nov/glassbones.asp

[Online]. London: Royal Society of Chemistry. [Accessed 31/03/2014 2014].
CONSTANTZ, B. R., ISON, I. C., FULMER, M. T., POSER, R. D., SMITH, S. T., VANWAGONER, M., ROSS, J., GOLDSTEIN, S. A., JUPITER, J. B. & ROSENTHAL, D. I. 1995. Skeletal Repair by in-Situ Formation of the Mineral Phase of Bone. *Science,* 267**,** 1796-1799.
COSTANTINO, P. D., FRIEDMAN, C. D., JONES, K., CHOW, L. C., PELZER, H. J. & SISSON, G. A., SR. 1991. Hydroxyapatite cement. I. Basic chemistry and histologic properties. *Arch Otolaryngol Head Neck Surg,* 117**,** 379-84.
COSTANTINO, P. D., FRIEDMAN, C. D., JONES, K., CHOW, L. C. & SISSON, G. A. 1992. Experimental hydroxyapatite cement cranioplasty. *Plastic and Reconstructive Surgery,* 90**,** 174-85; discussion 186-91.
CURRY, N. A. & JONES, D. W. 1971. Crystal Structure of Brushite, Calcium Hydrogen Orthophosphate Dihydrate - Neutron-Diffraction Investigation. *Journal of the Chemical Society a -Inorganic Physical Theoretical***,** 3725-&.
DAVIES, E., DUER, M. J., ASHBROOK, S. E. & GRIFFIN, J. M. 2012. Applications of NMR Crystallography to Problems in Biomineralization: Refinement of the Crystal Structure and P-31 Solid-State NMR Spectral Assignment of Octacalcium Phosphate. *Journal of the American Chemical Society,* 134**,** 12508-12515.
DE YOREO, J. J. & VEKILOV, P. G. 2003. Principles of crystal nucleation and growth. *Biomineralization,* 54**,** 57-93.
DOROZHKIN, S. V. 2008. Calcium orthophosphate cements for biomedical application. *Journal of Materials Science,* 43**,** 3028-3057.
DOWEIDAR, H. 2009. Density-structure correlations in Na2O-CaO-P2O5-SiO2 bioactive glasses. *Journal of Non-Crystalline Solids,* 355**,** 577-580.
DRIESSENS, F. C. M., BOLTONG, M. G., BERMUDEZ, O. & PLANELL, J. A. 1993. Formulation and Setting Times of Some Calcium Orthophosphate Cements - a Pilot-Study. *Journal of Materials Science-Materials in Medicine,* 4**,** 503-508.
EDEN, M. 2011. The split network analysis for exploring composition-structure correlations in multi-component glasses: I. Rationalizing bioactivity-composition trends of bioglasses. *Journal of Non-Crystalline Solids,* 357**,** 1595-1602.
EDEN, M., SUNDBERG, P. & STALHANDSKE, C. 2011. The split network analysis for exploring composition-structure correlations in multi-component glasses: II. Multinuclear NMR studies of alumino-borosilicates and glass-wool fibers. *Journal of Non-Crystalline Solids,* 357**,** 1587-1594.
ELGAYAR, I., ALIEV, A. E., BOCCACCINI, A. R. & HILL, R. G. 2005. Structural analysis of bioactive glasses. *Journal of Non-Crystalline Solids,* 351**,** 173-183.
ELLIOTT, J. 1994. *Structure and Chemistry of the Apatites and Other Calcium Orthophosphates,* Amsterdam, Elsevier.

FERNANDEZ, E., GIL, F. J., GINEBRA, M. P., DRIESSENS, F. C. M., PLANELL, J. A. & BEST, S. M. 1999a. Calcium phosphate bone cements for clinical applications - Part I: Solution chemistry. *Journal of Materials Science-Materials in Medicine,* 10**,** 169-176.

FERNANDEZ, E., GINEBRA, M. P., BOLTONG, M. G., DRIESSENS, F. C., GINEBRA, J., DE MAEYER, E. A., VERBEECK, R. M. & PLANELL, J. A. 1996. Kinetic study of the setting reaction of a calcium phosphate bone cement. *Journal of Biomedical Materials Research,* 32**,** 367-74.

FERNANDEZ, E., PLANELL, J. A. & BEST, S. M. 1999b. Precipitation of carbonated apatite in the cement system alpha-Ca-3(PO4)(2)-Ca(H2PO4)(2)-CaCO3. *Journal of Biomedical Materials Research,* 47**,** 466-471.

FLAUTRE, B., DELECOURT, C., BLARY, M. C., VAN LANDUYT, P., LEMAITRE, J. & HARDOUIN, P. 1999. Volume effect on biological properties of a calcium phosphate hydraulic cement: Experimental study in sheep. *Bone,* 25**,** 35s-39s.

FLEET, M. E. & LIU, X. Y. 2004. Location of type B carbonate ion in type A-B carbonate apatite synthesized at high pressure. *Journal of Solid State Chemistry,* 177**,** 3174-3182.

FOWLER, B. O., MARKOVIC, M. & BROWN, W. E. 1993. Octacalcium Phosphate .3. Infrared and Raman Vibrational-Spectra. *Chemistry of Materials,* 5**,** 1417-1423.

FRIEDMAN, C. D., COSTANTINO, P. D., JONES, K., CHOW, L. C., PELZER, H. J. & SISSON, G. A., SR. 1991. Hydroxyapatite cement. II. Obliteration and reconstruction of the cat frontal sinus. *Arch Otolaryngol Head Neck Surg,* 117**,** 385-9.

FUKASE, Y., EANES, E. D., TAKAGI, S., CHOW, L. C. & BROWN, W. E. 1990. Setting Reactions and Compressive Strengths of Calcium-Phosphate Cements. *Journal of Dental Research,* 69**,** 1852-1856.

GAO, G. 2004. *Nanostructures and Nanomaterials: Synthesis, Properties and Applications,* London, United Kingdom, Imperial College Press.

GASHTI, M. P., BOURQUIN, M., STIR, M. & HULLIGER, J. 2013. Glutamic acid inducing kidney stone biomimicry by a brushite/gelatin composite. *Journal of Materials Chemistry B,* 1**,** 1501-1508.

GBURECK, U., BARRALET, J. E., HOFMANN, M. P. & THULL, R. 2004a. Nanocrystalline tetracalcium phosphate cement. *Journal of Dental Research,* 83**,** 425-428.

GBURECK, U., BARRALET, J. E., RADU, L., KLINGER, H. G. & THULL, R. 2004b. Amorphous alpha-tricalcium phosphate: Preparation and aqueous setting reaction. *Journal of the American Ceramic Society,* 87**,** 1126-1132.

GBURECK, U., GROLMS, O., BARRALET, J. E., GROVER, L. M. & THULL, R. 2003. Mechanical activation and cement formation of beta-tricalcium phosphate. *Biomaterials,* 24**,** 4123-4131.

GENTLEMAN, E., FREDHOLM, Y. C., JELL, G., LOTFIBAKHSHAIESH, N., O'DONNELL, M. D., HILL, R. G. & STEVENS, M. M. 2010. The effects of strontium-substituted bioactive glasses on osteoblasts and osteoclasts in vitro. *Biomaterials,* 31**,** 3949-3956.

GIBBS, J. W. 1957. *The collected works of J. Willard Gibbs',* New Haven, Yale University Press.
GIBSON, I. R. & BONFIELD, W. 2002. Novel synthesis and characterization of an AB-type carbonate-substituted hydroxyapatite. *Journal of Biomedical Materials Research,* 59**,** 697-708.
GIOCONDI, J. L., EL-DASHER, B. S., NANCOLLAS, G. H. & ORME, C. A. 2010. Molecular mechanisms of crystallization impacting calcium phosphate cements. *Philosophical Transactions of the Royal Society a-Mathematical Physical and Engineering Sciences,* 368**,** 1937-1961.
GRIFFITH, A. A. 1921. The phenomena of rupture and fluid flow in solids. *Philosophical Transactions of the Royal Society of London* 221**,** 163-198.
GROVER, L. M., HOFMANN, M. P., GBURECK, U., KUMARASAMI, B. & BARRALET, J. E. 2008. Frozen delivery of brushite calcium phosphate cements. *Acta Biomaterialia,* 4**,** 1916-1923.
GROVER, L. M., KNOWLES, J. C., FLEMING, G. J. P. & BARRALET, J. E. 2003. In vitro ageing of brushite calcium phosphate cement. *Biomaterials,* 24**,** 4133-4141.
GRUNDWALD, S. Publication year not stated. *Primary Mineral Components of Soils,* http://soils.ifas.ufl.edu/faculty/grunwald/teaching/eSoilScience/primary.shtml [Online]. Florida: University of Florida. [Accessed 31/03/2014 2014].
GRYNPAS, M. D., HAMILTON, E., CHEUNG, R., TSOUDEROS, Y., DELOFFRE, P., HOTT, M. & MARIE, P. J. 1996. Strontium increases vertebral bone volume in rats at a low dose that does not induce detectable mineralization defect. *Bone,* 18**,** 253-9.
GUO, D. G., XU, K. W. & HAN, Y. 2008. The influence of Sr doses on the in vitro biocompatibility and in vivo degradability of single-phase Sr-incorporated HAP cement. *Journal of Biomedical Materials Research Part A,* 86A**,** 947-958.
GUO, D. G., XU, K. W., ZHAO, X. Y. & HAN, Y. 2005. Development of a strontium-containing hydroxyapatite bone cement. *Biomaterials,* 26**,** 4073-4083.
GUO, H., SU, J. C., WEI, J., KONG, H. & LIU, C. S. 2009. Biocompatibility and osteogenicity of degradable Ca-deficient hydroxyapatite scaffolds from calcium phosphate cement for bone tissue engineering. *Acta Biomaterialia,* 5**,** 268-278.
HACKER, B. *Intorduction* [Online]. California: University of California, Santa Barbara. [Accessed 17/03/2014.
HENCH, L. L. 1993. Bioceramics - from Concept to Clinic. *American Ceramic Society Bulletin,* 72**,** 93-98.
HENCH, L. L. 2006. The story of Bioglass (R). *Journal of Materials Science-Materials in Medicine,* 17**,** 967-978.
HENCH, L. L. 2009. Genetic design of bioactive glass. *Journal of the European Ceramic Society,* 29**,** 1257-1265.
HENCH, L. L., SPLINTER, R. J., ALLEN, W. C. & GREENLEE, T. K. 1971. Bonding mechanisms at the interface of ceramic prosthetic materials. *Journal of Biomedical Materials Research,* 5**,** 117-141.

HENCH, L. L., XYNOS, I. D., EDGAR, A. J., BUTTERY, L. D. K., POLAK, J. M., ZHONG, J. P., LIU, X. Y. & CHANG, J. 2002. Gene activating glasses. *Journal of Inorganic Materials,* 17**,** 897-909.

HILL, R. 2012. Type to KENT, N.

HOLLOWAY, D. G. 1973. *The Physical Properties of Glass*, Wykeham Publications LTD.

HONDA, Y., ANADA, T., KAMAKURA, S., MORIMOTO, S., KURIYAGAWA, T. & SUZUKI, O. 2009. The Effect of Microstructure of Octacalcium Phosphate on the Bone Regenerative Property. *Tissue Engineering Part A,* 15**,** 1965-1973.

HWANG, J. J. H., SIEW, C., ROBINSON, P., GRUNINGER, S. E., CHOW, L. C. & BROWN, W. E. 1986. Functional-Evaluation of a New Calcium-Phosphate Cement. *Journal of Dental Research,* 65**,** 195-195.

ISHIKAWA, K. 2008. Calcium phosphate cement. *Bioceramics and Their Clinical Applications***,** 438-463.

ISHIKAWA, K. 2010. Bone Substitute Fabrication Based on Dissolution-Precipitation Reactions. *Materials,* 3**,** 1138-1155.

ISHIKAWA, K., TAKAGI, S., CHOW, L. C. & ISHIKAWA, Y. 1995. Properties and Mechanisms of Fast-Setting Calcium-Phosphate Cements. *Journal of Materials Science-Materials in Medicine,* 6**,** 528-533.

ISHIKAWA, K., TAKAGI, S., CHOW, L. C. & SUZUKI, K. 1999. Reaction of calcium phosphate cements with different amounts of tetracalcium phosphate and dicalcium phosphate anhydrous. *Journal of Biomedical Materials Research,* 46**,** 504-510.

JACK, V., BUCHANAN, F. J. & DUNNE, N. I. 2008. Particle attrition of alpha-tricalcium phosphate: effect on mechanical, handling, and injectability properties of calcium phosphate cements. *Proceedings of the Institution of Mechanical Engineers Part H-Journal of Engineering in Medicine,* 222**,** 19-28.

KAKEI, M. & YOSHIKAWA, M. 2003. Demonstration of octacalcium phosphate in dental calculus. *Journal of Dental Research,* 82**,** B76-B76.

KAY, M. I., YOUNG, R. A. & POSNER, A. S. 1964. Crystal Structure of Hydroxyapatite. *Nature,* 204**,** 1050-2.

KEELER, J. 2010. *Understanding NMR Spectroscopy,* Chichester, United Kingdom, Jon Wiley and Sons.

KLEIN, C. P. A. T., DEGROOT, K., DRIESSEN, A. A. & VANDERLUBBE, H. B. M. 1985. Interaction of Biodegradable Beta-Whitlockite Ceramics with Bone Tissue - an Invivo Study. *Biomaterials,* 6**,** 189-192.

KNAACK, D., GOAD, M. E. P., AIOLOVA, M., REY, C., TOFIGHI, A., CHAKRAVARTHY, P. & LEE, D. D. 1998. Resorbable calcium phosphate bone substitute. *Journal of Biomedical Materials Research,* 43**,** 399-409.

KOHNE, J. M., SCHLUTER, S. & VOGEL, H. J. 2011. Predicting Solute Transport in Structured Soil Using Pore Network Models. *Vadose Zone Journal,* 10**,** 1082-1096.

KOLMAS, J., JAKLEWICZ, A., ZIMA, A., BUCKO, M., PASZKIEWICZ, Z., LIS, J., SLOSARCZYK, A. & KOLODZIEJSKI, W. 2011. Incorporation of carbonate and magnesium ions into synthetic hydroxyapatite: The

effect on physicochemical properties. *Journal of Molecular Structure,* 987**,** 40-50.
KOLMAS, J. & KOLODZIEJSKI, W. 2012. Inverse P-31 -> H-1 NMR cross-polarization in hydrated nanocrystalline calcium hydroxyapatite. *Chemical Physics Letters,* 554**,** 128-132.
KUMAR, M., XIE, J., CHITTUR, K. & RILEY, C. 1999. Transformation of modified brushite to hydroxyapatite in aqueous solution: effects of potassium substitution. *Biomaterials,* 20**,** 1389-1399.
LAI, Y. K., HUANG, Y. X., WANG, H., HUANG, J. Y., CHEN, Z. & LIN, C. J. 2010. Selective formation of ordered arrays of octacalcium phosphate ribbons on TiO2 nanotube surface by template-assisted electrodeposition. *Colloids and Surfaces B-Biointerfaces,* 76**,** 117-122.
LAURENCIN, D., WONG, A., DUPREE, R. & SMITH, M. E. 2008. Natural abundance Ca-43 solid-state NMR characterisation of hydroxyapatite: identification of the two calcium sites. *Magnetic Resonance in Chemistry,* 46**,** 347-350.
LEGEROS, R. Z. 1985. Preparation of Octacalcium Phosphate (Ocp) - a Direct Fast Method. *Calcified Tissue International,* 37**,** 194-197.
LEGEROS, R. Z. 1991. *Calcium Phosphates in Oral Biology and Medicine,* New York, Karger.
LEGRAND, A. P., SFIHI, H., LEQUEUX, N. & LEMAITRE, J. 2009. P-31 Solid-State NMR Study of the Chemical Setting Process of a Dual-Paste Injectable Brushite Cements. *Journal of Biomedical Materials Research Part B-Applied Biomaterials,* 91B**,** 46-54.
LEWIS, G. 2006. Injectable bone cements for use in vertebroplasty and kyphoplasty: State-of-the-art review. *Journal of Biomedical Materials Research Part B-Applied Biomaterials,* 76B**,** 456-468.
LI, Z. Y., YUAN, N., LAM, R. W. M., CUI, Z. D., YANG, X. J. & LU, W. W. 2013. Preclinical evaluation of strontium-containing bioactive bone cement. *Materials Science & Engineering C-Materials for Biological Applications,* 33**,** 5100-5104.
LIU, C. S., SHEN, W. & CHEN, J. G. 1999. Solution property of calcium phosphate cement hardening body. *Materials Chemistry and Physics,* 58**,** 78-82.
LUSVARDI, G., MALAVASI, G., CORTADA, M., MENABUE, L., MENZIANI, M. C., PEDONE, A. & SEGRE, U. 2008. Elucidation of the structural role of fluorine in potentially bioactive glasses by experimental and computational investigation. *Journal of Physical Chemistry B,* 112**,** 12730-9.
MACFADDEN, B. J., LABS-HOCHSTEIN, J., QUITMYER, I. & JONES, D. S. 2004. Incremental growth and diagenesis of skeletal parts of the lamnoid shark Otodus obliquus from the early Eocene (Ypresian) of Morocco. *Palaeogeography Palaeoclimatology Palaeoecology,* 206**,** 179-192.
MAIER, F. J. 1947. Methods of Removing Fluorides from Water. *American Journal of Public Health,* 37**,** 1559-1566.
MALLETTE, L. E., LEBLANC, A. D., POOL, J. L. & MECHANICK, J. I. 1989. Cyclic Therapy of Osteoporosis with Neutral Phosphate and Brief,

High-Dose Pulses of Etidronate. *Journal of Bone and Mineral Research,* 4**,** 143-148.

MARIE, P. J., AMMANN, P., BOIVIN, G. & REY, C. 2001. Mechanisms of action and therapeutic potential of strontium in bone. *Calcified Tissue International,* 69**,** 121-129.

MATHEW, M., BROWN, W. E., SCHROEDER, L. W. & DICKENS, B. 1988. Crystal-Structure of Octacalcium Bis(Hydrogenphosphate) Tetrakis(Phosphate)Pentahydrate, Ca8(Hpo4)2(Po4)4.5h2o. *Journal of Crystallographic and Spectroscopic Research,* 18**,** 235-250.

MATHEW, R., STEVENSSON, B., TILOCCA, A. & EDEN, M. 2014. Toward a Rational Design of Bioactive Glasses with Optimal Structural Features: Composition-Structure Correlations Unveiled by Solid-State NMR and MD Simulations. *Journal of Physical Chemistry B,* 118**,** 833-844.

MCGIRT, M. J., PARKER, S. L., WOLINSKY, J. P., WITHAM, T. F., BYDON, A. & GOKASLAN, Z. L. 2009. Vertebroplasty and kyphoplasty for the treatment of vertebral compression fractures: an evidenced-based review of the literature. *Spine Journal,* 9**,** 501-508.

MIQUEL, J. L., FACCHINI, L., LEGRAND, A. P., MARCHANDISE, X., LECOUFFE, P., CHANAVAZ, M., DONAZZAN, M., REY, C. & LEMAITRE, J. 1990. Characterization and Conversion Study into Natural Living Bone of Calcium-Phosphate Bioceramics by Solid-State Nmr-Spectroscopy. *Interfaces in Biomaterials Sciences,* 13**,** 19-29.

MIRTCHI, A. A., LEMAITRE, J. & MUNTING, E. 1989. Calcium-Phosphate Cements - Action of Setting Regulators on the Properties of the Beta-Tricalcium Phosphate Monocalcium Phosphate Cements. *Biomaterials,* 10**,** 634-638.

MIRTCHI, A. A., LEMAITRE, J. & MUNTING, E. 1990. Calcium-Phosphate Cements - Study of the Beta-Tricalcium Phosphate Dicalcium Phosphate Calcite Cements. *Biomaterials,* 11**,** 83-88.

MIRTCHI, A. A., LEMAITRE, J. & MUNTING, E. 1991. Calcium-Phosphate Cements - Effect of Fluorides on the Setting and Hardening of Beta-Tricalcium Phosphate Dicalcium Phosphate Calcite Cements. *Biomaterials,* 12**,** 505-510.

MONMA, H. & KANAZAWA, T. 2000. The hydration of alpha-tricalcium phosphate. *Journal of the Ceramic Society of Japan,* 108**,** S75-S80.

MOREAU, J. L., WEIR, M. D. & XU, H. H. K. 2009. Self-setting collagen-calcium phosphate bone cement: Mechanical and cellular properties. *Journal of Biomedical Materials Research Part A,* 91A**,** 605-613.

MORENO, E. C. & VARUGHESE, K. 1981. Crystal-Growth of Calcium Apatites from Dilute-Solutions. *Journal of Crystal Growth,* 53**,** 20-30.

MORENO, E. C., ZAHRADNIK, R. T., GLAZMAN, A. & HWU, R. 1977. Precipitation of Hydroxyapatite from Dilute-Solutions Upon Seeding. *Calcified Tissue Research,* 24**,** 47-57.

MORIMOTO, S., ANADA, T., HONDA, Y. & SUZUKI, O. 2012. Comparative study on in vitro biocompatibility of synthetic octacalcium phosphate and calcium phosphate ceramics used clinically. *Biomedical Materials,* 7.

MORIWAKI Y, D. Y. K. T., AOBA T, TAKAHASHI J, OKAZAKI M 1983. *Mechanisms of Tooth Enamel Formation,* Tokyo, Quintessence Publishing Co.

MOSEKE, C. & GBURECK, U. 2010. Tetracalcium phosphate: Synthesis, properties and biomedical applications. *Acta Biomaterialia,* 6**,** 3815-3823.

MURAGALELLI, M. J., NARUSAWA, H., SHIMADA, T., IIJIMA, M. & AOBA, T. 1992. Effects of Fluoride on Precipitation and Hydrolysis of Octacalcium Phosphate in an Experimental-Model Simulating Enamel Mineralization during Amelogenesis. *Cells and Materials,* 2**,** 221-230.

NELSON, D. G. A. & MCLEAN, J. D. 1984. High-Resolution Electron-Microscopy of Octacalcium Phosphate and Its Hydrolysis Products. *Calcified Tissue International,* 36**,** 219-232.

NISHIMURA, N., YAMAMURO, T., TAGUCHI, Y., IKENAGA, M., NAKAMURA, T., KOKUBO, T. & YOSHIHARA, S. 1991. A New Bioactive Bone-Cement - Its Histological and Mechanical Characterization. *Journal of Applied Biomaterials,* 2**,** 219-229.

NURIT, J., MARGERIT, J., TEROL, A. & BOUDEVILLE, P. 2002. pH-metric study of the setting reaction of monocalcium phosphate monohydrate/calcium oxide-based cements. *Journal of Materials Science-Materials in Medicine,* 13**,** 1007-1014.

O'DONNELL, M. D., CANDARLIOGLU, P. L., MILLER, C. A., GENTLEMAN, E. & STEVENS, M. M. 2010. Materials characterisation and cytotoxic assessment of strontium-substituted bioactive glasses for bone regeneration. *Journal of Materials Chemistry,* 20**,** 8934-8941.

O'DONNELL, M. D., WATTS, S. J., HILL, R. G. & LAW, R. V. 2009. The effect of phosphate content on the bioactivity of soda-lime-phosphosilicate glasses. *Journal of Materials Science-Materials in Medicine,* 20**,** 1611-1618.

O'DONNELL, M. D., WATTS, S. J., LAW, R. V. & HILL, R. G. 2008a. Effect of P2O5 content in two series of soda lime phosphosilicate glasses on structure and properties - Part I: NMR. *Journal of Non-Crystalline Solids,* 354**,** 3554-3560.

O'DONNELL, M. D., WATTS, S. J., LAW, R. V. & HILL, R. G. 2008b. Effect of P2O5 content in two series of soda lime phosphosilicate glasses on structure and properties - Part II: Physical properties. *Journal of Non-Crystalline Solids,* 354**,** 3561-3566.

OGAARD, B., ROLLA, G., DIJKMAN, T., RUBEN, J. & ARENDS, J. 1991. Effect of Fluoride Mouthrinsing on Caries Lesion Development in Shark Enamel - an Insitu Caries Model Study. *Scandinavian Journal of Dental Research,* 99**,** 372-377.

OXTOBY, D. W. 1998. Homogeneous nucleation: theory and experiment (vol 4, pg 7627, 1992). *Journal of Physics-Condensed Matter,* 10**,** 897-897.

PEDONE, A., CHARPENTIER, T., MALAVASI, G. & MENZIANI, M. C. 2010. New Insights into the Atomic Structure of 45S5 Bioglass by Means of Solid-State NMR Spectroscopy and Accurate First-Principles Simulations. *Chemistry of Materials,* 22**,** 5644-5652.

PEDONE, A., CHARPENTIER, T. & MENZIANI, M. C. 2012. The structure of fluoride-containing bioactive glasses: new insights from first-principles calculations and solid state NMR spectroscopy. *Journal of Materials Chemistry,* 22**,** 12599-12608.

PHILLIPS, J. C. & THORPE, M. F. 1985. Constraint Theory, Vector Percolation and Glass-Formation. *Solid State Communications,* 53**,** 699-702.

PINA, S., TORRES, P. M., GOETZ-NEUNHOEFFER, F., NEUBAUER, J. & FERREIRA, J. M. F. 2010. Newly developed Sr-substituted alpha-TCP bone cements. *Acta Biomaterialia,* 6**,** 928-935.

PUURA, I. & NEMLIHER, J. 2001. Apatite varieties in Recent and fossil linguloid brachiopod shells. *Brachiopods Past and Present***,** 7-16.

RAY, N. H. 1978. *Inorganic Polymers*, Academic Press Inc.

RAY, R. D. & WARD, A. A., JR. 1951. A preliminary report on studies of basic calcium phosphate in bone replacement. *Surg Forum***,** 429-34.

REFFITT, D. M., OGSTON, N., JUGDAOHSINGH, R., CHEUNG, H. F., EVANS, B. A., THOMPSON, R. P., POWELL, J. J. & HAMPSON, G. N. 2003. Orthosilicic acid stimulates collagen type 1 synthesis and osteoblastic differentiation in human osteoblast-like cells in vitro. *Bone,* 32**,** 127-35.

RENNO, A. C. M., NEJADNIK, M. R., VAN DE WATERING, F. C. J., CROVACE, M. C., ZANOTTO, E. D., HOEFNAGELS, J. P. M., WOLKE, J. G. C., JANSEN, J. A. & VAN DEN BEUCKEN, J. J. J. P. 2013. Incorporation of bioactive glass in calcium phosphate cement: Material characterization and in vitro degradation. *Journal of Biomedical Materials Research Part A,* 101A**,** 2365-2373.

ROMIEU, G., GARRIC, X., MUNIER, S., VERT, M. & BOUDEVILLE, P. 2010. Calcium-strontium mixed phosphate as novel injectable and radio-opaque hydraulic cement. *Acta Biomaterialia,* 6**,** 3208-3215.

ROTHWELL, W. P., WAUGH, J. S. & YESINOWSKI, J. P. 1980. High-Resolution Variable-Temperature P-31 Nmr of Solid Calcium Phosphates. *Journal of the American Chemical Society,* 102**,** 2637-2643.

ROWLES, S. L. 1968. The precipitation of whitlockite from aqueous solutions. *Bull Soc Chim Fr***,** 5.

SAINZ-DIAZ, C. I., VILLACAMPA, A. & OTALORA, F. 2004. Crystallographic properties of the calcium phosphate mineral, brushite, by means of First Principles calculations. *American Mineralogist,* 89**,** 307-313.

SANDHU, S. K. & HAMPSON, G. 2011. The pathogenesis, diagnosis, investigation and management of osteoporosis. *Journal of Clinical Pathology,* 64**,** 1042-1050.

SHARMA, V. K., JOHNSSON, M., SALLIS, J. D. & NANCOLLAS, G. H. 1992. Influence of Citrate and Phosphocitrate on the Crystallization of Octacalcium Phosphate. *Langmuir,* 8**,** 676-679.

SHIWAKU, Y., HONDA, Y., ANADA, T., MORIMOTO, S., MASUDA, T., SASAKI, K. & SUZUKI, O. 2010a. Analysis of physicochemical properties of octacalcium phosphate prepared by hydrolysis and co-precipitation with fluoride ions. *Journal of the Ceramic Society of Japan,* 118**,** 402-405.

SHIWAKU, Y., HONDA, Y., ANADA, T., SASAKI, K. & SUZUKI, O. 2010b. Apatite formation from octacalcium phosphate with fluoride. *Interface Oral Health Science 2009***,** 286-287.

STRICKLAND-CONSTABLE, R. F. 1968. *Kinetics and Mechanism of Crystallization*, Academic Press.

SUDARSAN.K & YOUNG, R. A. 1969. Significant Precision in Crystal Structural Details - Holly Springs Hydroxyapatite. *Acta Crystallographica Section B-Structural Crystallography and Crystal Chemistry,* B 25**,** 1534-&.

SUN, J. Y., LI, J. Y., LIU, X. Y., WEI, L., WANG, G. C. & MENG, F. H. 2009. Proliferation and gene expression of osteoblasts cultured in DMEM containing the ionic products of dicalcium silicate coating. *Biomedicine & Pharmacotherapy,* 63**,** 650-657.

SUZUKI, O., KAMAKURA, S., KATAGIRI, T., NAKAMURA, M., ZHAO, B. H., HONDA, Y. & KAMIJO, R. 2006. Bone formation enhanced by implanted octacalcium phosphate involving conversion into Ca-deficient hydroxyapatite. *Biomaterials,* 27**,** 2671-2681.

TAKAGI, S., CHOW, L. C. & ISHIKAWA, K. 1998. Formation of hydroxyapatite in new calcium phosphate cements. *Biomaterials,* 19**,** 1593-1599.

TAKAGI, S., FRUKHTBEYN, S., CHOW, L. C., SUGAWARA, A., FUJIKAWA, K., OGATA, H., HAYASHI, M. & OGISO, B. 2010. In Vitro and in Vivo Characteristics of Fluorapatite-Forming Calcium Phosphate Cements. *Journal of Research of the National Institute of Standards and Technology,* 115**,** 267-276.

TAMIMI, F., SHEIKH, Z. & BARRALET, J. 2012. Dicalcium phosphate cements: brushite and monetite. *Acta Biomaterialia,* 8**,** 474-87.

TENHUISEN, K. S. & BROWN, P. W. 1994. The formation of hydroxyapatite-ionomer cements at 38 degrees C. *Journal of Dental Research,* 73**,** 598-606.

TENHUISEN, K. S. & BROWN, P. W. 1998. Formation of calcium-deficient hydroxyapatite from alpha-tricalcium phosphate. *Biomaterials,* 19**,** 2209-2217.

TILOCCA, A. & CORMACK, A. N. 2007. Structural effects of phosphorus inclusion in bioactive silicate glasses. *Journal of Physical Chemistry B,* 111**,** 14256-14264.

TILOCCA, A., CORMACK, A. N. & DE LEEUW, N. H. 2007. The formation of nanoscale structures in soluble phosphosilicate glasses for biomedical applications: MD simulations. *Faraday Discussions,* 136**,** 45-55.

TOFIGHI, A., MOUNIC, S., CHAKRAVARTHY, P., REY, C. & LEE, D. 2000. Setting reactions involved in injectable cements based on amorphous calcium phosphate. *Bioceramics,* 192-1**,** 769-772.

TOMAZIC, B. B., TUNG, M. S., GREGORY, T. M. & BROWN, W. E. 1989. Mechanism of Hydrolysis of Octacalcium Phosphate. *Scanning Microscopy,* 3**,** 119-127.

TSAI, T. W. T., CHOU, F. C., TSENG, Y. H. & CHAN, J. C. C. 2010. Solid-state P-31 NMR study of octacalcium phosphate incorporated with succinate. *Physical Chemistry Chemical Physics,* 12**,** 6692-6697.

TSENG, Y. H., MOU, C. Y. & CHAN, J. C. C. 2006. Solid-state NMR study of the transformation of octacalcium phosphate to hydroxyapatite: A mechanistic model for central dark line formation. *Journal of the American Chemical Society,* 128**,** 6909-6918.

TSENG, Y. H., ZHAN, J. H., LIN, K. S. K., MOU, C. Y. & CHAN, J. C. C. 2004. High resolution P-31 NMR study of octacalcium phosphate. *Solid State Nuclear Magnetic Resonance,* 26**,** 99-104.

TUNG, M. S., CHOW, L. C. & BROWN, W. E. 1985. Hydrolysis of dicalcium phosphate dihydrate in the presence or absence of calcium fluoride. *Journal of Dental Research,* 64**,** 2-5.

VOGEL, W. 1985. *Chemistry of Glass,* Columbus, The American Ceramic Society.

WALLACE, K. E., HILL, R. G., PEMBROKE, J. T., BROWN, C. J. & HATTON, P. V. 1999. Influence of sodium oxide content on bioactive glass properties. *Journal of Materials Science-Materials in Medicine,* 10**,** 697-701.

WALTHER, M. M., EANES, E. D., DELANEY, T. F. & TRAVIS, W. D. 1996. Bladder calcifications after photodynamic therapy: Analysis of a rare complication. *Urology,* 47**,** 831-835.

WEI, J., WANG, J. C., LIU, X. C., MA, J., LIU, C. S., FANG, J. & WEI, S. C. 2011. Preparation of fluoride substituted apatite cements as the building blocks for tooth enamel restoration. *Applied Surface Science,* 257**,** 7887-7892.

WHITE, D. J., BOWMAN, W. D., FALLER, R. V., MOBLEY, M. J., WOLFGANG, R. A. & YESINOWSKI, J. P. 1988. 19F MAS-NMR and solution chemical characterization of the reactions of fluoride with hydroxyapatite and powdered enamel. *Acta Odontologica Scandinavica,* 46**,** 375-89.

WHITE, T., FERRARIS, C., KIM, J. & MADHAVI, S. 2005. Apatite - An adaptive framework structure. *Micro- and Mesoporous Mineral Phases,* 57**,** 307-401.

WHITE, T. J. & DONG, Z. L. 2003. Structural derivation and crystal chemistry of apatites. *Acta Crystallographica Section B-Structural Science,* 59**,** 1-16.

XIE, J., RILEY, C. & CHITTUR, K. 2001. Effect of albumin on brushite transformation to hydroxyapatite. *Journal of Biomedical Materials Research,* 57**,** 357-365.

XYNOS, I. D., EDGAR, A. J., BUTTERY, L. D. K., HENCH, L. L. & POLAK, J. M. 2001. Gene-expression profiling of human osteoblasts following treatment with the ionic products of Bioglass (R) 45S5 dissolution. *Journal of Biomedical Materials Research,* 55**,** 151-157.

XYNOS, I. D., HUKKANEN, M. V. J., BATTEN, J. J., BUTTERY, L. D., HENCH, L. L. & POLAK, J. M. 2000. Bioglass (R) 45S5 stimulates osteoblast turnover and enhances bone formation in vitro: Implications and applications for bone tissue engineering. *Calcified Tissue International,* 67**,** 321-329.

YESINOWSKI, J. P. & ECKERT, H. 1987. Hydrogen Environments in Calcium Phosphates - H-1 Mas Nmr at High Spinning Speeds. *Journal of the American Chemical Society,* 109**,** 6274-6282.

YU, T., YE, J. & WANG, Y. 2009. Preparation and characterization of a novel strontium-containing calcium phosphate cement with the two-step hydration process. *Acta Biomaterialia,* 5**,** 2717-27.
ZACHARIASEN, W. H. 1932. The atomic arrangment in glass. *J. Am. Chem.,* 10**,** 10.
ZARZYCKI, J. 1991. *Glasses and the Vitreous State*, Cambridge University Press.
ZOLOTOYABKO, E. 2014. *Basic Concepts of X-Ray Diffraction,* Weinheim, Germany, Wiley.

Appendix

Appendix A: Required statement of originality for inclusion in research degree theses

I, Niall William Kent, confirm that the research included within this thesis is my own work or that where it has been carried out in collaboration with, or supported by others, that this is duly acknowledged below and my contribution indicated. Previously published material is also acknowledged below.

I attest that I have exercised reasonable care to ensure that the work is original, and does not to the best of my knowledge break any UK law, infringe any third party's copyright or other Intellectual Property Right, or contain any confidential material.

I accept that the College has the right to use plagiarism detection software to check the electronic version of the thesis.

I confirm that this thesis has not been previously submitted for the award of a degree by this or any other university.

Signature: Niall Kent
Date: 13/05/2014

Details of collaboration and publications:
See further Appendix for Publication, Collaboration and Patent.

APPENDIX B:

APPENDIX C:

APPENDIX D: